UFL/COEL-84/004

COASTAL ENGINEERING INVESTIGATION AT JUPITER INLET, FLORIDA

by

William T. Buckingham

March 1984

Submitted to:

Jupiter Inlet District
and
Palm Beach County

Coastal & Oceanographic Engineering Department
433 Weil Hall • P.O. Box 116590 • Gainesville, Florida 32611-6590

UNIVERSITY OF
FLORIDA

UFL/COEL-84/004

COASTAL ENGINEERING INVESTIGATION AT JUPITER INLET, FLORIDA

by

William T. Buckingham

March 1984

Submitted to:

Jupiter Inlet District
and
Palm Beach County

REPORT DOCUMENTATION PAGE

1. Report No.	2.	3. Recipient's Accession No.

4. Title and Subtitle	5. Report Date
COASTAL ENGINEERING INVESTIGATION AT JUPITER INLET, FLORIDA	March, 1984
	6.

7. Author(s)	8. Performing Organization Report No.
William T. Buckingham	UFL/COEL-84/004

9. Performing Organization Name and Address	10. Project/Task/Work Unit No.
Coastal and Oceanographic Engineering Department University of Florida 336 Weil Hall Gainesville, FL 32611	11. Contract or Grant No. R-82-878

12. Sponsoring Organization Name and Address	13. Type of Report
Jupiter Inlet District Jupiter, FL and Palm Beach County Palm Beach, FL	Technical
	14.

15. Supplementary Notes

16. Abstract

A fixed-bed hydraulic model of Jupiter Inlet, Florida, was constructed for the purpose of testing measures designed to remedy problems of sediment erosion and deposition in the inlet area. Both tide-induced flows as well as waves were simulated in the model which was built on an undistorted scale of 1:49. Model verification was based on prototype measurements of waves, tides and currents. Results have been interpreted in terms of the influence of various proposed remedial schemes on flow velocity magnitude, distribution and wave height at various locations within the study area. A stability parameter has been utilized for evaluating the degree of sediment erosion or deposition at a given location.

Various structural solutions were examined in the model. It is proposed that, in the initial phase of solution implementation, sediment removal/nourishment methods be used primarily to mitigate the existing problems. New structures, as per model test results, should be installed under subsequent phases, only if sediment management procedures do not prove to be adequate. The currently followed procedure of periodic sand trap dredging may be extended to include the new dredging/nourishment requirements.

17. Originator's Key Words		18. Availability Statement
Erosion	Sediment Management	
Hydraulic Model	Sedimentation	
Inlet Hydraulics	Tidal Entrance	
Physical Model	Tidal Inlet	

19. U. S. Security Classif. of the Report	20. U. S. Security Classif. of This Page	21. No. of Pages	22. Price
Unclassified	Unclassified	245	

FOREWORD

The investigation reported here was conducted by Mr. William T. Buckingham under the supervision of Drs. A. J. Mehta, H. Wang and R. G. Dean of the Coastal and Oceanographic Engineering Department. Contents of this report have also been published separately under the title, "Physical Modeling of a Tidal Inlet," by Mr. William T. Buckingham, as a Master of Engineering Thesis, University of Florida, 1984.

The investigation was supported by the Jupiter Inlet District and the County of Palm Beach. Considerable technical assistance was in addition provided by Robert Owen & Associates, Inc., of West Palm Beach. This support and assistance are sincerely acknowledged.

ABSTRACT

A fixed-bed hydraulic model of Jupiter Inlet, Florida, was constructed for the purpose of testing measures designed to remedy problems of sediment erosion and deposition in the inlet area. Both tide-induced flows as well as waves were simulated in the model which was built on an undistorted scale of 1:49. Model verification was based on prototype measurements of waves, tides and currents. Results have been interpreted in terms of the influence of various proposed remedial schemes on flow velocity magnitude, distribution and wave height at various locations within the study area. A stability parameter has been utilized for evaluating the degree of sediment erosion or deposition at a given location.

Various structural solutions were examined in the model. It is proposed that, in the initial phase of solution implementation, sediment removal/nourishment methods be used primarily to mitigate the existing problems. New structures, as per model test results, should be installed under subsequent phases, only if sediment management procedures do not prove to be adequate. The currently followed procedure of periodic sand trap dredging may be extended to include the new dredging/nourishment requirements.

TABLE OF CONTENTS

LIST OF TABLES

LIST OF FIGURES

CHAPTER I

INTRODUCTION

1.1 Introductory Note

Jupiter Inlet is located in northern Palm Beach County on the southeast coast of Florida, about 28 km south of St. Lucie Inlet and 21 km north of Lake Worth Inlet (Figs. 1.1 and 1.2). It is a natural waterway connecting the Atlantic Ocean with the Loxachatchee River. Along both banks of the inlet, erosion and sedimentation problems have become a matter of concern in recent years. An investigation to examine these problems and to recommend appropriate remedial measures was conducted. This investigation is described here.

Although Jupiter Inlet is relatively small, it is important for its aesthetic and recreational values, its value as a prime residential development, and because it is the primary waterway connecting the Loxahatchee River Estuary to the Atlantic Ocean. The physical and biological characteristics of the inlet are typical of other such waterways in the general geographic location; the bottom consists primarily of sand interspersed with sea grasses and occasional oyster beds, and the shoreline vegetation consists mainly of pine, scrub oak and mangrove. The inlet covers approximately 50 hectares that are circumscribed by 8 km of shoreline. The average volume of water present in the inlet at any one time is approximately 1 million cubic meters (McPherson et al., 1982).

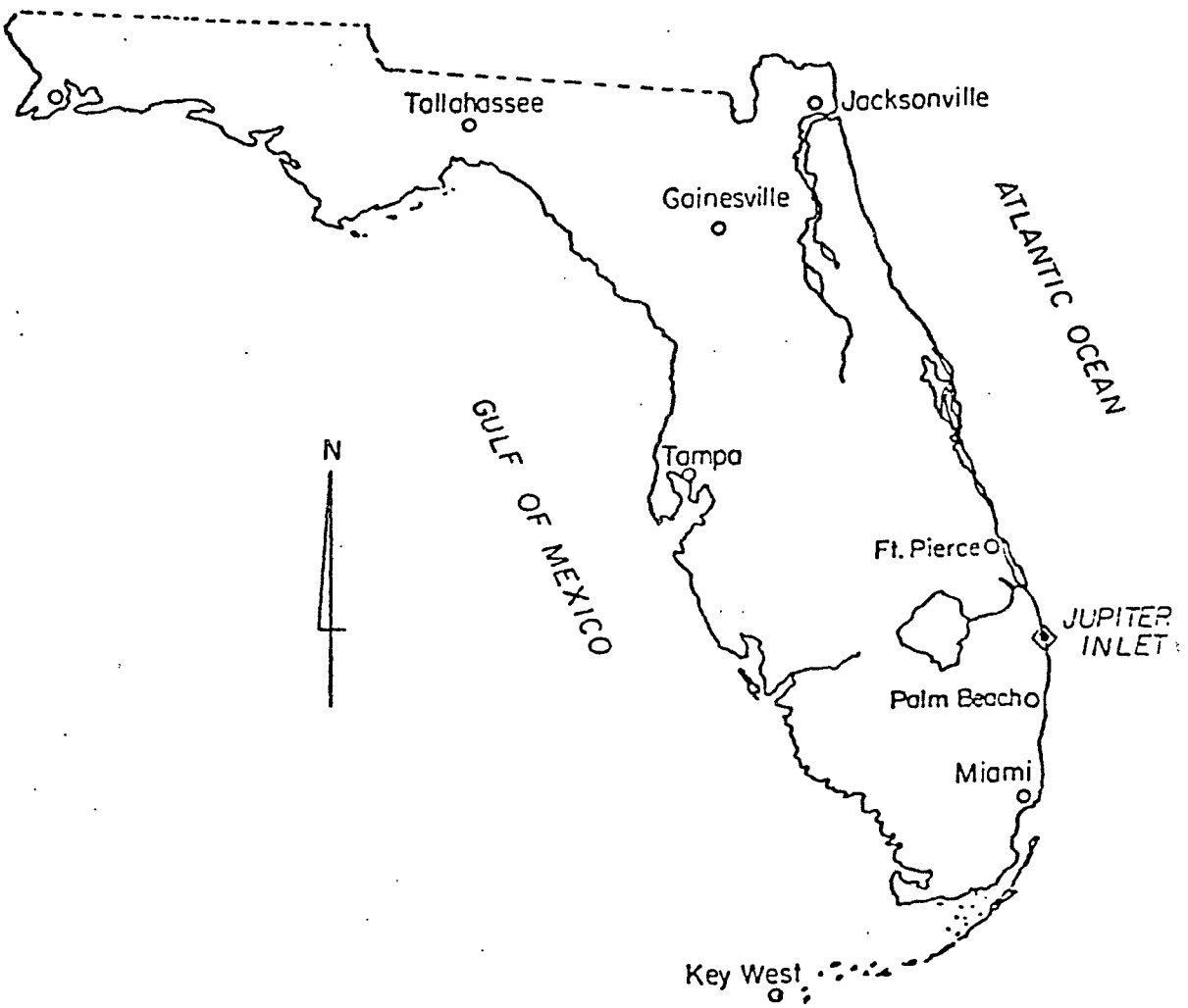

Fig. 1.1. Location Map of Jupiter Inlet.

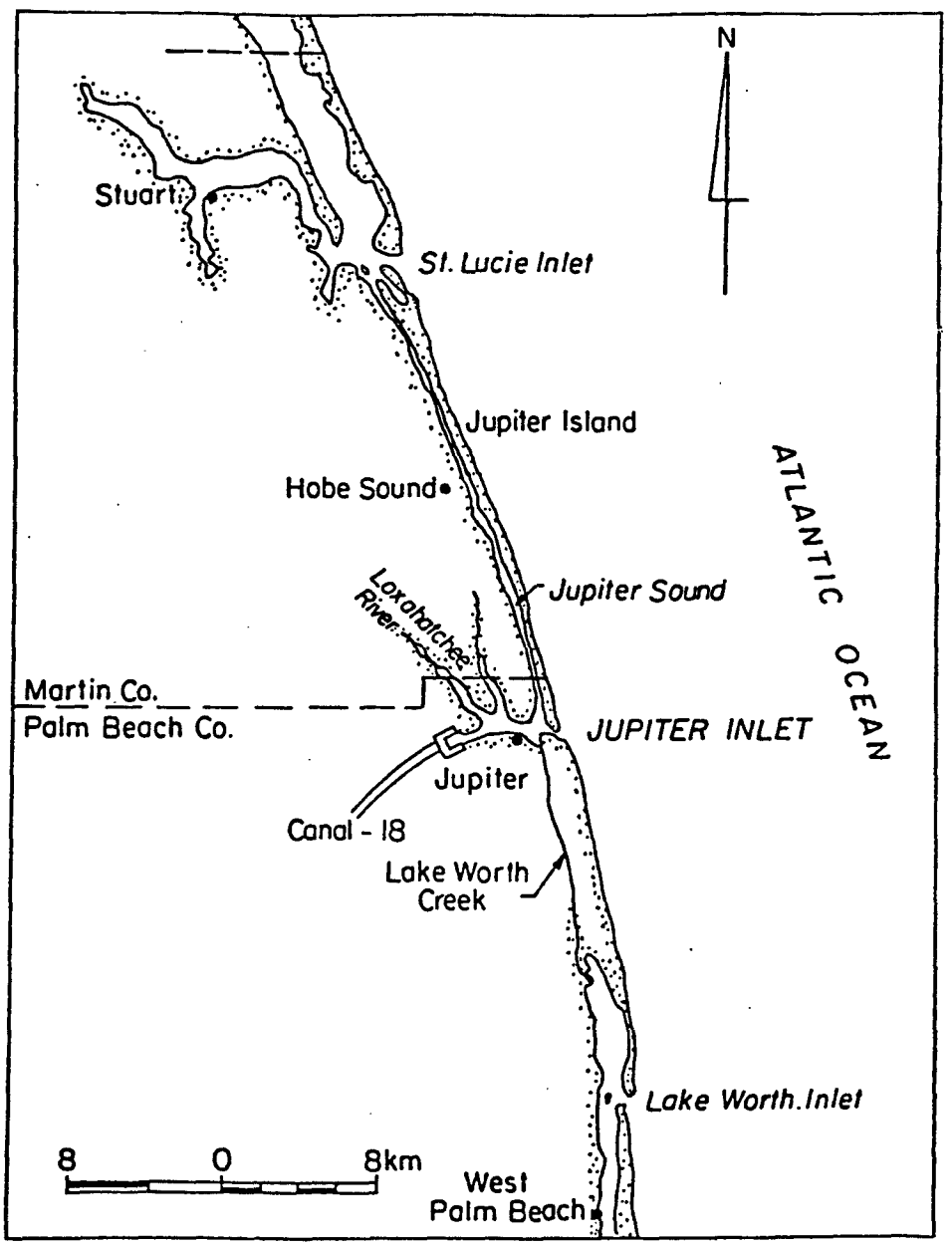

Fig. 1.2. Area Map of Jupiter Inlet.

1.2 Inlet History

Jupiter Inlet has existed as a natural waterway for at least 300 years according to historical records (McPherson, et al., 1982). The first such record, consisting of explorers charts, indicates the presence of the inlet in the year 1671. Originally, the inlet served as the only outlet for the Loxahatchee River, Lake Worth Creek and Jupiter Sound (Fig. 1.2), and as one of several outlets for the St. Lucie and Indian Rivers. The resulting discharge from these sources was of sufficient magnitude to prevent closure of the inlet except in events of severe storm action that sometimes resulted in temporary closure. The creation of St Lucie Inlet in 1892, the Intracoastal Waterway between Jupiter Sound and Lake Worth Creek in 1896 and Lake Worth Inlet in 1918 resulted in a diversion of much of the flow through Jupiter Inlet. As a result of this loss of flow through the inlet, the frequency and duration of inlet closure greatly increased until 1947 when a regular inlet maintenance schedule, primarily consisting of dredging, was initiated by the Jupiter Inlet District (Escoffier and Walton, 1979). This schedule of periodic dredging has since prevented closure of the inlet and has maintained it in a navigable state. However, there are other inherent problems that have yet to be solved.

1.3 Problems of Present Concern

As is the case with any coastal inlet exposed to littoral drift from one predominant direction, Jupiter Inlet is beset by, 1) navigational difficulties due to hazardous wave and current action as well as shoaling near the mouth of the inlet, and 2) beach erosion downdrift (south) of the inlet. In addition, erosion of the shoreline, including that which has been armored by bulkheads as well as that in

its natural state, has taken place at a noticeable rate along the inner banks of the inlet. Figures 1.3 and 1.4 show examples of this erosion. Problems of shoaling well inland of the inlet mouth have occurred along the northern bend of the Intracoastal Waterway, in the public marina located on the south shore of the inlet and in the Dubois Park Lagoon. A hydraulic sand bypassing scheme has been satisfactorily maintaining a navigable channel through the mouth and mitigating erosion downdrift of the inlet; this study focuses on the problems of erosion and sedimentation along the shoreline within the inlet. Figure 1.5 shows the locations of these problem areas.

Sites marked A through I are of particular concern. Along the north shore (A, B and C) the overall problem is one of erosion. The entire reach (with the exception of the northernmost portion of site C) is bulkheaded to protect valuable residential property in the Jupiter Inlet Colony. At site A there appears to be some problem in retaining sand in front of the bulkhead to act as a buffer against wave attack and currents. This area has been used as a recreational beach cum partially sheltered cove (formed between the beach and the rocks forming the western extension of the north jetty) by people using the clubhouse nearby. Elsewhere along this reach, various segments of the bulkhead (erected by the property owners) are in different states of repair. While some segments appear relatively undamaged, in other areas cracks have occurred and subsidence has become a problem. In some cases segments of the outer protective sheeting have collapsed thus exposing the piles and inner sheeting. At site B and adjacent reaches, waves and strong currents are believed to be the cause of the damage. Sand at the bulkhead toe has eroded away except in pockets where it offers

Fig. 1.3. Example of Shoreline Erosion at the Inlet.

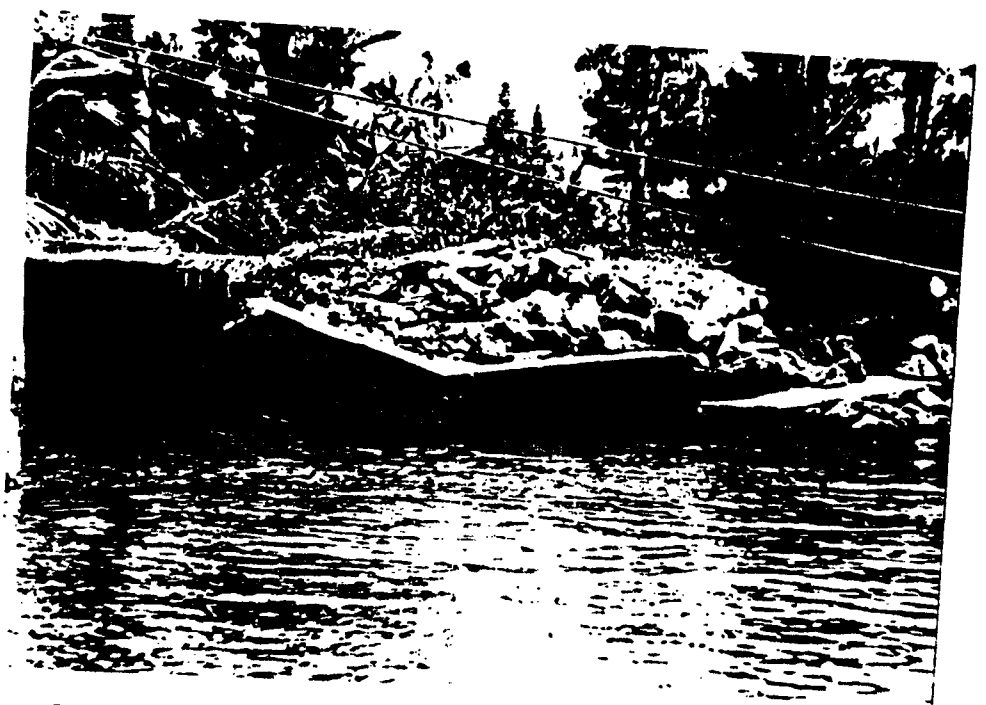

Fig. 1.4. Example of Bulkhead Failure at the Inlet.

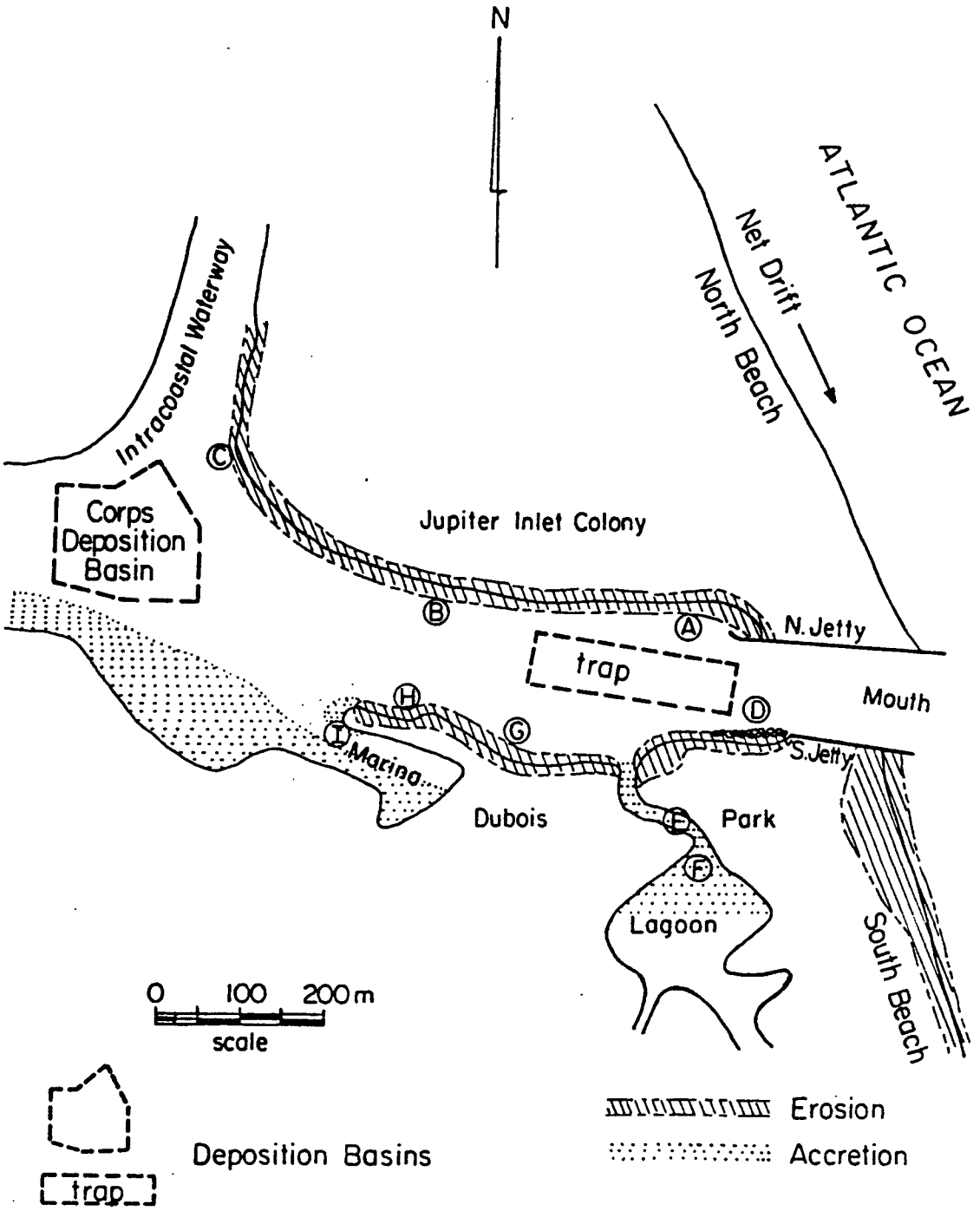

Fig. 1.5. Problem Areas of Erosion and Accretion.

protection against direct wave and current attack. At site C and adjacent reaches bulkhead damage and shoreline erosion is believed to be due to currents and boat wakes (resulting from traffic through the Intracoastal Waterway). Wave activity is observed to be lower here.

Location D corresponds to the shoreline behind rocks which form the western extension of the south jetty. Here, the sand has eroded away leaving an erosion scarp. Some Australian pines have fallen as a result. This area is heavily utilized as it is a part of the Dubois Park. The lagoonal channel (site E) and a portion of the lagoon itself (site F) have experienced shoaling due to sand deposition. The lagoon serves as a drainage basin for a rather extensive watershed. The channel is the only draining outlet for the lagoon into the inlet. Furthermore, tidal exchange between the inlet and lagoonal waters is essential for flushing and water renewal. Small boats use the channel at high tide to commute between the inlet and upstream residential areas. The topography and vegetation of the area have been conducive to the use of the channel area for picnics and other recreational activity. It is essential to maintain the channel and minimize shoaling there or in the adjacent waters.

At site G a public beach has been created by providing two short groin-like structures with a sandy beach in between. The beach consists of a curved shoreline stabilized by concrete on which sand has been deposited. In recent years there has been a depletion of the sand here. It is believed that wave and current attack is responsible for this problem. The problem is compounded by the concrete which causes significant reflections of the wave energy and enhanced scour. The shoreline west of the beach (G) has as well been stabilized by rocks and

concrete. There is, however, concern that continued wave and current attack might penetrate these defenses and erode the land. At site H the promontory between the marina and the inlet is rather narrow. It serves as a parking lot and picnic area and its erosion must be prevented. At site I, the problem is one of deposition (near the tip of the promontory). This has reduced docking space in the marina along its north bank. Two or three docks are now useless as the bottom is exposed at low tide. Furthermore, deposition is beginning to constrict the channel for boat access. The specific causes of and solutions to these problems are the main focus of this study and are addressed individually in Chapters III and V but are presented briefly as follows.

It is apparent that the causative forces for sand transport and attack on structures in the inlet area are contingent upon tide-induced currents and waves. The latter include approaching swells from the ocean as well as boat wake-induced waves. With respect to sand transport, waves primarily provide a mechanism for resuspension while currents can resuspend and also transport sediment. The relative magnitude of the influences of currents and waves differ in different locations. There are regions of strong main or primary currents and also regions of secondary cells or eddies where the strength is typically much lower. Waves from the ocean generally penetrate in a manner such that the wave crest is more or less normal to the jetties. However once inside, their direction is altered due to refraction resulting from depth changes, as well as due to diffraction. Refraction causes the crests to bend both towards the north as well as the south shorelines in a manner such that the shorelines become exposed to a relatively direct attack as waves break on the shore. Such a phenomenon

at inlet channels is not uncommon (COEL, 1970). Additional effects come from diffraction which produces a fairly complex wave field within the confines of the channel.

At site A, the importance of refracted and diffracted waves and eddy currents as causative forces of erosion are in that order. At site B it is currents and refracted waves. Main currents and boat wakes are the causative forces of erosion at site C. At site D, it is currents that exist during very high tides. At sites E and F the problem is not of currents or waves but of sand input from erosion at site D during very high tides. Refracted waves and eddy currents cause the erosion at site G. Main currents and refracted waves result in the erosion at site H while the deposition at site I is due to sediment transport due to currents.

Solutions to these problems must therefore, 1) reduce current strength and/or wave activity in areas of erosion, 2) supply sand in the same areas and 3) reduce the sand supply in areas of shoaling. The major ongoing activity of relevance is the periodic dredging of the sand trap and the Corps of Engineers dredging basin (every 2-4 years on the average) and the placement of the spoil downdrift of the inlet. This activity has been beneficial in that it controls downdrift erosion and keeps the inlet channel as well as the Intracoastal Waterway in a navigable state. It is evident therefore that any proposed solutions for the problems of erosion and shoaling must be viewed in conjunction with the dredging and spoil deposition routine which must continue as such.

1.4 Purpose and Scope of the Study

The purpose of this study was to formulate and recommend a remedial scheme that would mitigate the problems of erosion and sedimentation at Jupiter Inlet. Specifically, this scheme must consist of measures, either structural or non-structural, that would: 1) eliminate or at least substantially decrease erosion along the shoreline inland of the inlet mouth and 2) minimize shoaling at specified problem areas within the study area. The study consisted of, 1) field work in which prototype data were collected and on-site inspections and observations were made, 2) data analysis for evaluating the hydraulic and sedimentary characteristics of the inlet, and 3) a physical model in which solution options were tested.

1.5 Previous Studies

Very few previous studies can be found that have attempted to address all of the problems associated with the maintenance of Jupiter Inlet. Specifically, over the period in which this study was conducted, no previous investigations related to the shoaling and erosion problems inland of the inlet mouth were found. The primary issue addressed in previous studies of the inlet area has been the problems associated with beach erosion of Jupiter Island and shoaling in the immediate area of the inlet mouth.

The U.S. Army Corps of Engineers published a survey of the inlet in 1966 proposing federal maintenance of the inlet channel as a connection between the Intracoastal Waterway and the ocean together with a weir-jetty at the north side of the inlet for transferring littoral drift across the inlet. This proposal was not approved; channel maintenance remained the responsibility of the Jupiter Inlet District and the north jetty remained unchanged (Corps of Engineers, 1966).

The University of Florida Department of Coastal and Oceanographic Engineering conducted a study of the inlet during the period 1967-1969 (COEL, 1969). This study was a combination of field, model, and office investigations and again focused primarily on the problems of inlet shoaling and erosion of the south beach. The conclusions reached in this report consisted of recommendations to: 1) increase the lengths of both the north and south jetties, 2) construct a weir section at the north jetty that would direct littoral drift into an adjoining sand trap, and 3) enlarge the overall sand trap volume near the mouth.

With the exception of studies documenting the bypassing of sand from the sand trap to the south beach and periodic maintenance dredging of the Intracoastal Waterway by the Corps of Engineers, there are believed to be no published reports regarding recommended maintenance procedures for the inlet since 1970.

1.6 Selected Methodology

Physical modeling is a recognized method for providing accurate predictions of the performance of a particular design project. The fact that such a model is a scaled-down version of its prototype allows for accurate reproduction of the geometric, kinematic and dynamic characteristics of the prototype. In addition, physical modeling allows identification of problem areas and features that may not be of initial concern in the prototype and which may have otherwise been overlooked. The primary drawbacks are the costs and time of construction and maintenance as well as considerable set-up time between the testing of different situations in the model.

The type of model employed for this investigation was an undistorted, fixed-bed model of the study area. An undistorted model

maintains the same scale ratio in both the vertical and horizontal dimensions. Fixed-bed indicates that the prototype sediment transport phenomena are not reproduced in the model. This combination of a fixed bed and no distortion enables the simulation of tides, waves and currents (the three primary components causing sediment transport in the inlet) simultaneously with the necessary degree of overall accuracy (Sager and Hales, 1976). While the actual sediment transport phenomena were not modeled, the hydraulic forces which cause these phenomena were simulated. This resulted in an understanding of the causes of the problems at the inlet, rather than a mere reproduction of these problems. The model served as the means by which remedial measures were tested so as to predict their effectiveness and to expose any detrimental side-effects that they may have caused. A more detailed discussion of the physical model is presented in Chapter IV.

The three main phases of the study are presented as follows: Chapters II and III discuss the data collection and analysis phase, Chapter IV describes the model construction phase, and Chapters V and VI present potential solutions developed for the inlet and the testing of these solutions. Chapter VII presents a summary of the study and the resulting recommendations. Nine appendices have been included. Appendix A presents a procedure by which flow velocities corresponding to a storm surge were calculated. Appendix B describes the depth-correction factor applied to velocity profile measurements. Appendix C presents dimensionless transverse velocity profiles obtained at four cross-sections in the inlet and an interpretation of these profiles. Appendix D describes the procedure by which friction slopes and bed roughness calculations were carried out for each of the four

cross-sections. Appendix E provides an example of and the overall results from the calculations of the refraction of the predominant deep water wave directions offshore of the inlet into shallow water. Appendix F includes a map of the inlet bathymetry from which the model was constructed. Appendix G presents the theory behind and practical application of the "snake-type" wave generator that was used to produce the directional waves determined in Appendix E. Appendix H describes the procedure by which the weirs used in the model to simulate tidal conditions were calibrated. Appendix I presents a discussion of the theory behind and calculations made in determining the number and location of roughness elements in a physical model. Finally, in Appendix J, test results representing measurements and the stability parameter are reported.

CHAPTER II

FIELD INVESTIGATION

2.1 Overview

Data collection was carried out over a six month period from September 1982 through February 1983. Tidal records were obtained and velocity profiles, sediment samples, hydrographic surveys and drogue and dye studies were carried out over the study area as defined by the following boundaries: from the seaward limit of the study area corresponding to a distance 1050 m offshore (ten inlet widths) to the north and west limits as defined by the Intracoastal Waterway, and along the southern limit of the study area as determined by the south shore of the inlet including the lagoon extending into the Dubois Park area. These boundaries are shown in Fig. 2.1. The following paragraphs describe the methods employed for data collection.

2.2 Hydrographic Surveys

Hydrographic survey information on the inlet was obtained from various sources. This information included surveys of the bathymetry seaward of the mouth as well as surveys of the entire inlet study area up to + 1.5 m elevation; with the exception of the northwest shore area and the southshore marina area which were surveyed during the field study. Comparative historical surveys were also available which show beach erosion over the past 100 years near the inlet as well as relative erosion and accretion levels offshore in the last 30 years. An interpretation of these data are provided in Figs. 2.2 and 2.3. In

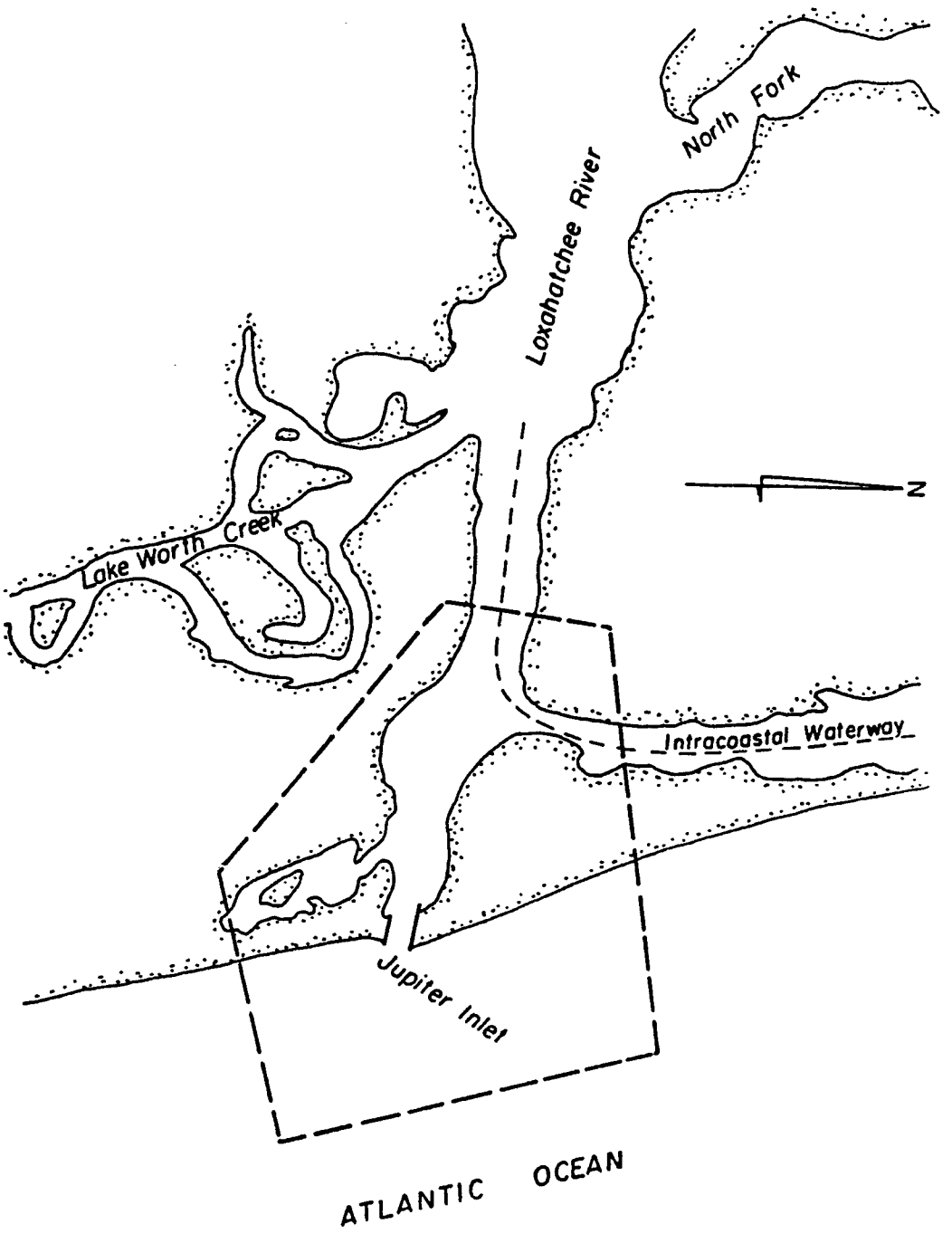

Fig. 2.1. Boundaries of the Inlet Study Area.

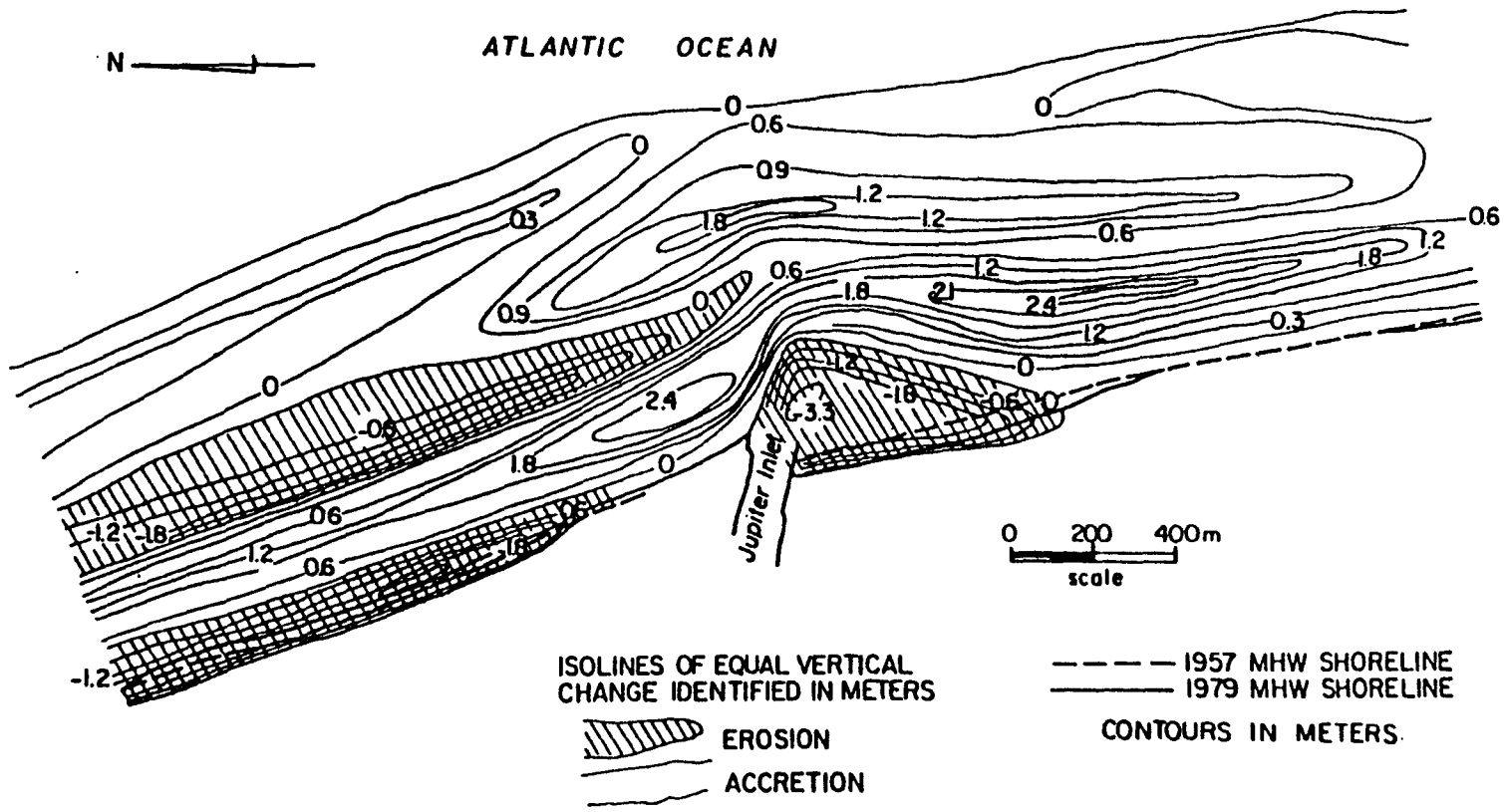

Fig. 2.2. Areas of Relative Erosion and Accretion between 1957 and 1979.

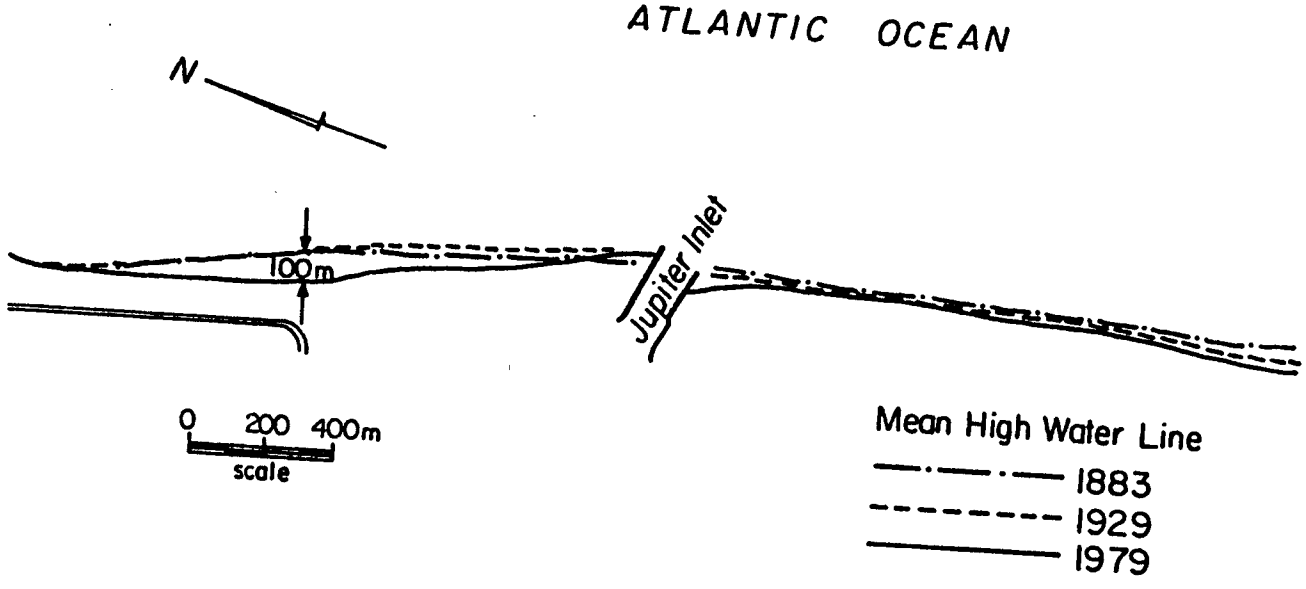

Fig. 2.3. Mean High Waterline Changes near Jupiter Inlet between 1883 and 1979.

addition, surveys were performed at cross-sections where velocity profiles were taken (see Fig. 2.4) so as to provide accurate measurement of the areas and depths at these cross-sections. Survey data were available for the Intracoastal Waterway portion within the study area.

2.3 Water Surface Elevations

Variations of water surface elevations due to tides were obtained by employing Stevens Type F gages at seven locations in the inlet. These gages were leveled with reference to the 1929 NGVD and were adjusted to provide continuous records over periods of eight days. Every eighth day, the gages were reset and outfitted with new chart paper. This procedure was continued over the six month data collection period. A few problems, mainly due to equipment failure or otherwise, were encountered. Tide gages were placed at each of the extreme boundaries of the inlet as well as at locations near the problem areas of erosion and deposition. Figure 2.4 shows the locations.

Gage T-1: This gage was located at the west end of the south jetty cap defining the entrance to the inlet and the eastern boundary of the study area.

Gage T-2A: This gage was located on a private dock on the north bank of the inlet, corresponding to an area of erosion.

Gage T-2B: This gage was located on a dock in the marina located in the southwest basin of the inlet, corresponding to an area subject to shoaling.

Gage T-2C: This gage was located on a private dock situated on the northeast bend where the inlet meets the northern reach of the Intracoastal Waterway. This area also corresponds to one of erosion.

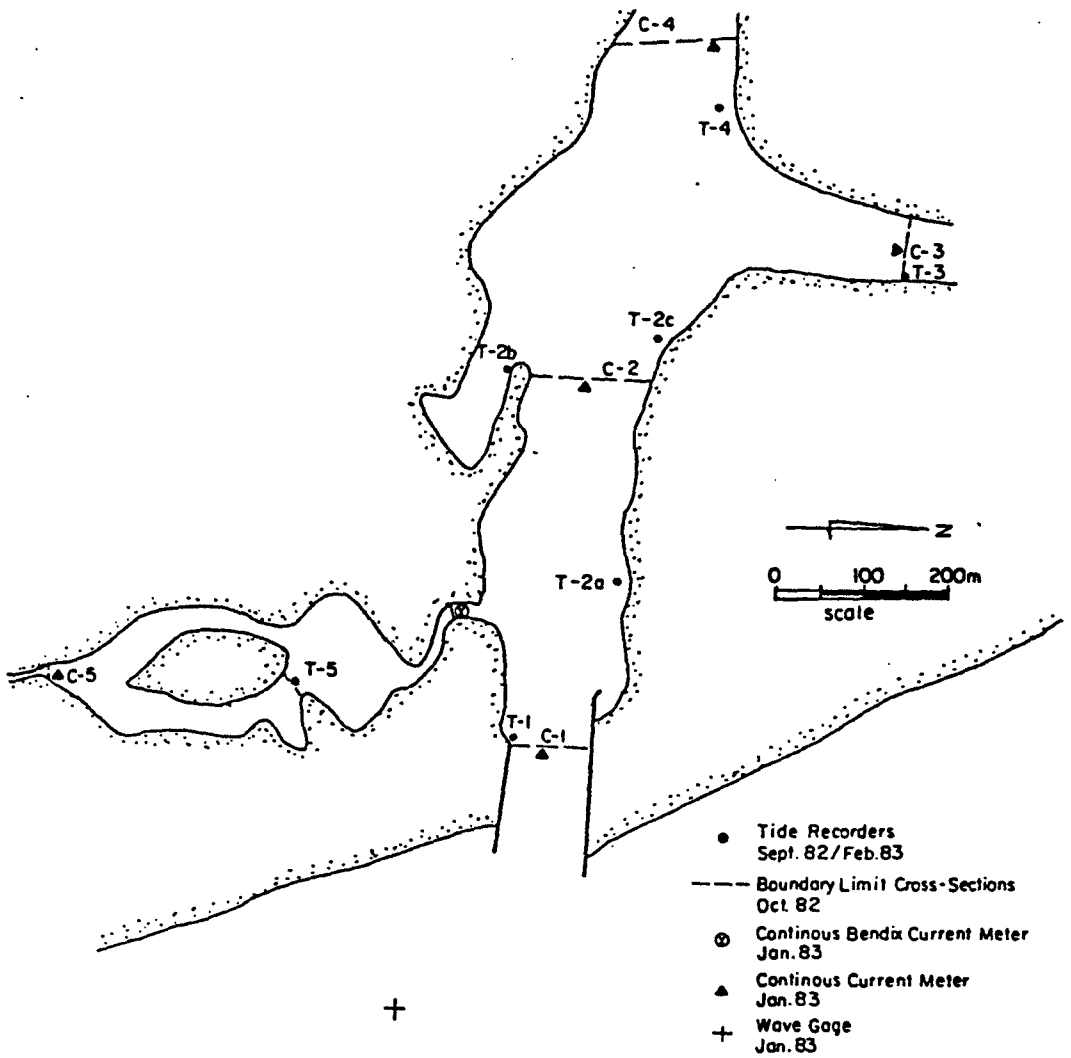

Fig. 2.4. Locations and Dates of Operation of Tide Recorders, Current Meters and Wave Gage.

Gage T-3: This gage was also located on a private dock, situated on the east bank of the northern reach of the Intracoastal Waterway. This location corresponds to the northernmost boundary of the study area.

Gage T-4: This gage was located on a dock owned by the U.S. Coast Guard situated at the west end of the north bank of the inlet and corresponding to the westernmost boundary of the study area.

Gage T-5: This gage was located on a walkway overpassing the lagoon immediately southwest of the inlet entrance and extending into the Dubois Park area. This location represents the southernmost boundary of the study area.

An example of a tidal record is shown in Fig. 2.5.

2.4 Extreme High Water Levels

High winds and relatively large atmospheric pressure gradients associated with tropical storms and hurricanes can cause water levels in the ocean as well as inside an inlet to be much higher than the astronomical levels predicted by the National Ocean Survey Tide Tables. This phenomenon is referred to as storm surge and may result in the flooding of land areas near the ocean or an inlet. Such flooding is especially severe if conditions conducive to storm surge occur during a spring tide.

According to Bruun et al. (1962), for the coastal regions of North Palm Beach County the return period for various levels of storm surge greater than or equal to the level indicated is predicted as follows:

1.25 m or higher above MSL	6 - 7 years
1.5 m or higher above MSL	12 - 14 years
2.0 m or higher above MSL	20 - 22 years

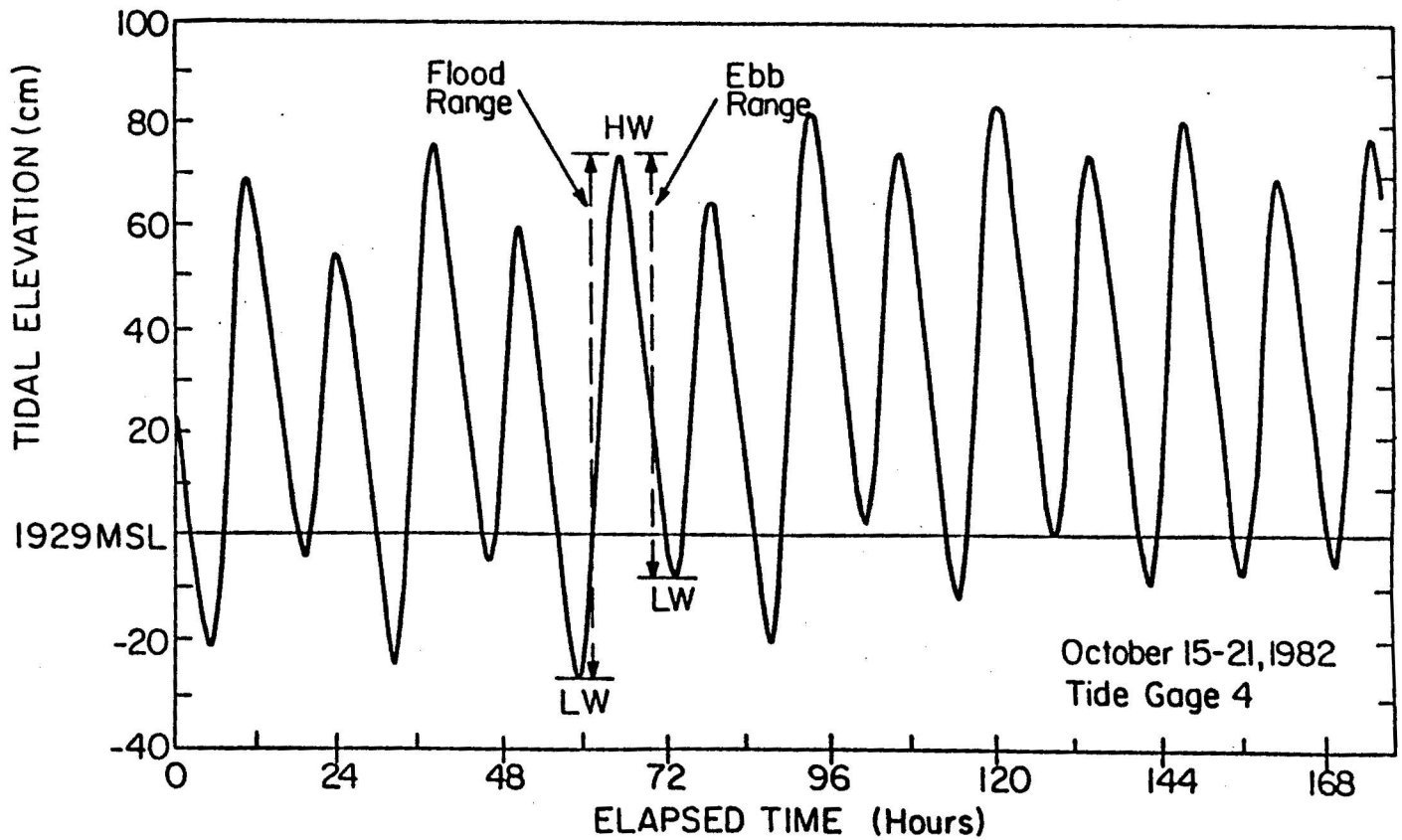

Fig. 2.5. A Sample Tide Record for Lighthouse Crossing C-4. HW = High Water; LW = Low Water.

2.5 m or higher above MSL	34 - 36 years
3.0 m or higher above MSL	58 - 60 years
3.5 m or higher above MSL	100 years

2.5 Flow Cross-Sections and Current Profiles

Five locations were chosen for cross-sectional current velocity and discharge measurements. These locations are indicated in Fig. 2.4. The selection of four of these locations was based on the location of the study area boundaries. The fifth cross-section (C-2) was chosen so that in the event of measurement failure or error at C-1, C-2 could serve as the control volume (between C-2, C-3, and C-4) boundary for the study area. Each of the five locations corresponds to the positioning of a tide gage.

Hydrographic surveys were obtained in detail at the cross-sections with exception of C-5. The profile of cross-section C-5 consisted of a rectangular culvert and was easily determined. The resulting profiles and calculated areas are shown in Fig. 2.6.

2.5.1 Instantaneous Velocity Profiles

Vertical velocity profiles were obtained at representative points across each of the cross-sections with the exception of C-5. The measurements were obtained from a boat (the position of which was held constant by a surveying crew) using an (model number 19089) Ott meter. Measurements were made at every 0.5 m of depth at four locations along each cross-section. Figures 2.7 and 2.8 illustrate the procedure used in obtaining the velocity profiles. As expected, the strongest currents were recorded at the mouth (C-1) where velocities approaching 2.2 meters per second were obtained; the lowest values were recorded in the Intracoastal Waterway (C-3) where the flow was visibly much slower.

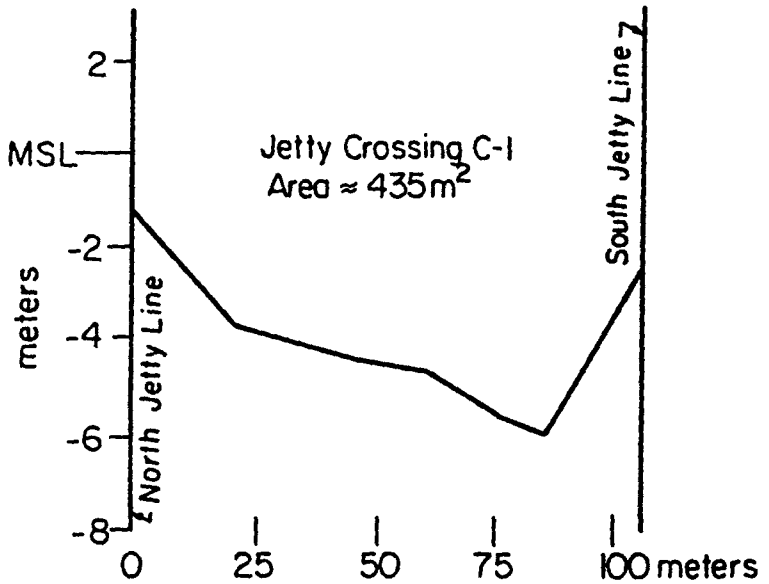

Fig. 2.6a. Profile of Jetty Crossing C-1. MSL Refers to NGVD.

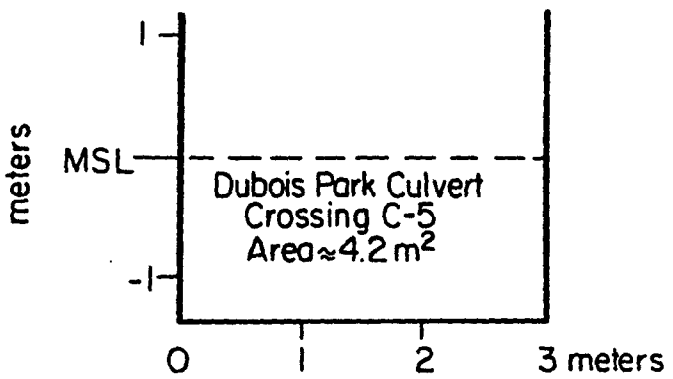

Fig. 2.6b. Profile of Culvert Crossing C-5.

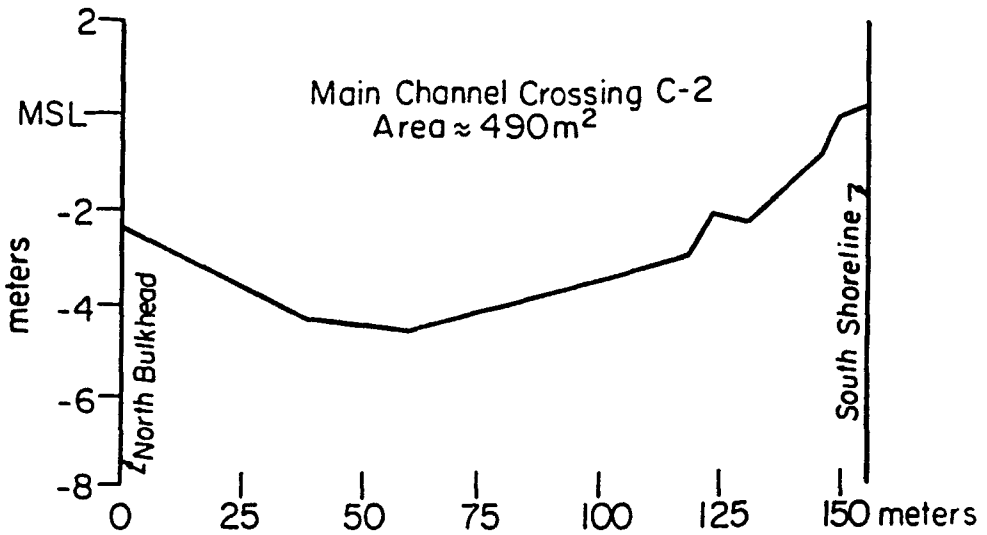

Fig. 2.6c. Profile of Main Channel Crossing C-2.

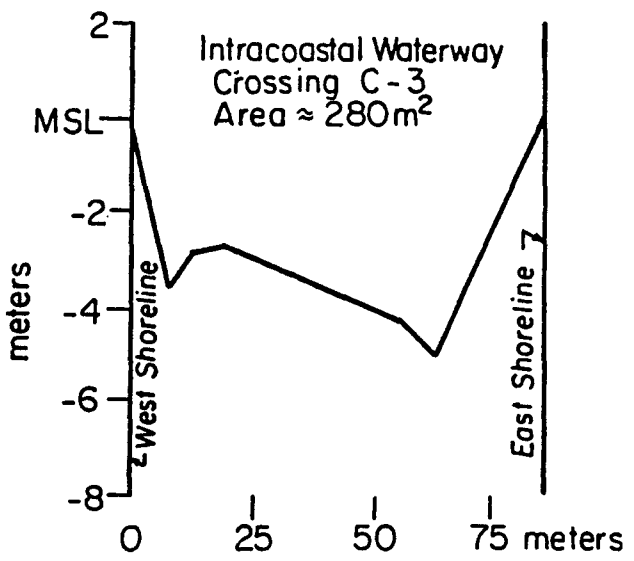

Fig. 2.6d. Profile of Intracoastal Waterway Crossing C-3.

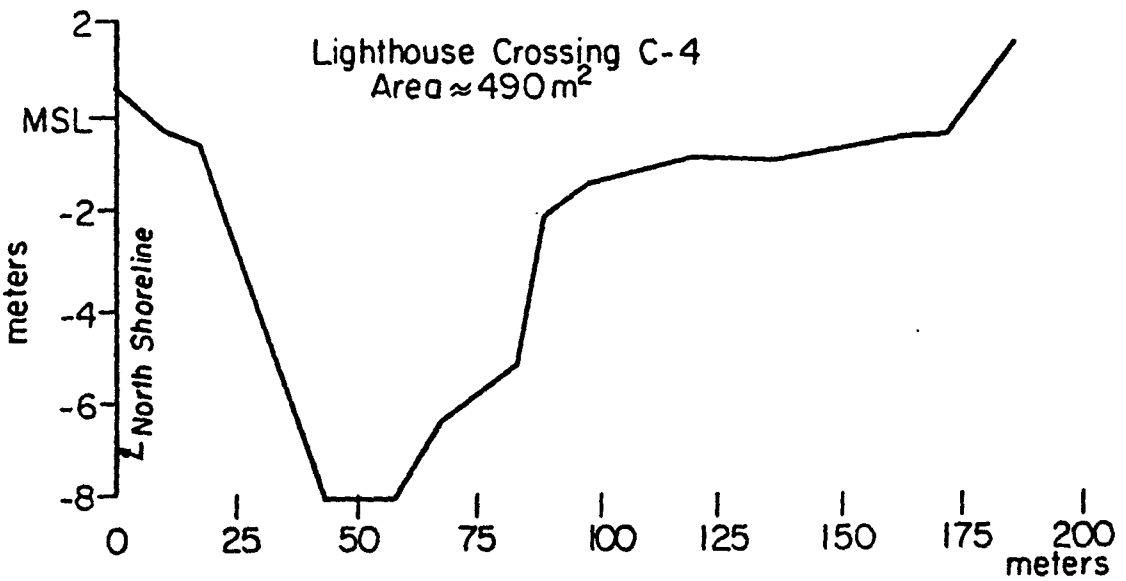

Fig. 2.6e. Profile of Lighthouse Crossing C-4.

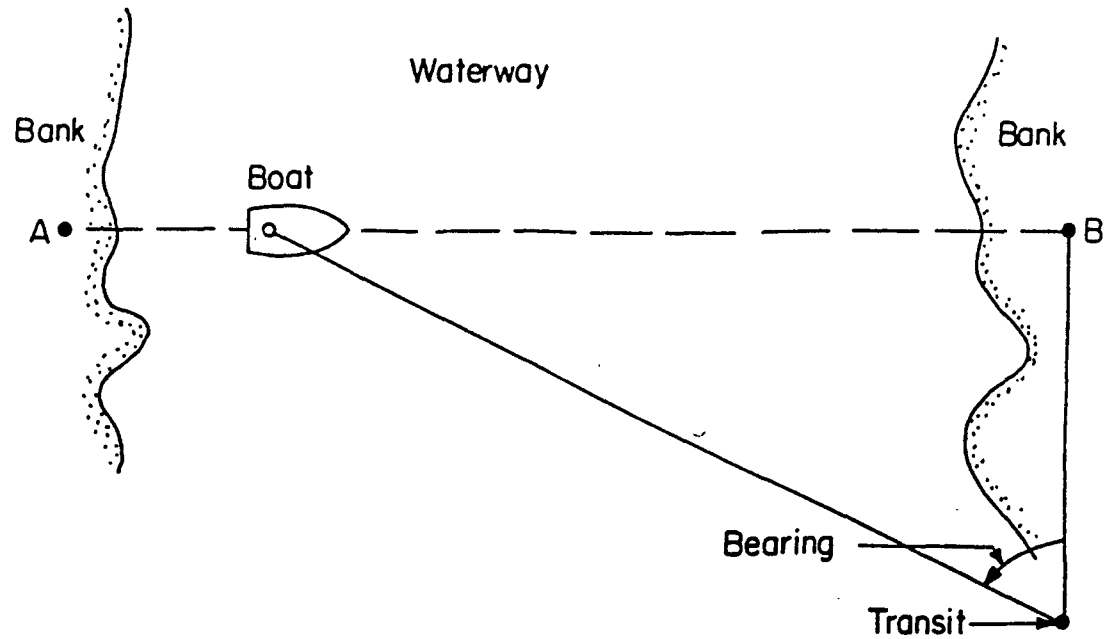

Fig. 2.7. Positioning Procedure for Obtaining Velocity Profiles (Hayter and Mehta, 1979).

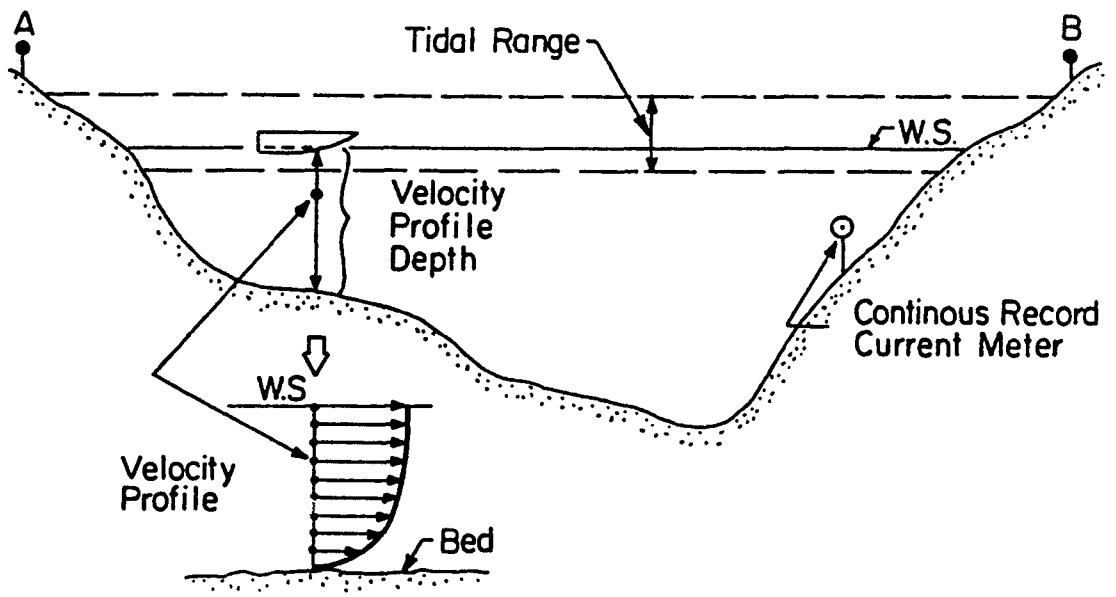

Fig. 2.8. Cross-Sectional View of Procedure for Obtaining Instantaneous Velocity Profiles and Continuous Velocity Record (Hayter and Mehta, 1979).

2.5.2 Continuous Velocity Measurements

In the last month of data collection, Marinco Inc. Type B-10 current meters were installed at all cross-sections with the exception of C-5 where a Bendix Q-16 current meter was installed. These meters provided a continuous current velocity record at a fixed position in each cross-section. These data, combined with those of the tidal cycle and geometry of each cross-section, were used to estimate the corresponding time-discharge records for each cross-section using a previously developed procedure (Hayter, 1979). The data collection was fairly continuous over time; some interruptions occurred when the meters became clogged with seaweed or fishing line and did not operate for a period of some hours. Figure 2.8 gives a schematic of the placement scheme for the continuous current meters, while Table 2.1 gives their specific locations at each cross-section.

Table 2.1. Current Meter Positions for Continuous Time-Velocity Measurements

Cross-Section No.	Horizontal (m)	Elevation* (m)
C-1	28 (from north jetty)	- 3.0
C-2	23 (from north bulkhead)	- 2.5
C-3	23 (from east shoreline)	- 1.0
C-4	19 (from north shoreline)	- 2.0
C-5	1.5 (center of culvert)	- 1.0

*Relative to 1929 MSL

2.6 Drogue Study

A drogue study was carried out on November 18, 1982 during a flood tide corresponding to a tidal elevation of +0.75 m at the inlet. The primary purpose of these studies was to determine the direction and magnitude of the flow as well as the locations of regions of high flow velocities. Figure 2.9 provides an example of the resulting plot of a drogue course over time. Three drogues were used consisting of 0.1 m thick styrofoam circles with directional anchors extended approximately one meter from the center by nylon rope (Fig. 2.10). Each drogue was a separate color so that they could be distinguished when tracking their separate paths. The drogues were launched from a boat at one minute intervals and were tracked by aerial photography.

2.7 Dye Studies

Dye studies were carried out over the same two day period during flood tides at the inlet. These studies served primarily to indicate: 1) mean flow directions in the channel, 2) regions along the banks where flow circulation occurs as a result of eddies driven by the flow in the main channel, and 3) relative degree of flow dispersion taking place at the surface. Figure 2.11 provides a chronological series of dye study observations as interpreted from aerial sketches and photographs. The dye Rhodamine B (red in color), was injected near the north jetty while Flourescein (a green dye), was injected at the south jetty.

2.8 Wave Information

A Viatran (absolute pressure transducer) wave measuring gage was placed approximately 800 meters offshore of the inlet at a depth of approximately 6 m. The gage recorded wave heights and periods for a seventeen minute interval once every hour over the period

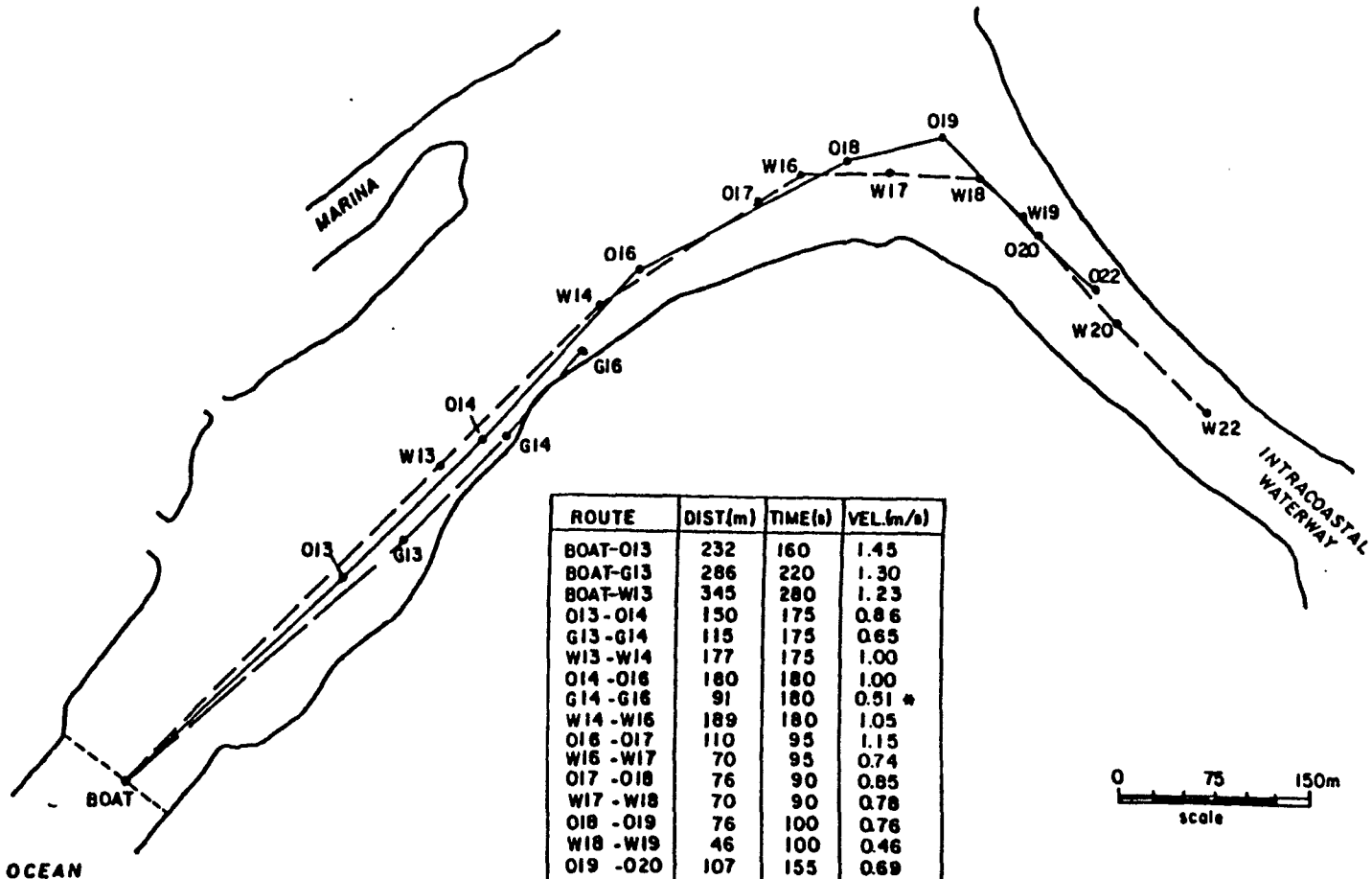

ROUTE	DIST(m)	TIME(s)	VEL.(m/s)
BOAT-013	232	160	1.45
BOAT-G13	286	220	1.30
BOAT-W13	345	280	1.23
013-014	150	175	0.86
G13-G14	115	175	0.65
W13-W14	177	175	1.00
014-016	180	180	1.00
G14-G16	91	180	0.51 *
W14-W16	189	180	1.05
016-017	110	95	1.15
W16-W17	70	95	0.74
017-018	76	90	0.85
W17-W18	70	90	0.78
018-019	76	100	0.76
W18-W19	46	100	0.46
019-020	107	155	0.69
W19-W20	110	155	0.71
020-022	61	310	0.20*
W20-W22	100	310	0.33*

* - DROGUE PICKED UP AT THIS POINT

Fig. 2.9. Plot of Drogue Course over Time.

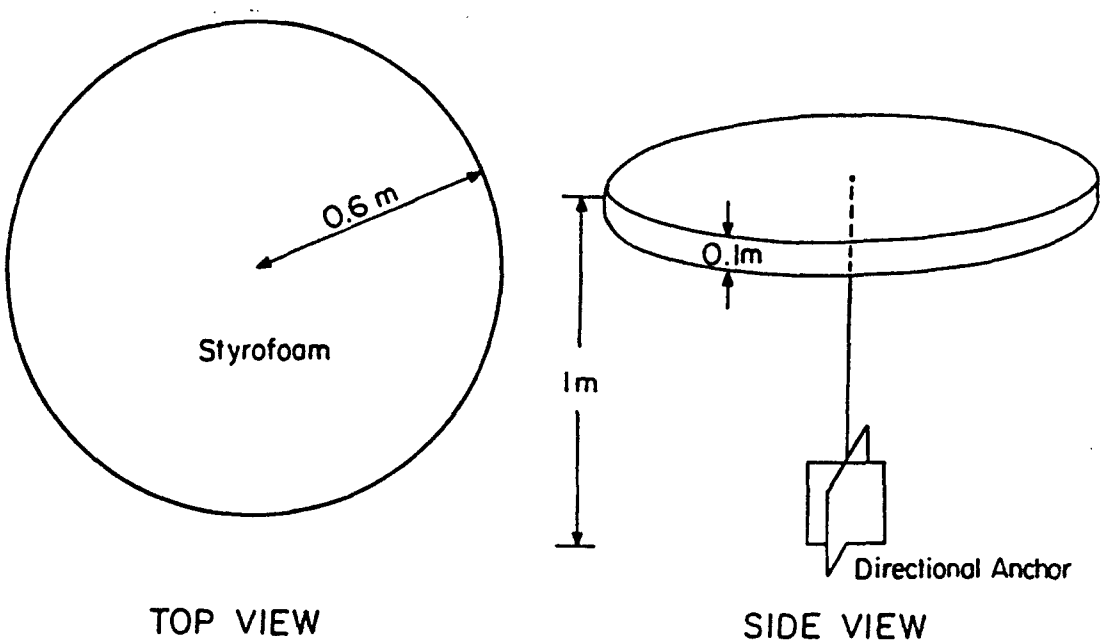

Fig. 2.10. Design of Drogue.

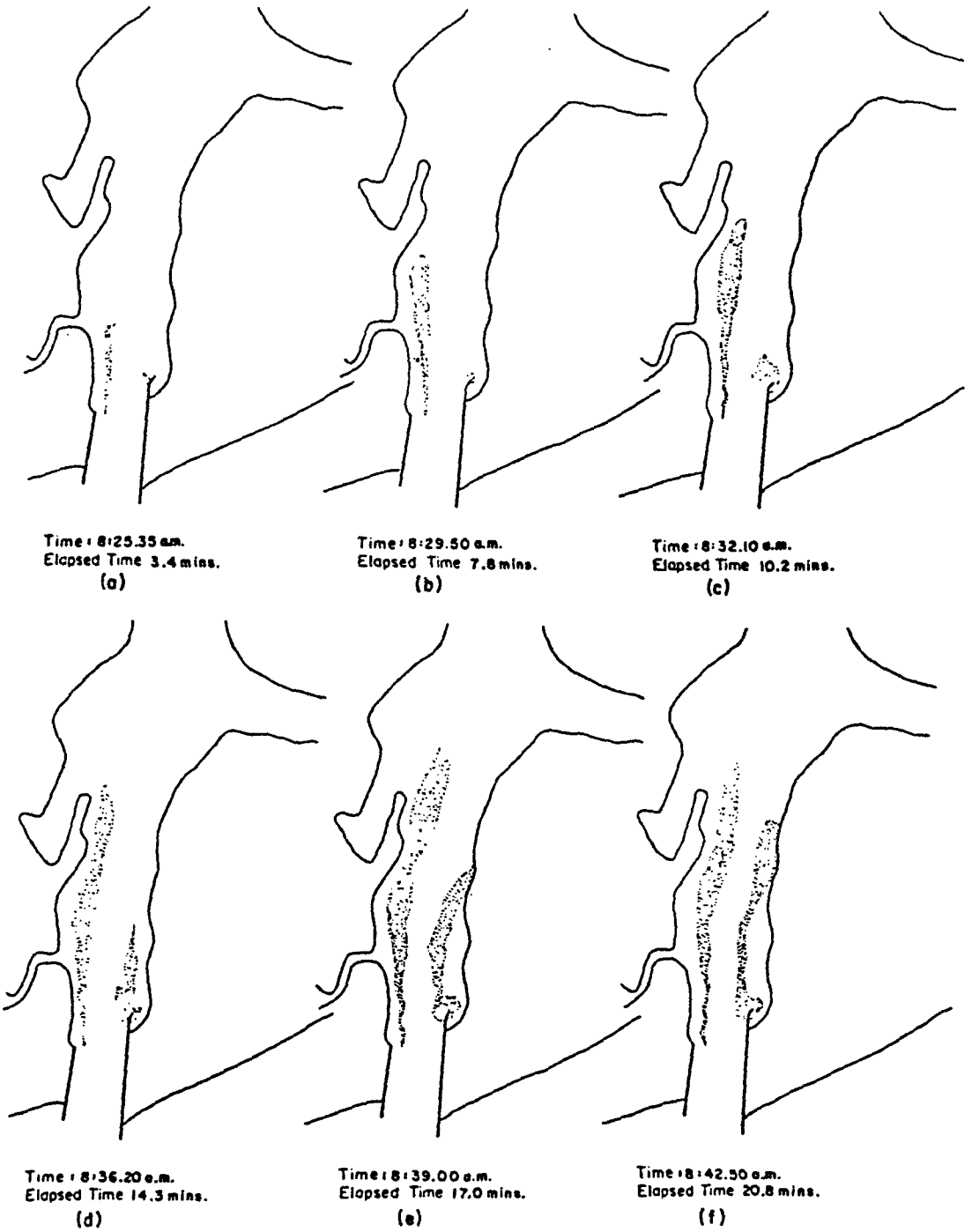

Fig. 2.11. Elapsed Time Plot of Dye Movement, Nov. 18, 1982.

January 27-30, 1983. In addition, data were obtained from a similar permanently installed wave gage (one of nine comprising the University of Florida Coastal Data Network) located offshore of West Palm Beach, Florida (20 km south of the inlet), in 10 meters of water. As neither of these gages measure wave direction, information on the predominant directions from which waves reach inlet was derived from Volume 4 of the Summary of Synoptic Meteorological Observations (SSMO) published by the U.S. Naval Weather Service Command (1970). Table 2.2 provides a one year summary of the wave climate at West Palm Beach including the period in which the field investigations were made.

2.9 Sediment Samples

Sediment samples were taken from several locations at the inlet in two phases. Each phase consisted of samples taken in a different location and each was performed with a different objective in mind. Fig. 2.12 indicates the location of all sediment samples taken. The analysis of all samples taken is presented in Section 3.9. In the first phase, samples were taken at specified locations as a means of determining the nature and source of the sediment in areas where deposition (shoaling) had occurred. Sample locations were chosen either as areas of immediate deposition, areas adjacent to areas of deposition, areas along the route over which the deposited sediment was transported, or potential source areas of sediment. Locations denoted by numbers 1 through 21 in Fig. 2.12 indicate the sample sites in this phase.

The second phase of sediment sampling was conducted with the purpose of determining the nature of the sand deposited in the sand trap (and subsequently transferred to the south beach). Accordingly, samples were taken at locations in and around the sand trap and were analyzed by

Table 2.2. Wave Data for West Palm Beach

	April 1982	May 1982	June 1982	July 1982	August 1982	September 1982	October 1982	December 1982	January 1983	February 1983	March 1983	Average Value
T_{avg} (sec)	4.5	5.0	4.5	4.6	4.7	9.3	8.2	5.2	4.7	4.7	5.0	5.9
T_{max} (sec)	9.0	9.0	11.0	8.5	10.5	11.5	12.0	12.0	11.0	12.0	12.0	10.7
H_{avg} (m)	0.30	0.52	0.25	0.21	0.25	0.33	0.52	0.76	0.4	0.75	0.52	0.43
H_{max} (m)	1.3	1.5	1.55	1.2	1.5	1.65	1.9	2.2	1.6	2.1	1.9	1.7

NOTE: No data were obtained for November, 1982.

T_{avg} = average wave period

T_{max} = maximum period

H_{avg} = average wave height

H_{max} = maximum wave height

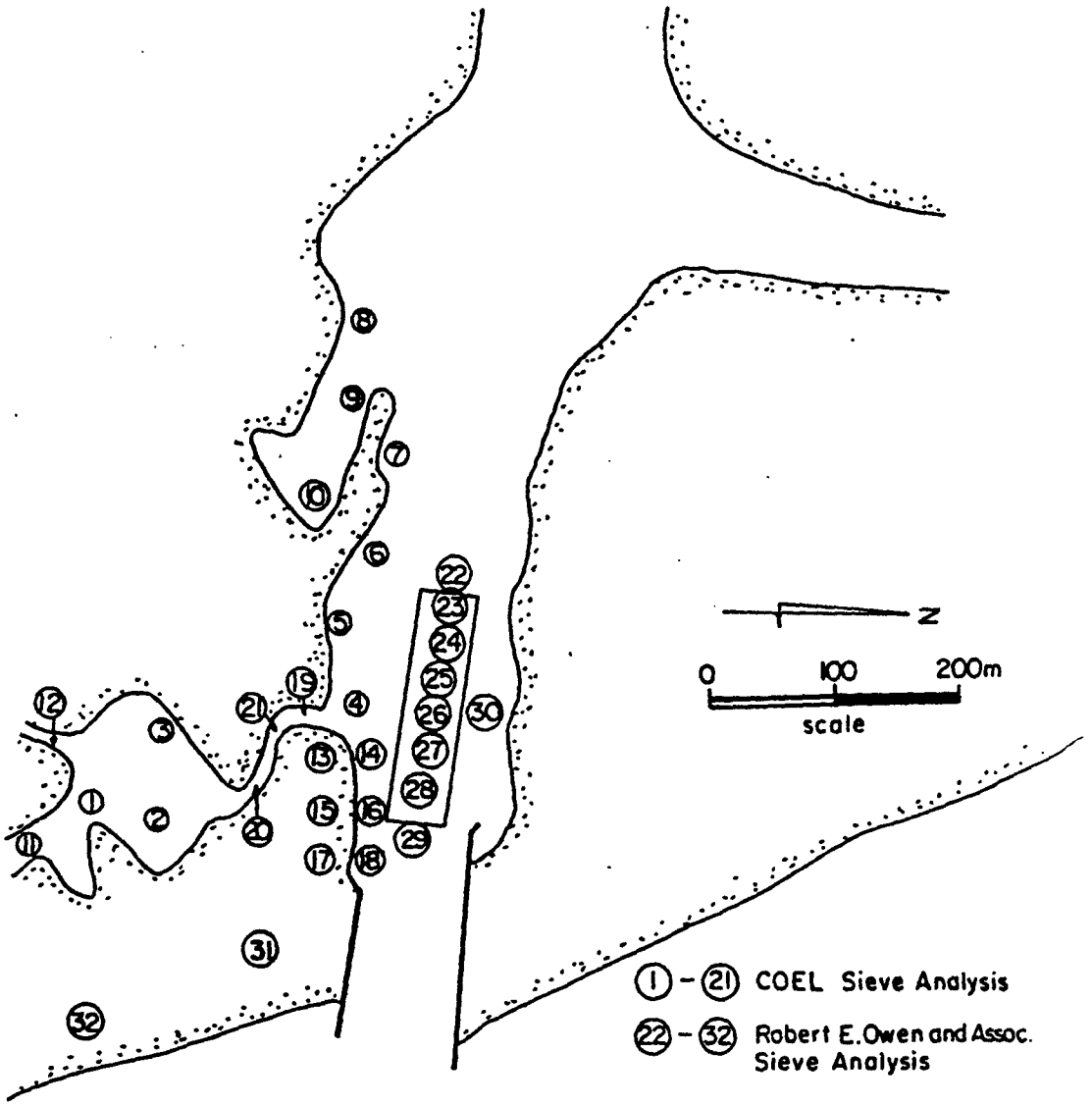

Fig. 2.12. Sediment Sample Sites.

Robert E. Owen and Associates of West Palm Beach, Florida. Locations denoted by numbers 22 through 32 in Fig. 2.12 indicate the sample sites for this phase.

2.10 Runoff

Data concerning the contribution to the overall discharge through the western boundary (Intracoastal Waterway) of the study area by tributaries in the form of freshwater inflow were obtained from the U.S. Geological Survey Water-Data Report (1981). Table 2.3 lists the maximum, minimum and average daily discharge values for each tributary as recorded for the water year October 1980 to September 1981. The tributaries are grouped according to their contribution to one of the three primary tributaries discharging directly upstream (west) of Jupiter Inlet. These three primary tributaries, Canal C-18 and the north and northwest forks of the Loxahatchee River, compromise the three forks of the Loxahatchee River Estuary and are shown in Fig. 1.2.

Table 2.3. Freshwater Inflow into the Three Forks of the Loxahatchee River Estuary

Tributary	Maximum Daily Discharge (m^3/sec)	Minimum Daily Discharge (m^3/sec)	Average Daily Discharge (m^3/sec)
Northwest fork			
Kitchings Creek	0.63	0.00	0.14
Cypress Creek	7.41	0.03	1.12
Hobe Groves Ditch	4.67	0.01	0.20
Loxahatchee River at State Road 206	16.21	0.20	1.61
North fork			
Unmaned	1.87	0.00	0.10
Southwest fork			
Canal-18	9.43	0.00	0.88

2.11 Winds

Data concerning the wind conditions at West Palm Beach were obtained from records compiled by the National Climatic Center (NOAA, 1980-81). Maximum and average wind speed from different directions as well as the percentage of occurrence of these speeds and directions were compiled over the period January 1980 - December 1981. The wind conditions at the inlet should not differ much from those in the West Palm Beach area.

Interpretation of the wind data reveals that velocities are greater from the northeast sector but the duration and percentage of occurrence are greater from the southeast sector. The yearly average wind velocity from the northeast sector is about 18 km/hr while that from the southeast sector is about 14.5 km/hr.

CHAPTER III

DATA ANALYSIS

3.1 Overview

Data were analyzed and interpreted so as to provide information on the hydraulic and sedimentary characteristics of the inlet. This information yielded necessary input parameters for both the computational procedures utilized and the physical modeling of the inlet. In addition, this information provided for a better understanding of the causes of the problems at the inlet. The following paragraphs describe the procedures involved in the data analysis and interpretation.

3.2 Hydrographic Surveys

The hydrographic survey of June, 1981, detailing the bathymetry of the inlet helped in providing: 1) a general description of the bathymetry of the inlet and surrounding areas, 2) an understanding of the field observations and hypotheses regarding bathymetric trends in the inlet, and 3) estimates of sediment volumes present at specific locations within the inlet.

The survey of October, 1981, describing the bathymetry of the offshore region immediately seaward of the inlet indicated the presence of a relatively small ebb tidal shoal or bar. This corresponded with observations made during the field investigation and compliments estimates of the offshore bar volume made in this study (Section 3.10.2). These surveys along with aerial photographs also indicated

that shoaling had indeed occurred in the Dubois Park lagoon, the southshore marina area and the bend in the Intracoastal Waterway. Calculations (made from the surveys) of the volume of sand deposited in the sand trap resulted in a value of 92,000 m^3 and were found to be in good agreement with prior sand trap dredging records which indicated an average volume of 86,000 m^3 between 1970 and 1979 (Jones, 1976).

The survey data were interpreted so as to determine bathymetric profiles extending offshore of the inlet shoreline areas that have undergone erosion. This provided the necessary information to calculate sand volumes required to renourish these areas. The surveys also indicated that (as detailed in Fig. 2.6c) the inlet area immediately west of the mouth is progressively deeper from south to north across the channel. This bottom feature causes waves entering the inlet to refract towards the Dubois Park Beach, thereby accelerating the erosion rate there. This phenomenon was first observed during the field investigation.

A cross-section of the "empty" sand trap was superimposed over a representative cross-section of the inlet area where the trap is located in order to determine the change in cross-sectional area when the trap is dredged (Fig. 3.1). The resulting cross-sectional area, A_c, showed an increase from 534 m^2 to 708 m^2. Calculations similar to those in Appendix A based on tidal inlet relationships developed by Keulegan (1967) were then made in order to determine the resulting change in maximum flow velocity expected from the dredging of the trap. The maximum flood velocity decreases from 1.95 m/sec to 1.65 m/sec while the maximum ebb velocity decreases from 2.25 m/sec to 1.90 m/sec as a result of dredging the sand trap according to the specifications of Fig. 3.1.

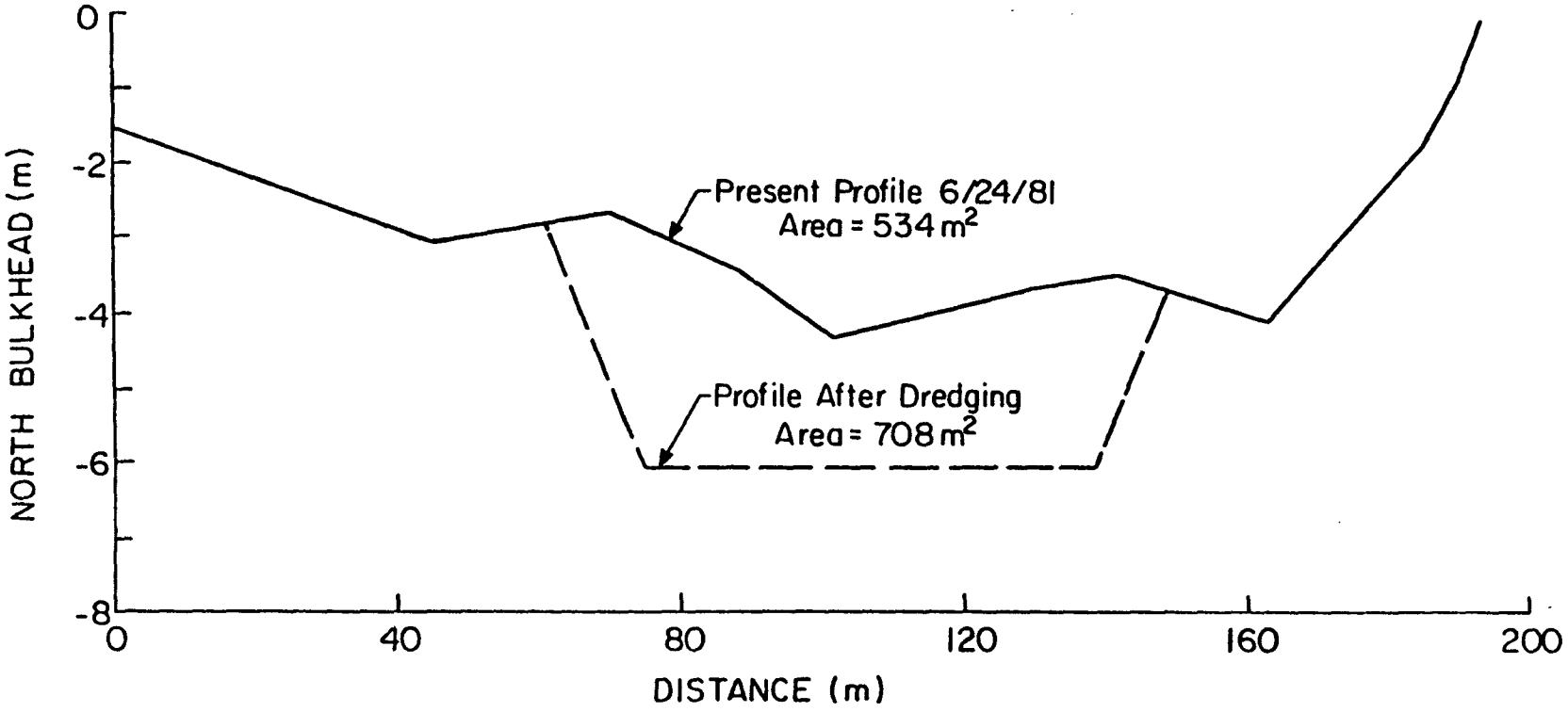

Fig. 3.1. Illustration of the Change in Area of a Typical Main Channel Cross-Section when the Sand Trap is Dredged.

The effect of this decrease in flow velocity will be to decrease the magnitude of the erosive forces along the shoreline while increasing the likelihood of deposition in the trap (as opposed to areas further inland). As the trap begins to fill up the cross-sectional area of the inlet decreases and the flow velocities increase, thereby increasing the magnitude of the erosive forces along the shoreline and decreasing the tendency of deposition in the trap until conditions equivalent to those when the trap is full exsit. As a result, it may be concluded that conditions most conducive to erosion along the shoreline and deposition of the eroded material further inland exist when the trap is full. Based on this conclusion, model testing was limited to conditions corresponding to the filled trap.

3.3 Tide Records

Data obtained at the seven tide gages were utilized in the computation of inlet hydraulic parameters as well as in the calibration of the physical model. Analysis of these data resulted in the determination of tidal ranges at each gage, ratios of these ranges relative to that of the inlet mouth (gage T-1), and lags of high water and low water at each gage relative to high and low water at gage T-1. These data are presented in Table 3.1. In addition, as an illustration, a cumulative histogram of the tide record from gage 2A over the time period September 30 to November 7, 1982 is provided in Fig. 3.2. Data from the National Ocean Survey (NOS) Tide Tables indicate an average tide range of 0.75 m and a spring tide range of 1.1 m for the inlet vicinity. The tidal ranges measured corresponded well with the NOS predictions in terms of magnitude (within 0.1 m) but were found to be less comparable in terms of the time of occurrence (within 30 minutes).

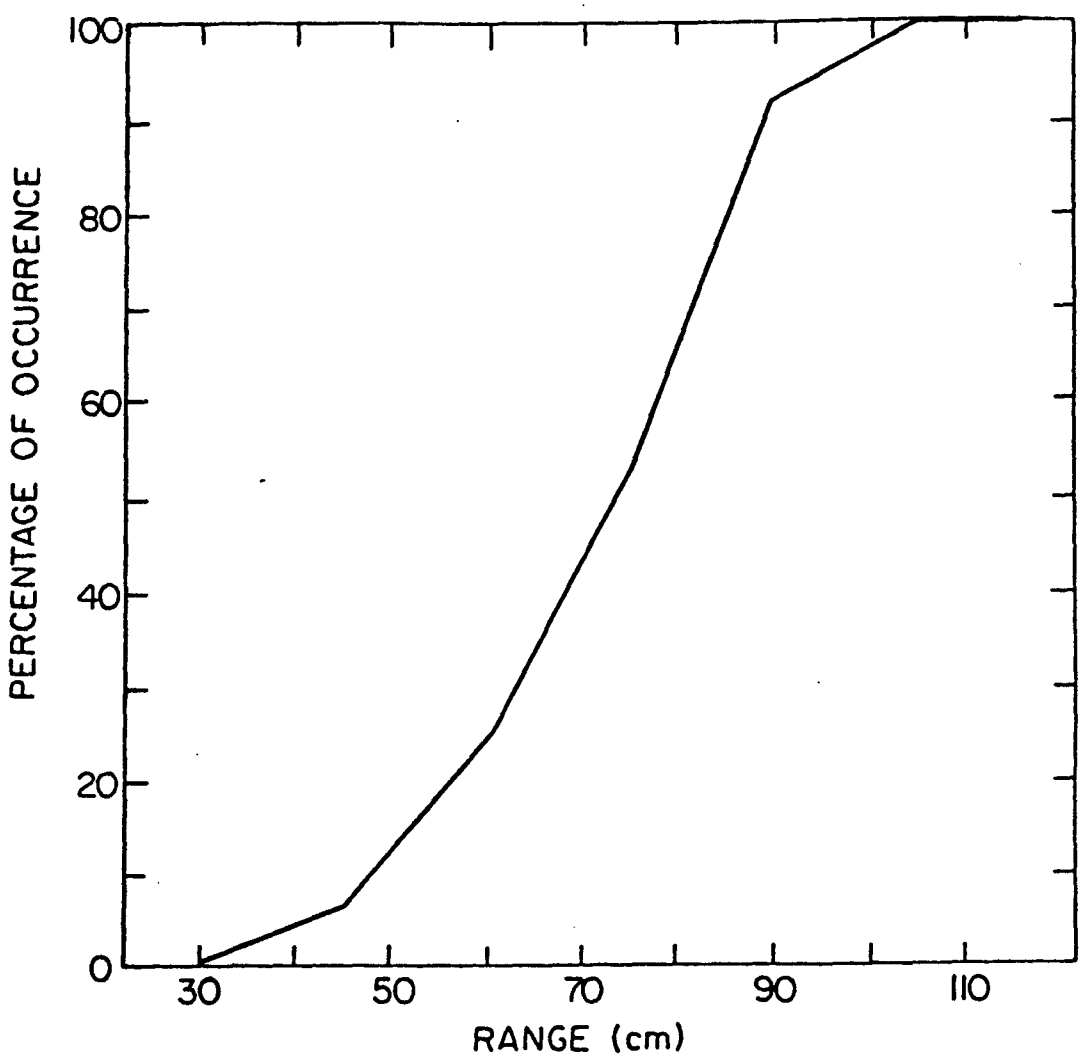

Fig. 3.2. Cumulative Histogram of Wave Heights (cm) at Gage 2-A over the Period September 30 - November 7, 1982.

Table 3.1. Tidal Ranges, Lags and Range Ratios Relative to Inlet Mouth, January 26 - February 2, 1983

Location	Maximum Range (m)	Range Ratio*	Lag (High) (min)	Lag (Low) (min)
Inlet Vicinity**	1.10	0.90	-15	-10
Ocean***	1.10	0.90	-48	-12
Gage T-1	1.22	1.00	0	0
Gage T-2A	1.05	0.86		4
Gage T-2B****	0.80	0.65	10	12
Gage T-2C	0.82	0.67	5	6
Gage T-3	0.76	0.62	29	16
Gage T-4	0.91	0.75	44	9
Gage T-5	0.43	0.35	234	151

*Relative to gage T-1.

**Obtained from NOS prediction for Jupiter Inlet, Longitude 80°05' West Latitude 26°57' North.

***Obtained from water level data from the offshore wave gage. Negative sign indicates high or low tide occurred before that of the inlet.

****Data obtained over the period January 19 - January 26, 1983.

3.4 Storm Surge

Data from historical storm surge records were compiled by Bruun et al. (1962) so as to provide a prediction of the return period for various surge levels (Section 2.4). Normally, this information would be used to determine a design storm surge level corresponding to a 50 or 100 year return period to be used as a worst-case condition for testing in the model. However, because the solution options (Chapter V) were all to be implemented within the inlet and not on the land area above +1.5 m, a storm surge of +1.5 m, corresponding to a fifteen year return period was chosen as the worst-case condition. In addition, the model

provides an accurate representation of the topography of the inlet study area only up to an elevation of +1.5 m. As a result, a storm surge greater than +1.5 m would not be accurately modeled and, therefore, neither would the effects of such a surge on the proposed solution options.

Field data similar to those obtained for normal flood and ebb flows were not available for storm surge conditions. As a result hydraulic relationships developed by Keulegan (1967) were utilized in order to determine the resulting maximum flow velocities due to a 1.5 m storm surge at the inlet. Appendix A presents relevant calculations by which these flow velocities were determined.

3.5 Analysis of Vertical Velocity Profiles

3.5.1 Vertical Velocity Profiles

Figure 3.3 shows typical profiles of the vertical velocity distributions for the jetty cross-section C-1. These measurements were made on October 14, 1982 between 1800 and 1900 hours. However for the purpose of further analysis it will be assumed that they represent instantaneous values at time 1830 hours. Figure 3.4 presents a corresponding logarithmic plot for the same profile. These profiles, as well as most others obtained from the collected data, exhibited the characteristic (for turbulent open channel flows) logarithmic velocity decay with increasing depth. The depth-averaged velocities, $\bar{u}$, for each of the measurement locations, were determined by integrating (over the depth of flow) the vertical velocity profiles, and are included in Fig. 3.3.

At locations where the flow velocity exceeded approximately one meter per second, the depths at which velocity measurements were taken

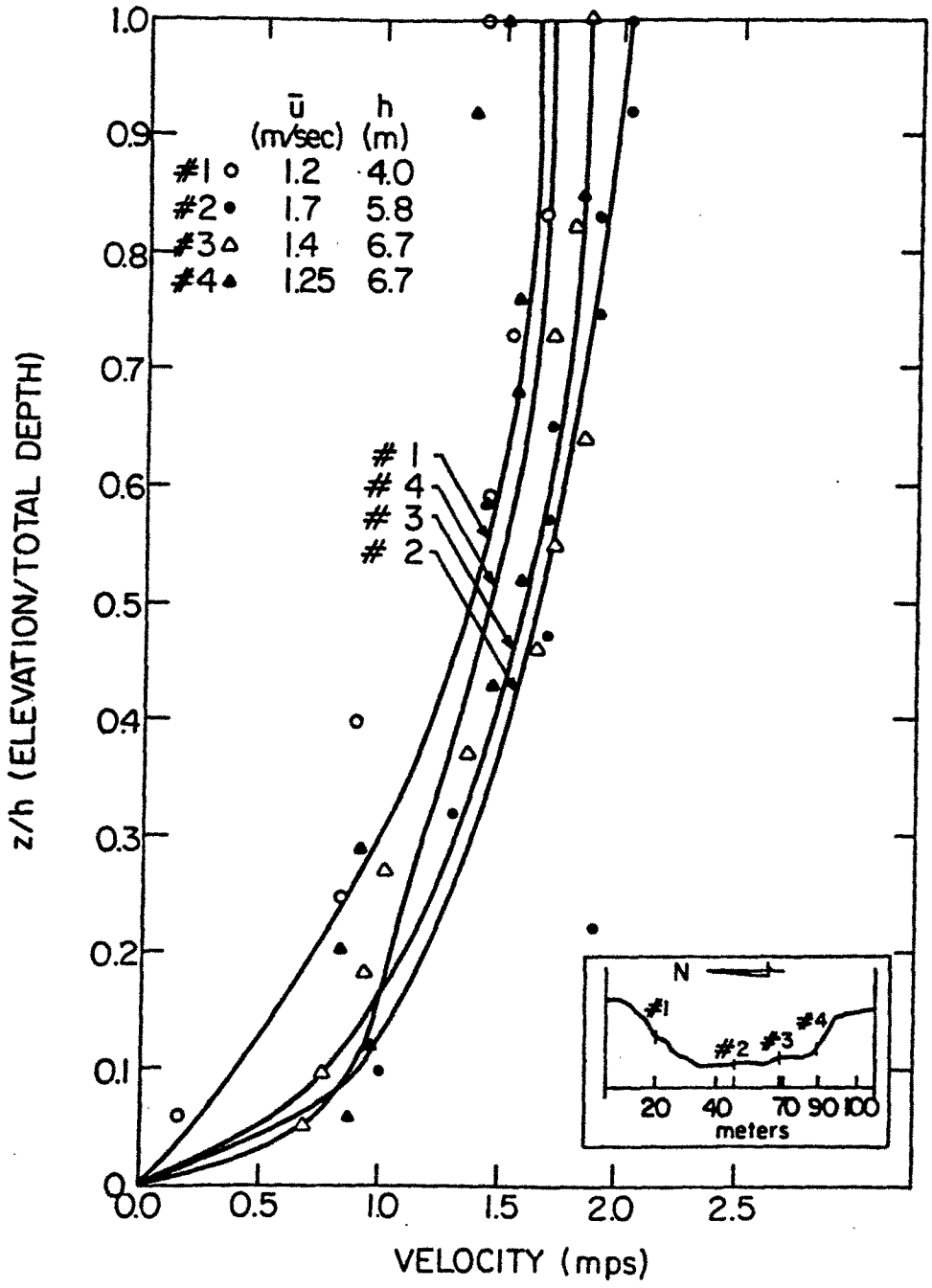

Fig. 3.3. Vertical Velocity Profiles for Jetty Cross-Section C-1 taken October 14, 1982 at 1830 Hours.

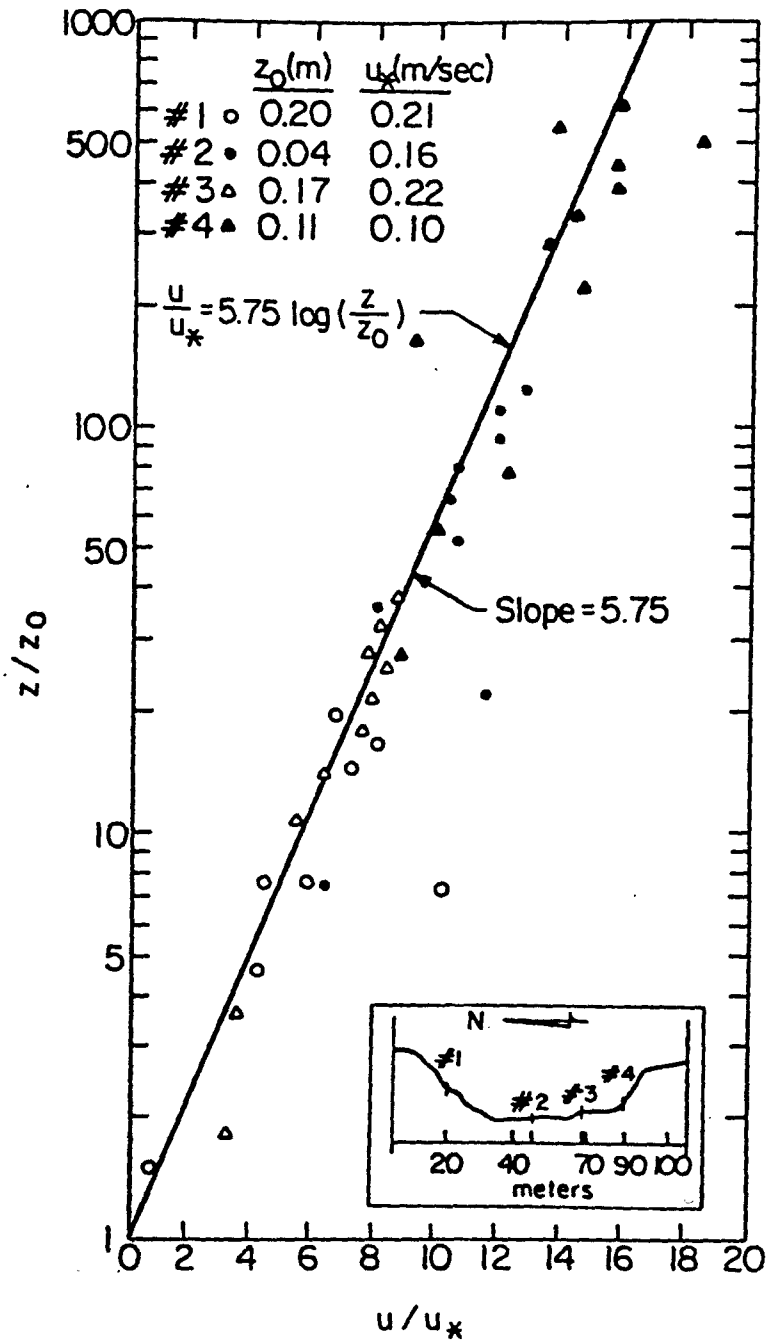

Fig. 3.4. Logarithmic Plot of the Vertical Velocity Profiles for Jetty Cross-Section C-1.

were corrected to account for horizontal displacement and the resulting vertical displacement of the Ott current meter due to drag forces associated with higher flow velocities. Appendix B presents the depth-correction calculations.

3.5.2 Depth-averaged Transverse Velocity Profiles

Figure 3.5 shows a plot of depth averaged velocity, $\bar{u}$, based on the vertical profiles in Fig. 3.3, against the location of the profile as measured from the indicated shoreline. The curve connecting these points is assumed to represent a continuous transverse velocity profile for the indicated cross-section. Values of $\bar{u}$, profile position, and the mean time corresponding to the cross-sectional velocity measurements were non-dimensionalized and plotted in the manner shown in Fig. 3.6 in order to present the results in a generalized manner. Similar plots for the non-dimensionalized transverse velocity profiles obtained at each cross-section are presented in Appendix C. The parameters describing the tidal conditions corresponding to the measurements on which these plots are based are defined as follows (Mehta and Sheppard, 1977):

W = width of the flow cross-section at the time the vertical velocity profiles were measured,

x = distance from the shore on which the tide box was installed to the location of the stations where the profiles were obtained,

$K = x/W$ = dimensionless parameter to normalize the abscissa,

$\bar{u}$ = vertically averaged horizontal velocity obtained from averaging the vertical velocity profile measured at each station,

g = acceleration due to gravity,

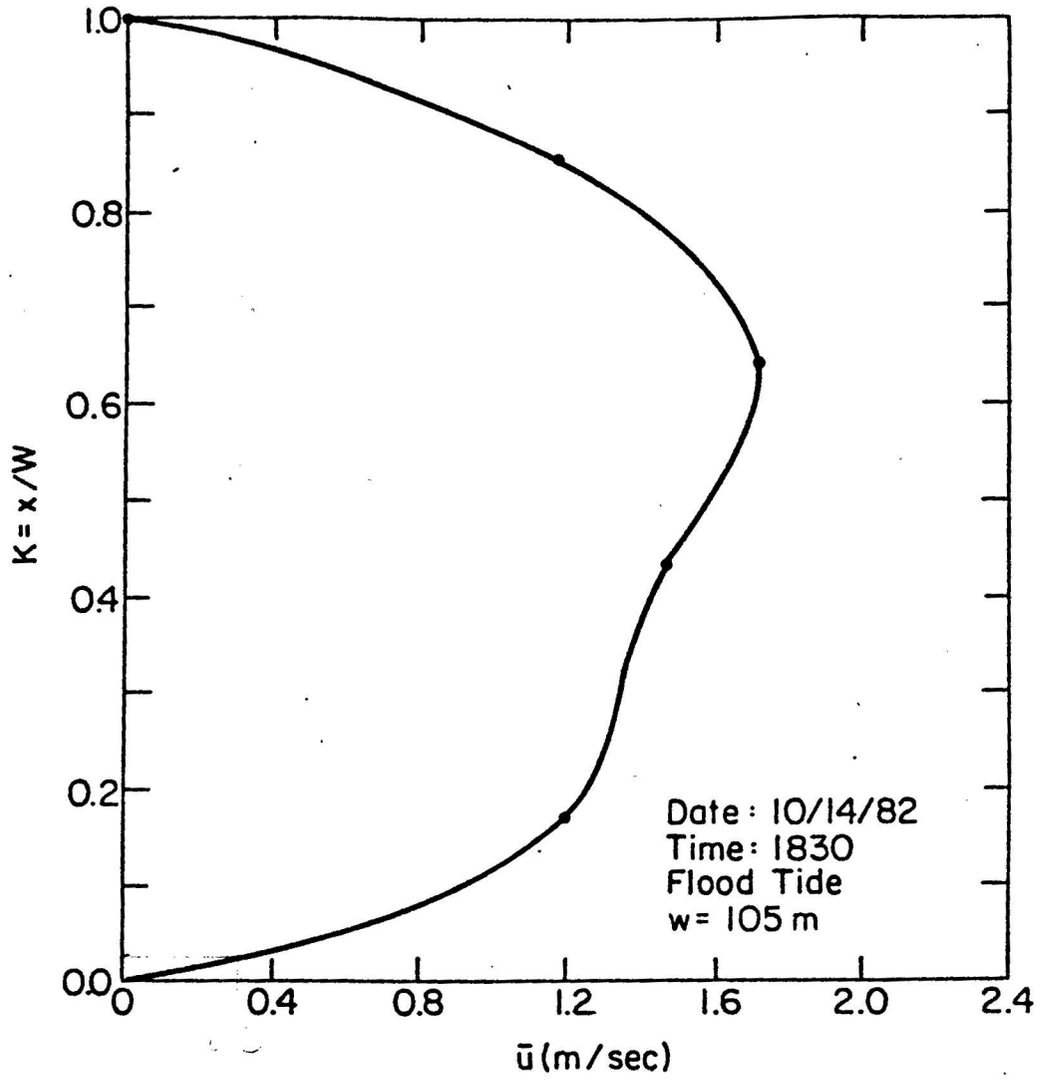

Fig. 3.5. Plot of Transverse Depth-averaged Velocity Profile for Jetty Cross-Section C-2.

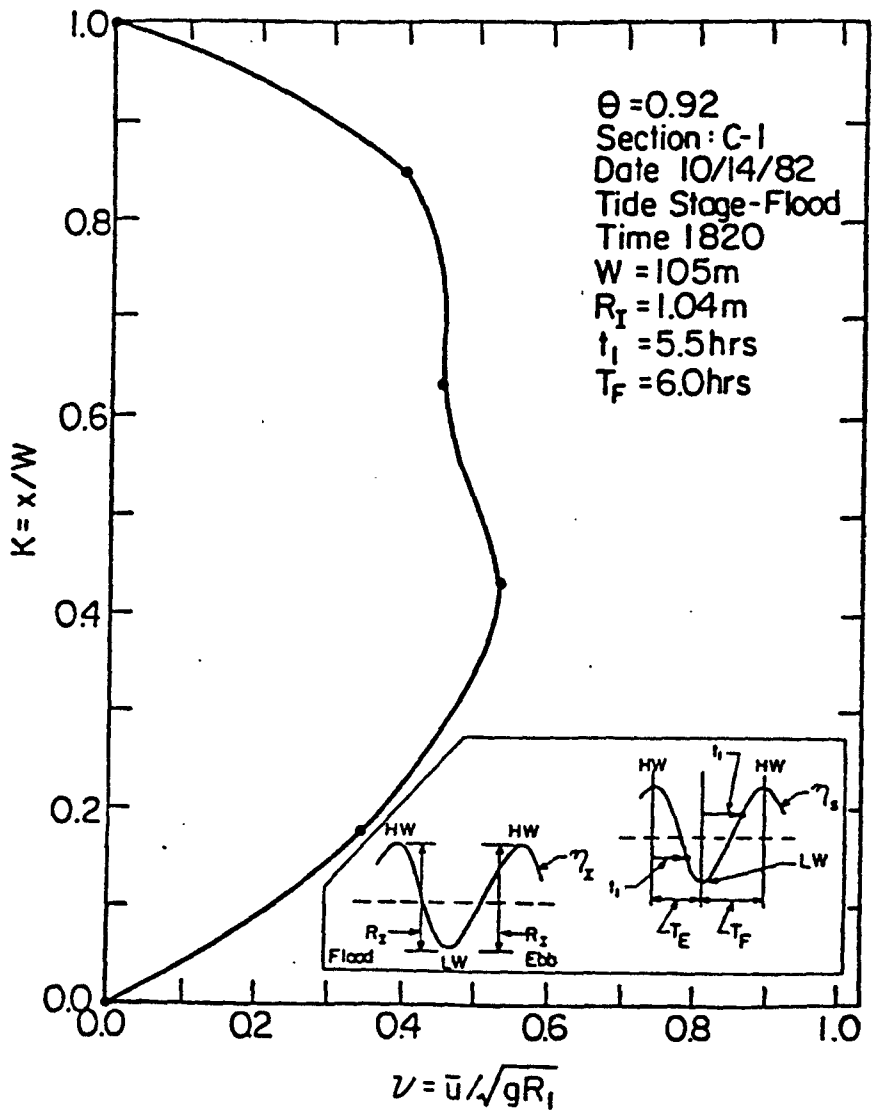

Fig. 3.6. Dimensionless Transverse Velocity Profile for Jetty Cross-Section C-1.

R_I = range of tide at the cross-section during the same stage of the tidal cycle during which the velocity profiles were obtained (see inset of Fig. 3.6),

$\nu = \bar{u}\sqrt{gR_I}$ = dimensionless parameter to normalize the ordinate,

T_F or T_E = time interval of flood or ebb tide (see inset of Fig. 3.6) determined from the tide record by the gage at the cross-section,

t_1 = time interval from the beginning of flood or ebb flow to the time the velocity profiles were obtained, and

$\theta = t_1/T_F$ or t_1/T_E = dimensionless parameter to determine during what stage of flood or ebb tide the velocity profile was measured.

3.5.3 Continuous Velocity Measurements

In each of the five cross-sections, continuous velocity measurements were obtained over minimum time periods of 50 hours. Figure 2.8 shows a typically located current meter. Records were obtained over the period January 26 - February 2, 1983. Current magnitude and direction recorded on chart paper as shown in Fig. 3.7 by the meter at cross-section C-5 were later digitized. Similar data for the other four cross-sections were recorded in digital form. Table 2.1 lists the locations where the current meters were installed at each cross-section.

3.5.4 Discharge Computations

The continuous velocity data were utilized in a single point-velocity discharge computational procedure (Hayter, 1979) to obtain continuous discharge records for each of the cross-sections. In addition to the continuous velocity data, the computer program requires

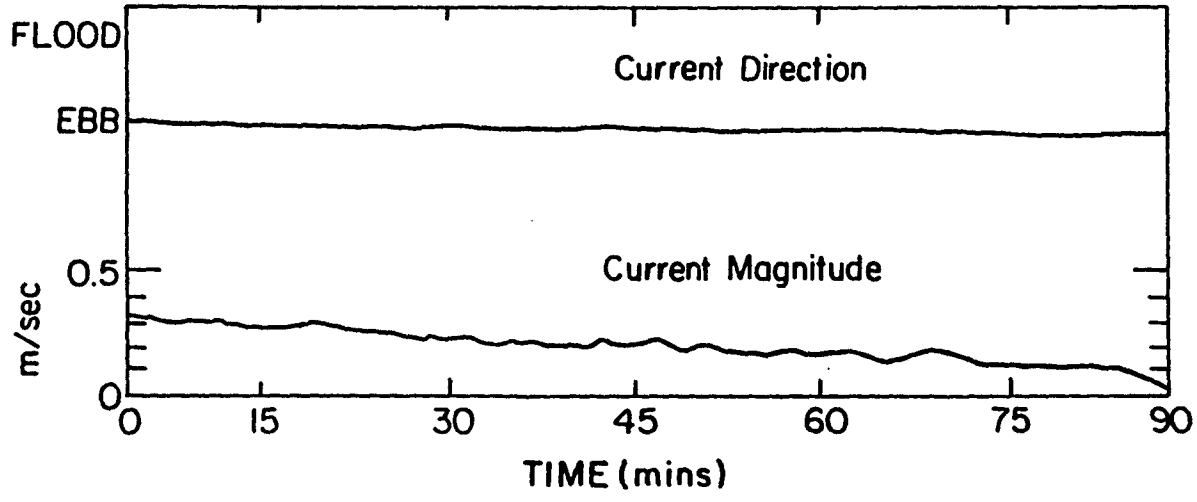

Fig. 3.7. Typical Current Meter Chart Record for Lagoon Cross-Section C-5.

input in the form of water surface elevation, bed roughness and geometry of each cross-section. If the bed roughness value of a specific cross-section is unknown, the computer program has the capability to calculate this value given the instantaneous measured water surface elevation and discharge as well as the friction slope for the cross-section. The instantaneous values for the discharge and the friction slope were calculated from the vertical velocity profiles (see Fig. 3.8). The corresponding water surface elevations were obtained from the tide records. Friction slopes and bed roughnesses were determined as described in Appendix D.

Table 3.2 presents the maximum flood and ebb discharges through each cross-section and their time of occurrence relative to maximum discharge at the inlet mouth. Figure 3.9 gives the flood and ebb discharges at each cross-section at the time of maximum discharge at the inlet mouth. The data included in Table 3.2 and Fig. 3.8 are based on the results of the aforementioned computations.

Analysis of Fig. 3.9 reveals a considerable difference in the discharge through the inlet mouth during ebb and flood flows. That the discharge during ebb is much greater than that during flood is believed to be due to two phenomena: 1) Discharge through the mouth during flood flow is due entirely to tide-induced flow. Discharge through the mouth during ebb flow, while due primarily to tide-induced flows, also contains an additional contribution from the Loxahatchee River Estuary in the form of freshwater runoff from inlet areas. 2) It is believed that a significant contribution to the ebb discharge is made from the reach of the Intracoastal Waterway extending west and south of the inlet. Some of the water entering the larger Lake Worth Inlet south

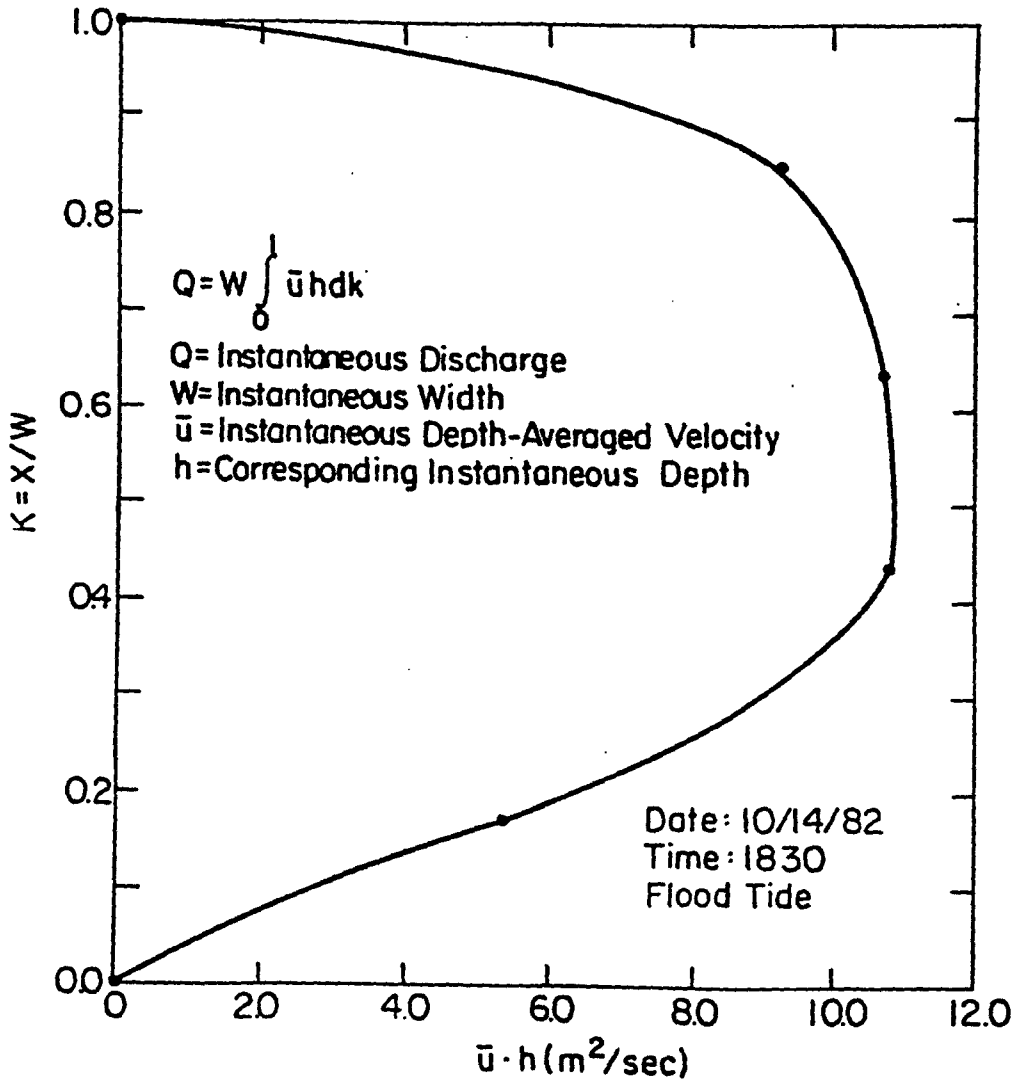

Fig. 3.8. Plot of the Product of the Depth-averaged Velocity and the Depth at Each Location Against Dimensionless Width K. Integration of this Plot Results in the Instantaneous Discharge Through the Jetty Cross-Section C-1 at 1830 hr on 10/14/82.

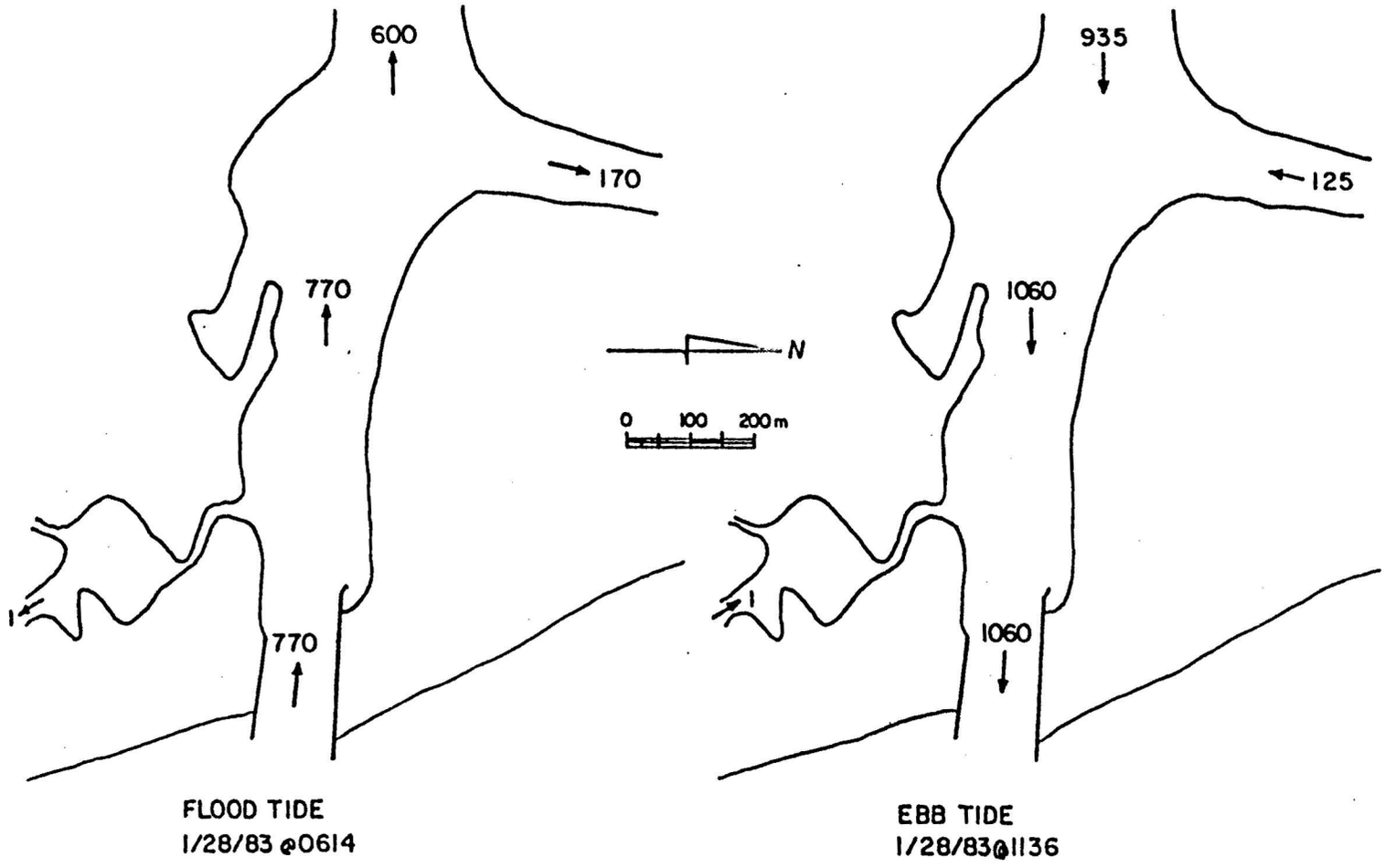

Fig. 3.9. Discharge Through Each Cross-Section Corresponding to Maximum Discharge Through the Inlet Mouth.

during flood flow probably returns to the ocean through Jupiter Inlet via the Intracoastal Waterway (van de Kreeke, 1976). The combined effect of these three phenomena is considered to be of sufficient magnitude so as to result in the observed difference in ebb and flood discharge rates.

Table 3.2. Maximum Discharge through Each Flow Cross-Section*

Ebb			Flood		
Section Number	Maximum Discharge (m^3/sec)	Lag** (Minutes)	Section Number	Maximum Discharge (m^3/sec)	Lag** (Minutes)
C-1	1060	---	C-1	770	---
C-2	1060	-2	C-2	770	4
C-3	143	-12	C-3	200	101
C-4	936	-1	C-4	651	46
C-5	2	224	C-5	3	151

*Data based on results from single point-velocity discharge computation procedure (Hayter, 1979).

**Lag is in reference to time of maximum discharge at inlet mouth. Negative sign means maximum discharge was earlier than that at the inlet mouth.

3.6 Drogue Study

Drogue motion over time plots, such as that shown in Fig. 2.9, revealed that flood flow is concentrated along the north bank of the inlet. In addition, the paths indicated that the flood tidal velocity vector exhibits a component normal to the shore. This component is suggested by the fact that the drogues tended to drift towards the north bank of the inlet as they travel westward. One drogue, as indicated in Fig. 2.9, actually made contact with the shore, ceased its westward movement, and had to be picked up. This characteristic of the flow is

believed to result in the deeper depths due to scouring along the north bank as well as the shoreline erosion and bulkhead failure occurring in this region.

Comparisons were made between the velocities of the drogues as they drifted past cross-section C-2 and the velocities calculated from the transverse velocity profile measured by a current meter at this location. Drogue velocities in fact correspond to the velocity of their anchor (see Fig. 2.10) and were therefore compared to the velocities at that flow depth (1 m). Both velocities were normalized by dividing by $\sqrt{gR}$, where R is the tidal range and g is acceleration due to gravity, to account for the difference in tidal range when the measurements were taken. Table 3.3 provides the results of this comparison. As can be seen, the agreement between the normalized velocities is good.

Table 3.3. Comparison of Normalized Drogue Velocities to Velocities Obtained from Current Meter Measurement at C-2

Current Meter Velocity (Oct. 14, 1982) (1m depth, R = 0.70 m)		Drogue Velocity (Nov. 18, 1982) (Cross-Section C-2, R = 0.86 m)	
Velocity (m/sec)	Normalized Velocity	Drogue Velocity (m/sec)	Normalized Velocity
0.80	0.31	W14-16 = 1.05	0.36
		014-16 = 1.00	0.35

3.7 Dye Study

Dye progression over time provides a further indication of the nature of flood flow through the inlet. Figure 2.11 supports the conclusions reached from the drogue study (Section 3.6) that flood flow

is concentrated on the north bank at a location directly across from the southshore marina. This phenomenon is clearly seen in the last two frames of Fig. 2.11.

In addition, the dye study revealed eddy activity along the north bank, just inland of the inlet mouth. This eddy formation is indicated by the tendency of the dye to remain in that area only to become more concentrated there; the dye did not begin to be transported inland until 14 minutes after injection. This phenomenon is especially noticeable when one compares the westward transport rate of the dye on the northshore to that of the dye on the southshore (see Fig. 2.11). This eddy formation during flood, coupled with wave activity, serves as the mechanism initiating sediment transport, and hence erosion, in this region.

3.8 Wave Information

Wave data (significant height and period) at the location shown in Fig. 2.4 were obtained over a period of only four days (January 27-30, 1983) and therefore could not be considered as representative over a longer duration. Comparisons of similar data taken at a permanent wave gage off of West Palm Beach at a depth of 10 m (COEL, 1983) over this same four day period were made. The purpose of this was to determine if the measured inlet waves were sufficiently comparable to those of West Palm Beach so as to justify using the more representative wave record of the latter in the model study.

Wave measurements were taken every hour at the inlet gage but only every six hours at the West Palm Beach gage. Ten concurrent readings were obtained from the two gages. The resulting data from these readings are plotted in Figs. 3.10 and 3.11. Figure 3.10 (Shore

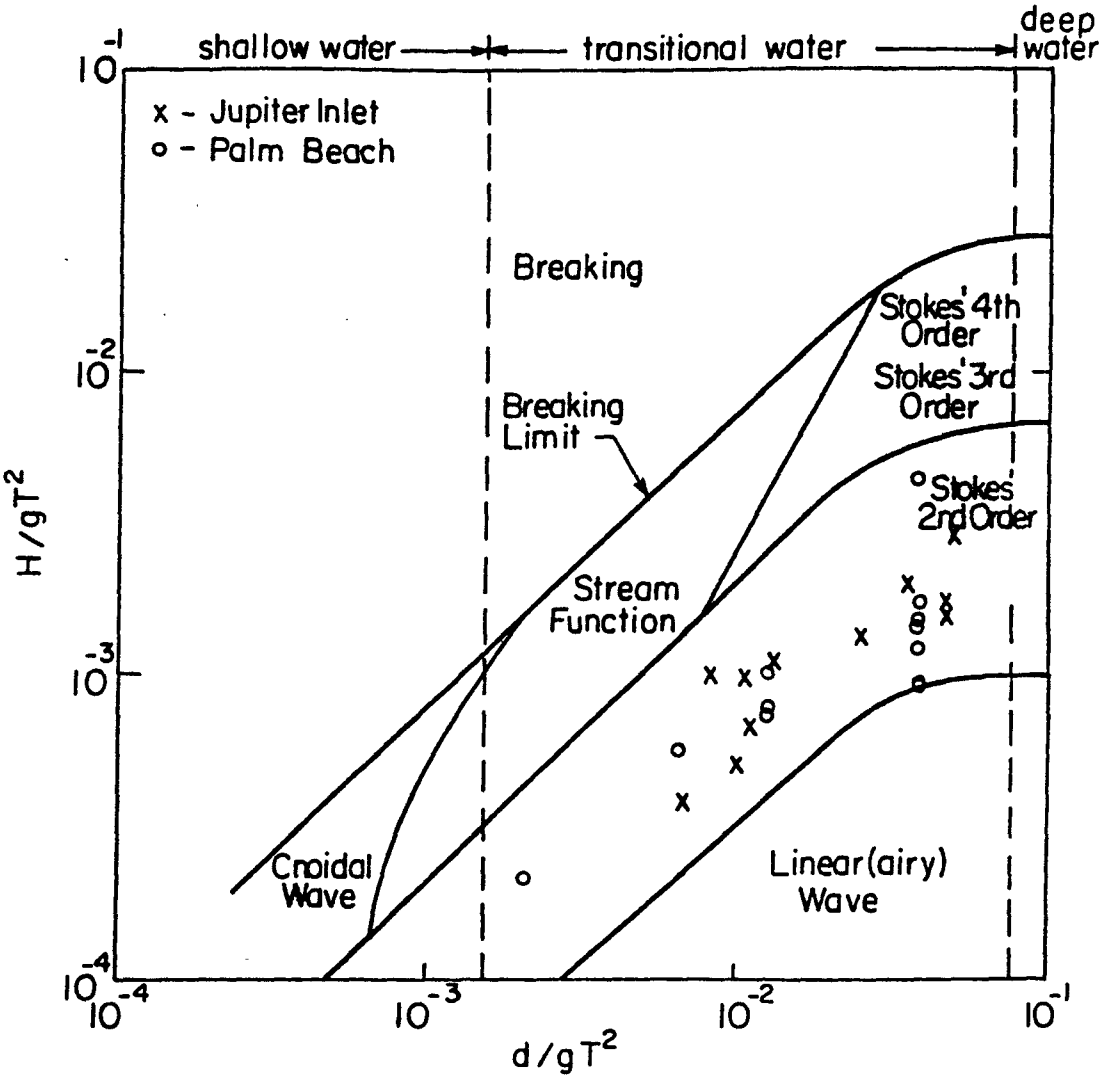

Fig. 3.10. Plot of Concurrent Jupiter Inlet and West Palm Beach Wave Data. Plot Indicates that All Waves may be Described by Stoke's Second Order Theory.

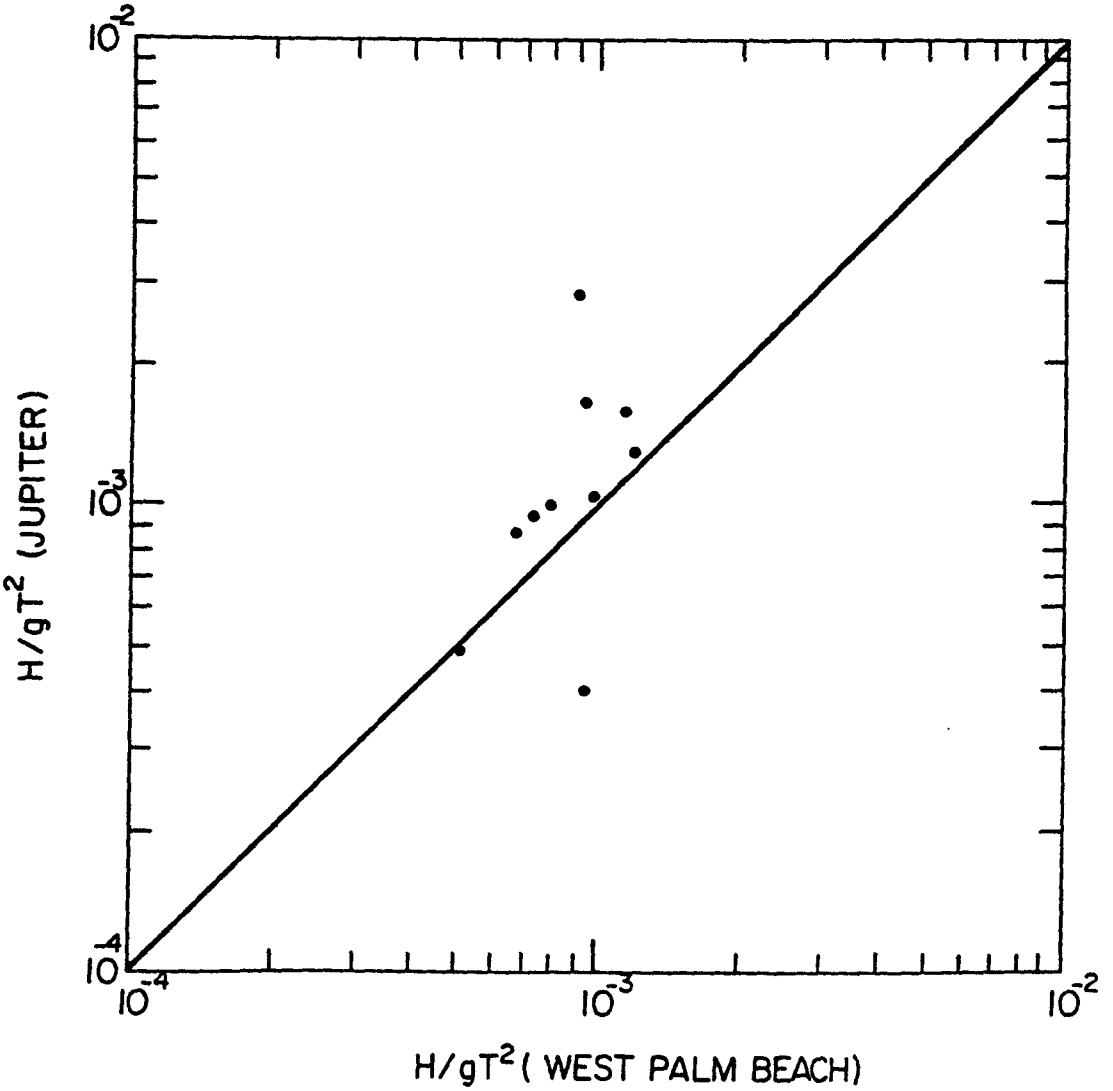

Fig. 3.11. Comparison of Concurrent Wave Data for Jupiter Inlet and West Palm Beach over the Period January 27-30, 1983.

Protection Manual, 1976) indicates that the non-breaking waves recorded at both gages were in a transitional stage between deep and shallow water and that they may be best described by employing Stokes' second order theory. Waves described by Stokes' theory demonstrate crest amplitudes that are greater and more peaked than their troughs. The fact that waves measured concurrently at the inlet and West Palm Beach were all non-breaking and may be described by Stokes' theory indicates that the waves at both locations were basically similar thereby indicating that a more specific comparison of heights and periods is justifiable. Figure 3.11 presents a plot of the dimensionless parameter, H/gT^2, where H is the significant wave height, g is the accelertion due to gravity and T is the significant wave period. This plot indicates that the wave conditions at both gages were reasonably similar. This plot, along with the one shown in Fig. 3.10, provides justification for using the West Palm Beach wave data as representative of the prevailing wave climate at the inlet.

The West Palm Beach wave data were next used to determine the mean and the maximum wave conditions (height and period) at the inlet. Wave data were averaged monthly for the one year period as shown in Table 2.2. Values for the mean wave height and period were taken directly from this averaged record as H_s = .43 m, T = 5.9 sec. The maximum wave conditions were determined in the same manner as $H_{s_{max}}$ = 1.7 m, and T_{max} = 10.7 sec.

Neither the wave gage at West Palm Beach nor the one at the inlet provided directional information. As a result, the directions corresponding to the highest frequency of incoming waves were determined from volume 4 of the Summary of Synoptic Meteorological Observations

(SSMO) published by the U.S. Naval Service Weather Command (1970). These directions were determined as Northeast, East, and Southeast; a "wave fan" of 90°. These waves are refracted from deep water so as to align themselves with the shoreline (Dean, 1983). Refraction calculations (Appendix E) resulted in a directional wave fan of approximately 60°.

3.9 Sedimentary Analysis

3.9.1 Procedure

The analysis of the sediment samples consisted primarily of determining the median diameter D_{50} and the sorting coefficient $\sqrt{D_{75}/D_{25}}$ of each sample. The median diameter of each sample provides a description of the sediment size for the specific location and can often give an indication of the source and mode of transport of that sediment. The sorting coefficient provides an indication of the range of grain sizes present at a specific location. A sorting coefficient value of 1.0 - 1.3 indicates a well sorted (or poorly graded) sediment sample while a value greater than 1.3 indicates a poorly sorted (well graded) sample. Table 3.4 lists the results of sediment analyses for each location. The results provide an indication of the sources and mechanisms of the sediment deposition in the Dubois Park and southshore marina areas.

Sample locations were grouped into eight different zones as shown in Fig. 3.12. Values of median diameters and the sorting coefficient for each sample in a given zone were averaged so as to provide a representative description of the sediment in each zone. The values of both of these sediment characteristics for the locations in each zone were very similar and, as a result, averaging them did not significantly

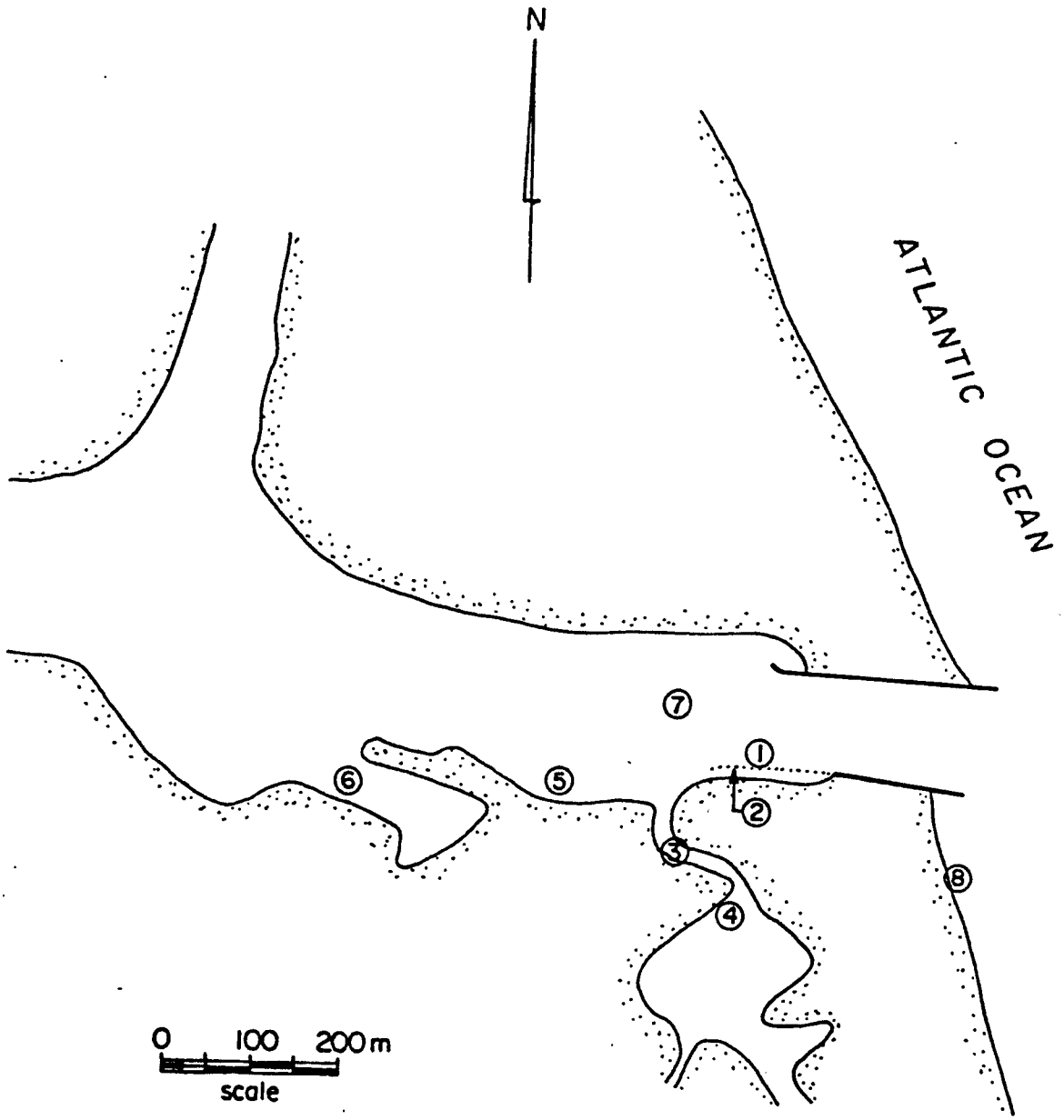

Fig. 3.12. Zones of Similar Sedimentary Characteristics.

Table 3.4. Sedimentary Analysis

Sample Number*	D_{50} (mm)	$\sqrt{D_{25}/D_{75}}$	Sample Number*	D_{50} (mm)	$\sqrt{D_{25}/D_{75}}$
1	**	well sorted	17	0.61	1.64
2	**	well sorted	18	0.25	1.37
3	**	well sorted	19	0.7	poorly sorted
4	0.3	1.89	20	0.9	1.57
5	0.62	2.36	21	0.42	1.51
6	0.38	1.54	22	0.88	1.74
7	0.36	1.51	23	0.77	1.61
8	**	well sorted	24	0.75	1.56
9	0.37	1.53	25	1.00	1.57
10	**	well sorted	26	0.78	1.61
11	**	well sorted	27	0.79	1.61
12	**	well sorted	28	0.80	1.54
13	0.50	1.54	29	1.08	1.71
14	0.34	1.88	30	0.35	1.30
15	0.60	poorly sorted	31	0.36	1.96
16	0.43	1.45	32	0.50	2.0.

*See Fig. 2.12 for locations of sample numbers.

**Indicates sediment primarily in the fine size range (less than 0.06 mm)

compromise the representative sediment characteristics of each zone. These characteristics, and the sediment samples (as indicated in Fig. 2.12) included in that zone are presented as follows:

Zone 1: This zone consisted of sample numbers 14, 16, and 18. The mean diameter for this zone was 0.34 mm while the sorting coefficient was 1.57.

Zone 2: This zone consisted of sample numbers 13, 15, and 17. The mean diameter for this zone was 0.57 mm, while the sorting coefficient was 1.59.

Zone 3: This zone consisted of sample numbers 19, 20, and 21. The mean diameter for this zone was 0.68 mm while the sorting coefficient was 1.51.

Zone 4: This zone consisted of sample numbers 1, 2, 3, 11, and 12. Qualitative analysis of these samples (taken at a maximum depth of 0.5 m) indicated very fine sediment (less than 0.06 mm diameter) that was well sorted (low sorting coefficient).

Zone 5: This zone consisted of sample numbers 4, 6, and 7. The mean diameter for this zone was 0.35 mm while the sorting coefficient was 1.65.

Zone 6: This zone consisted of sample numbers 8, 9, and 10. The mean diameter for this zone was 0.37 mm while the sorting coefficient was 1.50.

Zone 7: This zone consisted of sample numbers 22 through 30 (corresponding to the sand trap). The mean diameter for this zone was 0.80 mm while the sorting coefficient was 1.59.

Zone 8: This zone consisted of sample numbers 31 and 32. The mean diameter for this zone was 0.44 mm while the sorting coefficient was 1.99.

It should be noted that with the exception of zone 4, all zones exhibited a relatively high sorting coefficient indicating the presence of well graded sediments at each of these locations. As a result, only the mean diameter values served to differentiate between the sediment characteristics at each location.

3.9.2 Interpretation of Sediment Analysis

The mean diameter and sorting coefficient of the sediment in a particular zone provide an indication of the sources and mode of

transport of the sediment in that zone. Flow velocities in each zone act as the primary driving mechanism for sediment transport. By evaluating the sediment characteristics and flow velocities in each zone, hypotheses were made as to the causes of sediment deposition or erosion in each zone. Figure 3.13 shows a plot of sediment size versus velocity necessary to initiate transport (critical velocity), as based on Shield's diagram for turbulent flows (Section 6.3.2), that was used in part to base these hypotheses.

Zones 1, 2, 3 and 4: During a storm flood tide condition, water floods over and behind the rock protection just west of the south jetty (from zone 1 to zone 2). This water is channeled westward behind (south of) the rocks, continually increasing in velocity (Fig. 3.14) and results in the scouring of the sediment in zone 2. Velocities measured in the model indicated prototype values of 1.10 to 1.80 m/sec in this zone during storm conditions. These values are of sufficient magnitude to initiate scour in zone 2. The relatively large grain size of the remaining sediment in zone 2 suggests that primarily the finer grain sizes are scoured from this zone. No erosion was observed in zone 1 indicating that there is no net transport of sediment in this zone over time. Zone 1 was considered to be representative of the overall sediment characteristics of the inlet region along the south jetty both in mean diameter and sorting coefficient.

The channeled flow in zone 2 and the sediment that is scoured by this flow are diverted into the Dubois Park lagoon where the sediment would eventually settle out in zones 3 and 4. Velocities corresponding to 0.75 to 0.90 m/sec measured in zone 3 indicate that only the relatively larger grain sizes will remain in this zone. Analysis of the

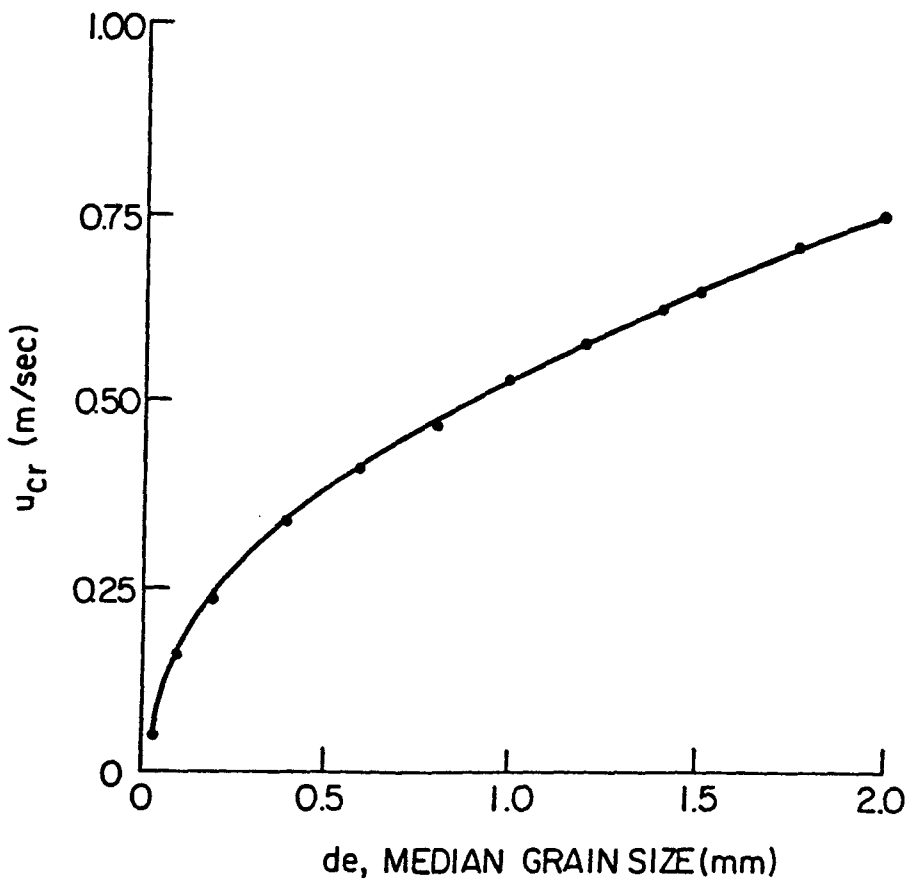

Fig. 3.13. Plot of Critical Velocity Versus Grain Size Based on Shield's Diagram.

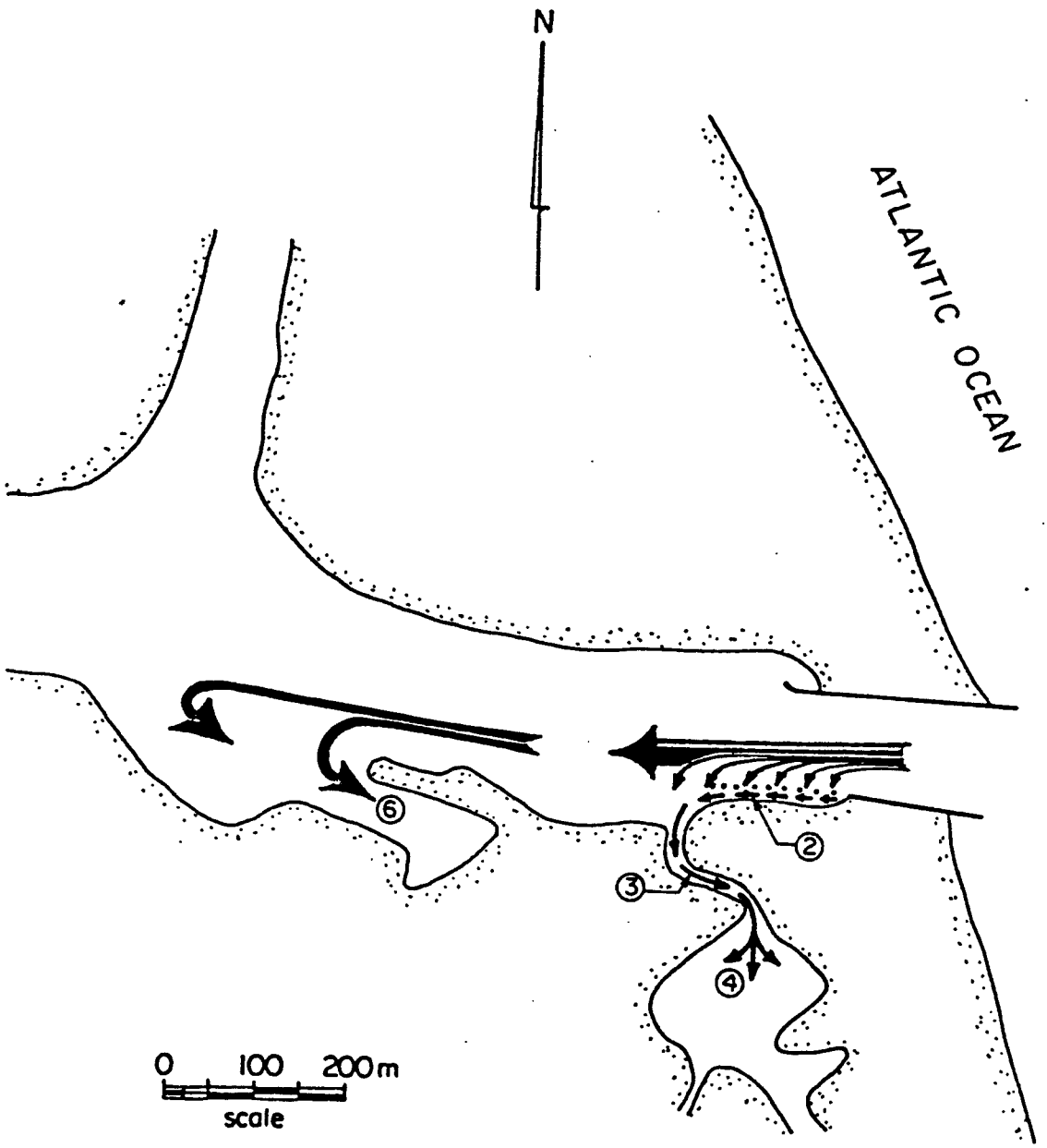

Fig. 3.14. Modes of Sediment Transport into Zones 3, 4, and 6; and out of Zone 2 (ref. Fig. 3.13).

sediment in zone 3 (D_{50} = 0.68 mm) substantiated the presence of larger grain sizes there. When the lagoon widens rather abruptly into zone 4, the flow velocity decreases to 0.1 to 0.2 m/sec. This decrease allows the finer grains to deposit in this region. Qualitative analysis of the sediment in zone 4 substantiated the presence of fine grain sizes here. In addition, calculated volumes of erosion and deposition shown in Fig. 3.15, indicate that the volume of sediment scoured from region 2 (N-2 = 1,500 m^3) was of the same magnitude as that deposited in zones 3 and 4 (S-2 = 2,300 m^3). These observations support the hypothesis that the erosion of sediment from zone 2 serves as the source of sediment deposition in zones 3 and 4.

Zone 5: At all stages of flood flow, sediment is transported into the inlet. In regions of higher flow velocity, only the larger particles are deposited; as the flow velocity decreases, finer particles begin to settle out. This phenomenon is the primary factor in determining the characteristics of the sediment found in zone 5. Maximum velocities measured in the model 15 to 30 m off the south shore of the inlet correspond to values of 0.50 to 0.80 m/sec in the prototype. These velocites and the flow vortices they create near the shoreline along with the previously mentioned wave action (Section 3.2) are of sufficient magnitude to scour the finer sediments from the south shoreline, and deposit them at locations further west within the inlet area. Some of this finer sediment is redeposited along the south shoreline during ebb flow but volume calculations (Fig. 3.15) and field observations indicate a net state of erosion in zone 5. Analysis of sample number 5 (Fig. 2.13), taken from the beach area of zone 5, gave a mean grain size of 0.62 mm. This relatively high value of grain size implies that the finer sediments have been gleaned from this zone.

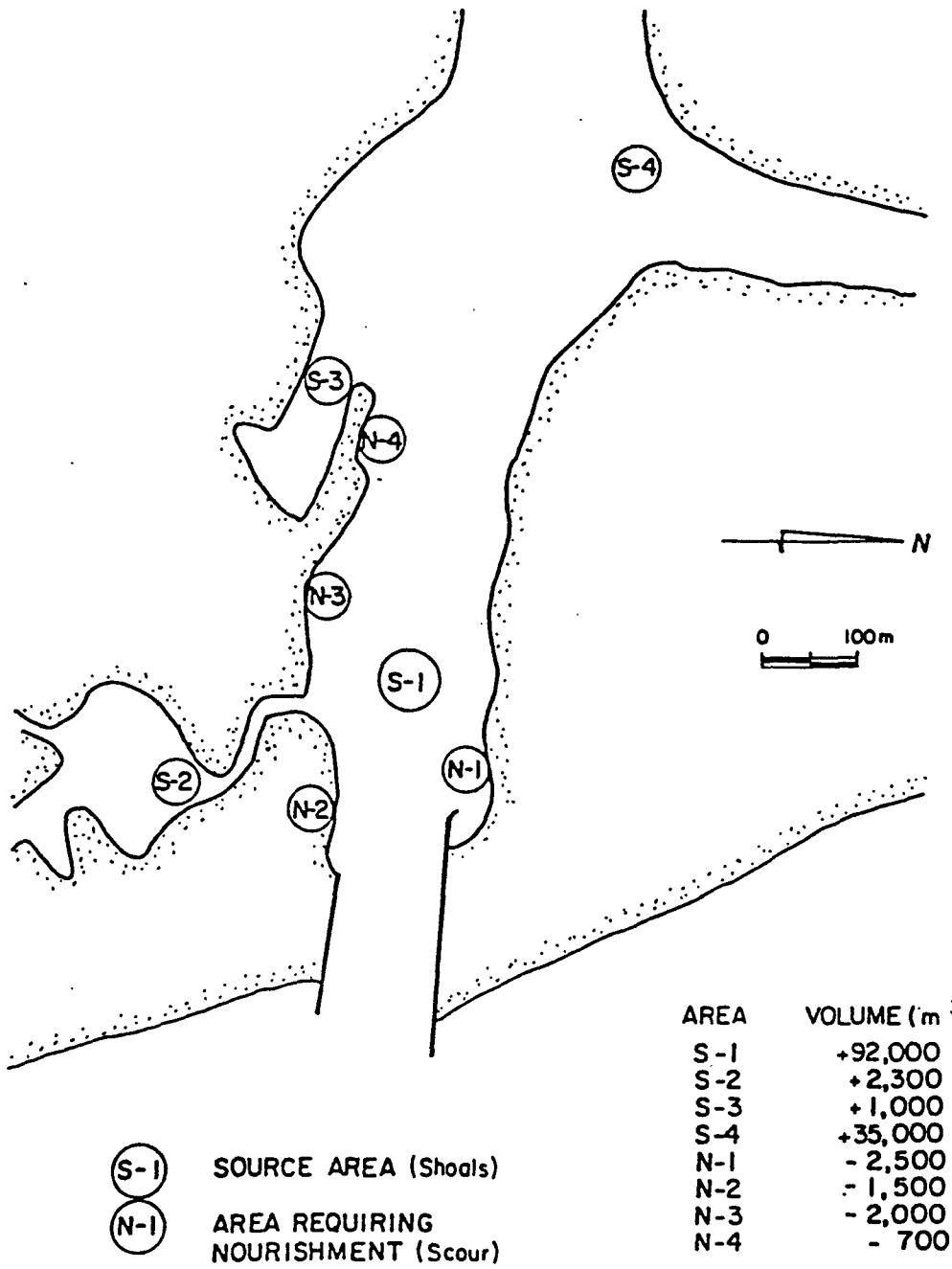

Fig. 3.15. Areas of Erosion (-) and Sedimentation (+) Corresponding to Areas Requiring Nourishment and Areas Acting as Sediment Sources in the Inlet.

Zone 6: Flow velocities measured in the model at the mouth of the southshore marina correspond to values of 0.1 to 0.2 m/sec in the prototype. These values are conducive to the deposition of sediment in this zone. It is hypothesized that this deposition takes place during both the flood and ebb flows. Sediment scoured from the south shoreline of the inlet is deposited near the mouth of the marina, an area of low flow velocities, during flood flow. Although most of this sediment is transported back along the south shoreline during ebb flow, a small portion of this sediment is carried into the marina. The low flow velocities in the marina are of insufficient magnitude to resuspend the sediment and transport the sediment out of the marina and, as a result, a net state of deposition occurs there.

Zone 7: The relatively large grain sizes in this zone (D_{50} = 0.80 mm) would be expected due to the fact that the high flow velocities here (1.6 to 1.8 m/sec) allow only the larger grain sizes to be deposited.

Zone 8: The relatively large grain sizes here (D_{50} = 0.44 mm) result from the fact that the sediment deposited in zone 7 (the sand trap) are mechanically bypassed to this zone. That the grain sizes here are smaller than those in zone 7 is likely to be due to the fact that some of the littoral drift (D_{50} = 0.25 mm) bypasses the inlet mouth and deposits in this zone. This explanation is substantiated by the very high sorting coefficients found in this zone.

3.10 Sand Budget

3.10.1 Overview

Examination and analysis of littoral drift estimates (Walton, 1976), hydrographic surveys (Corps of Engineers, 1966 and 1983) and dredging records (Robert E. Owen & Associates, 1979; Corps of Engineers,

1983) for Jupiter Inlet provide the basis for an estimate of a sand budget for the inlet. The basis for the formulation of the sand budget are discussed in the following paragraphs.

3.10.2 Littoral Transport and Distribution

The predominant direction of littoral drift at the inlet is from north to south; from June through August there is a northerly sand drift (COEL, 1969). This drift is distributed in three general modes as it reaches the inlet: it may be carried offshore by "jetted" ebb tidal flows, it may naturally bypass the inlet by either bar-bypassing or tidal flow bypassing, or it may be transported into and deposited in the inlet.

As is the case with most inlets with jetties, a portion of the littoral drift is believed to be lost offshore as it attempts to bypass Jupiter Inlet. This is due to the jet action of the inlet caused by the ebb tidal flow into the ocean. A portion of the drift may be directly transported offshore as it bypasses the updrift jetty or it may first enter the inlet and subsequently move offshore during ebb flow.

Some of the drift bypasses the inlet naturally via a process known as bar-bypassing. In this process, littoral drift moves around the mouth of the inlet in the form of a shifting sand bar. This phenomenon usually results in a hindrance to navigation and is often mitigated by jetties and maintenance dredging. It is believed that prior to 1966 seventy-five percent of the net littoral drift bypassed the inlet in this manner (Corps of Engineers, 1966).

Littoral drift entering the inlet either settles out and remains in the inlet, thereby resulting in shoaling of the inlet, or is eventually transported down-drift by means of tidal flow bypassing. This latter

form of transport is driven by the alternating ebb and flood tidal currents which carry the sediment in and out of an inlet eventually directing it down-drift of the inlet. While sediment will enter an inlet during a flood current, it is constantly directed towards the inlet mouth throughout the tidal cycle. During flood flow, the sediment is directed towards the mouth by the flow converging on the mouth from all seaward directions. During ebb flow, lateral mixing of the jet induces eddy formations on each side of the mouth thus resulting in nearshore currents directed towards the mouth from both sides. These currents transport the sediment towards the mouth where it is deposited only until the subsequent flood tide transports the material inside the inlet (O'Brien, 1969). Figure 3.16 qualitatively illustrates this process for Jupiter Inlet.

The refraction of waves by the sand bar near the inlet mouth as well as by ebb currents results in the concentration of the wave energy towards the mouth and currents directed towards the mouth from the surf zone. Such waves also act to suspend sediment thereby providing the initial mechanism for suspended sediment transport. These two phenomena also result in the transport of sediment into an inlet (O'Brien, 1969).

Based on the intended effect of jetty lengthening since 1970 to decrease the offshore bar volume, and based on field observations, it would be expected that the inlet would exhibit primarily tidal flow bypassing. This conjecture is supported by relationships developed to quantitatively characterize inlet bypassing mechanisms and offshore bar volume.

Bruun (1958) developed a "bypassing parameter" which characterizes an inlet as tidal flow bypassing, bar-bypassing, or a combination of the two as follows:

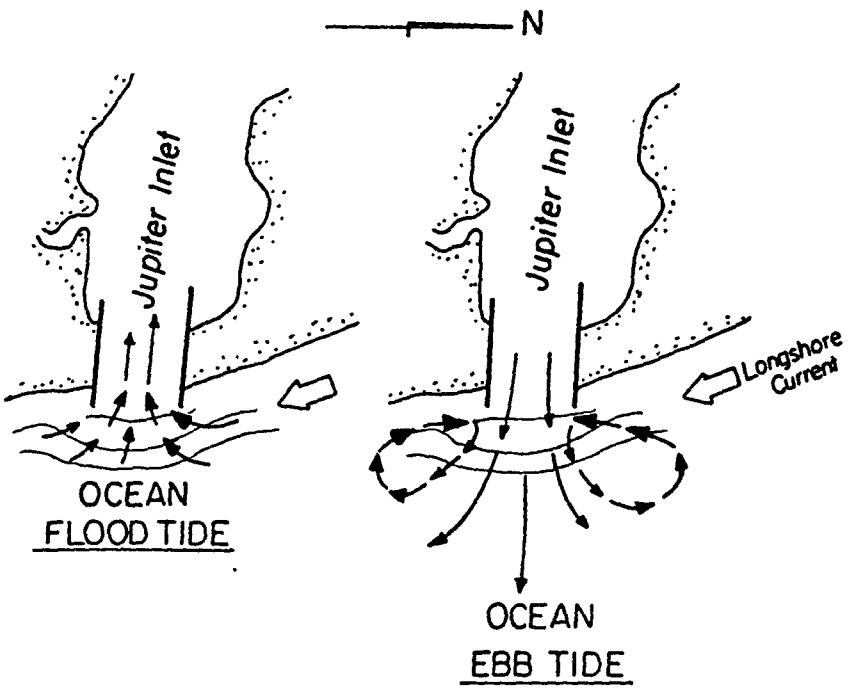

Fig. 3.16. Qualitative Illustration of Sand Transport towards the Inlet Mouth during Both Stages of a Tidal Cycle.

$$r = \frac{\Omega_s}{M_T} \tag{3-1}$$

where r is the bypassing parameter, M_T is the net annual littoral drift encountered by the inlet (1.76×10^5 m^3) and Ω_s is the spring tidal prism. Values of r greater than 100 indicate that the inlet undergoes tidal flow bypassing while values of r less than 50 indicate bar bypassing as the mechanism by which sand bypasses the inlet. Values of r in between 50 and 100 indicate a combination of these two mechanisms, weighted towards one or another depending on whether r is closer to 50 or 100. The value of Ω_s may be estimated by the following relationship (Mehta, et al., 1975):

$$\Omega_s = \Omega_m \left(\frac{a_{os}}{a_{om}}\right)^{1/2} \tag{3-2}$$

where Ω_m is the mean of the flood and ebb tidal prisms (1.205×10^7 m^3), a_{om} is the tidal amplitude corresponding to the measured tidal prism (0.4 m), and a_{os} is the spring tidal amplitude (0.65 m). Substitution of the appropriate values into equation (3-2) results in an Ω_s value of 1.536×10^7 m^3. Substituting the values for Ω_s and M_T into equation (3-1) results in an r value of 87. This value of r indicates a combination of the two mechanisms of sand bypassing, tending slightly towards tidal flow bypassing.

Walton and Adams (1976) developed a relationship between outer bar volume and spring tidal prism for sandy inlets on moderately exposed (to waves) coastlines as:

$$V = 10.5 \times 10^{-5} \Omega_s^{1.23} \tag{3-3}$$

where V is the outer bar volume and Ω_s as the spring tidal prism. For Jupiter Inlet, this relationship indicates an outer bar volume of 71,000 m^3. This corresponds to a low value for inlets on the east coast of Florida, strongly indicating that Jupiter Inlet undergoes tidal flow bypassing. The resulting sand budget also supports this conclusion. This tidal flow bypassing mechanism is never fully operative because approximately 70 percent of the sand entering the inlet settles in the sand trap and is mechanically bypassed to the south beach during regular maintenance dredging.

At this point it is worthwhile examining the relationship between the spring prism Ω_s and the throat cross-sectional area of the inlet, A_c. For inlets in sedimentary equilibrium, the well-known relationship is (O'Brien, 1969)

$$A_c = b\Omega_s^m \tag{3-4}$$

where b and m are empirical coefficients. For inlets with two jetties on the Atlantic Coast, mean values of b and m are 5.77×10^{-5} and 0.95, respectively, where Ω_s is measured in cubic feet and A_c in square feet (Jarrett, 1976). For Jupiter Inlet, $\Omega_s = 1.536 \times 10^7$ m^3 = 5.43×10^8 ft^3 and $A_c = 435$ $m^2 = 4{,}683$ ft^2 (cross-section C-1 in Fig. 2.4). For this value of Ω_s, Eq. (3-4) yields $A_c = 11{,}461$ ft^2 which is 2.45 times larger than the actual area. Ninety-five percent confidence limits have also been established by Jarrett (1976). These limits indicate that while 11,461 ft^2 is the mean value, the range can be between 5,100 ft^2 and 28,000 ft^2. It is clear that the actual

cross-section is considerably smaller than the expected equilibrium value. Erosion of the banks is not unexpected therefore, since the flow section attempts to adjust to its equilibrium value.

3.10.3 Sand Budget

As previously stated, the net annual southerly littoral drift rate near the inlet is 176,000 m^3. Out of this amount 134,000 m^3 is estimated (from dredging records) to enter the inlet, 1500 m^3 are lost offshore without entering the inlet (Corps of Engineers, 1966), leaving 40,500 m^3 of sand that is naturally bar bypassed each year.

Of the 134,000 m^3 of sand entering the inlet, 92,000 m^3 settle in the sand trap, 35,000 m^3 settle in the Intracoastal Waterway and 2,000 m^3 are deposited in the southshore marina (in recent years). Approximately 6,000 m^3 of sand are transported out of the inlet during ebb tidal flow and are lost offshore. The 92,000 m^3 deposited in the sand trap is mechanically bypassed to the south beach. Figure 3.17 provides a schematic drawing of the sand budget. In some cases records of sediment accumulation were only available for periods greater than one year. Data were interpreted in these cases, so as to determine a corresponding yearly average of sediment accumulation. Specifically, quantities of sediment dredged from the sand trap and the Corps of Engineers deposition basin were divided by the time period between successive dredgings to obtain yearly average accumulation of sediment.

3.11 Runoff

The contribution due to runoff in the form of freshwater inflow from the three primary tributaries of the Loxahatchee River Estuary was inherently included in the discharge calculations made from field measurements. Analysis of the data presented in Section 2.10 provided

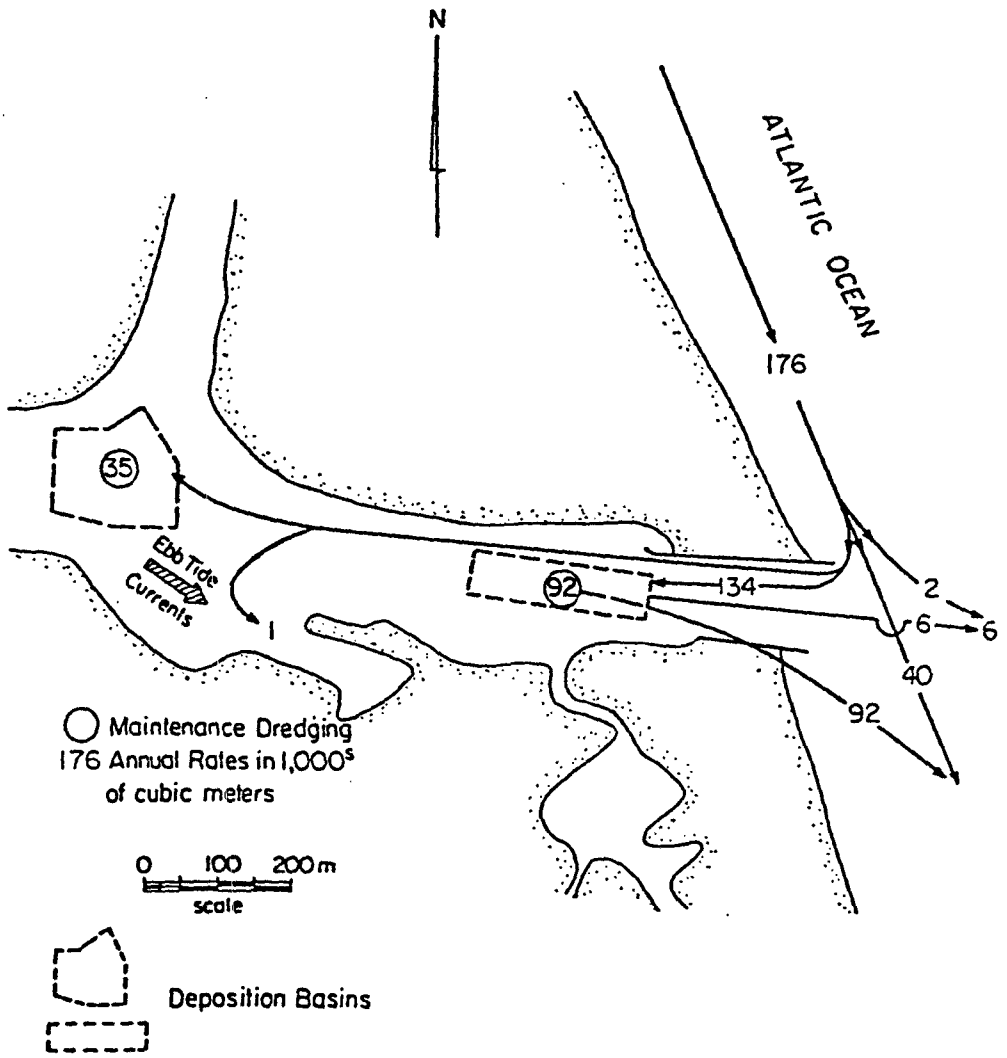

Fig. 3.17. Sand Budget for Jupiter Inlet.

an indication of the net change in this contribution that may occur due to maximum runoff conditions and the effect of this condition on the tidal prism at the inlet. Summation of the maximum daily discharge values in Table 2.3 results in a maximum freshwater contribution to the discharge through the western boundary of the inlet of 40.22 m^3/sec. Assuming this value to be constant over one-half of the 12.4 hour tidal cycle (equivalent to the time period over which a tidal prism is defined) results in a total contribution of 9.0×10^5 m^3 to the tidal prism. This corresponds to 6% of the estimated spring tidal prism of 1.536×10^7 m^3 (Section 3.10).

This value of 6% is considered to be much higher than the actual contribution due to the following reasons: 1) the maximum contributions of each tributary did not all occur on the same day although they were all added together in this calculation and 2) the maximum contributions from the north and northwest fork correspond to the period during which Hurricane Dennis occurred (mid-August, 1981) which would result in a much greater tidal prism in addition to the abnormally high freshwater discharges. A more accurate estimate of the net change in the freshwater contribution to the tidal prism at the inlet during maximum runoff conditions is believed to be in the range of 2 to 3%. As a result the additional contribution to the tidal prism due to maximum runoff conditions was disregarded when determining the maximum flow conditions over a tidal cycle.

3.12 Wind

While wind data are an essential characteristic in describing the overall climatic conditions of an area, it was not considered as an important factor in explaining the hydraulic and sedimentary phenomena

at the inlet. The water surface flows generated as a result of shear stresses exerted by winds were assumed negligible when considered relative to the magnitude of the tide-induced flows. Local wind-generated waves are of insufficient magnitude to compound the effects due to the longer waves entering the inlet from the ocean. In addition, the inlet shoreline may be described as "low-lying" in terms of the degree of exposure to wind and protection from the erosive forces of wind is provided by trees surrounding the inlet. For these three reasons, wind was not considered as an important characteristic to replicate in the model.

CHAPTER IV

THE PHYSICAL MODEL

4.1 Model Facility

The wave generator used in the study is classified as "snake-type" and is of French manufacture (Sogréah Institute, Grenoble, France). The stroke, phase angle and the frequency of the paddles can be varied to produce wave fronts up to 60° from parallel to the generator face, up to 1.5 second wave periods, and with wave heights up to 10 cm. The generator imparts these waves into a basin 50 m long and 35 m wide (Macrae, 1977). A system made up of pumps, weir gates and weir boxes was developed to provide a means to simulate flow conditions at the inlet.

4.2 Model Scale

The model was constructed using an undistorted scale; the same scale was used in both the vertical and horizontal direction. The choice of scale was determined by a compromise between economics and the technical requirements for similitude.

The economic aspects of choosing a scale consist primarily of constructing the model within size limitations determined by the dimensions of the modeling facility. The fact that the model was to be undistorted narrowed the range of scale choices even further. In order to maintain a reasonable vertical scale, so that phenomena dependent upon vertical dimensions are accurately simulated, the scale should not exceed 1:100. An undistorted scale of such magnitude results in a

considerably large plan (horizontal) area of interest, accompanied by higher cost and considerable construction time (Sager and Hales, 1976).

Satisfying technical requirements for similitude involves achieving and maintaining geometric, kinematic and dynamic similarities. In addition, the range of scales to be considered had to be such that the inertia of the fluid (water) would be predominant over the forces due to viscosity and surface tension thereby preventing any scale effects related to these two fluid parameters.

The physical nature of the model was such that the flow phenomena would be dominated by inertial and gravitational forces. As a result, similarity in the model was based on the Froude modeling laws. The Froude number represents the ratio of inertial force to gravitational force as $V/\sqrt{gL}$, where V is a characteristic velocity, L is a characteristic length and g is the acceleration due to gravity. This ratio must have the same value in both the model and the prototype, and can be expressed in terms of scales (relating the model to the prototype) as $n_V = \sqrt{n_g n_L}$. A useful result of Froude modeling is that, for an undistorted model, the velocity scale n_V is equal to the square root of the length scale, i.e. $n_V = \sqrt{n_L}$ (since $n_g = 1$).

Having predetermined the approximate range of scales that would satisfy both the economic and similarity criteria, a length scale of $n_L = 49$ was chosen. This conveniently corresponds to a velocity scale of $n_V = 7$. Other scales (these are for an undistorted model only) were obtained as follows (Bruun, et al., 1966):

Volume	$n_V = n_L^3 = 117649$
Cross-Section Area	$n_A = n_L^2 = 2401$

Time	$n_T = n_L/n_V = 7$
Discharge	$n_Q = n_W/n_T = 16807$
Slope	$n_S = n_L/n_L = 1$
Roughness	$n_f = n_S n_L/n_V^2 = 1$

4.3 Model Construction

The area replicated in the model (Figs. 2.1 and 4.1) encompassed the study area plus sufficient margins such that any boundary conditions would not be altered as a result of: 1) the physical boundaries of the model or 2) later modification of the study area. Construction of the model consisted of the following four phases:

4.3.1 Templates, Sand, and Concrete

The construction of the model was based on a template scheme that resulted in a fixed-bed, concrete bottom replica of the study area. The templates, cut from masonite, corresponded to a grid system superimposed over a topographic map of the study area up to plus 1.5 m elevaton. The templates were cut and labeled according to their respective elevation corresponding to their location on the grid. They were then placed on the basin floor and leveled relative to mean sea level (1929 N.G.V.D.) with surveying instruments. Appendix F gives the topographic map, which was composed from several surveys.

The construction procedure consisted of filling each grid section, measuring 1.2 m (0.6 m in locations requiring fine detail) by 2.4 m, with sand. This sand was compacted and maintained at a level 5 cm below the top of the templates. Concrete was then poured up to the template levels and graded to produce continuous bathymetry. Figure 4.2 is a schematic drawing of the template scheme. The sidewalls (boundaries) of the model were formed from concrete building blocks.

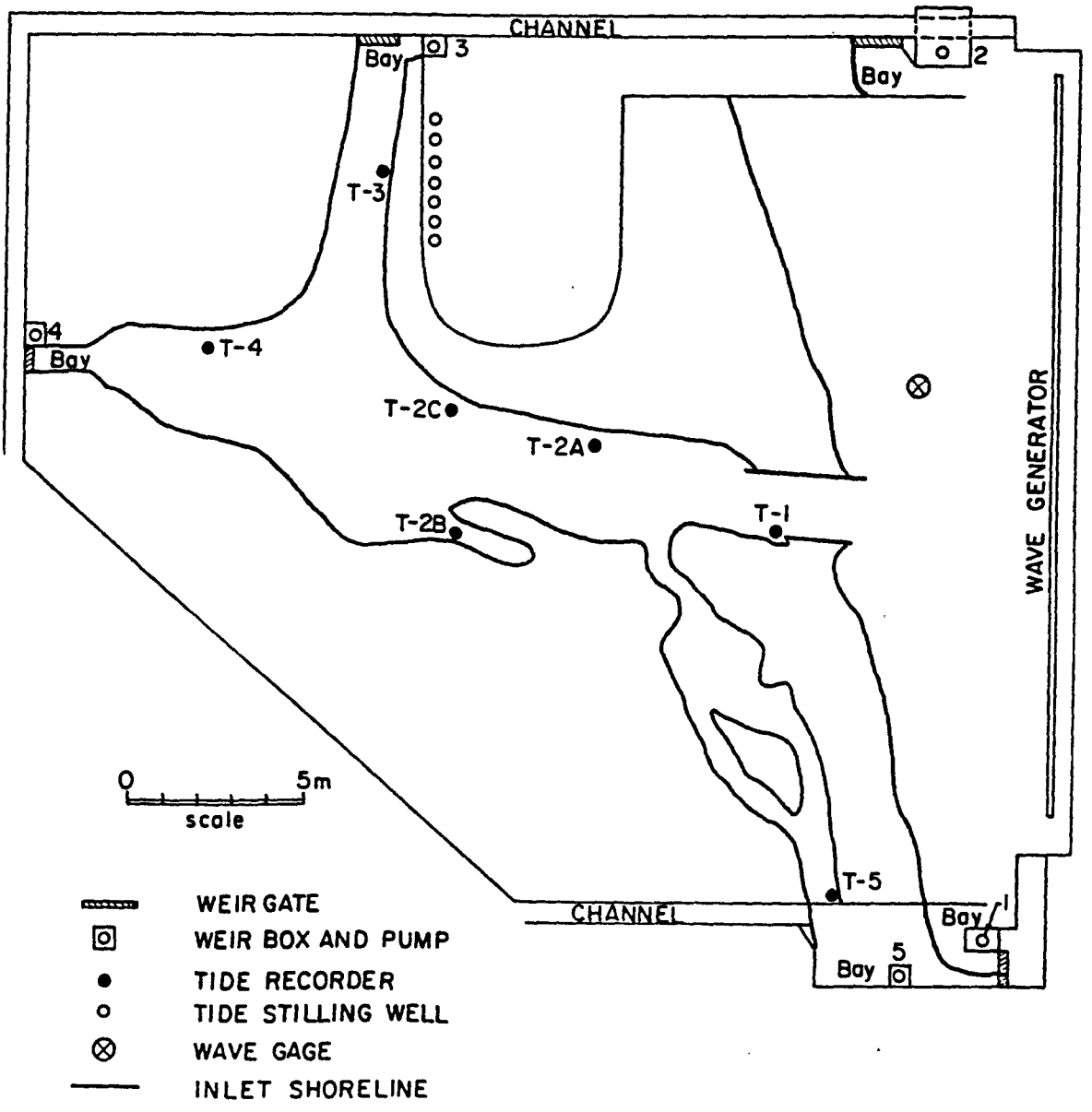

Fig. 4.1. Schematic Layout of the Physical Model.

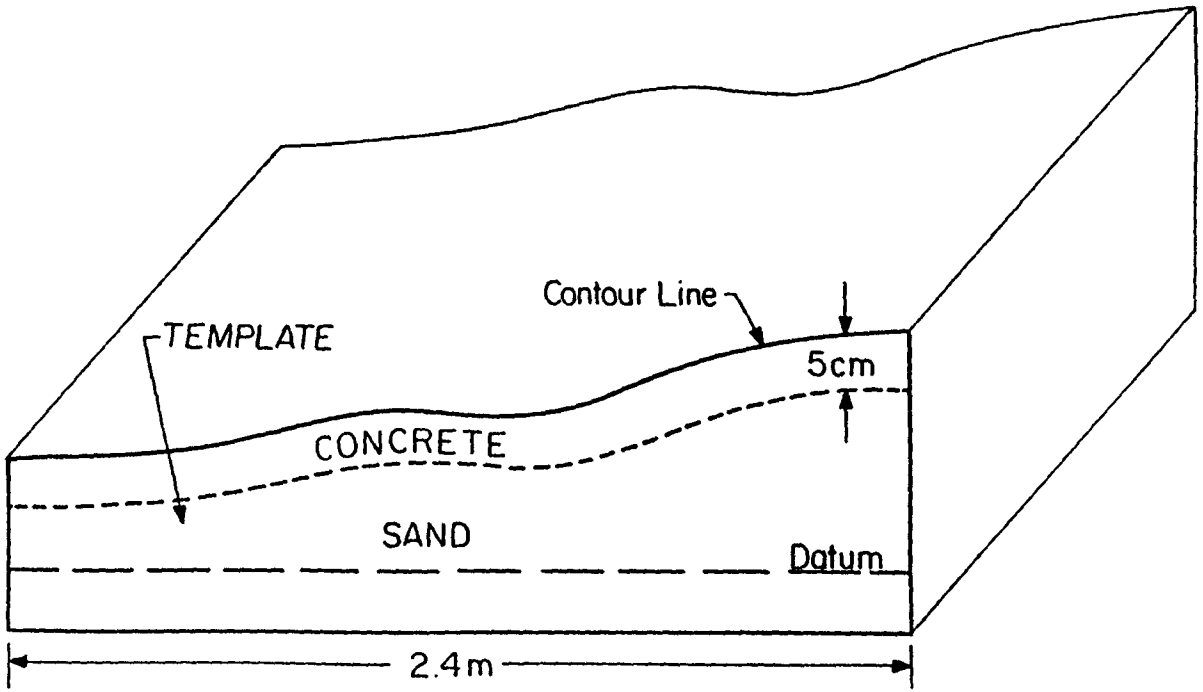

Fig. 4.2. Schematic Drawing of the Template Scheme to Reproduce the Bathymetry in the Model.

4.3.2 Seawall, Channel, Jetty and Rip-Rap

In certain areas of the model, topographical discontinuities such as seawalls and channels occur. Through an examination of aerial photographs and bathymetric surveys, the location and nature of these discontinuities were accounted for and the concrete appropriately graded. Features such as groins and flow deflectors (implemented as potential solution measures) were simulated by small stones and wooden templates.

The jetties and rip-rap along the shoreline of the inlet were simulated in accordance with available engineering and construction blueprints and field observations. Granite rock of scaled-down dimensions (12 to 16 cm^3) was used to model these as well as other structures tested in the model (Chapter VI).

4.3.3 Dredging Simulation

The model was constructed so as to simulate the condition where the sand trap was nearly full to capacity and the beach south of the inlet was considerably eroded. This trap area was marked in the model. Calculations based on the relationships developed by Keulegan (1967) were made (Section 3.2) to determine changes in the flow conditions brought about when the trap is dredged.

4.3.4 Aesthetics

Upon completion of construction, the model was painted so as to provide an aesthetic quality as well as a clearer representation of the overall layout. The model was painted blue, white, and beige to represent water, sand, and vegetation (land) respectively and to indicate the boundaries between these regions.

As mentioned, the model area was extended beyond the immediate study area so that the flow boundary conditions would not be altered by later modifications within the study area. In addition, these modifications were not expected to have any considerable effect on the amount of inflow or outflow taking place during a tidal cycle and, therefore, no significant change in the flow conditions at the boundaries were expected (or subsequently observed as noted in Section 6.4).

Figure 4.1 shows the layout of the model while Fig. 4.3 shows a view of the completed model.

4.4 Instrumentation

In addition to bathymetry, proper modeling of the hydraulic characteristics requires accurate simulation of wave height, direction and period, as well as flow velocities and water surface elevations. Simulation of these parameters is achieved by instrumenting the model with means to both induce and measure specific values of these parameters. The following five sections describe the instrumentation employed in the model so as to insure accurate reproduction and measurement of hydraulic parameters.

4.4.1 The Wave Generator

Prototype wave conditions were simulated by a snake-type wavemaker described in Section 4.1. The wave maker was modified by the addition of a continuous motor driven frequency alternator as well as a counter for the paddle cycle such that the wave period (or frequency) could be automatically varied and measured simultaneously, thereby allowing for fine-tuning of the wave period. Appendix G presents the theory and calculations involved in generating the properly modeled waves for this study.

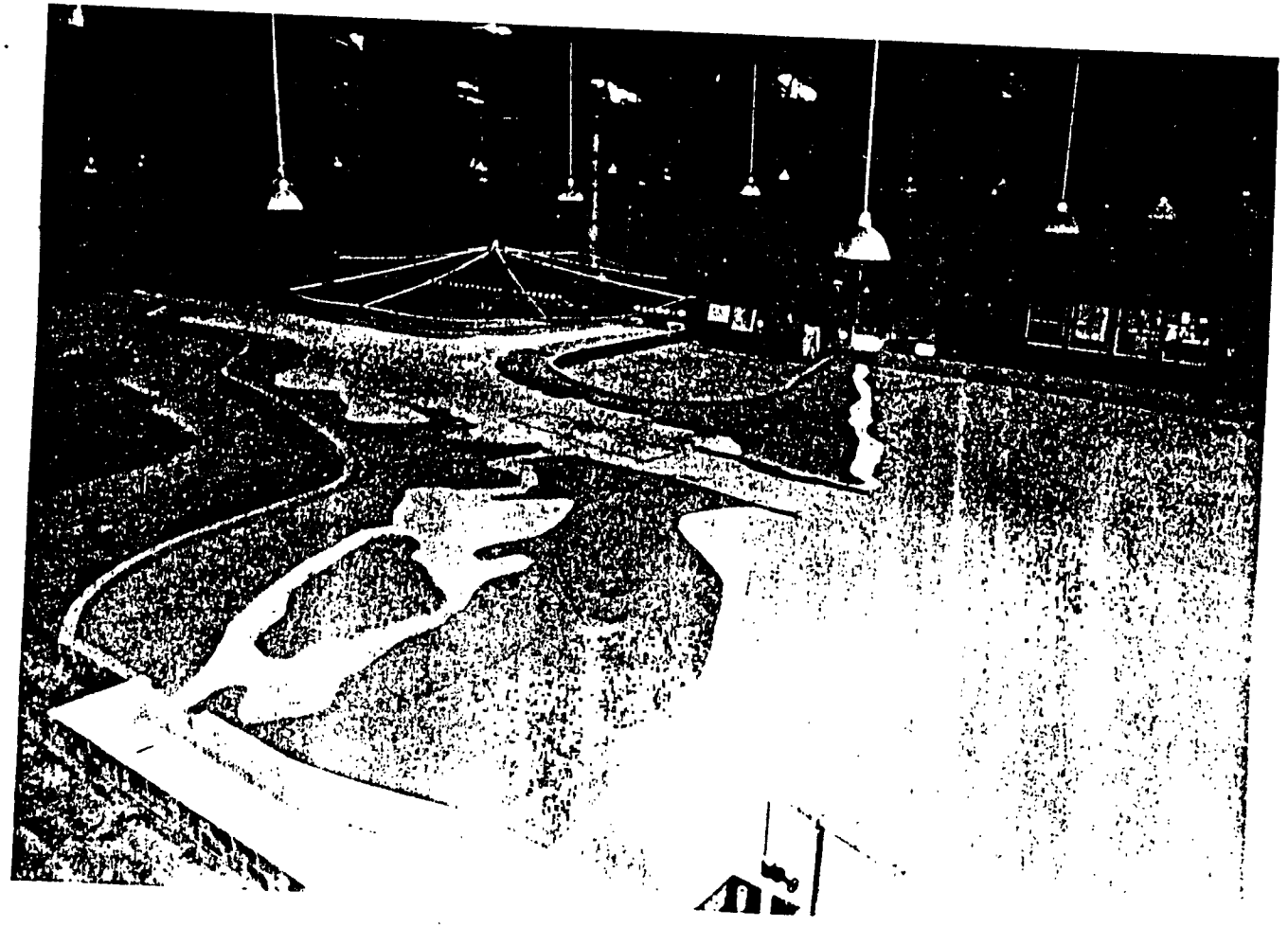

Fig. 4.3a. A View of the Model.

Fig. 4.3b. A View of the Model as Seen from Offshore.

4.4.2 Capacitance Wave Gage

A capacitance type wave gage was installed in the ocean portion of the model at a depth corresponding to 3 m in the prototype. The purpose of this gage was to ensure that the waves induced by the wave generator were of the scaled-down height and period corresponding to the required prototype wave conditions at this depth. The gage was statically calibrated for height when the wave basin was flooded or drained by recording 1 cm depth increments on a strip chart. Wave period was determined from the strip chart for a given chart speed. A north arrow was drawn at the base of the gage relative to the shoreline orientation for determining wave direction at this point.

A portable capacitance-type gage was also constructed for the purpose of measuring the wave activity at different locations inside the inlet. This gage was calibrated in a similar fashion.

4.4.3 Pumps, Weir Boxes and Weir Gates

Currents were simulated through a system of pumps, weir boxes and weir gates incorporated into five bays in the model as shown in Fig. 4.1. Flood currents were achieved by pumping water through the weir boxes into bays 1 and 2 and lowering the weir gates in bays 3, 4, and 5 thereby causing the water to flow into the inlet. Ebb currents were simulated in the converse manner by pumping water through the weir boxes into bays 3, 4, and 5 and lowering weir gates in bays 1 and 2. Figure 4.4 shows a typical pump and weir box system and Fig. 4.5 shows a typical weir gate used in the model.

4.4.4 Current Meters

A Kent mini-flow impeller meter and a Marsh-McBirney electromagnetic meter were used to measure flow velocities at specific

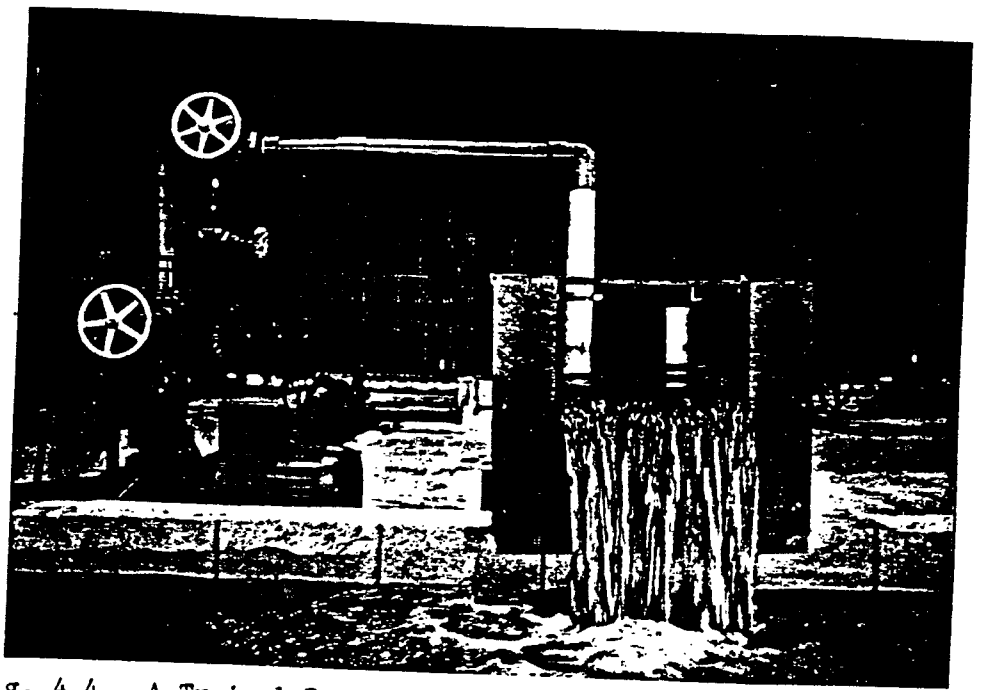

Fig. 4.4. A Typical Pump and Weir Box System Used in the Model.

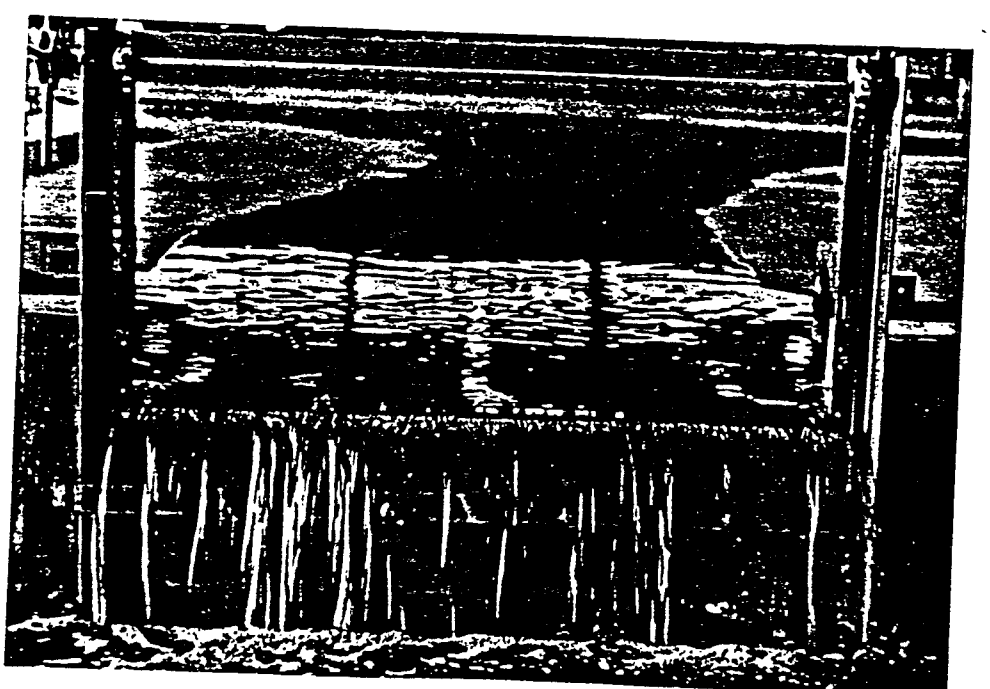

Fig. 4.5. A Typical Weir Gate Used in the Model.

locations in the model. The meters were first used for model calibration to ensure proper simulation of the flow velocities in the ebb, flood and storm surge conditions. The meters were then used to determine flow velocities at specific locations in the inlet under its existing condition as well as after solution options were implemented.

4.4.5 Stilling Wells

Seven stilling wells were employed in the model so as to provide for the measurement of the tidal elevations in the study area. A PVC pipe connected each of the stilling wells to a point on the model bottom that corresponded to one of the tide boxes installed in the prototype (see Fig. 4.6). The water level in each stilling well (equal to the water level at the corresponding tide gage location) was measured by a Lory Type-C (0.1 mm) hook gage.

4.5 Calibration and Verification

The model was calibrated and verified to ensure that the prototype hydraulic conditions were accurately simulated. Model calibration involved calibrating the weir boxes, stilling wells and the wavemaker. Verification entailed conducting tests so as to ensure that the hydraulic characteristics at all locations in the inlet were simulated appropriately. Model data and prototype data were then compared for specific locations so as to determine the accuracy with which the model reproduced the prototype. For a fixed-bed, undistorted model, these data consist of flow velocities and water surface elevations, or more specifically, the difference between these elevations, at different locations in the inlet. The following two sections provide a discussion of the two main components of the calibration and verification scheme.

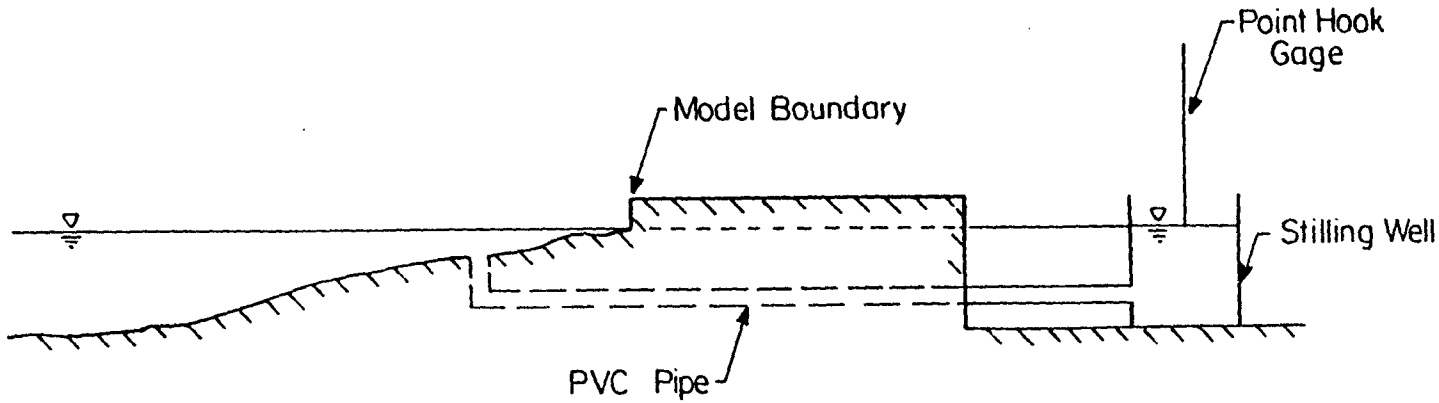

Fig. 4.6. Stilling Well Scheme.

4.5.1 Flow Calibration

Simulation of current velocities was achieved for the flood, ebb, and storm conditions by regulating the pump discharges and weir gate elevations until the desired conditions were obtained at all points in the model. The first step involved calibrating for the discharge through the weir boxes via the equations (King, 1976):

$$Q = \frac{8}{15} C_V \tan(\theta/2)\sqrt{2g}\, H^{5/2} \qquad (4\text{-}1)$$

$$Q = C_R L\, H^{3/2} \qquad (4\text{-}2)$$

Equation (4-1) applies to V-notched weirs while equation (4-2) applies to rectangular notched weirs. A description of the parameters in Equations (4-1) and (4-2) is provided in Fig. 4.7. The coefficients C_V and C_R were determined by measuring the time required for each weir box to fill a 75 liter bucket (resulting in a discharge value), noting the geometry of the notch and the height of the water flowing through the notch. Appendix H presents the procedure.

The proper distribution of discharges into the different reaches of the model (and hence the proper flow velocity in each reach) was achieved by regulating the heights of the respective weir gates. The weir gate elevations were varied based on educated guessing and a knowledge of the inlet flow characteristics while the velocities at each location listed in Table 4.1 were continuously monitored by the Kent flow meter. When the velocities were obtained for each location in accordance with Table 4.1 (or as near as possible to these values) the elevation of each weir gate was recorded so that the condition could be reproduced. Several times over the course of the study, flow velocities were measured at these weir gate settings to verify that the desired flow conditions were reproduced at these settings.

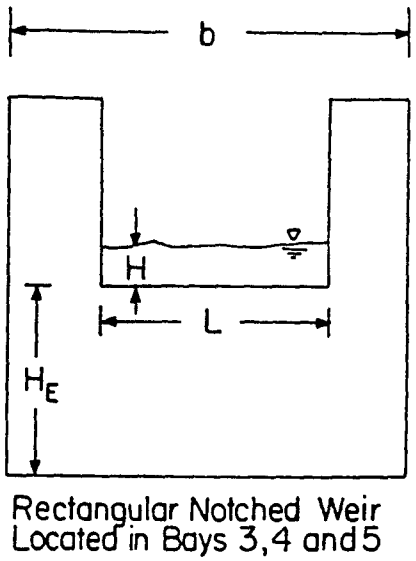

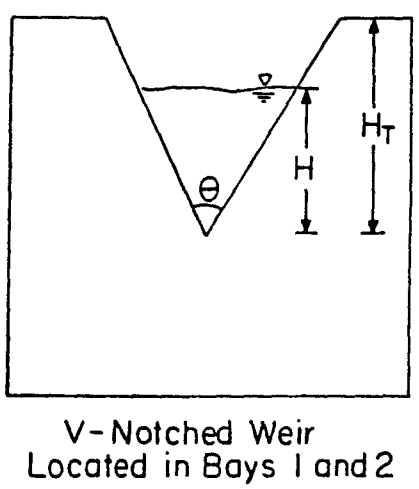

Fig. 4.7. Two Types of Weir Boxes Used in the Model.

Table 4.1. Verification of Flow Velocities

TIDE	FLOOD			STORM-FLOOD*			EBB		
Location	Req.** (mps)	Ob.** (mps)	% Diff. (Flood)	Req. (mps)	Ob. (mps)	% Diff. (Storm)	Req. (mps)	Ob. (mps)	% Diff. (Ebb)
T-1	0.31	0.31	0.0	0.48	0.48	0.0	0.37	0.37	0.0
T-2A	****	****	--	****	****	--	****	****	--
T-2B	****	****	--	****	****	--	****	****	--
T-2C	0.31	0.28	9.7	0.46	0.42	8.7	0.27	0.27	0.0
T-3	0.12	0.12	0.0	0.17	0.17	0.0	0.07	0.07	0.0
T-4	0.15	0.15	0.0	0.24	0.18***	25.0	0.27	0.21***	22.2
T-5	0.08	0.08	0.0	0.13	0.13	0.0	0.07	0.07	0.0

*1.5 meter storm surge
**"Req." refers to values necessary for exact scale reproduction while "Ob." refers to values obtained in the model.
***Velocity is suspected to be lower due to flooding over the bulkheads
****Represents locations where no velocity records were taken

4.5.2 Tide Level Calibration

The stilling wells were calibrated by first determining the hook gage reading (water surface elevation) corresponding to the mean sea level. The difference between this reading and that taken at several different still water elevations revealed acceptable consistency and accuracy in all seven stilling wells.

Tidal elevation differences at different locations in the inlet occur when water flows through the inlet and energy is dissipated due to bottom friction resulting in a head loss between two locations. These differences were obtained from the prototype tide records at each of the seven tide gages. If the model is accurately constructed, the flow velocities properly simulated and the prototype data correct, then the water surface elevation differences in the model (as indicated by the stilling wells) should be accurately scaled according to the prototype conditions.

4.6 Roughness Elements

In theory (Bruun et al., 1966), for an undistorted model, water surface slopes caused by energy losses due to bottom friction should be of the same value in the model as in the prototype (i.e. $n_{slope}=1$), provided the flow velocities are properly scaled. This was an area of concern for the inlet model due to the differences in the bed roughness between the natural sand bottom in the prototype and the concrete bottom of the model. In addition, the sand in the prototype constantly shifts throughout the tidal cycle thereby continually altering the effective bed roughness everywhere. Shifting sand is not accounted for in the model and this fact served as a possible contribution to likely inconsistencies between water surface slopes in the model and in the prototype.

In most cases where the model roughness does not properly scale that of the prototype, it is because the model roughness is not of sufficient magnitude to reproduce the bottom dissipation in the prototype. This in turn implies that surface slopes in the model will be less than those in the prototype. A possible method for compensating for this lack of roughness in the model is to place roughness elements at pre-determined locations so as to increase bottom dissipation and, correspondingly, the water surface slopes. Appendix E discusses the theory and calculations made in determining the location of roughness elements in an undistorted physical model.

4.7 Calibration and Verification Results

If the flow discharge conditions through the boundaries are simulated with reasonable accuracy, then the flow velocities and water surface elevations should be simulated accordingly. Tables 4.1 and 4.2 list the flow velocities and tidal elevations measured in the prototype and then reproduced in the model during the ebb and flood tidal stages corresponding to maximum flow velocities at the inlet mouth. These values are listed as well for a 1.5 m storm surge as based on the calculations in Appendix A. Observed percent differences are likely to be due to incorrect model construction or errors in prototype data collection. As seen in these tables, the velocities, tide levels and tide level differences were satisfactorily scaled, thereby verifying the model flow conditions.

One inconsistency was noted at the Lighthouse Location (T-4) where the model velocity was lower than that in the prototype during both ebb and storm flows. This inconsistency is attributed to the fact that water tended to flood over the bulkheads in this area of the model,

Table 4.2. Verification of Tide Elevations

TIDE	FLOOD			STORM-FLOOD*			EBB		
Location	Req.** (cm)	Ob.** (cm)	% Diff. (Flood)	Req. (cm)	Ob. (cm)	% Diff. (Storm)	Req. (cm)	Ob. (cm)	% Diff. (Ebb)
T-1	0.60	0.60	0.0	3.7	3.65	1.3	0.70	0.60	14.3
T-2A	0.50	0.42	16.0	3.60	3.50	2.8	0.50	0.60	16.7
T-2B	***	0.45	--	***	3.50	--	***	0.50	--
T-2C	0.50	0.40	20.0	3.60	3.50	2.8	0.60	0.70	14.3
T-3	0.24	0.26	7.7	3.34	3.30	1.2	1.00	1.00	0.0
T-4	0.70	0.58	17.2	3.80	3.40	7.7	0.90	0.80	11.1
T-5	0.40	0.40	0.0	3.50	3.50	0.0	0.20	0.20	0.0

*1.5 meter storm surge
**"Req." refers to values necessary for exact scale reporduction while "Ob." refers to values obtained in the model.
***Data inadequate

thereby resulting in velocities that were 20 to 25 percent lower than the scaled prototype values. It should be noted however that the proper discharge through this area was maintained for each flow condition and therefore the contribution of this area to the overall flow regime was accurately modeled.

CHAPTER V

POTENTIAL SOLUTIONS

5.1 Overview

Certain options are available as potential solution schemes to the problems of erosion and deposition at the inlet. These schemes each consist of two parts: the solution plan and the means to execute this plan.

Solution schemes were chosen after review and consideration of the hydraulic and sedimentary processes occurring at the inlet. These schemes consisted of a combination of structural and non-structural designs. The schemes were modeled and tested (Chapter VI) under maximum ebb flow, maximum flood flow and storm surge (flood) conditions. These conditions correspond to those during which rates of erosion and deposition are most likely to be of the greatest magnitudes.

Once the optimal solution schemes are decided upon, a method of implementing and maintaining them must be determined. To be considered feasible, this method must satisfy different requirements prior to implementation. These requirements include meeting economical and environmental criteria as well as maintenance efficiency and practicality.

The following section presents the solution options that were initially considered to be appropriate to remedy the problems at the inlet. These solutions are based on physical characteristics, existing and resulting flow conditions and the intended future use of the inlet

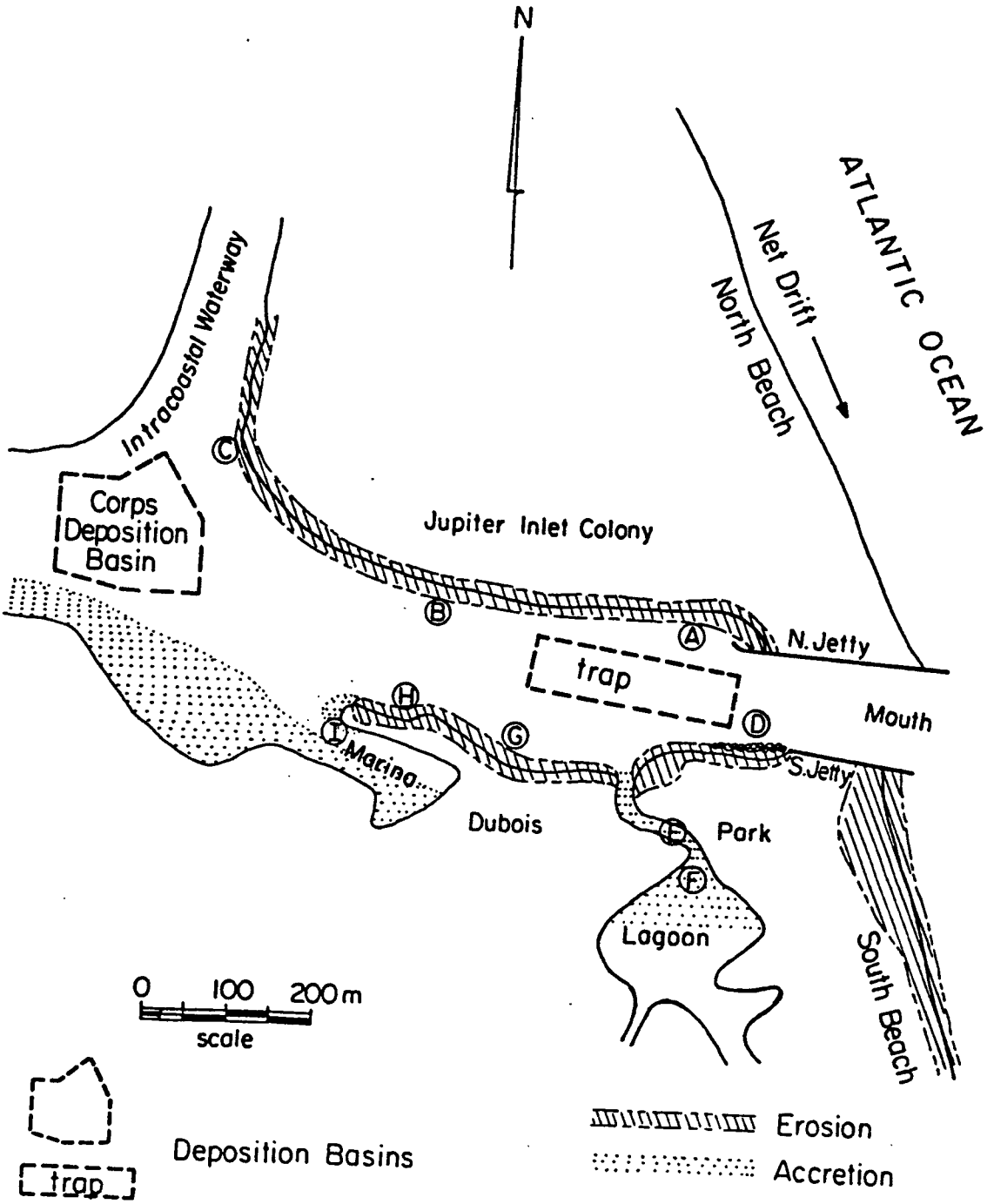

Fig. 5.1. Problem Areas of Erosion and Deposition.

shoreline and waterways. The results of the tests of these solutions are presented in Chapter VI.

5.2 Solution Options

The solution options initially developed were site specific within the study area. These sites are designated in Fig. 1.5 which has been reproduced as Fig. 5.1.

Site A encompasses the shoreline area just west of the north jetty. This area has undergone erosion of the beach within the cove area as well as deterioration of the bulkheads along the westward reach of this site. This erosion is believed to be due primarily to the observation that as waves enter the inlet they diffract and refract in such a manner that this shoreline becomes exposed to a relatively direct attack by the waves. Eddy currents, due to flow separation just inside the entrance at flood tide, also act as an erosive force as they resuspend sediment. All three phenomena (diffraction, refraction and eddies) were observed in the model. The resuspended sediment is carried away from this area by flood tidal currents as well as by set-up currents caused by the diffracting waves.

The solution proposed for testing in the model is illustrated in Fig. 5.2. A weir-groin would first be constructed in the location where there are presently the remains of a previous groin, and the area to the east of the groin would be nourished with sand. The weir-groin would be designed on a slope such that it maintains an elevation 0.3 m above the nourished profile at any point. The structure would then sharply taper to above high tide level at the bulkhead. This should result in a narrow beach at the bulkhead at all stages of the tidal cycle but would not starve the westward reach of the north shoreline as sediment could

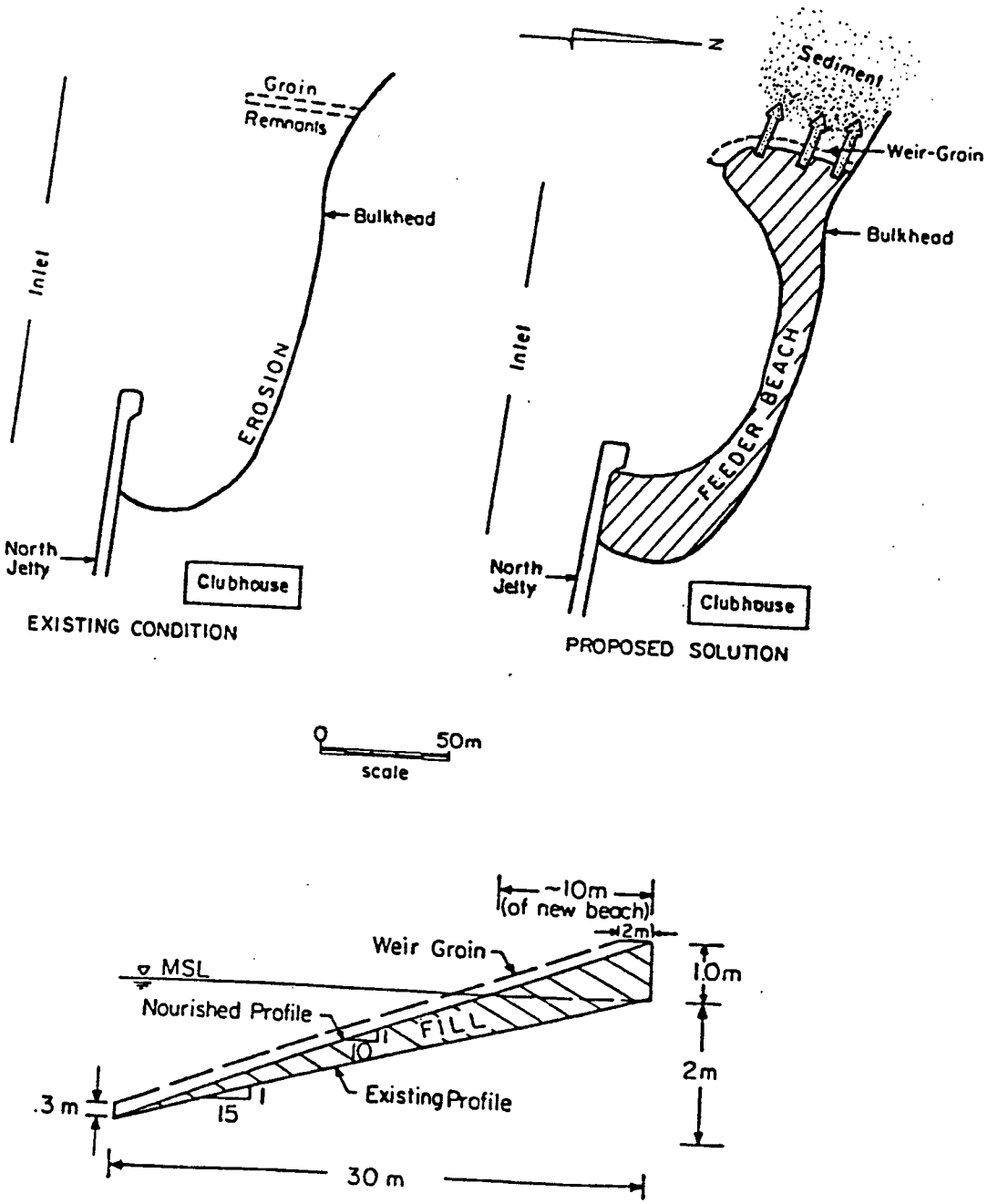

Fig. 5.2. Plan and Profile of the Existing Condition and Proposed Solution to Problem Site A.

be transported westward once it accreted to the elevation of the weir-groin. The beach east of the weir-groin would act as a feeder beach to the north shoreline and would therefore require periodic renourishing.

Bulkhead deterioration exists in different degrees along different segments of site B but is of the same general nature and is due to the same causative forces. Strong currents and waves concentrated along the shoreline here result in scour at the toe of the bulkhead. In addition, exposure to repeated wave action contributes to the long-term fatigue of the bulkheads.

Initially it was felt that a shoreline armoring scheme using rip-rap placed in accordance with the requirements of each site would be the solution to the problems associated with this shoreline. This rip-rap interspersed with sand from the adjoining feeder beach would provide a buffer zone protecting the bulkheads from waves as well as currents. This option was deemed unfavorable because of questions regarding financial liability should further bulkhead deterioration occur along a particular shoreline segment after the rip-rap was specifically placed to prevent such deterioration.

An alternative solution, shown in Fig. 5.3, consists of placing a sheet-pile flow deflector at an approximately constant distance from the shoreline and connecting with the shoreline at a location directly across the inlet from the west end of the Dubois Park beach. This deflector must be placed at an elevation just above that of the highest 28 day tide level (+1 m) and should be of sufficient length to prevent flood tidal flows from attacking the shoreline here. The flow would be diverted into the middle of the channel and into the north and west reaches of the Intracoastal Waterway. The deflector was tested at

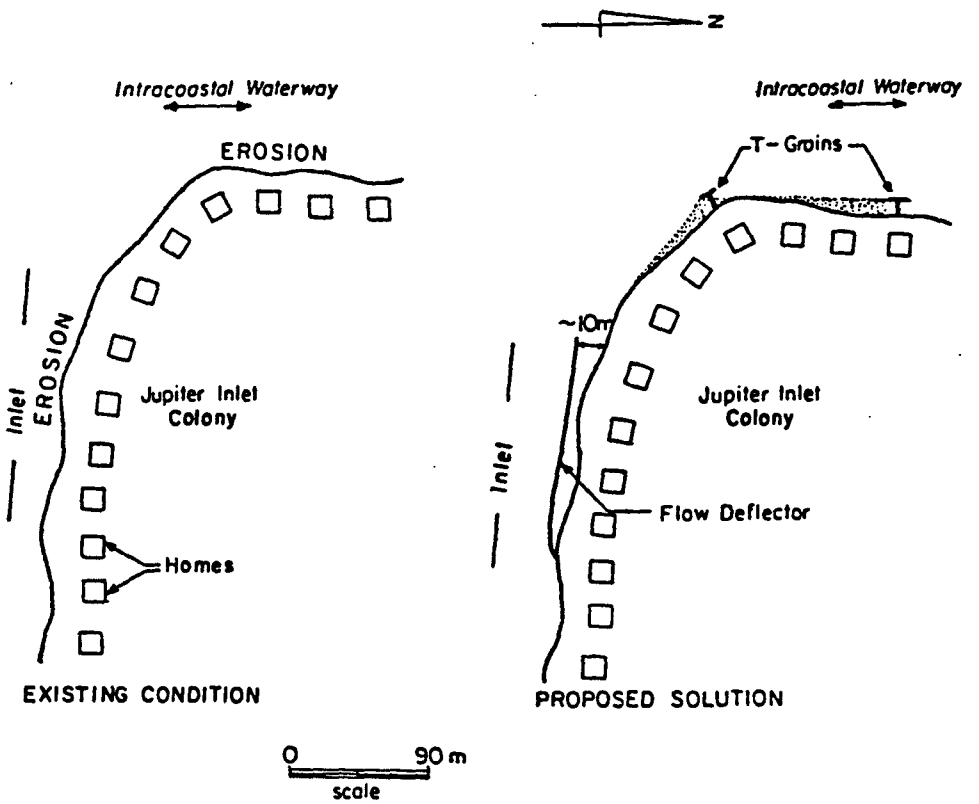

Fig. 5.3. Existing Conditions and Proposed Solution for Problem Sites B and C.

different lengths and with gaps at different locations to allow for water exchange. The tests also provided an indication as to the possibility of any adverse side effects resulting from the deflector during an ebb tidal flow.

Site C consists of the westward extent of the north shoreline as it winds into the northern reach of the Intracoastal Waterway. This shoreline is in various states of disrepair ranging from natural eroding beaches, beaches armored with rip-rap, bulkheads showing signs of imminent failure to bulkheads that have fallen into the water. This erosion and bulkhead deterioration is believed to be caused by a combination of boat wakes as well as scour induced by the high velocity flood currents existing at this site. Accordingly, recommendations to limit the magnitude of boat wakes by regulating boat speeds in this area have been made (Section 5.4). In addition, schemes consisting of the placement of different groin combinations (see Fig. 5.3) for the purpose of retaining sand along the shoreline, were proposed for testing in the model. These groins would be implemented in the event that the reduction of boat wake magnitudes is not by itself sufficient to remedy the problems here. It is also believed that the aforementioned flow deflector will divert the flood flow from directly attacking the shoreline here as it winds into the northern reach of the Intracoastal Waterway.

Site D consists of the area immediately west of the south jetty where erosion has occurred. As verified through sediment analysis (Section 3.9) this erosion is believed to be due to the channeling of the flow south of the rocks (comprising the west extension of the south jetty) towards the Dubois Park lagoon. This flow occurs during very

high flood tides (e.g. due to storm surge conditions) when the water level is such that it penetrates well behind these rocks. This water escapes by being channeled at a high velocity towards the lagoon and, in the process, scours the sediment behind the rocks and transports it around and into the lagoon. This process results in the shoaling problems at sites E and F.

Placing more rocks at this location will not prevent water from penetrating these rocks as the structure would still be permeable. Construction of an impermeable structure at the east side of the mouth of the lagoon, while preventing sediment from being channeled into the lagoon, may not significantly reduce erosion of the area east of the lagoon behind the rocks.

The structural solution (shown in Fig. 5.4) proposed to remedy the erosion problem at site D, and thereby the shoaling at sites E and F, consists of two phases. The first phase, considered as a minimal measure necessary to solve the problems at these sites, involves extending the rock structure west of the south jetty around into the lagoon until it meets the bulkhead on the east bank of the lagoon. The west end of this extension would be made impermeable by pouring concrete over the rocks here. This would prevent sediment from being channeled into the lagoon as previously described but is not likely to prevent the erosion at site D.

The second phase of this solution is designed to prevent both the channeling of sediment into the lagoon and the erosion of site D. As in the first phase, this phase involves extending the rock structure west of the south jetty around into the lagoon until it meets the bulkhead on the east bank of the lagoon and pouring concrete over the west end of

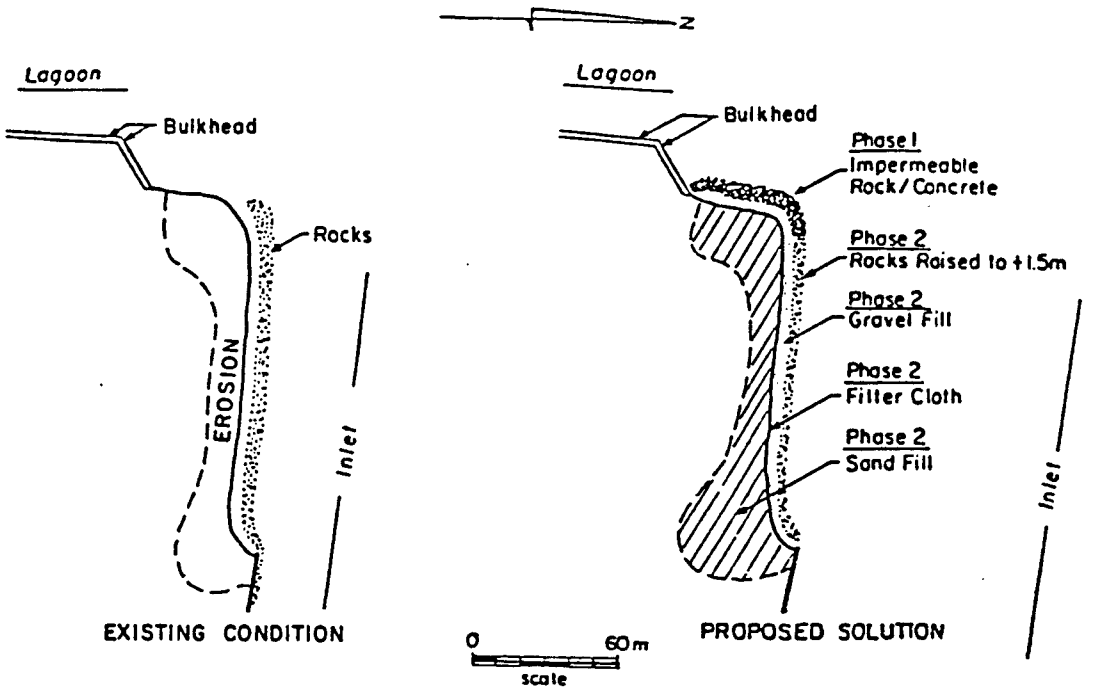

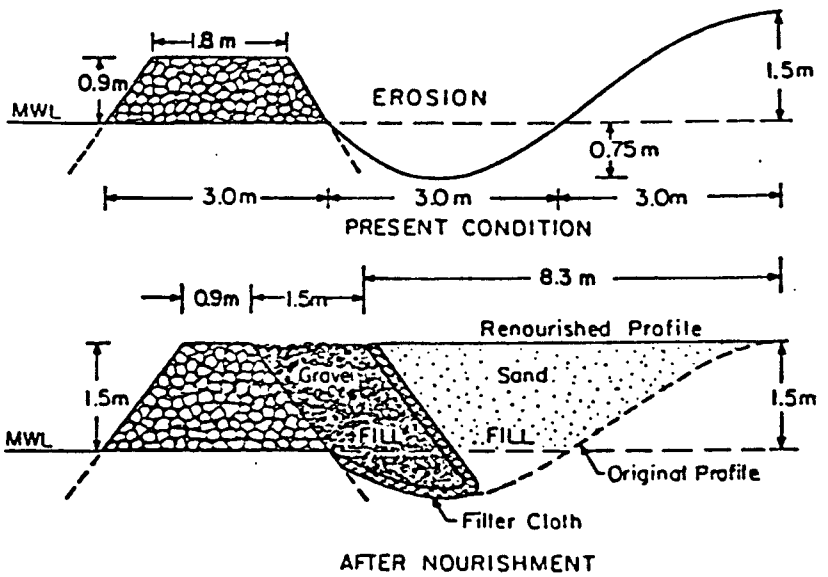

Fig. 5.4. Plan and Profile of the Existing Condition and Proposed Solution for Problem Site D (and subsequently, Sites E and F).

this extension. The elevation of this structure would then be raised to +1.5 m (same as the south jetty) and a 1.5 m layer of 1.3 - 5.0 cm gravel (5.0 cm standard sieve size) would be placed against its south side. Against this gravel, filter cloth would be placed (so that it tucks under the gravel) and sand would be filled south of this cloth to attain the desired topography. While the resulting structure will not be completely impermeable, the rocks and filter cloth should prevent the transport of high volumes of water and also prevent the sand from being carried away over and through the rocks. This phase is recommended if the erosion of site D is of major concern. If this is not the case, the first phase should be sufficient to prevent the shoaling of sites E and F.

Site G is located at the Dubois Park beach on the south shoreline of the inlet. This area once served as a popular swimming beach but has since eroded away. This erosion is believed to be due to: 1) refraction of waves entering the inlet such that they strike this beach, 2) the suspension and transport of sediment by current eddies near the shoreline and 3) transport of the sediment along the banks by the flood tidal currents. The proposed structural solution at this site (shown in Fig. 5.5) also consists of two phases. The first phase, consisting of the minimal measures, involves: 1) removing the existing concrete structures at the beach, 2) nourishing the beach with sand and 3) constructing groins at both end of the beach. Both groins would be curved (see Fig. 5.5) so as to retain the sand. Curving the east groin should also serve to attenuate the energy of the refracted waves reaching the beach here. The solution encompassing this first phase should reduce the erosive forces at this location and is anticipated to induce accretion immediately east and west of the beach.

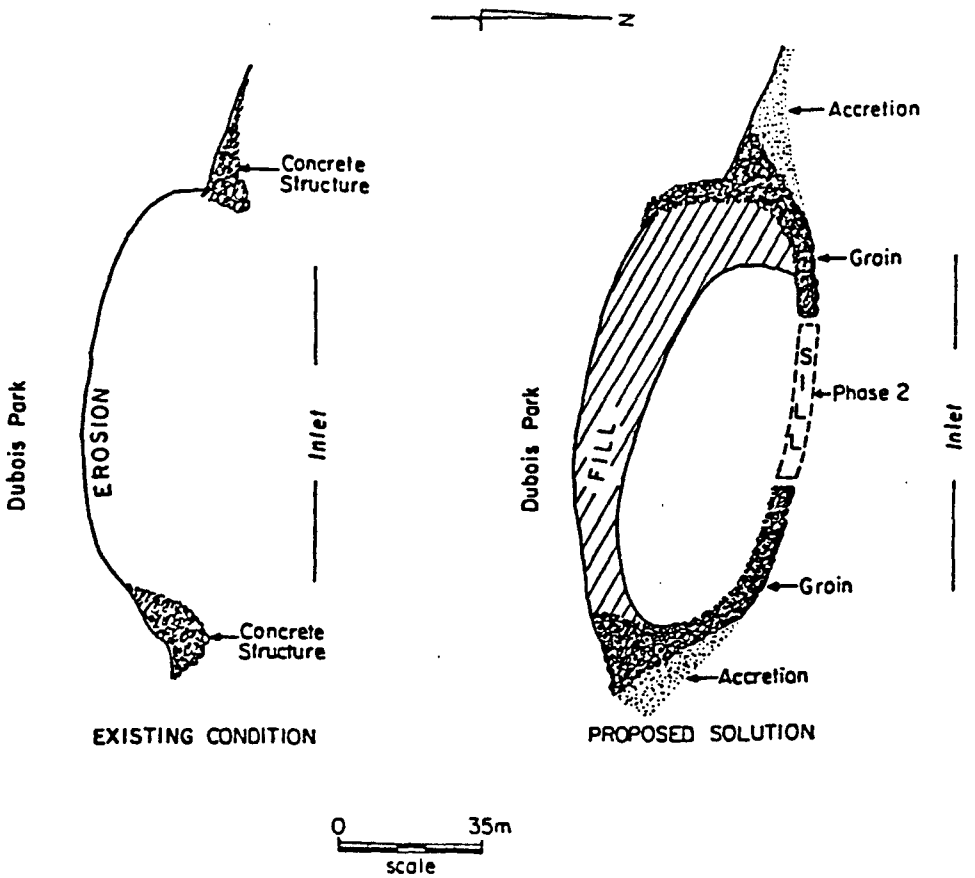

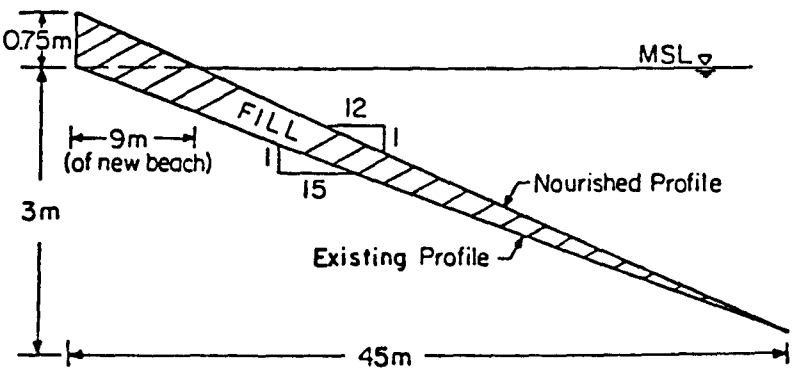

Fig. 5.5. Plan and Profile of the Existing Condition and Proposed Solution for Problem Site G.

The second phase consists of two options, both of which involve the placement of offshore sills parallel to shoreline. The first option consists of placing a sill between the two groins constructed in phase one (see Fig. 5.5). The elevation of the sill would be set at -0.5 m so that it is always below the waterline. The sill would serve to reduce the wave energy reaching the beach and to retain sand while still allowing for mixing and water exchange between the beach area and the inlet. The second option for this phase involves constructing a series of sills running offshore from the west end of the Dubois Park beach up to site H (see Fig. 5.6). As in option one the elevation of the sills would be set at -0.5 m so that they are always below the waterline and serve to attenuate wave energy and retain sand. Sills of various lengths and spacing were proposed for testing (see Fig. 5.6) so as to determine the optimum design for this option. These tests were also expected to provide an indication of the effect that the sills would have on the longhsore sediment transport in this region.

Site H encompasses the basin area on the north side of the promontory between the marina and the inlet. Problems in this area consist of shoaling in the eastern portion of the basin and erosion on the north side of the westward end of the promontory. Shoaling of the basin is believed to be due to the transport of sediment into this region by both flood and ebb tidal currents. Flow velocities in this basin are very low (0.1-0.2 m/s) such that any sediment transport into this basin will settle there. The erosion of the promonotory is believed to be a result of scour induced by high velocity currents passing this region as well as by both refracted waves and boat wakes striking this area.

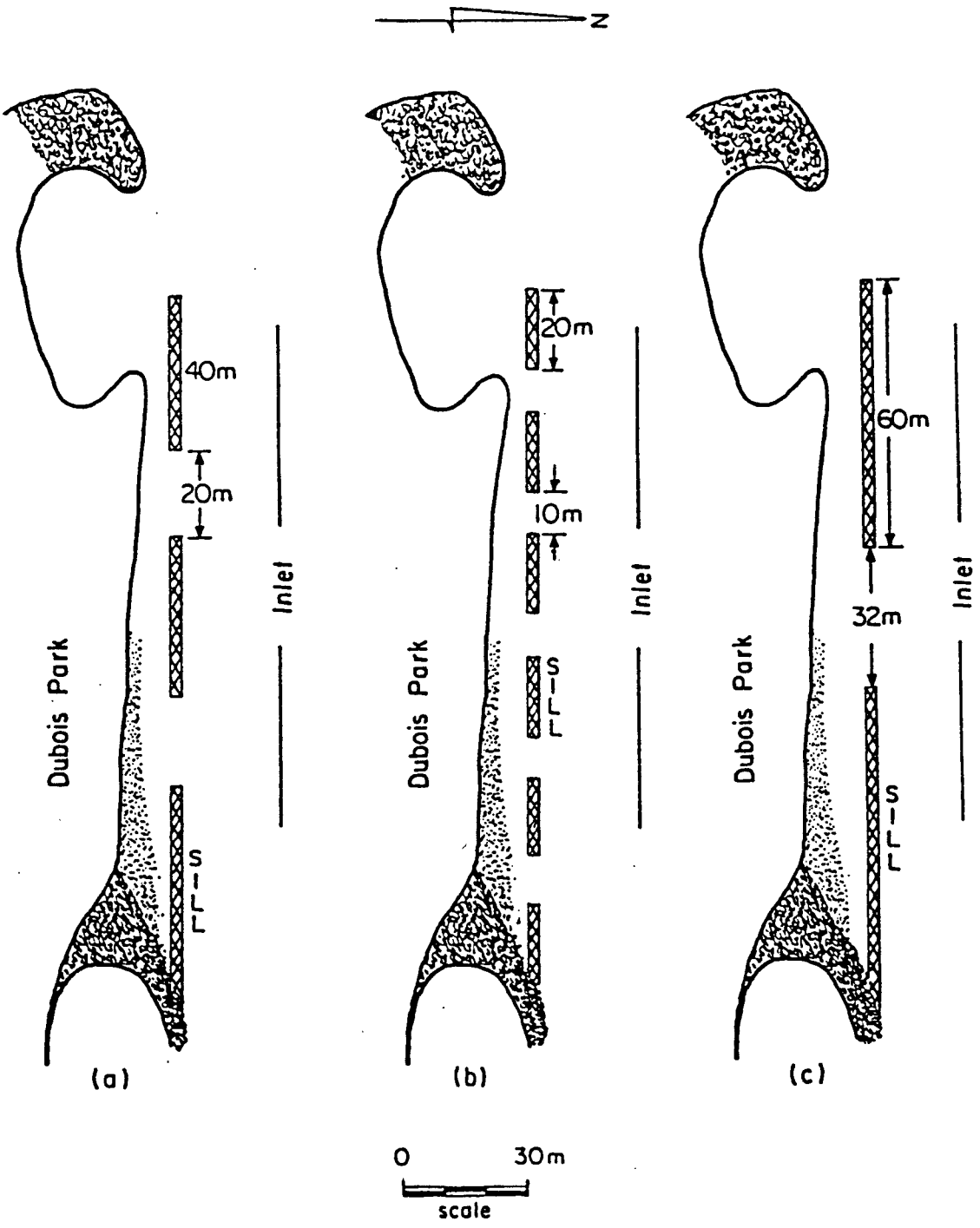

Fig. 5.6. Three Offshore Sill Schemes Tested as Possible Measures to Protect the Shoreline between Problem Sites G and H.

The solution proposed for this area, shown in Fig. 5.7, is designed to reduce erosion of the promontory but also includes an option to create a recreational beach here. The design for erosion prevention consists of extending (with rocks) the bulkhead that runs parallel to the promontory (see Fig. 5.7) up to the bulkhead running perpendicular to the promontory and removing this perpendicular section. The purpose of extending the parallel bulkhead with rocks would be to protect the north side of the promontory from wave and current attack. In addition, a structure acting both as a groin to retain sand and as an armoring measure to protect the tip of the promontory from waves and currents would be constructed at the west end of the promontory. The creation of a recreational beach along the north side of this promontory by nourishing this area exists as a possible option. The bulkhead plus rock extension and the groin would serve to retain the sand which would also act as a buffer further aiding in the prevention of the erosion of the promontory.

Site I consists of the westward portion of the marina area on the south side of the promontory where deposition is taking place. Two or three of the marina slips are now useless as the bottom is exposed at low tide. In addition, this deposition is beginning to constrict the marina channel thereby threatening boat accessibility. This deposition is believed to be due to the transfer of sediment into this area by currents. The flow velocities in the marina area are so slow (0.05-0.15 m/sec) that virtually all sediment transported here is permanently deposited. A large portion of this sediment is believed to be that which is eroded from the north side of the promontory as well as that which is transported along the north shore of the inlet by flood

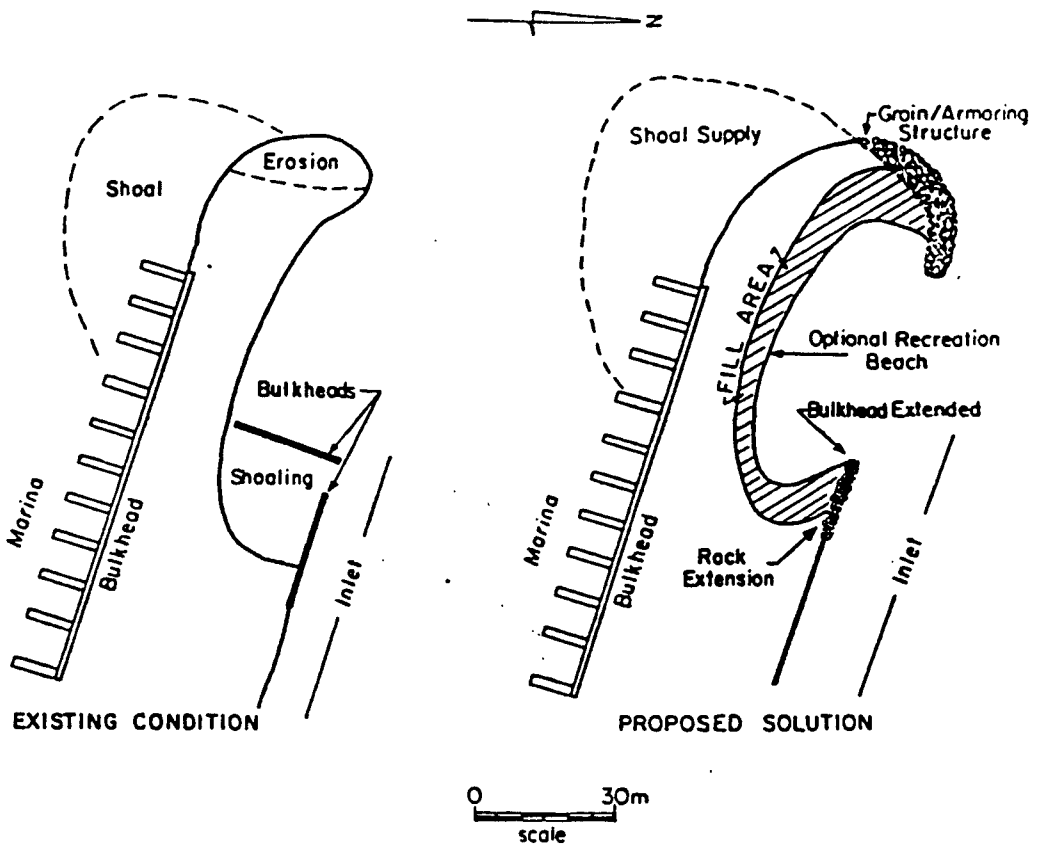

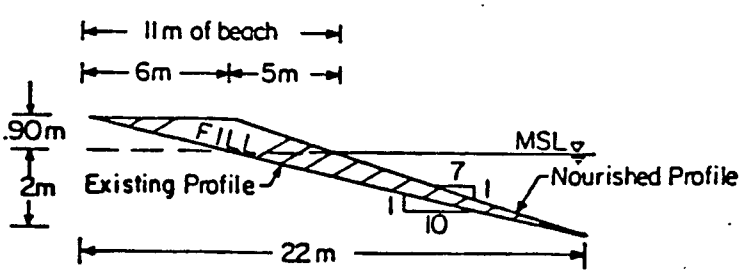

Fig. 5.7. Plan and Profile of the Present Condition and Proposed Solution for Problem Site H (and subsequently, Site I).

currents. It is believed that the solutions to the erosion at site H will reduce the amount of sediment available for deposition at site I. By minimizing the erosion of the north side and tip of the promontory, a part of the sediment supply to site I is cut off. Furthermore, the curved design of the groin at the tip of the promontory is expected to trap a significant portion of the sand transported inland by flood currents that may otherwise end up being deposited at site I.

5.3 Solution Implementation

Once the solution schemes to be tested in the model have been determined, it becomes necessary to develop a procedure for the implementation of these schemes in the prototype. Certain options exist as means of carrying out the various sand nourishment and removal measures. The objective would be that of providing for a self-contained maintenance program for the inlet area. This entails that, once the initial structures are put into place, the inlet will be self-sufficient in terms of sediment supply for areas where nourishment is proposed. This eliminates the option of trucking in sand from outside sources; an option that was previously ruled out due to inherent difficulties in accessibility to the problem areas by vehicle. Figure 3.15 substantiates the fact that there is a sufficient sand supply within the inlet to allow for continual nourishment of all the proposed shoreline areas. Sediment analysis (Section 3.9.2) reveals that there are sufficient quantities of sand (38,000 m^3) in the areas of the inlet undergoing shoaling to provide the sand volumes necessary for initial nourishment (6,000 m^3) as well as for continual maintenance at the locations for which this operation is proposed. Any additional sediment may be obtained from the sand trap area without any significant effect

on the overall sand volume (7% maximum) bypassed from the trap to stabilize the south beach.

Having established a supply of sand, the next question is one of transporting the sand from the supply locations to the locations requiring nourishment. Three methods are likely options; transport by 1) a single portable hydraulic dredge other than the one currently used in the bypassing operation, 2) a jet pump system or 3) the dredge currently used on occasions when the sand trap is dredged. These options will now be discussed further.

5.3.1 Portable Hydraulic Dredge

Portable hydraulic dredges, with their relatively high degree of mobility, small draft, single unit construction and sometimes even amphibious capabilities are available for "small volume maintenance" of areas such as Jupiter Inlet. The employment of such a dredge could provide a means to both excavate areas of sediment deposition and renourish areas of erosion in the inlet. In some instances, the sediment excavated from one area undergoing deposition could be directly transferred to another area of erosion. Such a dredge could satisfy the maintenance requirements of the inlet including the sand trap-bypassing operation. The portability of such a dredge would also allow for the dredge to be loaded onto and then operated from a flat-bed truck so as to excavate the Dubois Park lagoon.

A survey of portable dredges available in the United States was conducted by the Corps of Engineers (1983) and from this survey four dredges were chosen as possibly suitable for the requirements of the inlet. These dredges and their most pertinent specifications are listed in Table 5.1. It should be noted that the maintenance requirements of

Table 5.1. Dredge Summary Chart (Corps of Engineers, 1983)

Dredge/ Company	Length (m)	Width (m)	Weight kg	Draft (m)	Anchoring System	Cutter-Type	Digging Depth (m)	Production Rates m^3/HR	Pumping Distance (m)	Price[4] ($)	Operating Cost[5] $/HR
D-24-1/ MUDCAT[1]	10.5	3.0	15,500	0.55	Spuds & Winches	Cutter-Head	4.6	70-110	To 625	122,000	50
D-30/ MUDCAT	12.2	3.7	21,000	0.61	Spuds & Winches	Cutter-Head	7.6	85-150	To 625	156,000	65
MD-815B/ (VMI)	12.2	2.5	6,900	0.50	Hydraulic Winch	Horizontal Cutter	4.6	150	---[3]	123,500	65
MD-820/ (VMI)	14.0	2.5	11,350	0.50	Hydraulic Winch	Horizontal Cutter	6.1	150	---[3]	132,500	83

NOTES: 1 - Mud Cat Division of National Car Rental System, Inc.
2 - Vaughn Maitlen Industries (VMI)
3 - Calculated from Capacity
4 - 1983 Price
5 - 1983; includes depreciation, insurance, interest, taxes, repair parts, labor (2 men @ $12/hr).

the inlet, with the exception of the sand-bypassing operation, are of such low relative magnitude that the dredges best suited for implementation here are among the smallest available.

5.3.2 Jet Pump

A jet pump system consists of the pumping unit with several flexible pipes attached to provide pumping power from an onshore injector and to transfer the sand to its deposit site. The injector pump propels a high velocity water jet into the jet pump (see Fig. 5.8) which is located on the bed at the point where sand will be removed. This water passes through a venturi nozzle and is converted to a high velocity, low pressure jet stream within the pump. This low pressure induces suction resulting in a flow of surrounding water and sand (slurry) through the intake and into the mixing chamber. The momentum from the jet stream drives the slurry through the mixing chamber accelerating it for transfer through a discharge line to be deposited at the nourishment area (DeGraca, 1975).

Jet pumps have been employed at inlets in Florida and Virginia and have had fairly favorable results. The main drawback, however, has been in the maintenance requirements to keep the pump in operating condition and prevent clogging during times when it is not in use. These problems arise when the pump is in a permanent operating location, is not required year round, and as a result is often neglected during periods of non-use. It is possible, however to transport the pump from one location to another by filling the jet pump with air and floating it in place (DeGraca, 1975).

Such a transportability would be suitable for maintaining different areas of Jupiter Inlet. Due to the small volumes involved at each of

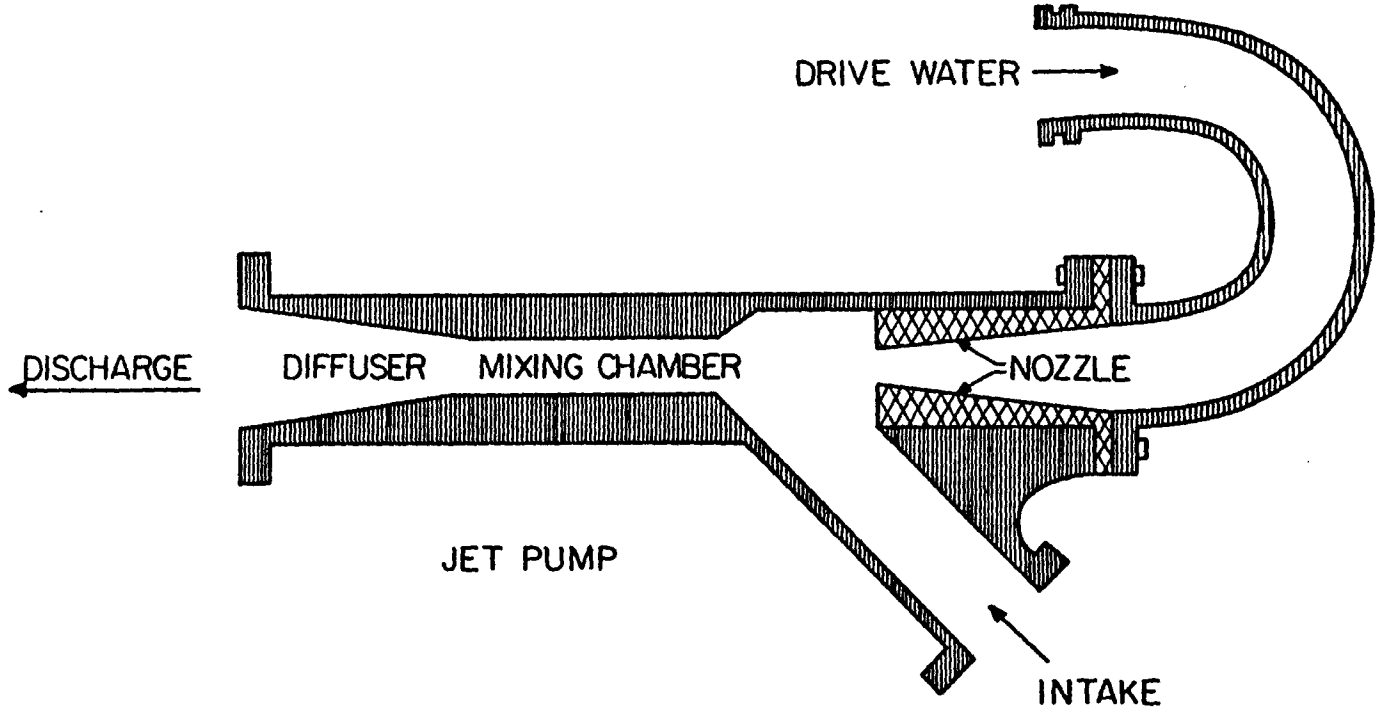

Fig. 5.8. Schematic of a Jet Pump (Jones, 1977).

the problem areas, the jet pump would only be needed for a relatively short time at any one site. The pump could be transported from one site to another temporarily and would thereby operate continually and avoid the aforementioned drawback. Indeed at any time when the pump was not needed to maintain the channel or shoreline areas, it could operate in the sand trap, bypassing sand to the south beach. In addition, the pumping house could be made portable by mounting it on a flat-bed trailer. This would allow the pumping house to be located as close as possible to the areas undergoing sediment removal and renourishment (within 200 m) thereby eliminating the need for a booster pump. The transportability of the jet pump combined with the relatively low cost, uninterruption of navigation, no moving parts (in the jet pump), and the virtual invisibility of the operation to an observer make the employment of a jet pump system a possible option for the channel and shoreline maintenance at the inlet. Figure 5.9 shows a possible layout of such a jet pump scheme.

5.3.3 Bypassing Dredge

Utilization of the dredge employed on occasions when the sand trap is dredged would appear to be an economical means of nourishing and dredging other areas of the inlet. Certain criteria would have to be met, however, for this option to be feasible.

The relatively large size of the dredge currently used at the sand trap may mean that problems of accessibility to areas within the inlet could be encountered. In addition a dredge of such large pumping capacity may not be capable of accurately placing the relatively small quantities of sand required for nourishment of the shoreline areas within the inlet. Another likely drawback is the fact that the sand

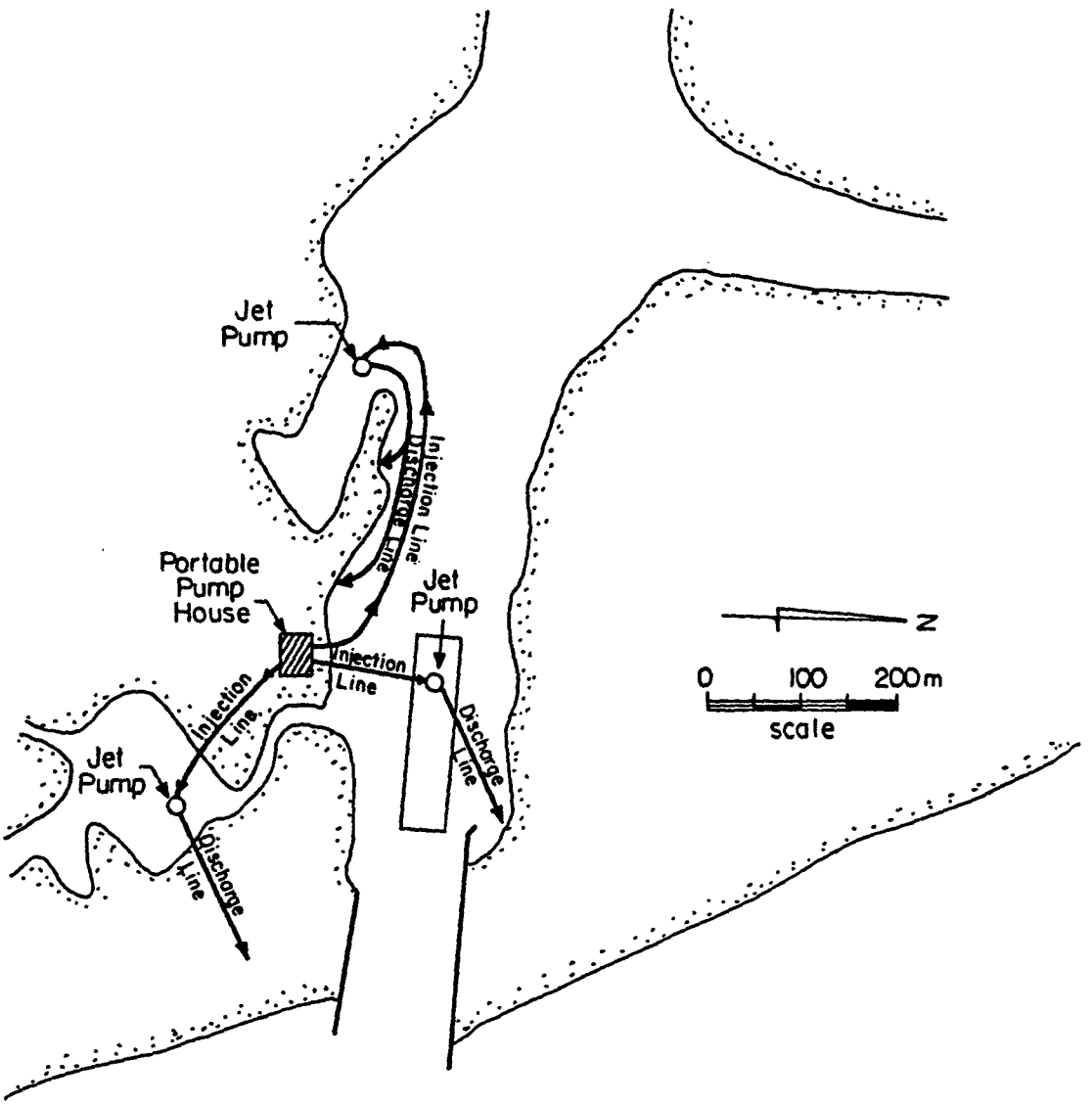

Fig. 5.9. Three Possible Modes of Employing a Single Portable Jet Pump at Jupiter Inlet.

trap dredging operation takes place once every two to three years. While the solutions involving nourishment include measures to retain sand, it is difficult to predict how often each site will require renourishment (particularly the feeder beach at site A). As a result, it is possible that the dredge may not be available when certain sites are in need of renourishment.

5.4 Boat Wakes

In addition to scour induced by currents, a significant cause of bulkhead failure and shoreline erosion at the inlet is believed to be the forces due to boat wakes. Shoreline erosion due to boat wakes is a direct result of the erosive forces of waves as they break onshore. Bulkhead failure results from the impact and resulting scouring forces exerted by waves. Although bulkheads are ideally designed to withstand the impact forces due to waves, occasionally the combination of 1) repeated exposure to these forces, 2) scour at the base of the bulkhead and 3) erosion of the land area behind the bulkhead in the event of flooding can result in failure. This appears to be the case at several locations along the northern shoreline.

The impact forces of non-breaking waves are directly proportional to the height of the waves as they come in contact with the bulkhead (Sainflou, 1928). Shoreline erosion due to waves may also be considered proportional to the wave height as this determines the extent of wave uprush which in turn determines the amount of shoreline exposed to these erosive forces. The height, pattern and phase of these waves are dependent upon the size, draft, speed and geometric form of the boat generating them as well as the depth of the water in which they are generated. With the exception of boat speed, none of these variables

are realistically controllable. As a result, it would appear that restricting boat speed in the inlet would constitute a possible solution for reducing shoreline erosion and bulkhead failure due to boat wakes.

Waves caused by boats act as shallow-water waves when their Froude number ($V/\sqrt{gd}$), either due to an increase in the boat speed (V) or a decrease in the water depth (d), exceeds 0.6. At this point, the waves become affected by the inlet bathymetry; the wave speed (celerity), wavelength, and wave height become dependent on depth. As the Froude number increases further, the boat-generated waves increase in size until they reach a maximum value when the Froude number is equal to 1.0. The boat velocity corresponding to a Froude number of 1.0, for a given depth, is the critical velocity. It is at this critical velocity that the boat-generated waves are the largest; the waves become smaller for larger velocities (Froude numbers greater than 1.0). It becomes obvious from this phenomenon that, in order to attenuate shoreline erosion due to boat wakes, boat speeds would have to be regulated at less than the critical velocity.

Figure 5.10 provides data obtained by Sorensen (1967) for various sized boat prototypes relating boat velocities and the resulting wave heights due to these velocities. These waves were measured at various distances from the sailing line, the range of which encompasses those distances from the channel to the shoreline at various locations in the inlet. The waves were measured in water depths varying from 1 to 2 meters which corresponds well to depths along the north bank of the main channel. A correction factor, denoted by k_s in Fig. 5.10, should be applied to the breaking wave height estimations for the shoreline along the Intracoastal Waterway to account for shoaling effects (Sorensen,

1978). Wave run-up may be estimated as 5/2 the breaking wave height (Bodge and Dean, 1984). This defines the swash zone along regions where the shoreline is not bulkheaded.

This figure may be used as a general indicator of the magnitudes of wave heights or run-up that would occur along the shoreline of Jupiter Inlet for different boat sizes and speeds. Currently there is no speed limit for the inlet; a "slow zone" exists in the northern reach of the Intracoastal Waterway. As it would be impractical to set different speed limits for different size boats, an all-encompassing limit must be imposed. The primary criteria in establishing such a speed limit is that it be of sufficiently low magnitude such that virtually no wake is produced by passing boats. Analysis of Fig. 5.10 suggests that establishing a maximum speed limit of 6 knots should limit wave heights to less than 0.2 m for the boats considered. Lowering this speed limit further should result in the elimination of virtually all significant wave action due to boats.

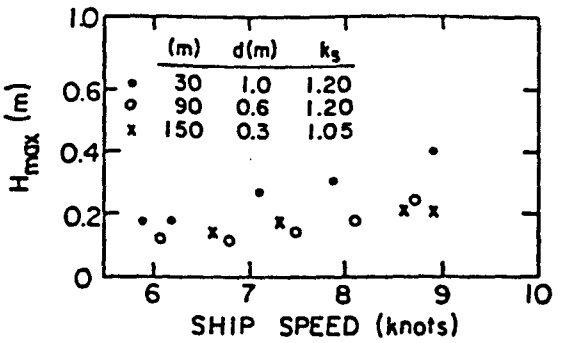

Fig. 5.10a. Maximum Wave Height as a Function of Ship Speed for the Tug "Merryfield"; Length 13.5 m, Draft 1.8 m, Beam 4 m, Displacement $\tilde{=}$ 29 Tons (Sorensen, 1967).

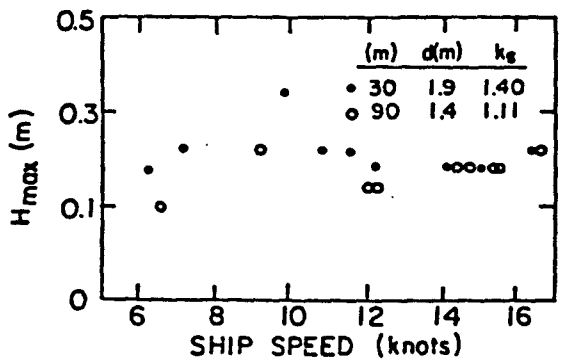

Fig. 5.10b. Maximum Wave Height as a Function of Ship Speed for a Cabin Cruiser; Length 7 m, Draft 0.5 m, Beam 2.5 m, Displacement $\tilde{=}$ 3 Tons (Sorensen, 1967).

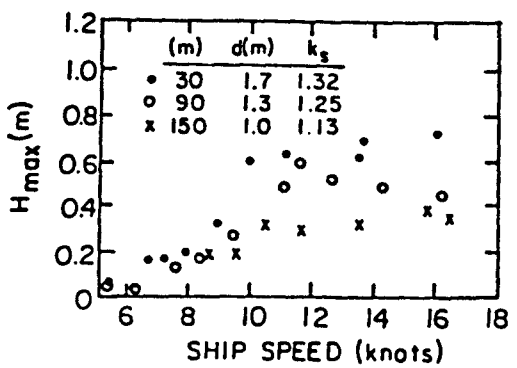

Fig. 5.10c. Wave Height as a Function of Ship Speed for the Fishing Boat "Miss Dragnet"; Length 19.5 m, Draft 0.9 m, Beam 3.9 m, Displacement $\tilde{=}$ 35 Tons (Sorensen, 1967).

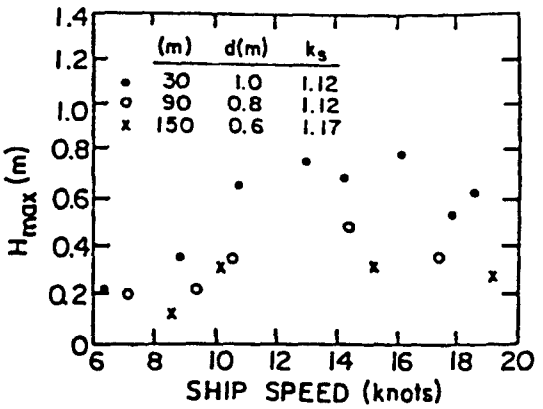

Fig. 5.10d. Wave Height as a Function of Ship Speed for a Coast Guard Cutter; Length 12.2 m, Draft 1.0 m, Beam 3.0 m, Displacement $\tilde{=}$ 10 Tons (Sorensen, 1967).

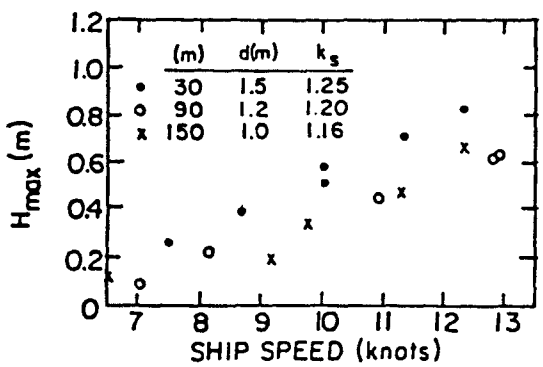

Fig. 5.10e. Wave Height as a Function of Ship Speed for City of Oakland Fire Boat; Length 30.5 m, Draft 3.5 m, Beam 8.5 m, Displacement $\tilde{=}$ 343 Tons (Sorensen, 1967).

CHAPTER VI

MODEL TESTING

6.1 Overview

Three hydraulic parameters were measured at various locations in the inlet in its existing condition and again each time a particular solution scheme was implemented. These parameters were flow velocities, flow patterns and wave heights. An evaluation of the effectiveness of a particular scheme was based on the extent to which its implementation altered these parameters. If they were altered in such a manner as to result in the attenuation of the problems at a specific location, then the scheme was considered to be effective.

Flow velocities and wave heights were measured at locations throughout the inlet by means of a flow meter and a portable capacitance wave gage, respectively (Section 4.4). Flow patterns were determined by photographing, at a four to six second shutter speed, the patterns formed by small styrofoam floats (packing material) placed at specified locations. Data obtained from these measurements were then analyzed by means of a procedure developed to predict sedimentary phenomena due to wave and current action. The results of this analysis provided the basis for the evaluation of each of the schemes.

6.2 Test Conditions

6.2.1 Initial Considerations

Conditions under which the different solution schemes were tested were initially chosen so as to represent 1) those conditions which, over

a normal lunar cycle, would be most likely to result in erosion and deposition problems at the inlet and 2) those which would represent the conditions occurring during a storm event. The first of these conditions were characterized by the average as well as extreme wave heights and periods occurring offshore of the inlet (Section 3.8) simultaneously with the ebb and flood tidal levels corresponding to maximum flow velocities at the inlet mouth. The second set of conditions consisted of maximum wave heights and periods offshore concurrently with tide levels and flow velocities corresponding to a 1.5 meter storm surge in the inlet.

While it is recognized that forces of sufficient magnitude to cause sediment transport resulting in the erosion and deposition problems at the inlet exist over a large portion of the tidal cycle and over an entire storm duration, the conditions chosen for simulation in the model were those that would result in the highest magnitudes of these forces. This decision was a result of the contention that if the solutions implemented significantly reduce the erosion and deposition problems during conditions corresponding to the highest magnitudes of the aforementioned forces, then they would be effective in reducing these problems during any other portion of the tidal cycle or storm event. Figure 6.1 illustrates the eighteen conditions (resulting from combinations of wave heights, wave directions and tidal conditions) that were initially considered for testing of the proposed solution options.

6.2.2 Test Conditions

It became apparent during initial tests that some of the combinations given in Fig. 6.1 produced conditions much more conducive to the problems associated with the inlet than did others.

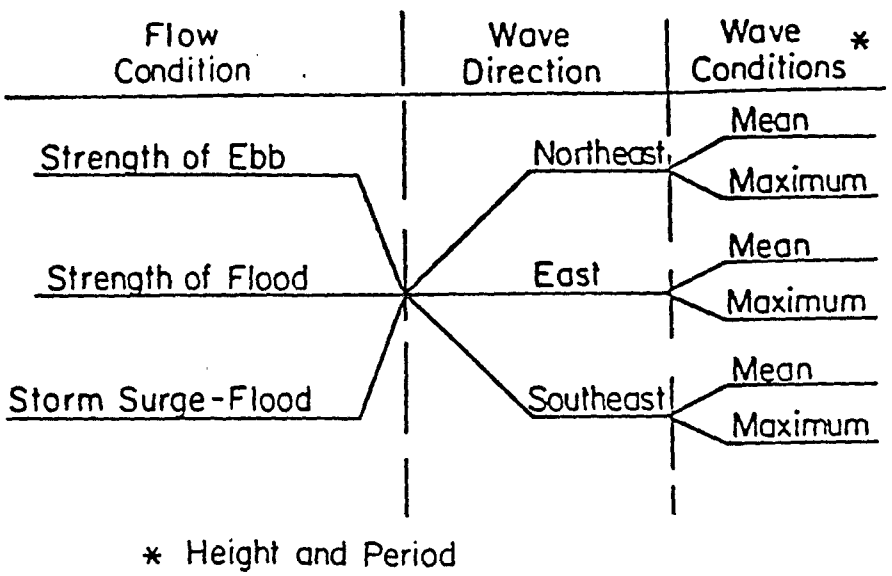

Fig. 6.1. Combinations of Wave Heights, Wave Directions and Tidal Stages Resulting in 18 Conditions Considered for Testing.

Specifically, certain combinations of wave height, wave direction and current produced significantly higher waves inside the inlet. The combinations resulting in the highest waves were considered as those most conducive to the problems at the inlet, and therefore, it was decided to conduct extensive testing under those combinations. Observations of wave action made in the prototype and corroborated in the model provided justification for the elimination of thirteen of the combinations shown in Fig. 6.1.

During periods of maximum ebb, waves directed at the inlet are "stalled" at the mouth by the high velocity flow leaving the inlet. These waves take the form of nearly standing waves and result in no observable wave penetration into the inlet. This phenomenon was also observed in the model (Fig. 6.2) and no wave action was measured inland of the mouth during ebb flow. As a result, tests were conducted for ebb flow conditions only; no wave conditions were simulated during ebb tide.

Observations made in the model study indicated that waves approaching the inlet from the Southeast did not result in any significant amount of wave action in the inlet relative to that due to waves from the East and Northeast. This is believed to be due to a combination of 1) wave refraction characteristics of the southeast waves and 2) dissipation of the energy of these waves resulting from reflection between the jetties. In addition a knowledge of the wave climate of southeast Florida (SSMO, 1970) indicates that the maximum wave conditions determined in Section 3.8 rarely occur from the Southeast. As a result of these observations, no in-depth testing was done under southeast wave conditions.

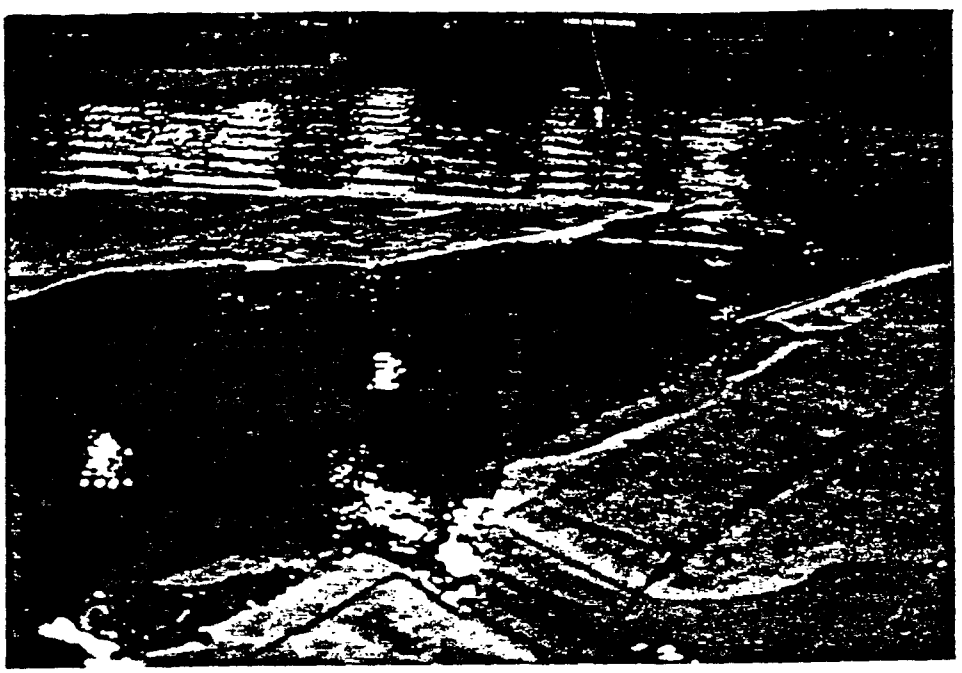

Fig. 6.2. Photograph Indicating the Inability of Waves to Penetrate into the Inlet on Ebb Tide.

The number of wave and current combinations for testing was further decreased by the elimination of the mean wave height condition for waves approaching from the East and Northeast. This decision was based on the aforementioned contention that solution schemes determined to be effective under the most severe conditions (in this case waves) would most likely be effective under those that were less severe.

The remaining combinations represented the conditions under which in-depth testing of each of the schemes was carried out. These conditions were: 1) maximum ebb flow without waves, 2) maximum flood flow combined with maximum wave conditions from the East and Northeast and 3) storm flood flow combined with maximum wave conditions from the East and Northeast. Table 6.1 lists the magnitudes (prototype) of these conditions. The results of the tests are presented in the following sections.

Table 6.1. Prototype Conditions Under Which Model Tests were Performed

Flow Condition	Current Velocity* ($^m/_s$)	Tide Level** (m)	Wave Height*** (m)	Wave Period (sec)	Wave Direction****
ebb	2.60	0.35	___	___	___
flood	2.20	0.30	1.7	10.7	E
flood	2.20	0.30	1.7	10.7	NE
storm	3.40	1.80	1.7	10.7	E
storm	3.40	1.80	1.7	10.7	NE

*current velocity at the inlet mouth.

**above 1929 NGVD sea-level.

***measured at the offshore gage shown in Fig. 2.4.

****generated at the wave-maker.

6.3 Data Analysis

6.3.1 Overview

The hydraulic parameters measured in the model represent the forces that initiate and perpetuate sediment transport in the inlet. Determining the flow patterns at a given location in the inlet provides a qualitative description of the velocity field, including the existence of current eddies, at that location. Current velocities and wave heights may be used to obtain a quantitative estimate of the degree to which the hydraulic forces will govern sediment transport.

6.3.2 Procedure

A procedure was developed to estimate the degree of erosion or deposition at a specific location given the current velocity, wave height, depth and sediment size at that location. The procedure incorporates the maximum bed velocity at a location due to the combination of tidal current velocity and the particle velocity due to waves. Whether a location will undergo erosion or deposition is based upon a bed stability parameter P defined as follows:

$$P = \left(\frac{\tau_{wc}}{\tau_{cr}} - 1 \right) \qquad (6\text{-}1)$$

where τ_{wc} = bed shear stress due to waves and current and τ_{cr} = critical bed shear stress. The bed shear stress is directly proportional to the square of the velocity under turbulent flows; therefore P may be expressed as

$$P = \left[\left(\frac{u_{wc}}{u_{cr}} \right)^2 - 1 \right] \qquad (6\text{-}2)$$

where u_{wc} = velocity due to waves and current and u_{cr} = critical velocity for erosion. Assuming the wave to be in shallow water, the horizontal particle velocity due to waves is directly proportional to wave height and inversely proportional to the square root of the depth (Sorensen, 1978). Based on this, an empirical relationship relating u_{wc} to the tidal current velocity u_c is assumed to be of the form:

$$u_{wc} = \left\{ 1 + k \left[\left(\frac{d_R}{d} \right)^{1/2} \left(\frac{H}{H_R} \right) \right]^m \right\} u_c \qquad (6\text{-}3)$$

where k = a coefficient to be determined, m = an exponent to be determined, H = wave height at the location, H_R = reference wave height, d = depth at the location and d_R = reference depth. Substitution of equation (6-3) into (6-2) results in the following expression for P:

$$P = \left\{ \left[1 + k \left[\left(\frac{d_R}{d} \right)^{1/2} \left(\frac{H}{H_R} \right) \right]^m \right]^2 \left(\frac{u_c}{u_{cr}} \right)^2 - 1 \right\} \qquad (6\text{-}4)$$

For situations where there is no wave activity, H=0 and $u_{wc}=u_c$; P therefore becomes:

$$P = \left[\left(\frac{u_c}{u_{cr}} \right)^2 - 1 \right] \qquad (6\text{-}5)$$

which is consistent with equation (6-2). The parameter P provides an indication as to whether deposition or erosion will occur as follows:

for $u_{wc} > u_{cr}$, erosion occurs and $P > 0$

for $u_{wc} = u_{cr}$, marginal instability occurs and $P = 0$

for $u_{wc} < u_{cr}$, deposition occurs and $P < 0$

As u_c and H increase, P increases as well. This is consistent with the increase in erosion that would be expected.

The parameters used in the application of equation (6-4) are as follows:

u_c = measured current velocity

u_{cr} = critical velocity obtained from Shields diagram

H_R = wave height at the offshore wave gage

H = wave height measured at the specific location

d_R = depth at the offshore wave gage

d = depth measured at the specific location

k = determined by iteration

m = determined by iteration

The value of u_{cr} for a specific location may be obtained from the following relationship (Mehta and Christensen, 1983):

$$\tau_{cr} = \frac{f}{4} \rho \frac{u_{cr}^2}{2} = 0.056(\gamma_s - \gamma)\, d_e \qquad (6\text{-}6)$$

where f = friction factor selected to be equal to 0.025 (Mehta, 1978)

ρ = density of water = 105 N/m^3

γ_s = unit weight of sand = 2650 kg/m^3

γ = unit weight of saltwater = 1030 kg/m^3

d_e = sand diameter in meters

0.056 = Shields entrainment coefficient for fully turbulent flows.

From this relationship, u_{cr} is calculated in meters per second as a function of sand diameter in millimeters:

$$u_{cr} = (0.2855\, d_e)^{1/2} \qquad (6\text{-}7)$$

A plot of u_{cr} versus d_e shown in Fig. 3.13 is based on equation (6-7).

Velocities were measured at locations in the model at a point two-thirds of the total depth above the bottom. These values, assumed to represent the depth-averaged velocity at that location, were multiplied by 1.17 in order to provide an estimate of the maximum (surface) velocity u_{max} (O'Brien and Clark, 1973). The one-seventh approximation relating u_{max} to velocity u at a prototype elevation z above the bottom (Schlichting, 1979) was then applied for an elevation (z) of 0.15 m in order to estimate the bottom velocity at any location. This bottom velocity was substituted for u_c in equation (6-4).

Although no specific data were available on the exponent m, it is likely to be between 1 and 2. The coefficient k was evaluated from observations that the Dubois Park beach was believed to have reached a point of marginal stability (virtually no erosion or deposition under normal conditions) and therefore P was assumed to be equal to zero here. Substituting measured values of H, d and u_c into equation (6-4) for this location and solving iteratively for m and k (with P=0) resulted in a range of m values of 1.3 - 1.7 and k values of 2.0 - 8.0.

Best-fit values of m and k were then determined iteratively by employing equation (6-4), using various combinations within these ranges of m and k, at each location for the inlet in its present condition. Resulting values of P for each combination were then analyzed to determine whether or not they were in accordance with the existing sedimentary phenomena at each location. The combination of m and k that resulted in the values of P most consistent with the sedimentary phenomena at all locations in the inlet were then chosen as the best-fit values for equation (6-4). These values were 1.4 for m and 7 for k.

Tests were performed in the model in order to assess the validity of equation (6-4). Coal dust (γ_s = 1250 kg/m^3, d_e = 0.50 mm) was placed at locations 11, 17 and 35 (shown in Fig. J-1) which correspond to areas of erosion, marginal stability and deposition, respectively, during flood tide in the prototype. Substitution of the appropriate model values for the parameters in equation (6-4) resulted in P values of 7.41 for location 11, -0.61 for location 17 and -0.98 for location 35. Upon placement of the coal at these locations the following observations were made: 1) considerable transport of the coal took place at location 11, 2) only a slight initial transport of the coal which soon ceased took place at location 17 and 3) no transport of coal took place at location 35. These observations correspond well with the calculated P values as well as the observed conditions at these locations in the prototype. Based on this corroboration, equation 6.4 was deemed valid for assessing the sediment transport characteristics at specific locations in the inlet.

An evaluation of the solution schemes proposed for various locations in the inlet was next made based on the calculated values of P. It should be noted that no correlation was established between the relative magnitude of P and the degree of erosion or deposition taking place at a given location. Equation 6.4 is such that it has no upper limit and a lower limit of minus one. While it is recognized that a greater magnitude of P indicates a greater degree of erosion or deposition, analyses of sedimentary phenomena made in this study were based solely on the sign and relative magnitude of a given P value.

6.4 Test Results and Interpretation

6.4.1 Overview

Model test results consisted of 1) wave and current data from which a sediment stability parameter P was calculated for each measurement location and 2) photographs of the flow patterns at each problem site. Measurements and photographs taken for the inlet in its present state were analyzed so as to verify that the flow conditions at each site were of appropriate magnitude to cause the problems taking place there. The flow conditions were then measured and photographed after the various aforementioned solution schemes were implemented in the model. The results of these tests as well as a more detailed account of the measurements made for the inlet in its existing condition are presented in the following section. Appendix J presents figures indicating the locations of measurements as well as tabulated data resulting from these measurements. All references to current velocities, wave heights and P values are taken from the data presented in Appendix J.

6.4.2 Results and Interpretation

6.4.2.1 Problem Site A

The current velocities and wave heights at problem site A (see Fig. 5.1) are known to cause erosion and bulkhead deterioration in the present condition. Current velocities ranging from 0.3 to 1.2 m/sec and wave heights of 0.2 to 0.5 m were measured here resulting in P values ranging from 1 to 29. In addition, photographs of this region indicate that a large circulation pattern exists within the sheltered cove area. This pattern acts to transport the sediment and is especially pronounced during ebb tide (see Fig. 6.3).

Fig. 6.3. Circulation Patterns within the Cove Area at Site A; Ebb Tide.

Fig. 6.4. Circulation Patterns near the Groin Remnants at Site A; Flood Tide.

Testing was done in an attempt to determine the overall contributions that the remains of the groin just west of the cove area made to the erosion problems along the north shoreline. As this groin is in an extreme state of disrepair, it has become permeable and is therefore incapable of retaining sand. It does however create considerable eddy circulation on flood tide thereby enhancing erosion along the shoreline (see Fig. 6.4). P values ranging from 1 to 143 were obtained for flood and storm tides at this location. Negative P values were obtained along the immediate shoreline here during ebb tide. No significant changes in current velocities, wave heights and, therefore, P values in this immediate area were observed upon removal of the groin (See Table J-2), however, the circulation was somewhat attenuated (Fig. 6.5).

With the exception of a reduction in the flow velocity immediately downdrift of the weir-groin, the implementation of this scheme resulted in no noticeable change in the flow velocities and patterns (Fig. 6.6) or the wave heights at the groin location in problem site A. This indeed was desirable for this location as the principle behind the feeder beach and weir-groin concept is that sediment will still be transported over the weir-groin and further inland so as to nourish the westward reach of the north shoreline once a buffer of sand has accumulated in the cove area. P values of 0.5 to 42 for locations downdrift of weir-groin indicate that sediment should continue to be transported westward on a flood tide. In addition, no adverse effects due to the installation of this weir-groin were observed at other locations along the shoreline during the testing. Based on these results, model tests appear to indicate that this scheme is likely to mitigate the erosion problems at site A.

Fig. 6.5. Attenuation of Circulation Patterns upon Removal of Groin Remnants at Site A; Flood Tide.

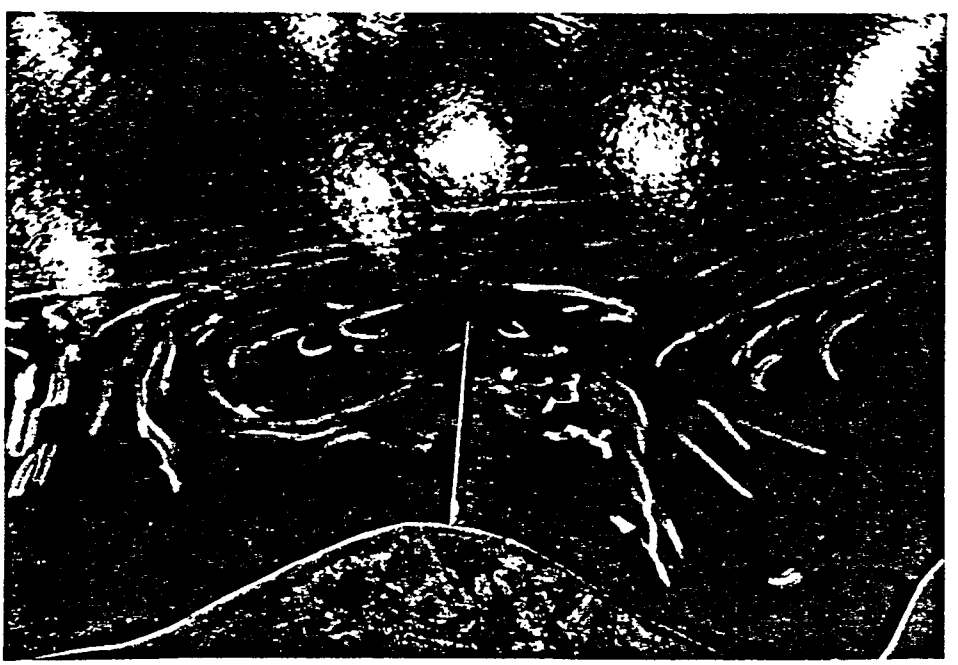

Fig. 6.6. Flow Patterns Induced by the Implementation of a Weir-groin at Site A; Flood Tide.

6.4.2.2 Problem Sites B and C

The flow velocities and patterns along with the wave heights at problem site B are known to cause the erosion problems there. Current velocities ranging from 0.5 to 1.9 m/sec and wave heights to 0.4 m, resulting in P values ranging from 2 to 54, were measured at this location in the model for the present condition. Figure 6.7 suggests the manner in which flood currents attack the shoreline here.

A flow deflector placed at approximately 10 and later 5 meters offshore as described in section 5.2 was tested with and without a six meter long gap at problem site B. In addition, these deflector configurations were tested in combination with a T-groin placed approximately 100 meters further west along the north shoreline where the channel begins winding north into the Intracoastal Waterway (see Fig. 5.3). The deflector was positioned approximately parallel to the shoreline and was curved at the west end so as to direct the flood currents towards the main channel and away from the shoreline. In addition the elevation of the deflector was such (+1 m) that it protected the shoreline from wave attack during normal ebb and flood tides. Tests were run with and without the T-groin in order to determine its effect on the flow patterns and velocities near the deflector, particularly during ebb tide.

Tests were first conducted for the deflector 10 meters offshore with no gap or T-groin but were discontinued when it became apparent that 5 meters offshore was a more practical location. This is based on the observation that while nearly the same flow patterns existed for both configurations (thereby posing no particular advantage in locating 10 meters offshore), navigational safety would be better served by

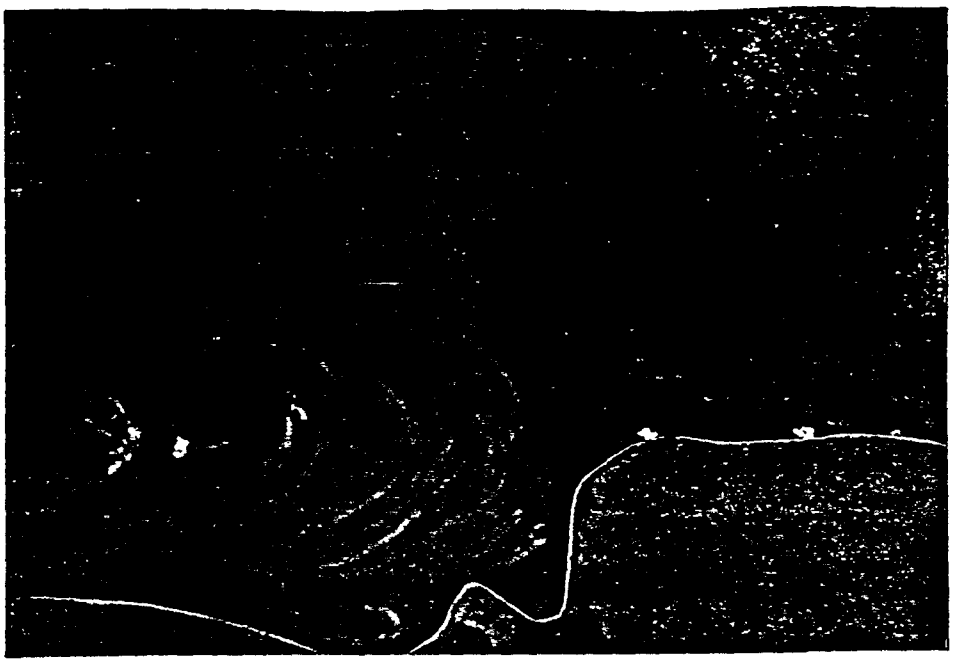

Fig. 6.7. Indication of the Manner in which Flood Currents Attack the North Shoreline (Site B).

Fig. 6.8. Illustration of the Diversion of Ebb Flow such that it does not Enter behind the Flow Deflector with no Gap; no T-groin.

placing the deflector close to the shore. One potential drawback to the deflector scheme, however, was alleviated during tests with the deflector 10 meters offshore. It was of particular concern what the flow patterns behind the deflector on an ebb tide might reveal. Specifically it was feared that flow forced through the open end and behind the deflector would result in a turbulent gyre that would further erode the shoreline there. As can be seen in Fig. 6.8, however, this was not found to be the case. It appears that once a small set-up occurs behind the deflector the forces exerted due to gravity and bottom shear stresses are sufficient to prevent further flow into that region. As a result, flow was directed around the open end of the deflector on ebb tide.

Tests were then carried out on the flow deflector 5 meters offshore with a 6 meter gap located as shown in figure 6.9. The purpose of this gap was to provide for flow circulation behind the deflector in order to prevent flow stagnation there. As can be seen in figure 6.9 this gap resulted in too much circulation; the gyre located behind the deflector caused flow velocities of 0.4 to 0.6 m/sec resulting in positive P values as high as 2.60 indicating that erosion could take place here. Such erosion would enhance scour at the base of the bulkhead and the deflector. This gyre and these positive P values were also observed on flood and storm tides.

It is possible that other combinations of gap widths and locations may attenuate the magnitude of the gyre formed behind the flow deflector. Further testing was proposed to study this effect but was later ruled out as unnecessary. Figure 6.10, taken on an ebb tide, indicates that a slow but definite water exchange takes place behind the

Fig. 6.9. Resulting Flow Patterns due to a Gap in the Flow Deflector; Ebb Tide, T-groin.

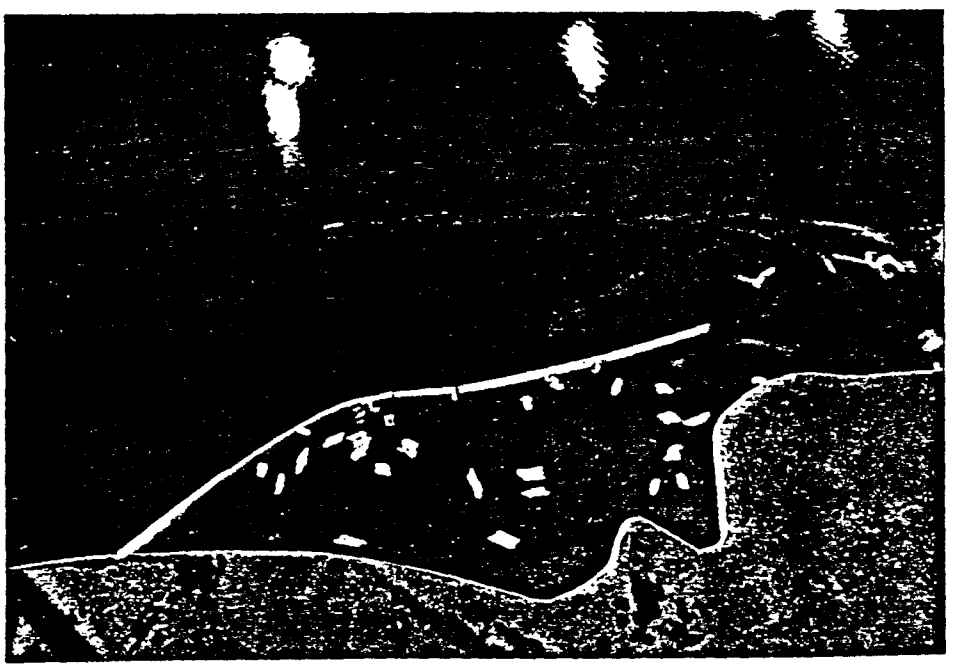

Fig. 6.10. Resulting Flow Patterns behind the Flow Deflector with no Gaps; Ebb Tide, T-groin.

deflector (when floats were placed there) despite the previously mentioned overall balance of forces. This slow exchange was observed on flood tides as well. As the sole purpose of the gap was to provide for mixing behind the deflector, and because this mixing took place at a more desirable rate in the absence of the gap, the gap was deemed unnecessary.

Figure 6.11 shows the flow patterns resulting from the placement of a T-groin at a location approximately 100 meters west of the deflector near the point where the channel winds into the northern reach of the Intracoastal Waterway (problem site C). The purpose of this groin would be to retain sand along the shoreline. One such groin was tested in the model although several could conceivably be employed in the prototype. Testing of the groin was done in order to determine the flow patterns and any adverse current velocities it may create as well as the effects it would have on the flow patterns near the deflector during ebb tide.

The shorter streaks made by the floats near the T-groin as shown in Fig. 6.11 indicate that the groin results in slower current velocities in its immediate vicinity. These currents are on the order of 0.2 m/sec for flood and ebb flows thereby resulting in P values ranging from -0.2 to -0.7 which indicate that deposition could take place here. Small circulation patterns were observed at the updrift side of the T-groin but these were not believed to be of sufficient magnitude to overcome the tendency for deposition indicated by the P values obtained. Figures 6.9 and 6.10 were obtained with this T-groin in place. No noticeable adverse effects on the flow patterns (i.e. increased eddy action) near the deflector were observed due to the T-groin and no significant changes in these flow patterns were observed upon its removal.

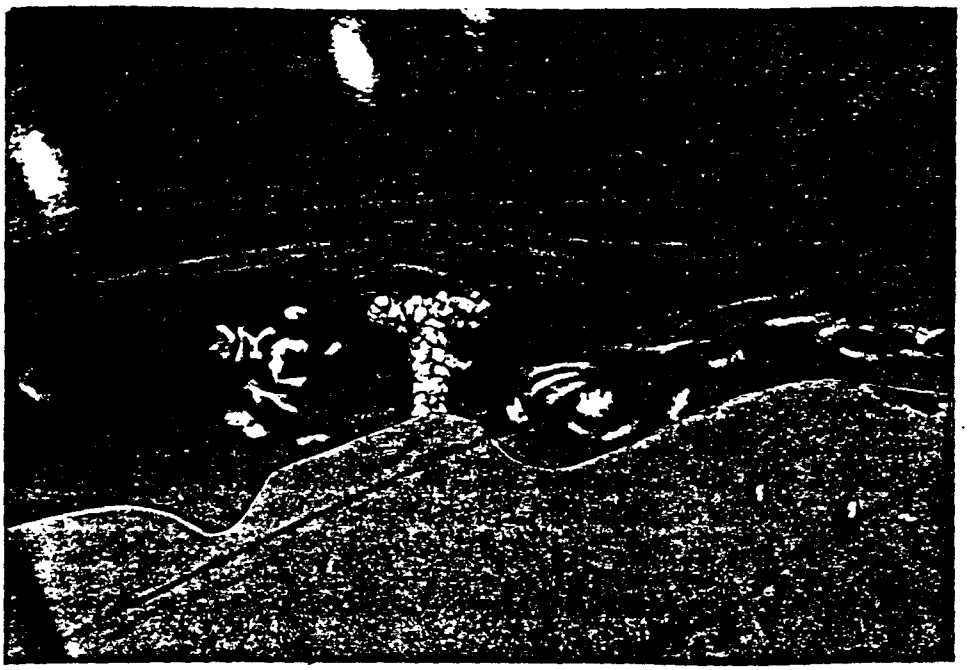

Fig. 6.11. Flow Patterns Induced due to the Placement of a T-groin along the North Shoreline at Site C; Ebb Tide.

Fig. 6.12. Flow Patterns at the Mouth of the Dubois Park Lagoon; Flood Tide.

6.4.2.3 Problem Sites D, E and F

The channeling of flow south of the west extension of the south jetty (site D) towards the Dubois Park Lagoon during abnormally high flood tides is believed to cause the erosion at problem site D (Section 5.2). Velocities ranging from 0.7 to 1.6 m/sec were measured resulting in P values ranging from 3 to 21 for a 1.5 meter storm surge tide in the present inlet condition. In addition, circulation patterns were observed at the lagoon mouth (Fig. 6.12). These patterns act to maintain sediment in suspension thereby providing for transport into the lagoon (sites E and F).

Placement of an impermeable structure at the west end of the rocks (in accordance with the solution proposed in Section 5.2) resulted in a flow velocity of 1.0 m/sec at the east end of these rocks (location 13 in Fig. J-1) decreasing westward to zero at the structure. This observation supports the assumption made in Section 5.2 that the placement of this structure would serve to prevent sediment from being directly transported into the Dubois Park Lagoon thereby significantly reducing the immediate sediment supply for the shoaling that has occurred at problem sites E and F. However, concurrent with this assumption, the resulting P values ranging from 1.3 to 7 at locations 13, 14 and 15 in Fig. J-1 indicate that erosion could continue to occur here.

A considerable portion of this eroded sediment should be transported by the re-directed flow over and through the rocks into the inlet channel and subsequently further westward along the south shoreline during storm conditions. As can be seen in Fig. 6.13 placement of the impermeable structure did nothing to significantly

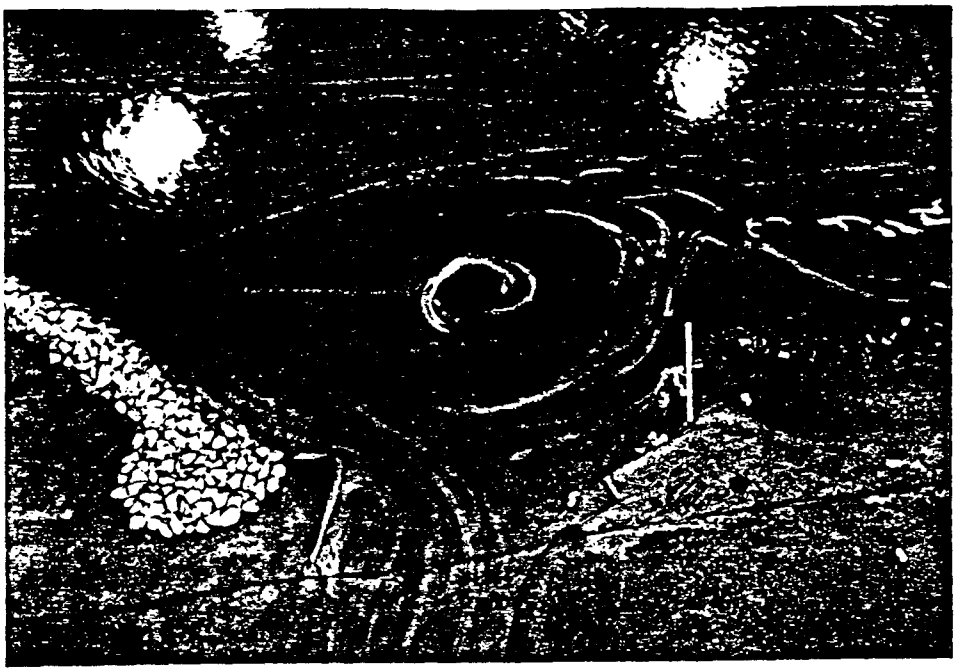

Fig. 6.13. Flow Patterns at the Mouth of the Dubois Park Lagoon due to the Placement of an Impermeable Structure at the West End of the South Jetty Rock Extension; Flood Tide.

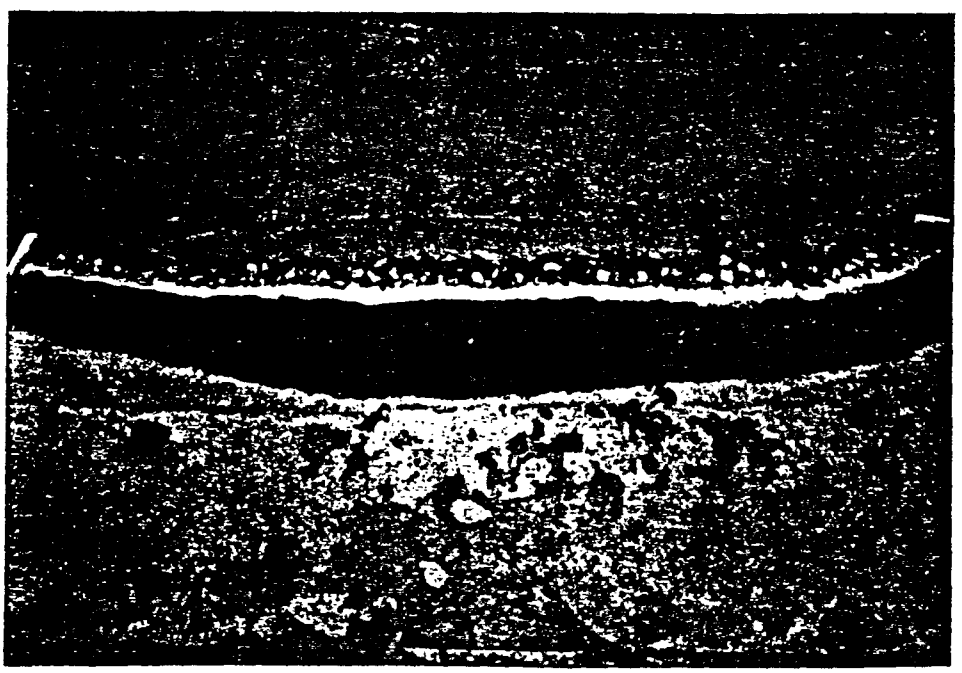

Fig. 6.14. Proposed Backfill of the West Extension of the South Jetty. White Layer Represents Gravel, Coal Represents Sand Fill, Filter Cloth is not Shown.

alter the circulation pattern at the mouth of the lagoon. As a result some of the sediment eroded from problem site D may continue to be transported into the lagoon by the combined effects of this circulation pattern and the flow into the lagoon during storm conditions. It appears that this circulation pattern at the lagoon mouth is of a permanent nature and that the only means to significantly reduce transport of sediment into the lagoon (and thereby attenuate the shoaling problems at sites E and F) is to cut off the supply from site D. This may best be accomplished by implementing the second phase of the solution scheme for this site as shown in Fig. 5.3 and again in Fig. 6.14.

6.4.2.4 Problem Site G

The erosion problems at the Dubois Park beach (problem site G) are believed to be due to the combination of 1) wave attack, 2) suspension and transport of sediment by current eddies, and 3) transport of sediment along the shoreline by tidal currents. Current velocities during flood tide corresponding to a range of 0.2 to 0.3 m/sec near shore (5 to 10 m from beach) and 0.3 to 0.7 m/sec further offshore (25 to 35 m from the beach) along with maximum wave heights of 0.3 m were measured at this location resulting in P values of 1 to 3 and 0 to 7.5, respectively. Negative P values were calculated for points near shore during ebb tide indicating deposition there, while positive P values ranging from 2 to 10 were calculated for all points at site G during a 1.5 m storm surge indicating erosion for this condition. In addition, Fig. 6.15 indicates the existence of a large circulation pattern immediately offshore of the beach during a flood tide. This pattern also was observed during both ebb and storm tides.

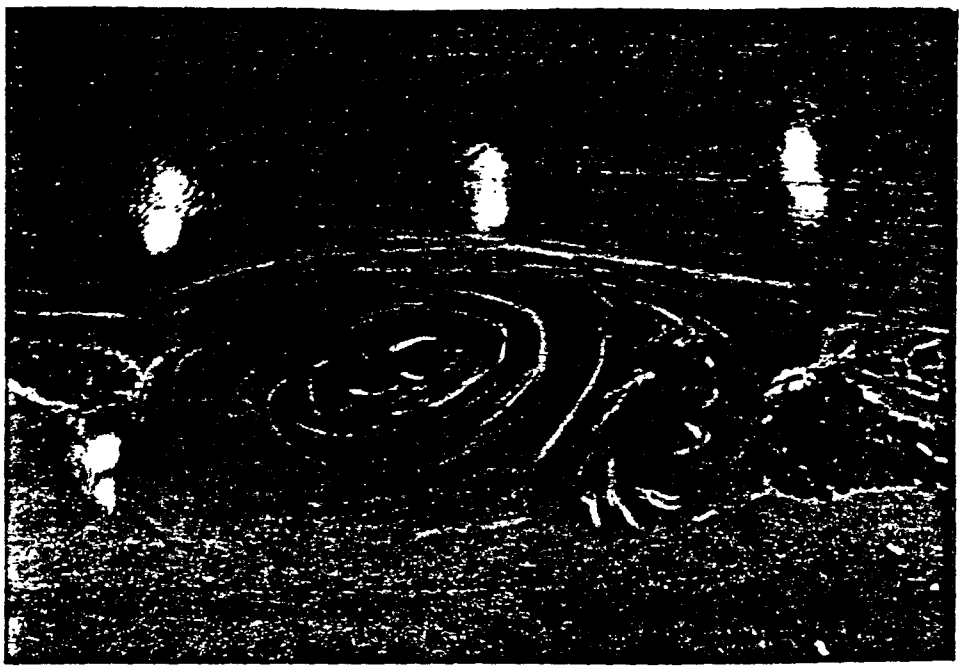

Fig. 6.15. Flow Patterns at Dubois Park Beach; Flood Tide.

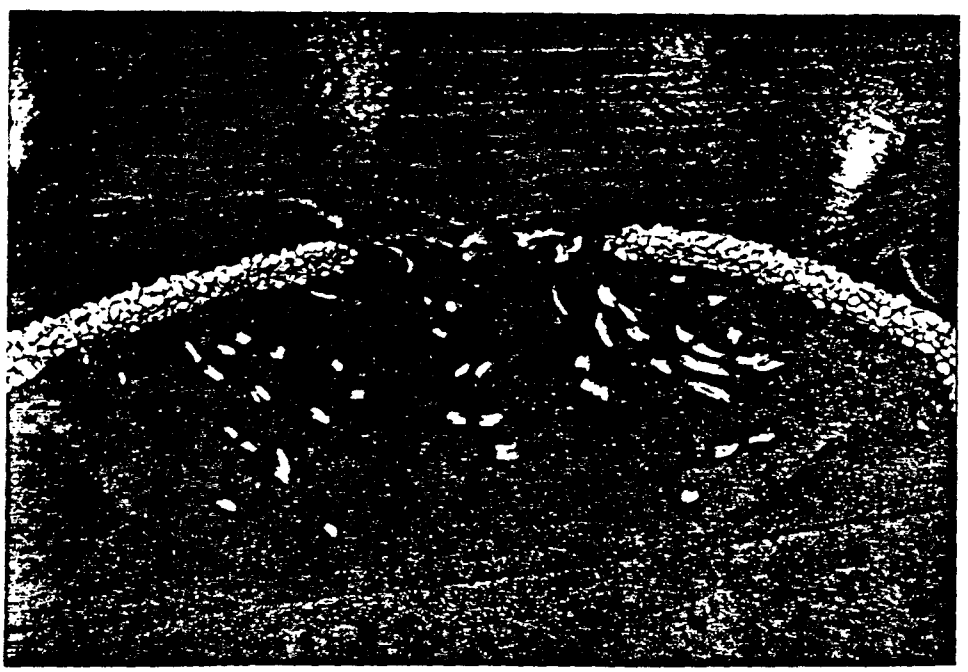

Fig. 6.16. Flow Patterns at Dubois Park Beach Resulting from the Placement of Two Curved Groins Extending from Each End of the Beach; Flood Tide.

In accordance with the solution scheme proposed for this site (Section 5.2), the existing rocks were removed from the site and a set of curved groins was put in their place (see Fig. 5.5). The resulting flow velocities and wave heights at locations within the groins were reduced by as much as 60 percent thereby resulting in P values ranging from -0.14 to -0.92. These values indicate conditions conducive to no significant sediment erosion within the groins even during storm surge conditions. Flow velocities outside the groins were observed to increase approximately 20 to 30 percent, presumably due to the added contribution of the concentrated flow around the groins. Figure 6.16 indicates that during a flood tide the groins attenuated the large circulation pattern that previously existed immediately offshore of the beach. It should be noted in Fig. 6.16 however, that a slow circulation within the groins as well as water exchange through the gap between the groins continued to occur. This slow circulation should serve to minimize flow stagnation within the groin area but, as indicated by the P values, should not be of sufficient magnitude to initiate significant sediment erosion. This behavior was observed during ebb and storm tides as well.

Supplemental measures to the proposed solution for this location consisted of two options, the first of which was to place an underwater sill between the two groins implemented in phase one (see Fig. 5.5). Measurements taken for this configuration indicated current velocities equal to and wave heights slightly less (20 percent) than those measured without the sill at locations near the shoreline. However, at locations immediately south of the sill the flow velocities and wave heights were approximately 10 to 30 percent higher than those at the same locations in the absence of the sill.

The higher flow velocities near the sill were believed to be due to the fact that the effective gap area for water flowing out to the inlet from the beach was reduced by anywhere from 50 to 75 percent (depending on the tide level) by the sill. In order to maintain the same discharge through the gap, the velocity must increase to offset this decrease in area. Figure 6.17 illustrates the acceleration of flow as the floats approach the sill. The higher wave heights immediately south of the sill were believed to be due to the fact that the waves steepen as they "feel" the sill and the higher flow velocities opposing their direction. The sill dissipates some of the wave energy thereby resulting in the ultimately lower wave heights measured near the beach. This steepening of waves at the sill is not believed to be detrimental to the beach proposed for this area. However, the increase in velocity directed away from the beach may result in sediment transport offshore, causing sand to pile up against the sill eventually flowing over the sill and into the inlet. P values ranging from 0.3 to 3.4 for this configuration support this hypothesis as they indicate that offshore sediment transport could take place near the sill.

The second option proposed as a supplement to the solution scheme for this area involved the placement of offshore sills parallel to the shoreline west of the Dubois Park beach as shown in Fig. 5.6. The primary purpose of these sills would be to attenuate wave energy; any sand that these sills may retain would be considered an added benefit. Current velocities corresponding to values ranging from 0.2 to 1.1 m/sec were measured in the model along this shoreline and wave heights corresponding to 0.1 to 0.3 m were measured here for the existing condition. These values result in P values ranging from 1 to 14 thereby

Fig. 6.17. Flow Patterns Resulting from the Placement of an Underwater Sill between the Two Groins Shown in Fig. 6.16; Flood Tide.

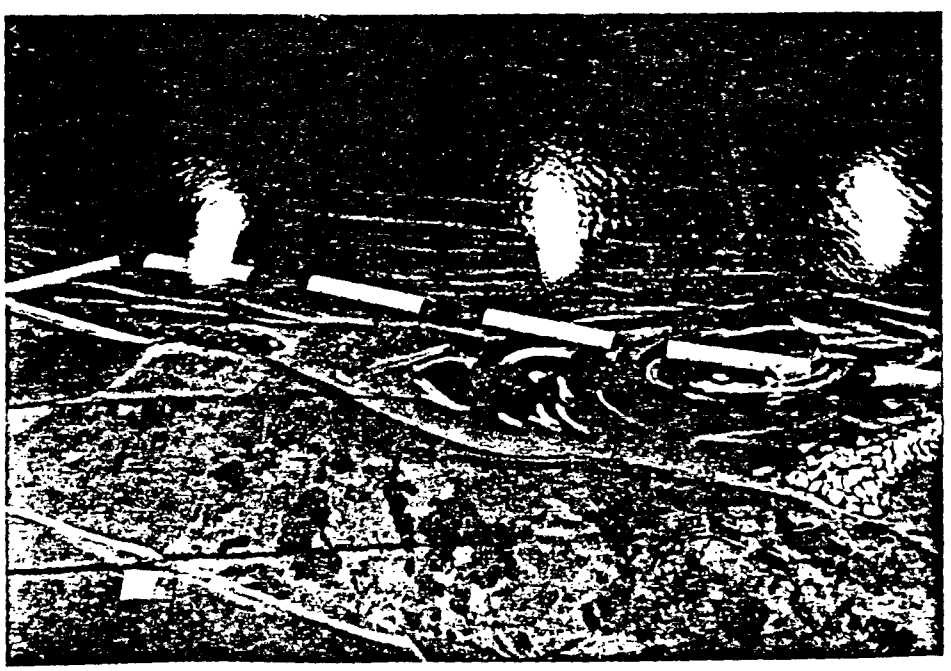

Fig. 6.18. Flow Patterns Resulting from the Implementation of Sill Plan b in Fig. 5.6; Flood Tide.

indicating conditions conducive to erosion. In addition, this shoreline is exposed to wave action in the form of boat wakes which are believed to contribute to the erosion of this shoreline.

Wave measurements made during the testing of the three sill schemes shown in Fig. 5.6 indicated that all three would reduce wave heights occurring at the shoreline by 10 to 30 percent. It is anticipated that the sills would have a similar damping effect on boat wakes. As can be seen in Table J-5, however, none of these schemes reduces the magnitudes of the current velocities enough to result in P values indicating a state of no erosion. These P values (0.2 to 18) indicate that scour at the base of the sills would be likely. This does not mean that the sills are entirely ineffective. By reducing wave heights, the sills may at least slow down the erosion rate by reducing the contribution to erosion made by waves and boat wakes.

The distinguishing feature differentiating the effectiveness of each sill scheme lies in the flow patterns and flow velocities through the gaps between the sills resulting from the various placement schemes. A comparison of Figs. 6.18, 6.19, and 6.20 provides a qualitative indication of the magnitude of circulation patterns resulting from the implementation of each of the three sill schemes. The overall sill length in each scheme is the same (approximately 130 m) but the individual sill lengths and the gaps between them are different (see Fig. 5.6). These figures indicate that the scheme providing a greater number of gaps produces circulation patterns of the least magnitude along the shoreline. In addition measurements of the flow velocities through the gaps in each scheme due to water exchange indicated that the lowest magnitudes (see Table J-5) of velocity

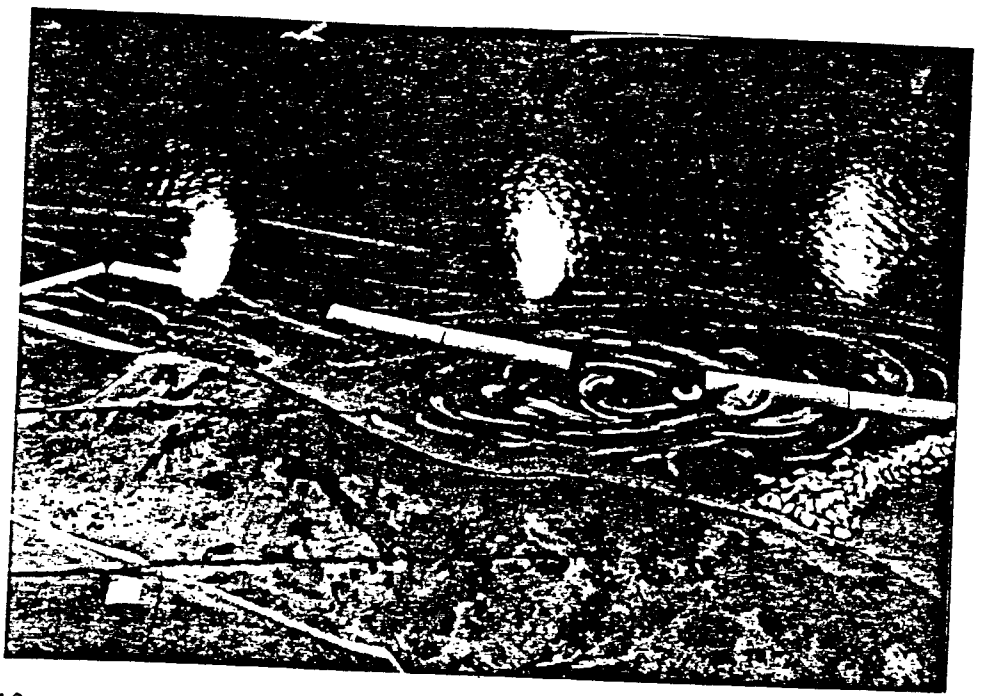

Fig. 6.19. Flow Patterns Resulting from the Implementation of Sill Plan a in Fig. 5.6; Flood Tide.

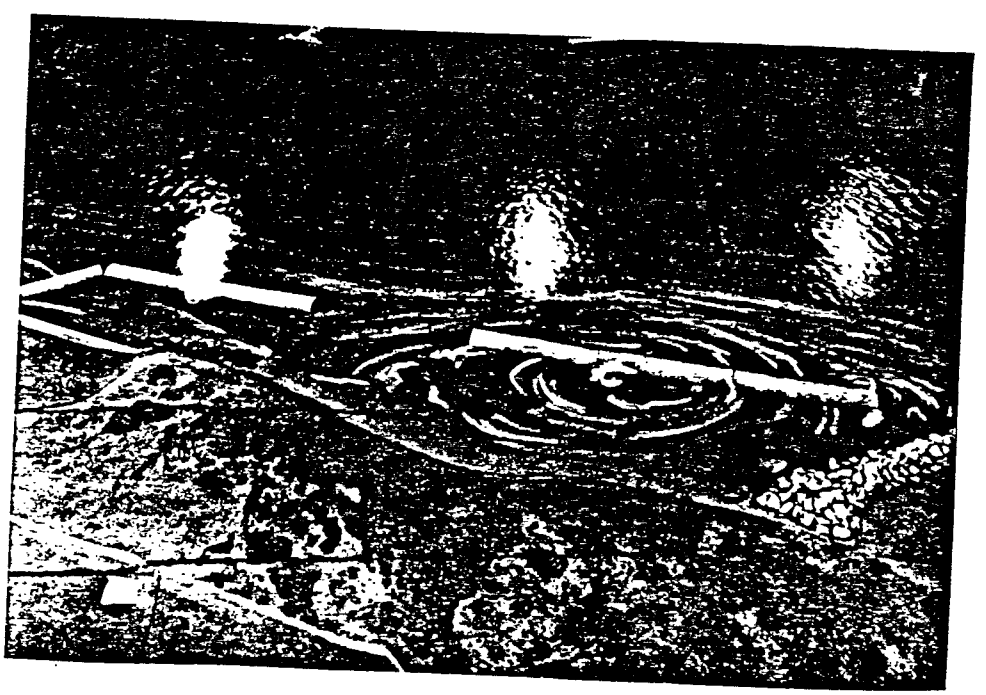

Fig. 6.20. Flow Patterns Resulting from the Implementation of Sill Plan c in Fig. 5.6; Flood Tide.

occurred for the scheme consisting of the greatest number of gaps. Based on these observations it would appear that sill scheme b in Fig. 5.6 would be the most favorable for implementation.

It should be noted that for expediency, PVC pipe was used to model the offshore sills. These sills would most likely be constructed from rock in the prototype thereby allowing for some water transfer through the sill. It is anticipated that actual velocities would be slightly lower and the circulation patterns of slightly smaller magnitude than those based on model measurements.

6.4.2.5 Problem Sites H and I

The problems existing in the area of the southshore promontory (sites H and I) consist of shoaling in the southshore marina and in the basin at the northeast end of the promontory as well as erosion of the west end of the promontory (see Fig. 5.7). Both cases of shoaling are believed to be due to the transport of sediment into these regions of low flow velocity (0.1 - 0.2 m/sec) whereby the sediment is deposited. Erosion of the west end of the promontory is believed to be due to the high current velocities (0.4 - 0.5 m/sec) existing at this location during ebb, flood and storm tides. P values ranging from 0.1 to 1.7 support the above hypotheses regarding the causes of erosion and deposition near the promontory. In addition, the flow patterns shown in Fig. 6.21 illustrate the flow around the promontory during a flood tide that acts to erode sediment here and deposit it at the mouth of the marina. Figure 6.22 illustrates the current attack on the promontory as well as the flow that tends to push sediment deposited at the marina into the marina on ebb tide.

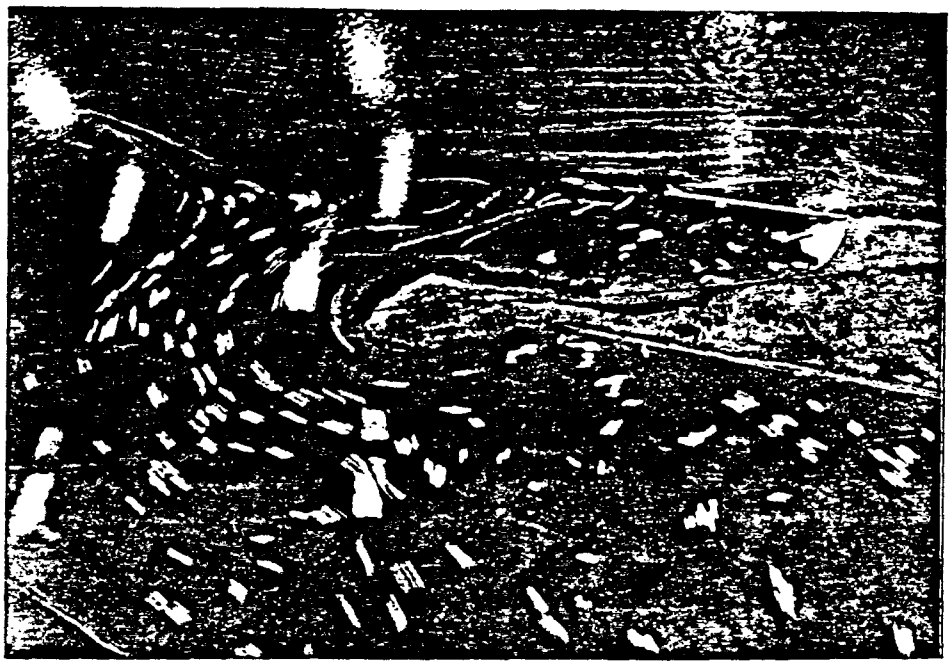

Fig. 6.21. Flow Patterns in the Southshore Promontory Area; Flood Tide.

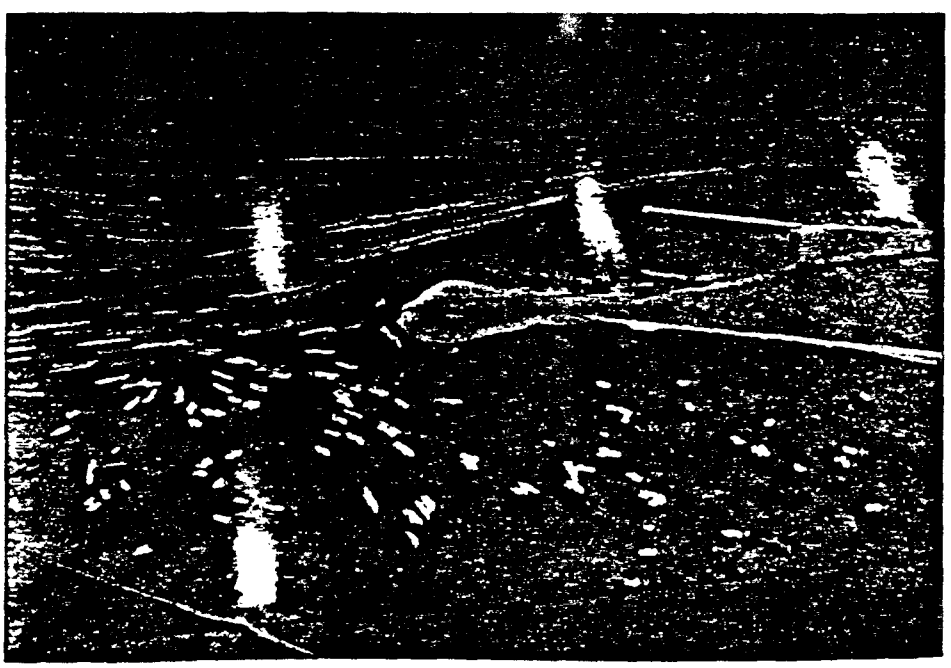

Fig. 6.22. Flow Patterns in the Southshore Promontory Area; Flood Tide.

The scheme proposed to remedy the erosion and deposition problems at the promontory consists primarily of armoring the west end of the promontory with a structure that extends north acting as a groin (Fig. 5.7). The purpose of this structure would be to control the erosion of the west end of the promontory by armoring it and to retain sand thereby minimizing the shoaling supply for the southshore marina. With the exception of lower current velocities near the west end of the promontory due to a redirection of flow further inland by the structure there, the current velocities at these sites were not altered significantly by the implementation of the solution scheme for this area. Figure 6.23 indicates, however that flood flows would no longer be directed around the promontory. This would eliminate the mechanism by which the promontory is eroded and the marina shoaled. Currents and flow patterns on the north side of the promontory indicate adequate mixing there but P values ranging from -0.55 to -0.98 suggest that shoaling could continue to occur. This, however, is concurrent with the recommendation that a recreational beach be created at this site. The negative P values indicate that any fill placed here should be relatively stable.

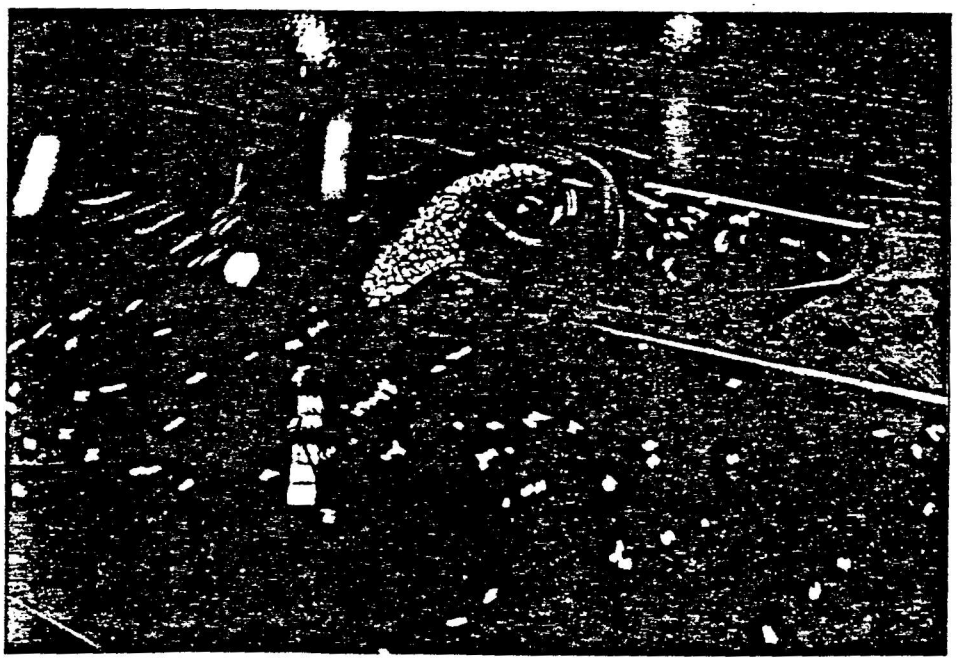

Fig. 6.23. Flow Patterns in the Southshore Promontory Area due to the Implementation of the Solution Scheme Proposed for this Site; Flood Tide.

CHAPTER VII

SUMMARY AND RECOMMENDATIONS

7.1 Summary

The purpose of this study was to identify the causes of the problems of shoreline erosion and sediment deposition at Jupiter Inlet and to develop and test potential solutions to these problems. An extensive field investigation that included hydrographic surveys, drogue and dye studies, continuous tide level records, current velocity measurements and sediment samples was carried out. The resulting data were analyzed and interpreted so as to provide an indication of the hydraulic and sedimentary characteristics of the inlet as well as the necessary information to construct a physical model of the inlet. The model was a fixed-bed, steady flow model with an undistorted scale of 1:49. After construction, the model was calibrated and adjusted until prototype flow conditions were accurately simulated.

Potential solution schemes were then proposed for testing in the model and three methods of implementing and maintaining these schemes were considered. The schemes consisted of a combination of structural and non-structural designs and were proposed and tested in two phases. The first phase consisted of measures considered as the minimum necessary to remedy the existing problems at the inlet. The second phase included optional measures to further stabilize the inlet if necessary as well as to create recreational beaches along the south shoreline.

The solution schemes were tested under maximum flood and ebb flow conditions as well as conditions resulting from a 1.5 m storm surge. Maximum wave conditions were simulated from east and northeast directions. Testing consisted of measuring current velocities and wave heights, as well as photographing flow patterns in the inlet.

7.2 Recommendations

Cost as well as aesthetic considerations suggest that remedial measures be implemented, if and when necessary, in a phased manner. The investigation has suggested a combination of sediment nourishment/removal methods coupled with the use of certain structures. The fact that structures are expensive and that they impose relatively permanent changes in the inlet system indicates that they should be constructed only if deemed absolutely essential. Specific structures were tested in the model. Whether or not a given structure is essential depends on the rate of sediment transport in the locality of interest. For example, if upon renourishment the Dubois Park beach were to remain stable for, say, a ten year period, a sand retaining structure such as a terminal groin may not be necessary. On the other hand, a relatively rapid rate of sand depletion, e.g. in a period of the order of a year, would mean that renourishment would be an expensive proposition in the absence of a groin.

Fixed bed hydraulic models are used to test the effects of various structural configurations and placements on flow characteristics. Sediment transport rates, on the other hand, are highly dependent on episodic events including storms and runoff, and long-term (e.g. on an annual basis) rates are strongly site-specific. At Jupiter Inlet the erosion problems are believed to be due to the jetties which have

essentially reduced the sediment transport rates along the banks while concentrating most of the transport from the sea within the middle portion of the channel so that the trap continues to receive sediment. Such a bank sediment-reducing rate of jettied inlets is a well-known and not uncommon phenomenon. The inlet, however, has been in existence in more or less its present state for over a decade, and one might expect the bank erosion/deposition rates to be relatively slow. This is of course an advantage in that it allows for the possibility of primarily using sediment nourishment/removal schemes as remedial measures as opposed to structural means.

The question that needs to be addressed concerns what to do and where to begin. The answer is that one must work with the forces of nature (and not against!) whenever necessary. In this sense, sediment nourishment/removal measures are relatively innocuous and allow for future corrections easily.

7.2.1 North Bank

It is proposed to nourish the feeder beach area with sand (volume $\cong$ 3,000 m^3). In addition, two relatively short test groins (using rocks or concrete-filled bags with appropriate foundation) should be constructed perpendicular to the shoreline. The feeder beach (terminating at the old groin west of the clubhouse beach) must be surveyed immediately after its placement and again one year later. The rate of sand depletion will give an indication as to the need for a weir-groin such as that studied in the model. If the beach lasts for a 2-3 year period, corresponding to the dredging frequency of the trap, it should not require a weir-groin. The test groins, of elevations up to mid-tide level at the bulkhead, should taper down to -2 m at a distance

of the order of 15 m, approximately equal to the length of some of the private docks in the area. Groin locations should be such that they do not inhibit boat traffic but that they are still useful in trapping sand. The sand trapping role is clearly suggested by the T-groin tests in the model. However, the amount retained at each groin will depend on the rate at which sand is depleted from the feeder beach. Figure 7.1 shows suggested locations for the test groins. The groins must be examined periodically to evaluate their sand trapping role. At the end of a one year period their efficacy will become apparent. If not effective, they should be removed.

It is evident that concentrated flood currents, waves and boat wakes are responsible for the erosion problem along the north bank where sediment supply is restricted by the presence of the north jetty at the entrance. A possible solution is to protect the entire shoreline by rocks placed against the bulkhead (or natural shoreline where there is no bulkhead) as well as short rock groins of the type noted above, for sand retainment (assuming of course that the groins are effective for this purpose). These groins and the rocks against the shoreline would also serve to attenuate the erosive forces due to currents, waves and boat wakes so that, regardless of their sand retaining capabilities, they may be useful. Long groins on the other hand will undoubtedly cause some adverse effects updrift as well as downdrift.

A problem with this scheme, however, is that placement of rocks against the bulkhead will not necessarily protect poorly designed bulkheads, or bulkheads in poor state of repair, from failure due to erosive forces which can be mitigated but not eliminated. A strict enforcement of boat speed limits should somewhat contain the bulkhead

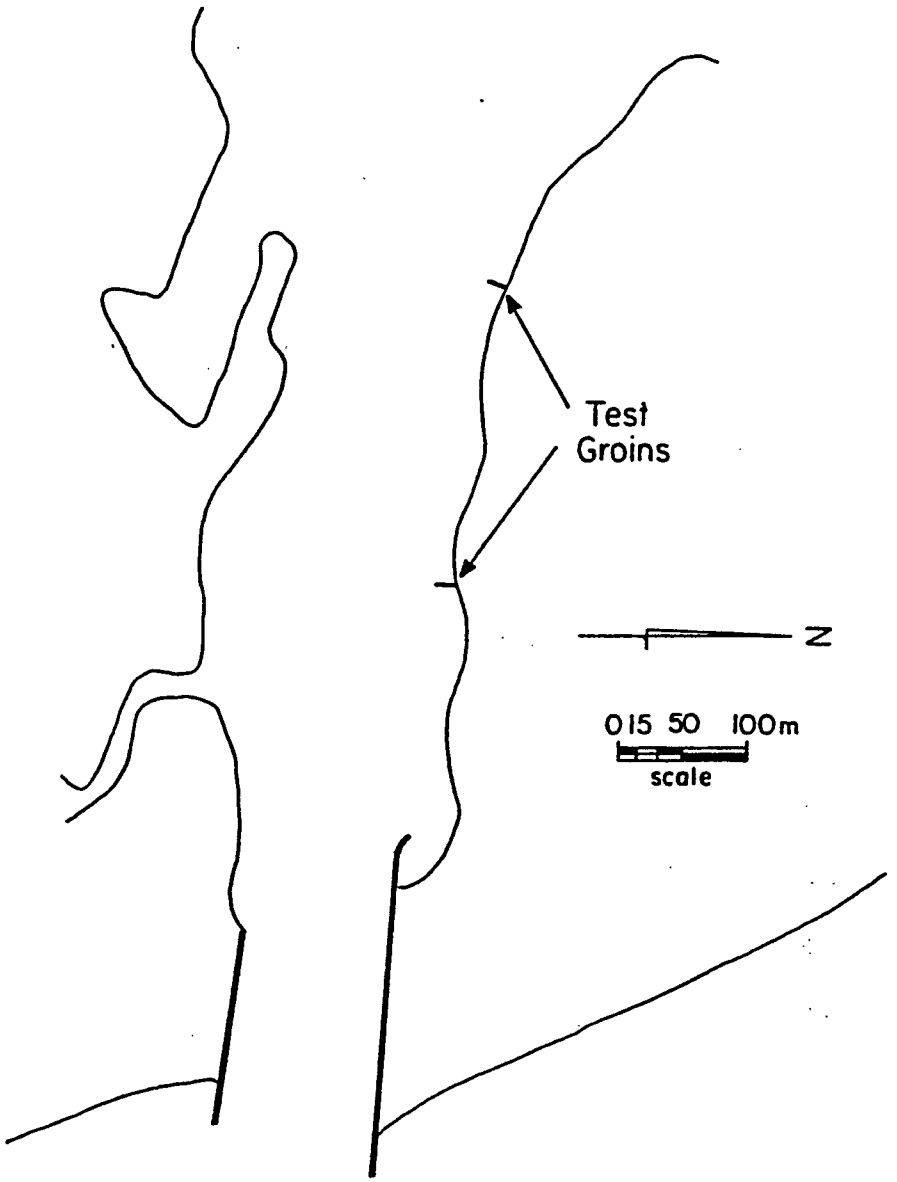

Fig. 7.1. Suggested Locations for Test Groins.

failure problem. In the first analysis, however, the poor bulkheads and the fact that placement of rocks against these could cause liability problems may restrict an effective solution.

The hope is that the feeder beach alone will be sufficient and that no weir-groin or rock groins along the shoreline will be necessary. If this does not turn out to be the case, then a minimal-sized weir-groin may be constructed. Furthermore, some short groins should be constructed along the shoreline both to retain sand and cut down the strength of flood flow.

A flow deflector may be considered in the future only as a last resort. Such a deflector, although effective in model tests, is expensive and sometimes develops a scour hole near its tip of sufficient dimensions to undermine the nearby bulkhead. One possibility is to construct the deflector (of configuration used in the model tests) or rocks to mid-tide level with piles driven at suitable intervals to provide for additional resistance to currents and waves. The piles would also serve to mark the location of the deflector for navigation purposes.

7.2.2 South Bank

The source of sediment in the Dubois Park lagoon is believed to be the region of erosion behind the south jetty rock extension. This does not, however, mean that no sediment could come from the inlet itself. Model tests have indicated the presence of a flow gyre at the mouth of the lagoonal channel which, during flood, could assist in the transport of sand from the inlet into the lagoon. An inspection of the lagoonal channel and the portion of the lagoon adjacent to the channel where sand deposition has occurred suggests no critical concern at present as far

as channel closure is concerned. It is best to inspect this area periodically, and if necessary in the future, to perform some dredging to keep the channel open.

The erosion scarp behind the rock extension of the south jetty is undesirable. The Australian pines here have fallen in places and root systems have been exposed. However, it is best not to do anything here unless the erosion becomes worse. It is recommended, however, that the connection between this area and the lagoonal mouth be blocked off as suggested through the model study. This may be done by constructing a bulkhead of relatively short length. Beyond this aspect, if reclamation of the eroded area is desired, a filter cloth-gravel-sand scheme may be implemented as suggested.

One cannot overemphasize the desirability to place vegetation wherever necessary and possible. From ecological as well as aesthetic points of view, the arguments in favor are strong. Although in the Australian pine area this may not be possible (unless of course the area is cleared which would reduce shade), there is an area near the parking lot next to the jetty where scour due to stormwater drainage has occurred. This appears to be a good site for some vegetative cover provided it is protected from people walking over.

A problem with the Dubois Park beach is the concrete between the two end groins. This must be removed without removing the groins themselves. The groins have been covered with concrete as well and there is an undesirable amount of wave reflection (which in turn erodes the sand). It should be easy to break up the concrete over each groin up to high tide level, converting it to rubble (as has already happened in places due to natural forces). This rubble will serve to absorb the

wave energy. It should be noted again, however, that the concrete beach between the groins including the steps must be removed, while the concrete turned into rubble at the groins themselves must be retained. After this, the beach must be renourished (volume $\cong$ 2,000 m^3).

If the existing groins fail to retain the sand over an adequate length of time, e.g. 2-3 years, then they must be extended as suggested in the model study. No sills are recommended.

The shoreline between the Dubois Park beach and the marina promontory has been lined with rocks and concrete. Here again it is desirable to break up the concrete cover in to rubble up to high tide level. In this study a possible recreational beach has been proposed near the west end of the bank. As such, the present configuration of the cove-like area will not retain sand. Modifications suggested in the model study, i.e. removal of an existing groin and lengthening the two end groins plus removal or at least breaking up of all concrete between the groins will be essential for retaining renourished sand here.

The source of the shoal in the marina is sediment which moves around the promontory during flood as well as material brought in from the inlet by ebb currents. This material should be dredged out. Some armoring of the eroding portion of the tip of the promontory with rocks is also recommended. The marina, by virtue of its existence, will continue to trap sand. However, it is believed that the rate of shoaling is not too high.

7.3 Inlet Maintenance

The primary component of this program would consist of a means to carry out various sand nourishment and removal operations. Data analysis suggests that the inlet is self-sufficient in terms of sand

supply necessary for the recommended nourishment of eroded areas and recreational beaches. Therefore, a method that would not require transport of sediment from sources outside the inlet may be employed.

Three such methods were discussed in Section 5.3 and two were deemed viable for the inlet: transport of sediment by a 1) portable hydraulic dredge or 2) a jet pump.

It is quite likely, however, that the currently followed procedure of periodic dredging of the sand trap would be at a lower unit cost than either of the aforementioned systems, both of which would involve new capital costs. It is therefore recommended that the present procedure be extended to cover the additional removal/nourishment requirements.

APPENDIX A

STORM SURGE FLOW VELOCITY

Calculations of flow velocities at various locations in the inlet due to a storm surge of +1.5 m are based on the use of tidal inlet hydraulic relationships of Keulegan (1951). The relationships originally developed apply to an ocean-inlet-bay system but may be applied to an ocean-inlet-estuary system through suitable interpretation of bay geometry (Mehta, 1975). This procedure was first tested by calculating the maximum inlet flow velocity u_{max} for a normal (measured) flood condition. A velocity of 2.35 m/sec was calculated which compared reasonably with the measured velocity of 2.15 m/sec. Based on this comparison, the procedure was deemed valid for the predictions of the flow velocity during a 1.5 m storm surge.

The calculation of storm surge flow velocity is based on the relationship between u_{max} and the coefficient of repletion K of the inlet (see Fig. A-1). This value of K is defined by:

$$K = \frac{T}{2\pi a_o} \frac{A_c}{A_B} \frac{\sqrt{2ga_o}}{\sqrt{F}} \qquad \text{(A-1)}$$

where T is the tidal period (12.4 hours), a_o is the tidal amplitude (0.55m), A_c is the inlet cross-sectional area at mid-tide (435 m^2), and A_B is the area of the bay. F represents the energy losses by the flow between the ocean and bay resulting from head losses due to flow convergence and expansion when entering and leaving the inlet as well as

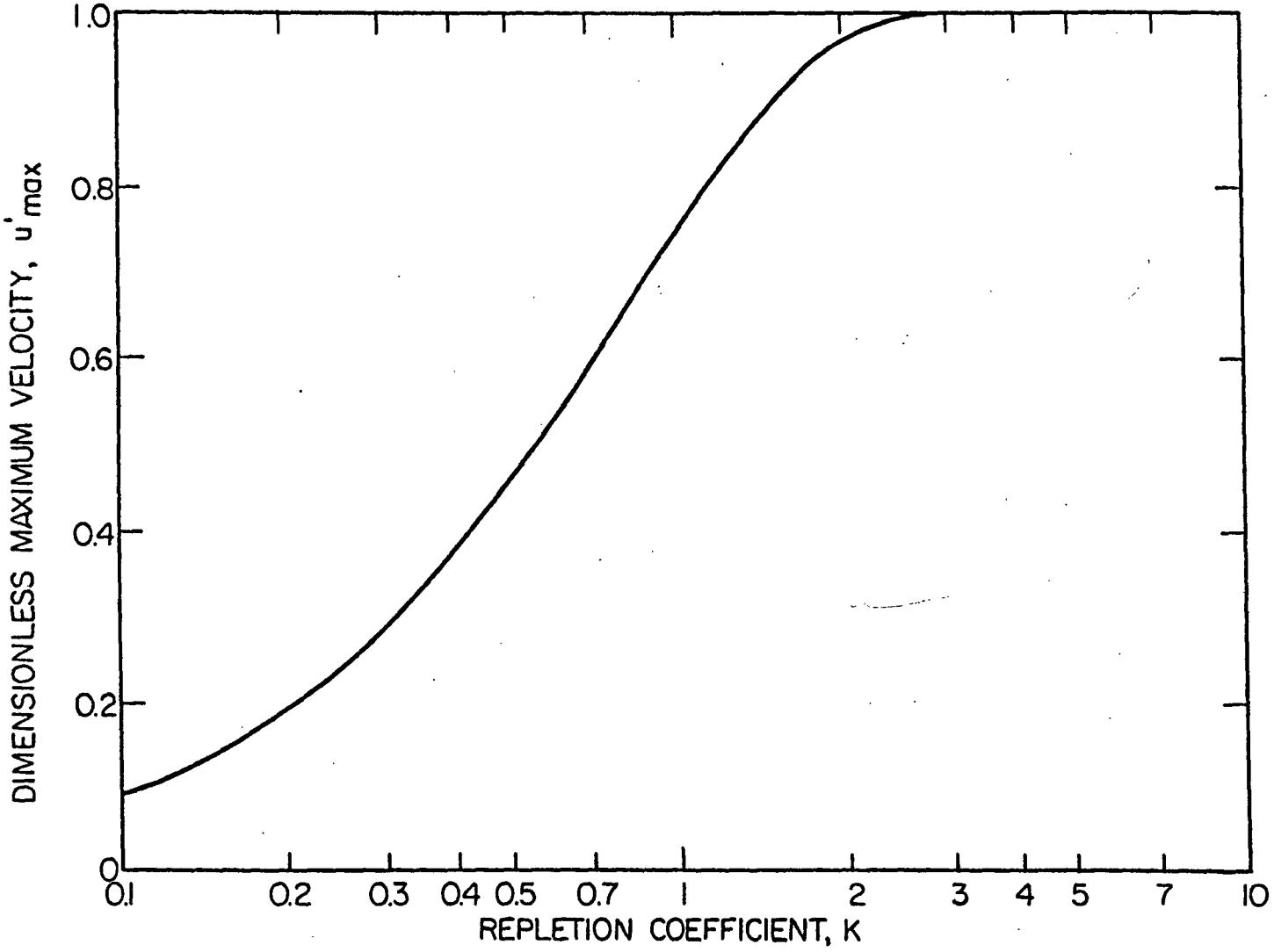

Fig. A-1. Dimensionless Maximum Velocity, u'_{max}, as a Function of Keulegan's Repletion Coefficient.

losses due to bottom friction in the inlet. It should be noted that the value for A_c was calculated based on 1929 NGVD sea level. That the sea level at the inlet has risen approximately 0.12 m since then (Hicks, et al., 1983) was not taken into account when calculating the value of A_c. In the event of a storm surge, the values of A_c and a_o increase significantly thereby altering K and as a result, the flow velocity through the cross-section.

All of the parameters on the right hand side of equation (A-1) were known for Jupiter Inlet with the exception of A_B and F. K may be determined if the time lag ε between high or low tide in the ocean and slack water in the inlet is known (see Fig. A-2). Based on comparisons between tide records taken at the inlet mouth and well offshore (Section 3.3), a time lag of 48 minutes was calculated. This corresponds to an ε value of

$$\frac{48 \text{ min.}}{12.4 \text{ hours}\left(60 \frac{\text{min.}}{\text{hour}}\right)} \times 360^0 \approx 23^0 \qquad \text{(A-2)}$$

With this value of ε, K is determined from Fig. A.2 as 1.2. The value of F was determined from the procedure prescribed by Mehta (1975) as follows:

$$F = K_{en} + K_{ex} + \frac{fL_c}{4R_c} \qquad \text{(A-3)}$$

where K_{en} and K_{ex} are the coefficients of head loss at the flow entrance (due to convergence of flow streamlines into the inlet) and flow exit (due to expansion of flow streamlines out of the inlet). K_{en} is assumed to be 0.05 while K_{ex} is equal to 1.0. The term $fL_c/4R_c$ represents the

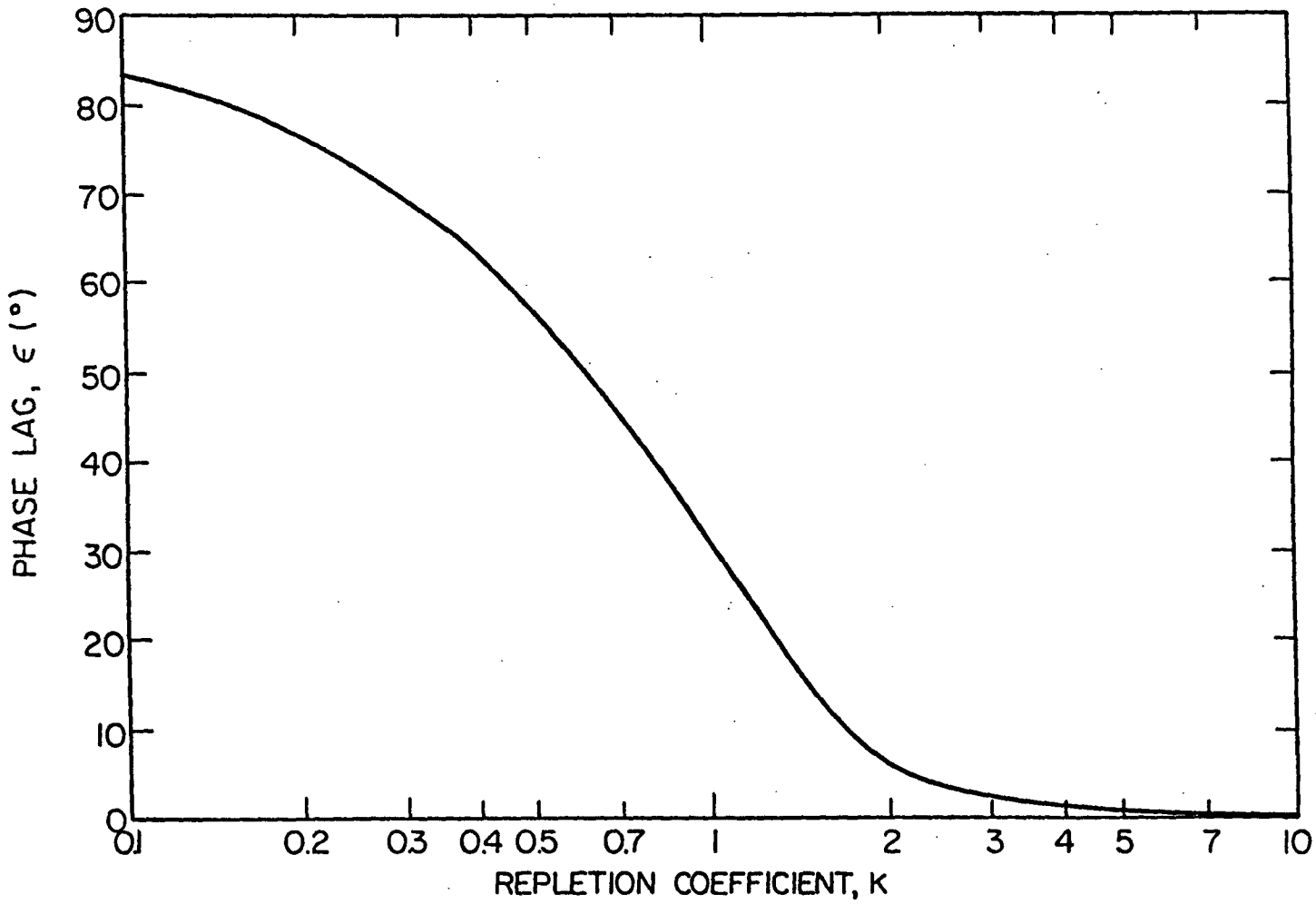

Fig. A-2. Lag ε in Degrees as a Function of Keulegan's Repletion Coefficient K.

gradual head loss due to bottom friction in the inlet of "equivalent length" L_c (see Mehta, 1975). R_c is the hydraulic radius of the "equivalent inlet", while f is the Darcy-Weisbach friction factor which is calculated as follows (Mehta, 1975):

$$\frac{1}{2\sqrt{f}} = 1.458 \left(\frac{R_c}{k}\right)^{1/6} \qquad \text{(A-4)}$$

k is the bed roughness which was estimated from discharge measurements as 0.234 m (Appendix D). From equation (A-4), an f value of 0.045 was calculated. By substituting these values of f, L_c (= 471 m using the procedure given by Mehta, 1975), and R_c (= 4.1 m) into equation (A-3), an F value of 2.35 was calculated.

Equation (A-2) may be used with these parameters to determine A_B as follows:

$$A_B = \frac{T A_c\sqrt{2ga_o}}{K2\pi a_o\sqrt{F}} = \frac{(12.4)(3600)(435)\sqrt{(2)(9.8)(0.55)}}{(1.2)(2\pi)(0.55)\sqrt{(2.35)}} \qquad \text{(A-5)}$$

$$= 9.94 \times 10^6 m^2$$

For a 1.5 m storm surge the inlet cross-sectional area increases from 435 m^2 to 591 m^2 and a_o from 0.55 m to 2.05 m. A K value corresponding to this storm surge condition may now be calculated.

$$K = \frac{(12.4)(3600)}{(2\pi)(2.05)} \frac{(591)}{(9.94)(10^6)} \sqrt{\frac{(2)(9.8)(2.05)}{(2.35)}} \qquad \text{(A-6)}$$

$$= 0.85$$

From Fig. A-1 a K value of 0.85 corresponds to a dimensionless velocity of 0.68 where

$$u'_{max} = \frac{T}{2\pi a_o} \frac{A_c}{A_B} u_{max} \qquad (A-7)$$

This results in a maximum velocity of

$$u_{max} = \frac{(2\pi)(2.05)}{(12.4)(3600)} \frac{(9.937)(10^6)}{(591)} (0.68)$$

$$= 3.30 \text{ m/sec}$$

Thus the maximum flow velocity at the inlet mouth during a 1.5 m storm surge is approximately one and one-half times that of a normal maximum flood velocity. This value corresponds to a model velocity of 0.48 m/sec and, as can be seen in Table 4.1, was accurately reproduced. It was assumed that the flow velocities in the other areas of the inlet increased by approximately the same ratio.

APPENDIX B

DEPTH CORRECTION FOR VELOCITY MEASUREMENTS

When taking velocity measurements in currents of high magnitudes, the drag forces induced by the flow past the current meter and its connecting weight cause a measurable horizontal and, as a result, vertical displacement of the current meter (Fig. B-1). This phenomenon must be accounted for when determining velocity profiles as they are dependent upon flow velocities corresponding to specific depths. The depth correction procedure used was as follows.

Parameters used in calculations correspond to the specifications of the Ott meter #19089 utilized in the field to measure current velocities.

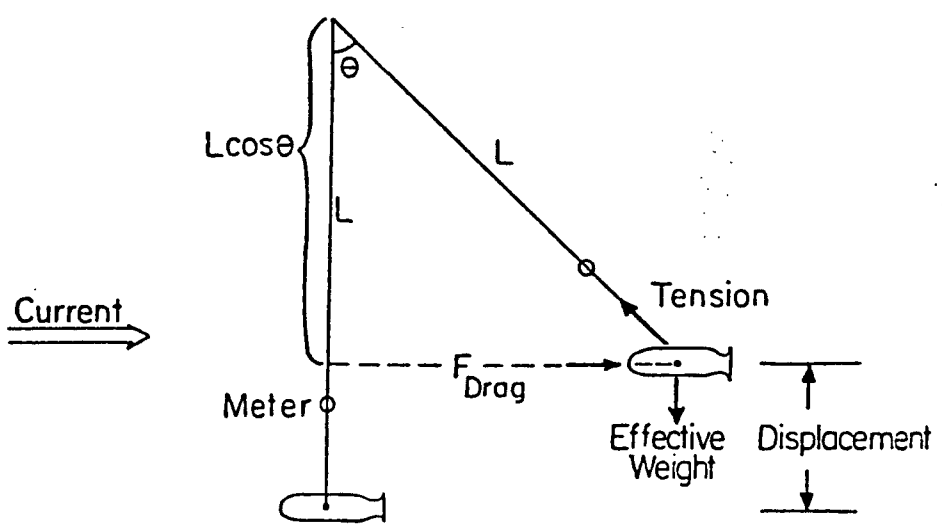

Fig. B-1. Vertical Displacement of the Current Meter due to Current-Induced Drag Forces.

A_w = Cross-sectional area of weight = $0.028\ m^2$

$\forall_w$ = Volume of weight = $1.9 \times 10^{-3}\ m^3$

W_w = Weight = 5.0 kg

A_m = Cross-sectional area of meter = $0.012\ m^2$(propeller)

$\forall_m$ = Volume of meter = $7.1 \times 10^{-4}\ m^3$

W_m = Weight of meter = 0.45 kg

C_{Dw} = Drag coefficient of weight* = 0.05

C_{Dm} = Drag coefficient of meter* = 0.99

ρ_{H_2O} = Density of salt water = $1030\ kg/m^3$

*Drag coefficients obtained from Meyers, et al. (1969).

$$\Sigma F_v: \quad T\cos\theta = \text{Effective weight} \tag{B-1}$$

$$\Sigma F_H: \quad T\sin\theta = F_{Drag} \tag{B-2}$$

$$T = \frac{\text{Effective Weight}}{\cos\theta} = \frac{F_{Drag}}{\sin\theta} \tag{B-3}$$

$$\therefore \tan\theta = \frac{F_{Drag}}{\text{Effective weight}} \tag{B-4}$$

For a given current velocity u (m/sec):

$$F_{Drag} = \left(C_{Dm}\rho_{H_2O}A_m \frac{u^2}{2}\right) + \left(C_{Dw}\rho_{H_2O}A_w \frac{u^2}{2}\right) \tag{B-5}$$

$$= u^2 \left[\left(\frac{(0.99)(1030)(0.012)}{(2)}\right) + \left(\frac{(0.05)(1030)(0.028)}{(2)}\right)\right]$$

$$= 6.84\ u^2 \text{ Newtons}$$

$$= 0.70\ u^2 \text{ kg}$$

Effective weight

$$= (W_m + W_w) - \rho_{H_2O}(\forall_m + \forall_w)$$

$$= (0.45 + 5.0) - (1030)(0.00071 + 0.0019)$$

$$= 2.76 \text{ kg} \qquad \text{(B-6)}$$

$$\therefore \tan\theta = \frac{F_{Drag}}{\text{Effective Weight}} = \frac{0.70\ u^2}{2.76} = \frac{u^2}{3.94}$$

$$\theta = \tan^{-1}\left(\frac{u^2}{3.94}\right) \qquad \text{(B-7)}$$

$$\text{corrected depth} = L\cos\theta = L\cos\left(\tan^{-1}\frac{v^2}{3.94}\right) \qquad \text{(B-8)}$$

For flow velocities less than 1 m/sec, $L\cos\theta \approx L$. In this case drag forces do not overcome the effective weight of the meter-weight system and no significant vertical displacement takes place. Figure B-2 shows a plot of vertical displacement versus flow velocity determined from equation B-8.

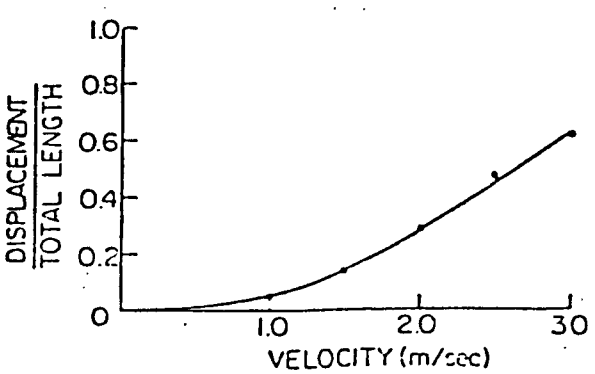

Fig. B-2. Vertical Displacement of the Current Meter versus Flow Velocity.

APPENDIX C

DIMENSIONLESS TRANSVERSE VELOCITY PROFILES

The plots presented in this appendix represent the dimensionless transverse velocity profiles for each of the cross-sections in the inlet (with the exception of C-5). They are based on data obtained from the velocity profiles taken at each cross-section (Section 3.5). These plots, as well as the parameters describing the tidal conditions on which they are based, are defined in Section 3.5.2 (Mehta and Sheppard, 1977). The plots provide information regarding the dominance of ebb and flood flows at different locations along the cross-section. As these plots are normalized, they provide a more representative indication of the dominant regions of flow throughout the tidal cycle. Table C-1 provides a summary of the information obtained from each profile taken at a given cross-section. Analysis and discussion of this information follows.

Information provided in Table C-1 for cross-section C-1 reveals that the transverse cross-sectional velocity profile is relatively uniform. The bathymetry is fairly constant here thereby preventing the channeling of flow into a region of higher velocity.

Profiles at cross-section C-2 clearly indicate a region of higher flow velocity along the north bank of the inlet. This is corroborated by analyses made from the drogue and dye studies (Sections 3.6 and 3.7) as well as with the observation that the deeper locations along this cross-section are near the north shore. These greater depths provide a

Table C-1. Location of Dominant Flow Along Each Cross-Section.

Cross-Section	Flow Condition	θ	Discharge (m^3)	Location of Dominant Flow
C-1 #1	Flood	0.92	396	Center
#2	Ebb	0.52	517	Center
#3	Ebb	0.68	623	Center
#4	Flood	0.64	413	Center
C-2 #1	Flood	0.83	444	North Bank
#2	Flood	0.33	366	North Bank
#3	Flood	0.54	337	North Bank
C-3 #1	Flood	0.42	78	West Bank
#2	Flood	0.66	160	Center
#3	Ebb	0.92	207	Center
C-4 #1	Flood	0.92	311	Center
#2	Ebb	0.12	182	Center
#3	Ebb	0.84	586	North Bank
#4	Ebb	0.95	393	North Bank

means for the flow to be channeled at high velocities in this location and contribute to the erosion problems along the north shoreline.

The profiles at cross-section C-3 indicate a fairly uniform cross-sectional transverse velocity distribution, with one exception showing flow concentrated towards the west bank of the Intracoastal Waterway. The paths taken by the drogues as they proceed into the Intracoastal Waterway (Section 3.6) tend to indicate flow concentration along the west bank as well.

Two of the profiles taken at cross-section C-4 indicate a high concentration of flow near the north shoreline. This location corresponds to that of the Intracoastal Waterway channel where, again due to the significantly greater depths, the flow is channelized at high velocities.

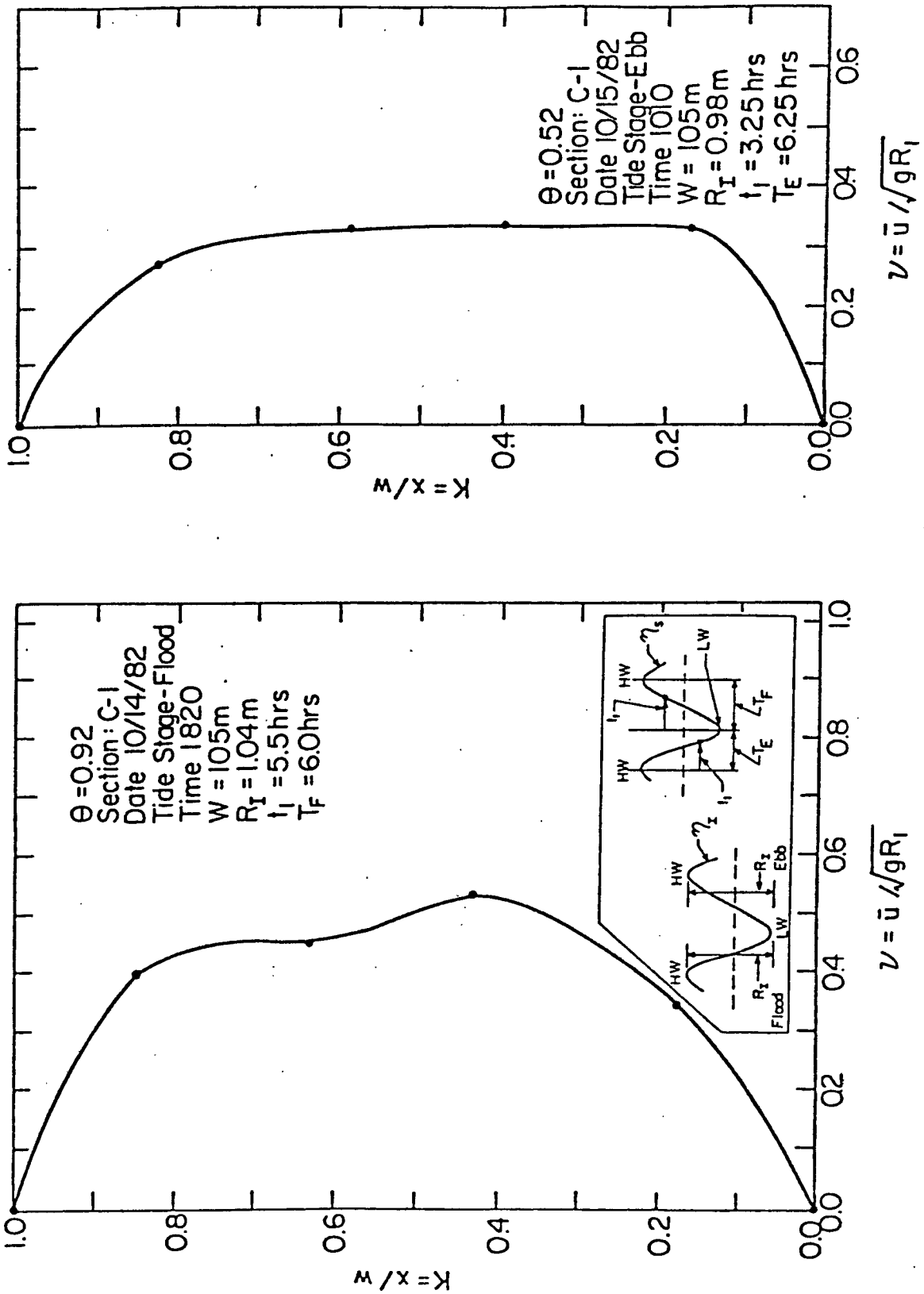
θ=0.52
Section: C-1
Date 10/15/82
Tide Stage-Ebb
Time 1010
W = 105m
R_I=0.98m
t_I =3.25hrs
T_E =6.25hrs
$\nu = \bar{u}/\sqrt{gR_I}$
K = x/w
θ=0.92
Section: C-1
Date 10/14/82
Tide Stage-Flood
Time 1820
W = 105m
R_I = 1.04m
t_I =5.5hrs
T_F =6.0hrs
HW
LW
Flood
Ebb
η_s
η_I
T_E
T_F
t_I
R_I

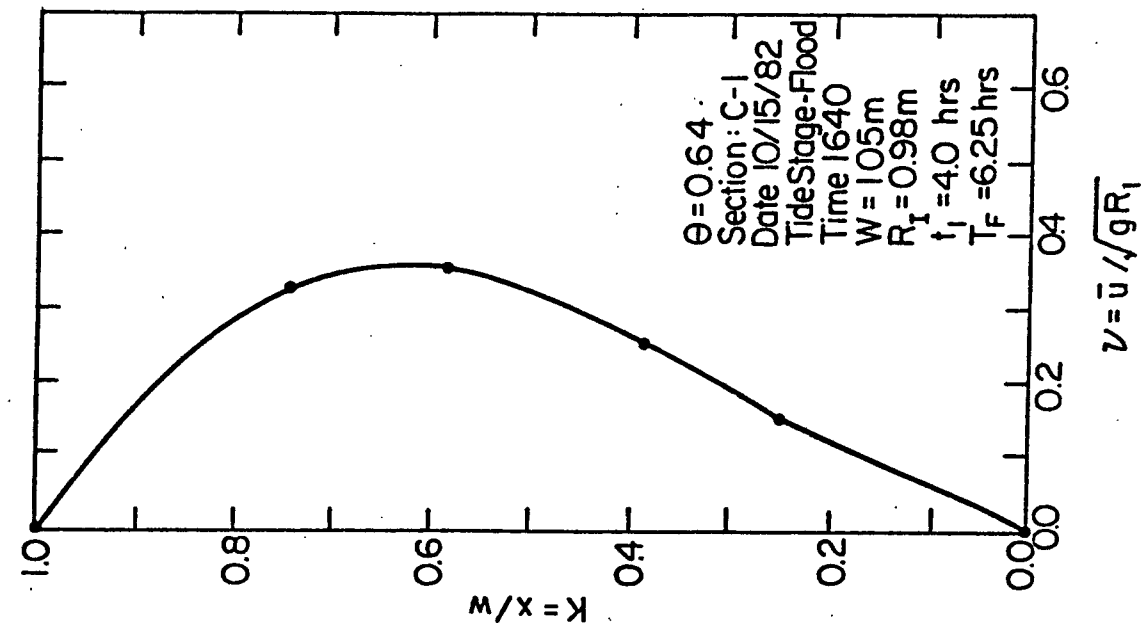
θ=0.64
Section: C-1
Date 10/15/82
TideStage-Flood
Time 1640
W = 105m
R_I = 0.98m
t_I = 4.0 hrs
T_F = 6.25hrs
K = x/w
$v = \bar{u}/\sqrt{gR_I}$
0.0
0.2
0.4
0.6
0.8
1.0

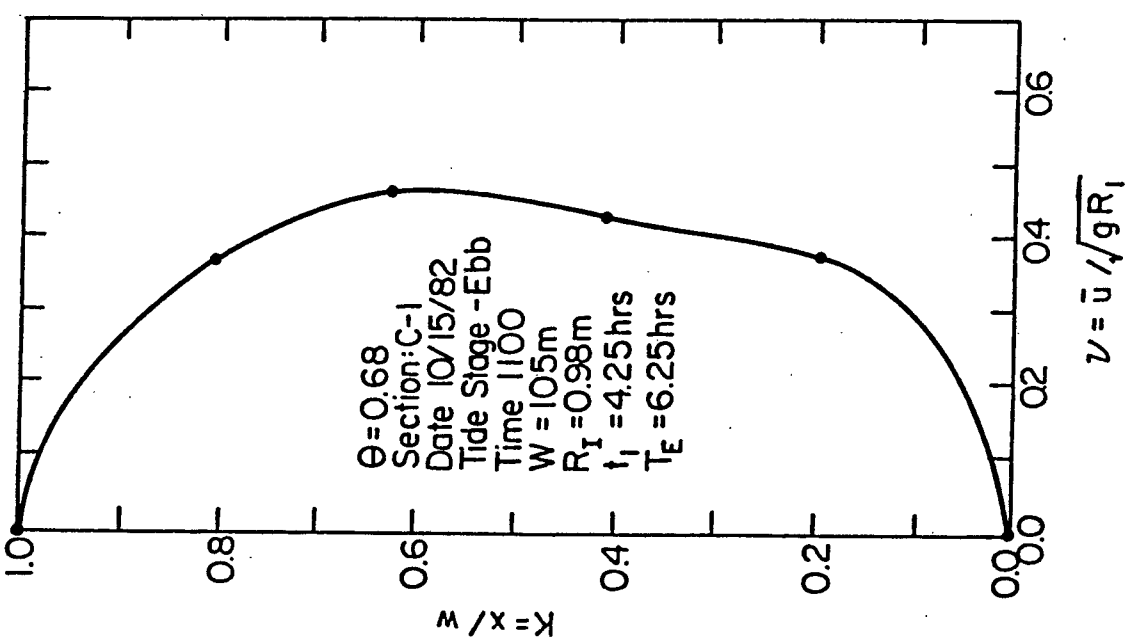
θ=0.68
Section: C-1
Date 10/15/82
Tide Stage - Ebb
Time 1100
W = 105m
R_I = 0.98m
t_I = 4.25hrs
T_E = 6.25hrs
K = x/w
$v = \bar{u}/\sqrt{gR_I}$
0.0
0.2
0.4
0.6
0.8
1.0

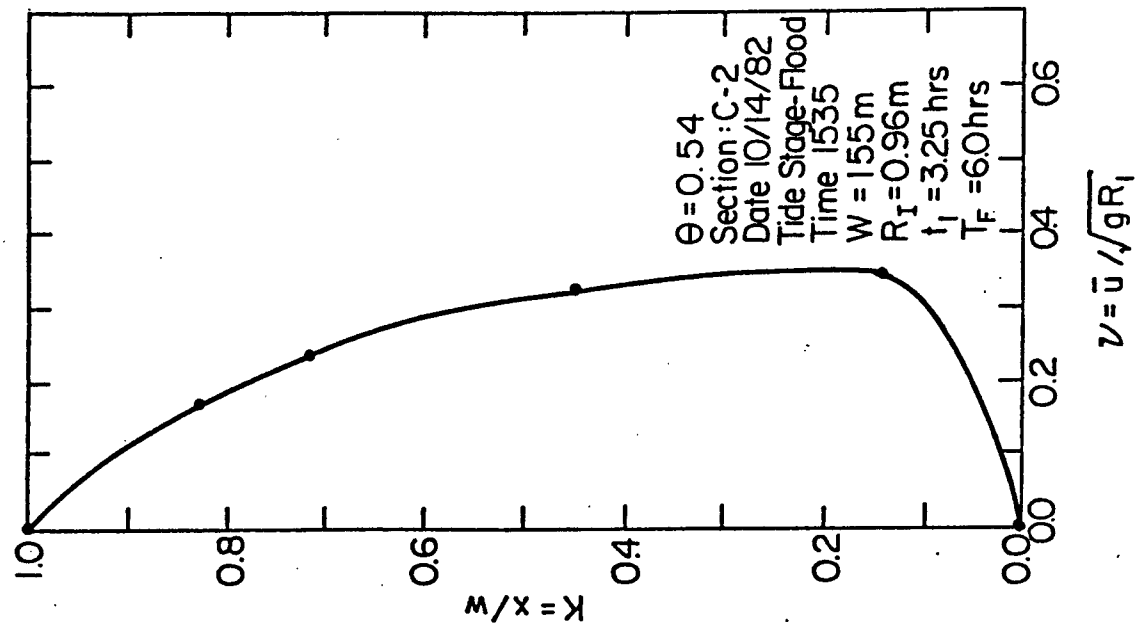
θ=0.54
Section: C-2
Date 10/14/82
Tide Stage-Flood
Time 1535
W = 155m
R_I=0.96m
t_I =3.25 hrs
T_F =6.0hrs
K = x/w
$v = \bar{u}/\sqrt{gR_I}$
1.0
0.8
0.6
0.4
0.2
0.0
0.0
0.2
0.4
0.6

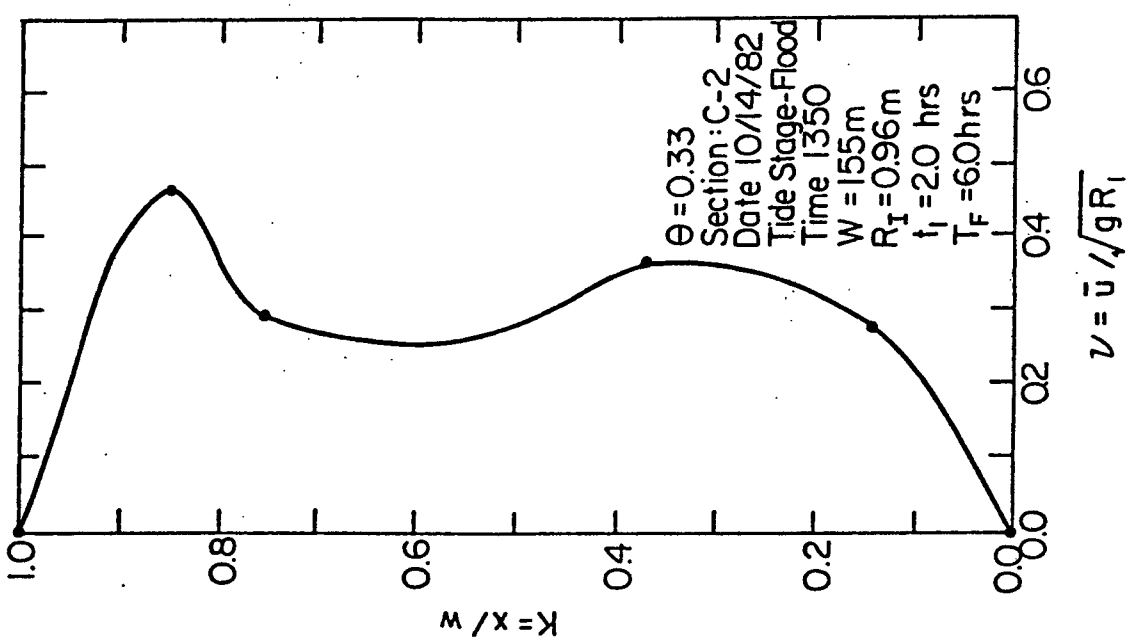
θ=0.33
Section: C-2
Date 10/14/82
Tide Stage-Flood
Time 1350
W = 155m
R_I=0.96m
t_I =2.0 hrs
T_F =6.0hrs
K= x/ w
$v = \bar{u}/\sqrt{gR_I}$
1.0
0.8
0.6
0.4
0.2
0.0
0.0
0.2
0.4
0.6

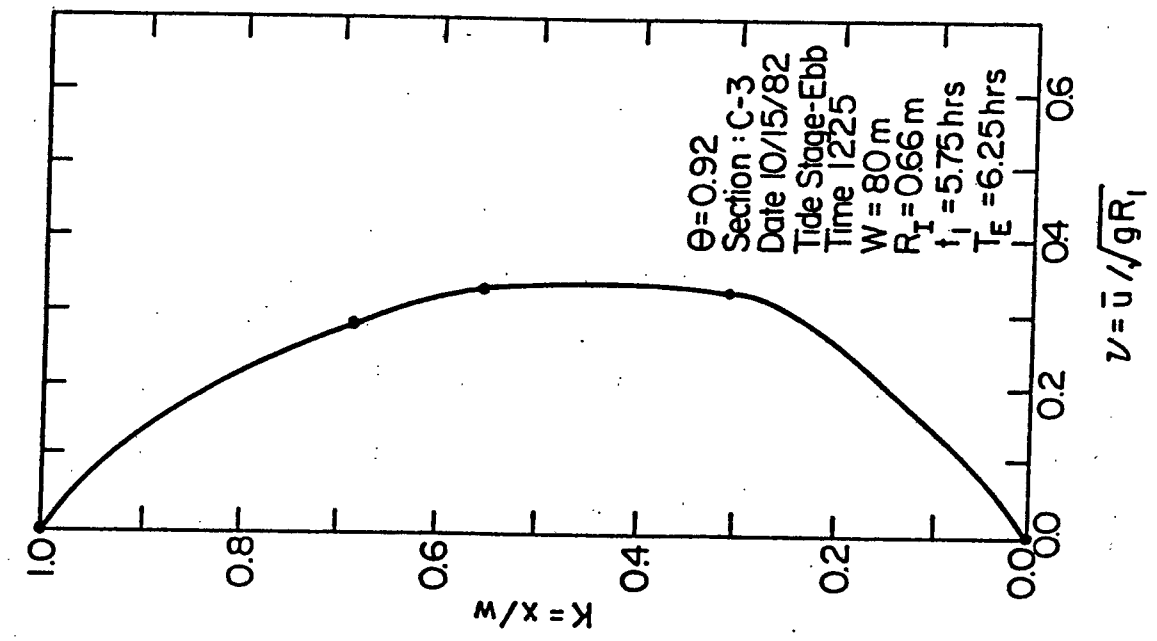
θ=0.92
Section : C-3
Date 10/15/82
Tide Stage-Ebb
Time 1225
W = 80 m
R_I = 0.66 m
t_I = 5.75 hrs
T_E = 6.25 hrs
K = x/w
$\nu = \bar{u} / \sqrt{g R_I}$
0.0
0.2
0.4
0.6
0.8
1.0

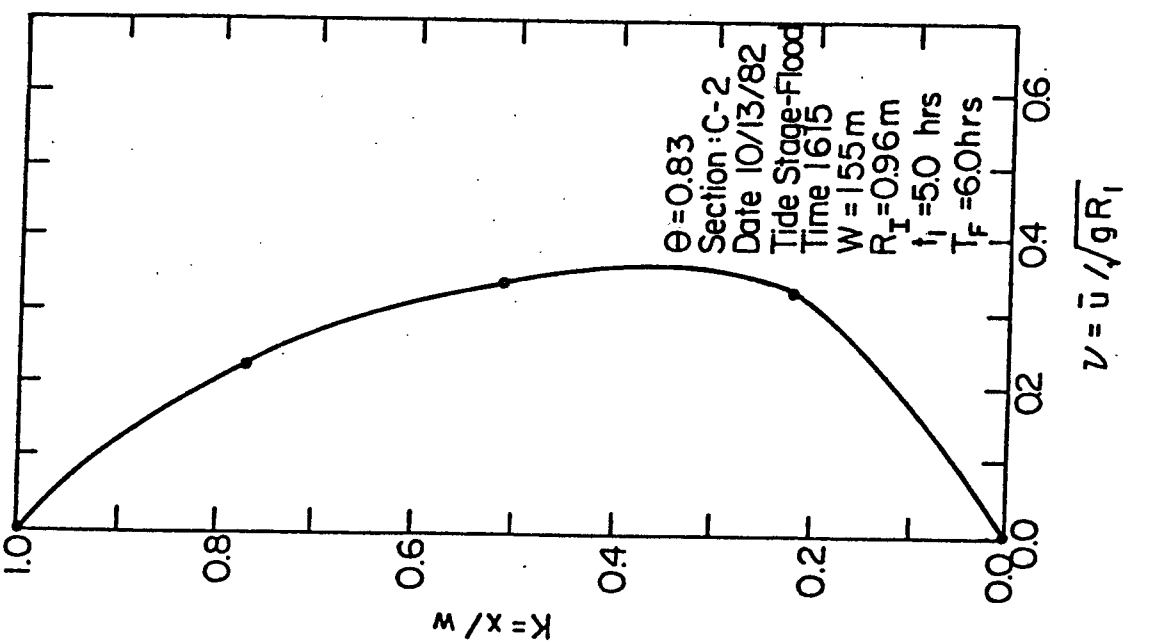
θ=0.83
Section : C-2
Date 10/13/82
Tide Stage-Flood
Time 1615
W = 155 m
R_I = 0.96 m
t_I = 5.0 hrs
T_F = 6.0 hrs
K = x/w
$\nu = \bar{u} / \sqrt{g R_I}$
0.0
0.2
0.4
0.6
0.8
1.0

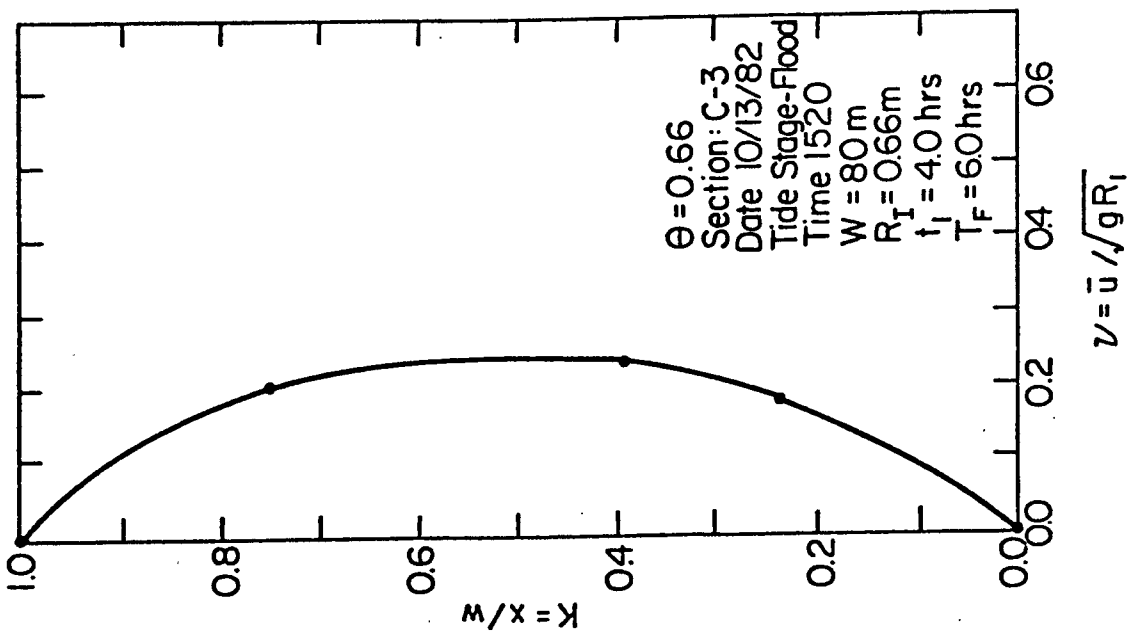
θ=0.66
Section: C-3
Date 10/13/82
Tide Stage-Flood
Time 1520
W = 80 m
R_I = 0.66m
t_I = 4.0 hrs
T_F = 6.0hrs
K = x/w
$\nu = \bar{u}/\sqrt{gR_I}$
0.0
0.2
0.4
0.6
0.8
1.0

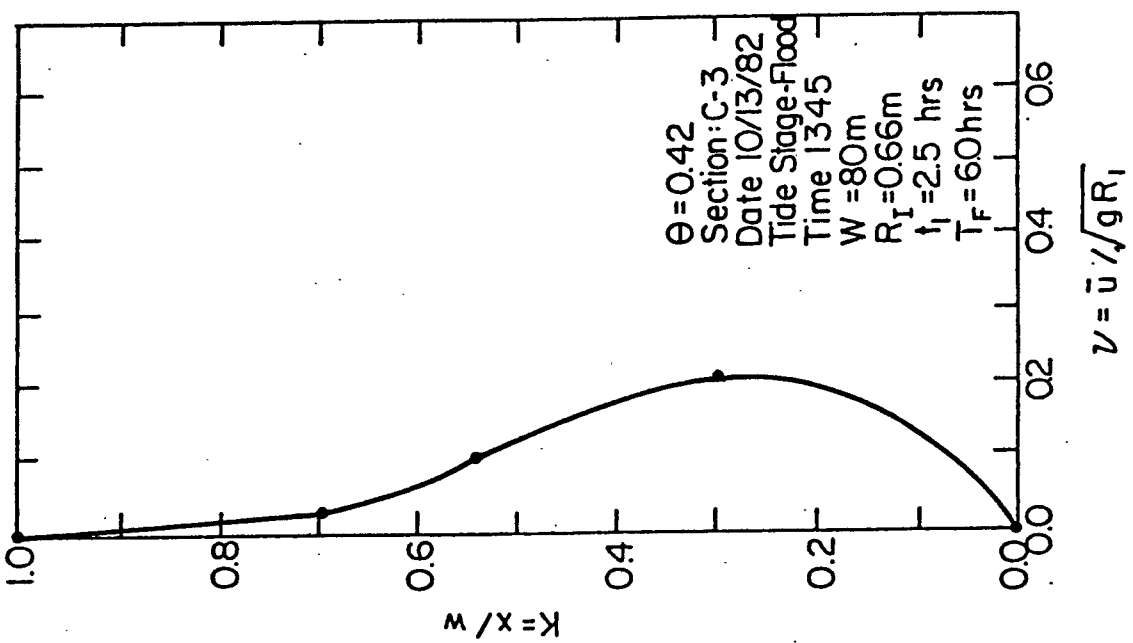
θ=0.42
Section: C-3
Date 10/13/82
Tide Stage-Flood
Time 1345
W =80m
R_I=0.66m
t_I =2.5 hrs
T_F=6.0hrs
K= x/w
$\nu = \bar{u}/\sqrt{gR_I}$
0.0
0.2
0.4
0.6
0.8
1.0

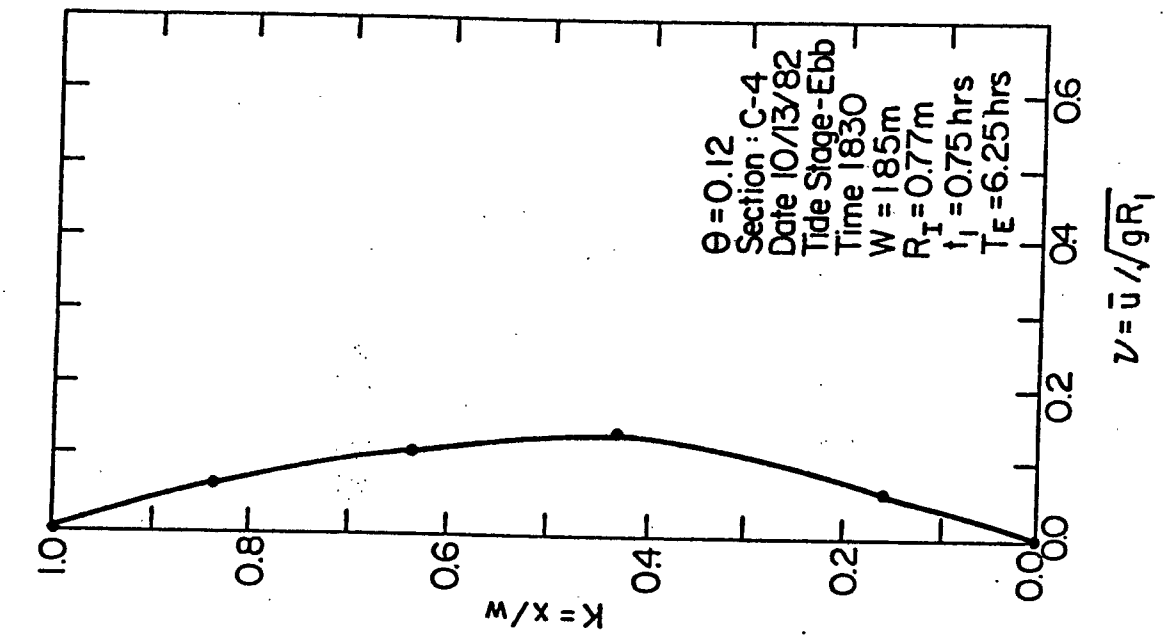
θ=0.12
Section: C-4
Date 10/13/82
Tide Stage-Ebb
Time 1830
W = 185m
R_I=0.77m
t_I=0.75hrs
T_E=6.25hrs
$\nu = \bar{u}/\sqrt{gR_I}$
K = x/w
0.0
0.2
0.4
0.6
0.8
1.0

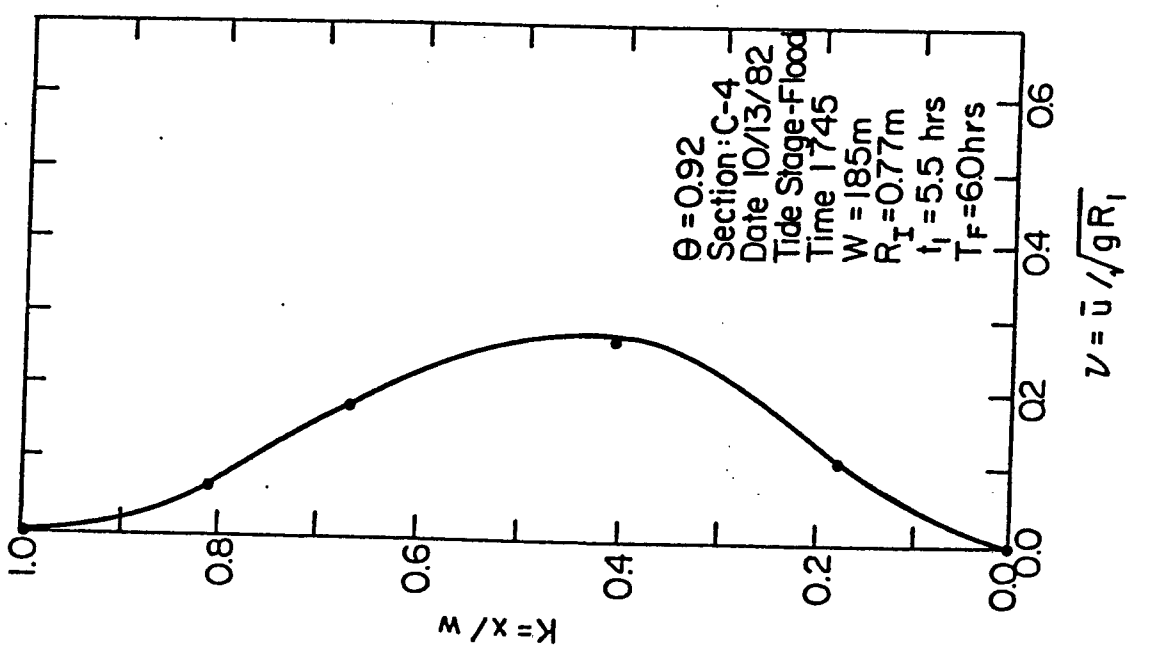
θ=0.92
Section: C-4
Date 10/13/82
Tide Stage-Flood
Time 1745
W = 185m
R_I=0.77m
t_I=5.5 hrs
T_F=6.0hrs
$\nu = \bar{u}/\sqrt{gR_I}$
K = x/w
0.0
0.2
0.4
0.6
0.8
1.0

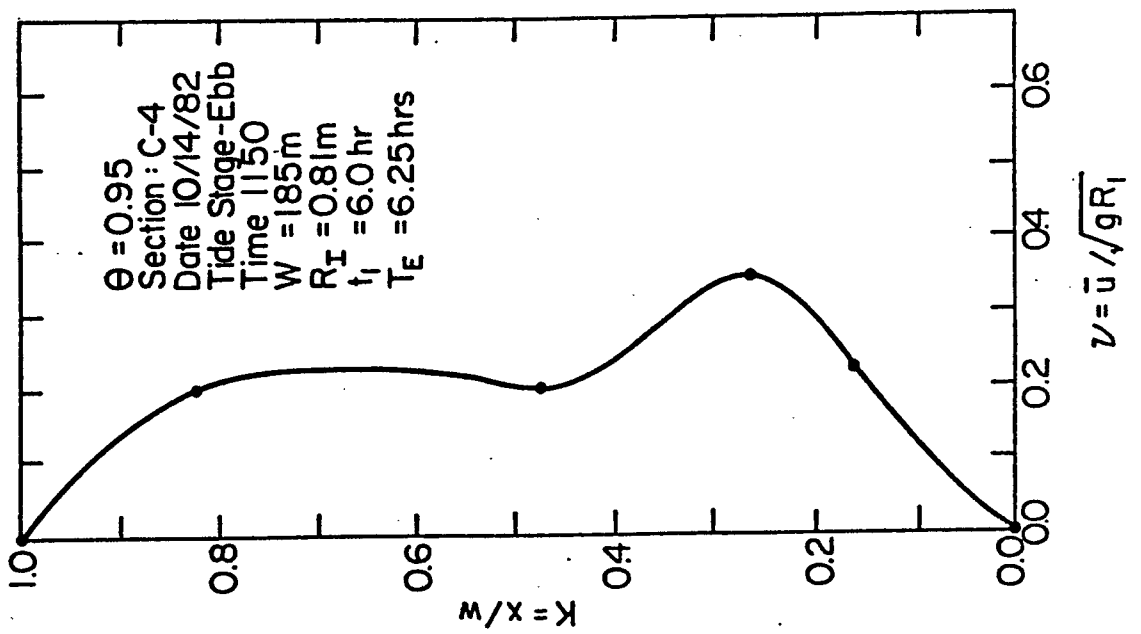
θ=0.95
Section: C-4
Date 10/14/82
Tide Stage-Ebb
Time 1150
W=185m
R_I=0.81m
t_I=6.0hr
T_E=6.25hrs
K= x/w
$\nu = \bar{u}/\sqrt{gR_I}$
1.0
0.8
0.6
0.4
0.2
0.0
0.6
0.4
0.2
0.0

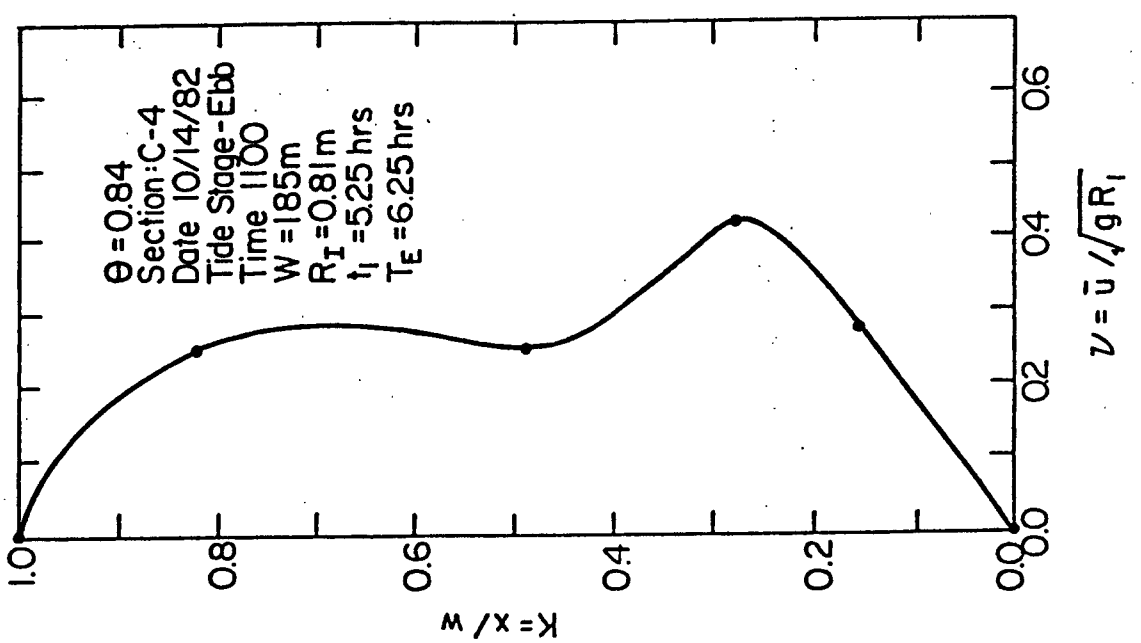
θ=0.84
Section: C-4
Date 10/14/82
Tide Stage-Ebb
Time 1100
W=185m
R_I=0.81m
t_I=5.25hrs
T_E=6.25hrs
K= x/w
$\nu = \bar{u}/\sqrt{gR_I}$
1.0
0.8
0.6
0.4
0.2
0.0
0.6
0.4
0.2
0.0

APPENDIX D

FRICTION SLOPE AND BED ROUGHNESS CALCULATIONS

Vertical velocity profiles taken at each flow cross-section were used to estimate friction slopes and bed roughness values, as was the case in this study. The method is described in detail by Hayter (1979) and is briefly outlined here.

The procedure consists of first calculating the friction velocity, u_*, at each point along the cross-section where velocity profiles were taken by employing the equation (Christensen and Walker, 1969) as follows:

$$u_* = 0.4(u_p - u_q)/\ell n(p/q) \qquad \text{(D-1)}$$

In this equation, values for u_p and u_q are velocities at p and q, respectively, and are obtained from a logarithmic plot of the vertical velocity profiles similar to the one in Fig. 3.3. The friction slope S_f is then computed via the equation

$$S_f = \frac{u_*^2}{gd} \qquad \text{(D-2)}$$

where d = local depth.

In all cases, calculated values of S_f were found to be of the same order of magnitude across a given profile. These values were not identical, however, and therefore a cross-sectional average value $\bar{S}_f$ was determined by integration (Fig. D-1). The resulting values of $\bar{S}_f$ calculated from each profile of a given cross section were then

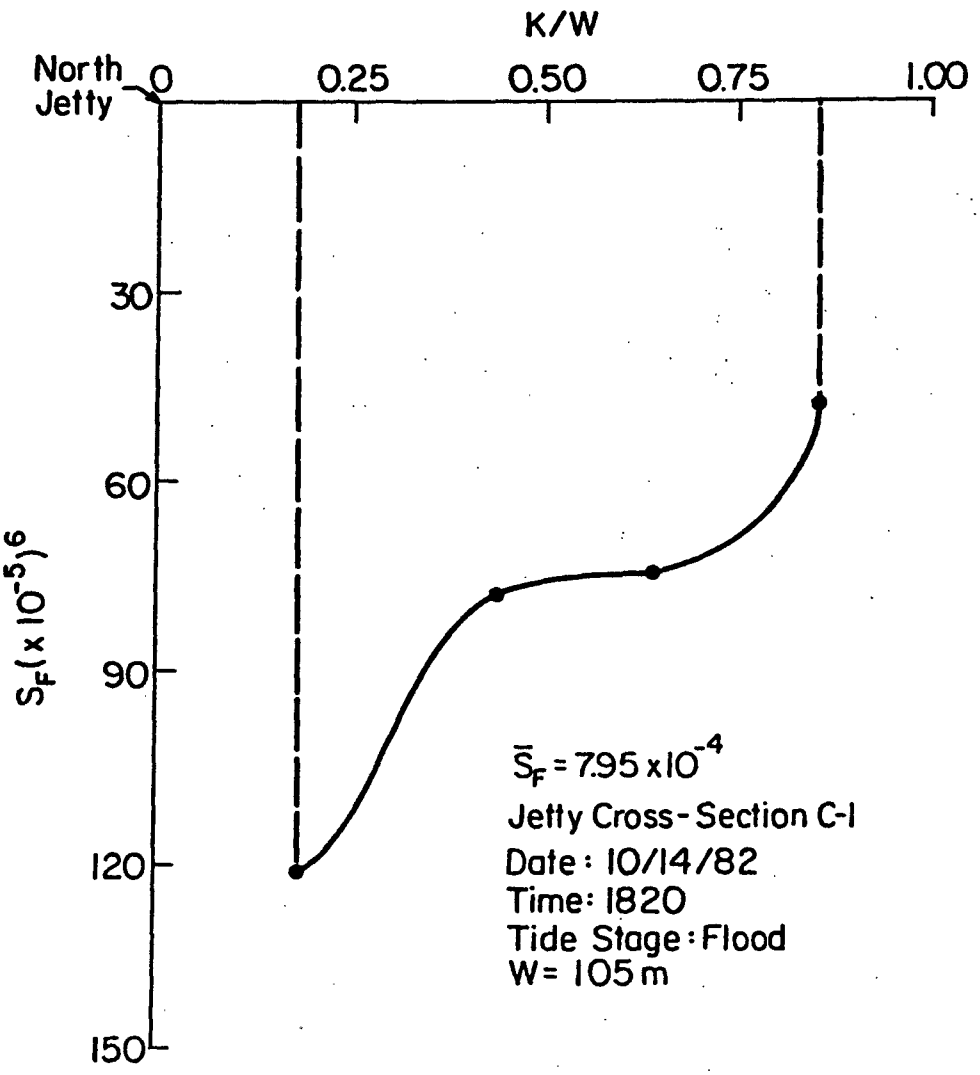

Fig. D-1. Lateral Distribution and Cross-Sectional Average of S_f at Jetty Cross-Section C-1, October 14, 1982, 1820 Hours.

utilized, along with values of tide elevation and instantaneous discharge, as input for determining the cross-section bed roughness (k) for each profile in the single point-velocity discharge computer program (Hayter, 1979). Values of $\bar{S}_f$ and k are presented in Table D-1. For a given cross-section, values of k obtained for each profile were averaged to obtain a representative bed roughness for that cross-section. These values are given in Table D-2.

Table D-1. Friction Slope ($\bar{S}_f$) and Bed Roughness (k) for Each Flow Cross-Section

Cross-Section	Date	Time (hrs)	$\bar{S}_f(*10^{-4})$	k(m)
C-1 #1	10/14/82	1640	3.40	0.23
#2	10/15/82	1820	2.17	0.11
#3	10/15/82	1010	7.35	0.21
#4	10/15/82	1100	7.95	0.38
C-2 #1	10/13/82	1615	4.67	0.13
#2	10/14/82	1350	3.26	0.09
#3	10/14/82	1535	2.83	0.07
C-3 #1	10/13/82	1345	1.96	1.40
#2	10/13/82	1520	2.92	2.10
#3	10/15/82	1225	0.74	0.90
C-4 #1	10/13/92	1745	2.80	17.75
#2	10/13/82	1830	2.78	19.44
#3	10/14/82	1100	1.23	12.36
#4	10/14/82	1150	0.58	12.02

Table D-2. Average Bed Roughness ($\bar{k}$) Values

Cross-Section	$\bar{k}$ (m)
C-1	0.23
C-2	0.10
C-3	1.47
C-4	15.40

APPENDIX E

DETERMINATION OF NEARSHORE WAVE DIRECTIONS

The predominant wave directions were determined from SSMO data as being from the Northeast, East and Southeast. The normal to the coastline at the inlet is at a 70° azimuth. Therefore, assuming straight and parallel depth contours (a reasonable assumption in the present case), the deep water wave directions correspond to -25°, 20° and 65°, respectively (where a wave direction normal to shore corresponds to 0° and directional angles are positive going clockwise). These waves were refracted (using Snell's law) to depths of 27 m and 3 m, respectively, to determine the resulting wave directions at the depth corresponding to the wavemaker and at the wave gage. Table E-1 presents the results of these calculations and an example is presented as follows:

Prototype Conditions: Wave Height H = 0.67 m, period T = 5.9 sec and water depths d = 27 m and 3 m, respectively.

Procedure: Plate C-6 in the Shore Protection Manual Volume III (1977) provides a graph of the change in wave direction angle from deepwater (α_o) to a specified depth based on the dimensionless parameter d/gT^2 where g is the acceleration due to gravity, d is depth and T is wave period. For the given prototype conditions:

$$d = 27 \text{ m} \quad ; \quad \frac{d}{gT^2} = \frac{(27)}{(9.81)(5.9)^2} = 0.079$$

$$d = 3 \text{ m} \quad ; \quad \frac{d}{gT^2} = \frac{(3)}{(9.81)(5.9)^2} = 0.0088$$

From plate C-6 given:

$$\alpha_o = 25^0 \quad , \quad \frac{d}{gT^2} = 0.079 \rightarrow \alpha = 25^0$$

$$\alpha_o = 25^0 \quad , \quad \frac{d}{gT^2} = 0.0088 \rightarrow \alpha = 13^0$$

TABLE E-1. Nearshore Wave Directions

Deepwater Direction*	Wave Period (sec)	Water Depth (m)	$\frac{d}{gT^2}$	Refracted Wave Direction*
-25°(NE)	5.9	3	0.0088	-13°
-25°(NE)	5.9	27	0.079	-25°
-25°(NE)	10.7	3	0.0027	- 8°
-25°(NE)	10.7	27	0.024	-20°
20°(E)	5.9	3	0.088	12°
20°(E)	5.9	27	0.079	20°
20°(E)	10.7	3	0.0027	6°
20°(E)	10.7	27	0.024	17°
65°(SE)	5.9	3	0.0088	30°
65°(SE)	5.9	27	0.079	65°
65°(SE)	10.7	3	0.0027	17°
65°(SE)	10.7	27	0.024	46°

*Wave direction is defined as 0° parallel to shore and positive clockwise from 0°.

The resulting α values at 3 m depth correspond to the nearshore wave directions reproduced in the model while the α values at 27 m depth correspond to the initial wave directions to be reproduced by the wave generator. Appendix G discusses the procedure by which these wave angles were reproduced.

APPENDIX F

INLET BATHYMETRY

The following figures represent the inlet bathymetry. The model grid and template scheme was selected (Section 4.3.1) using this bathymetry.

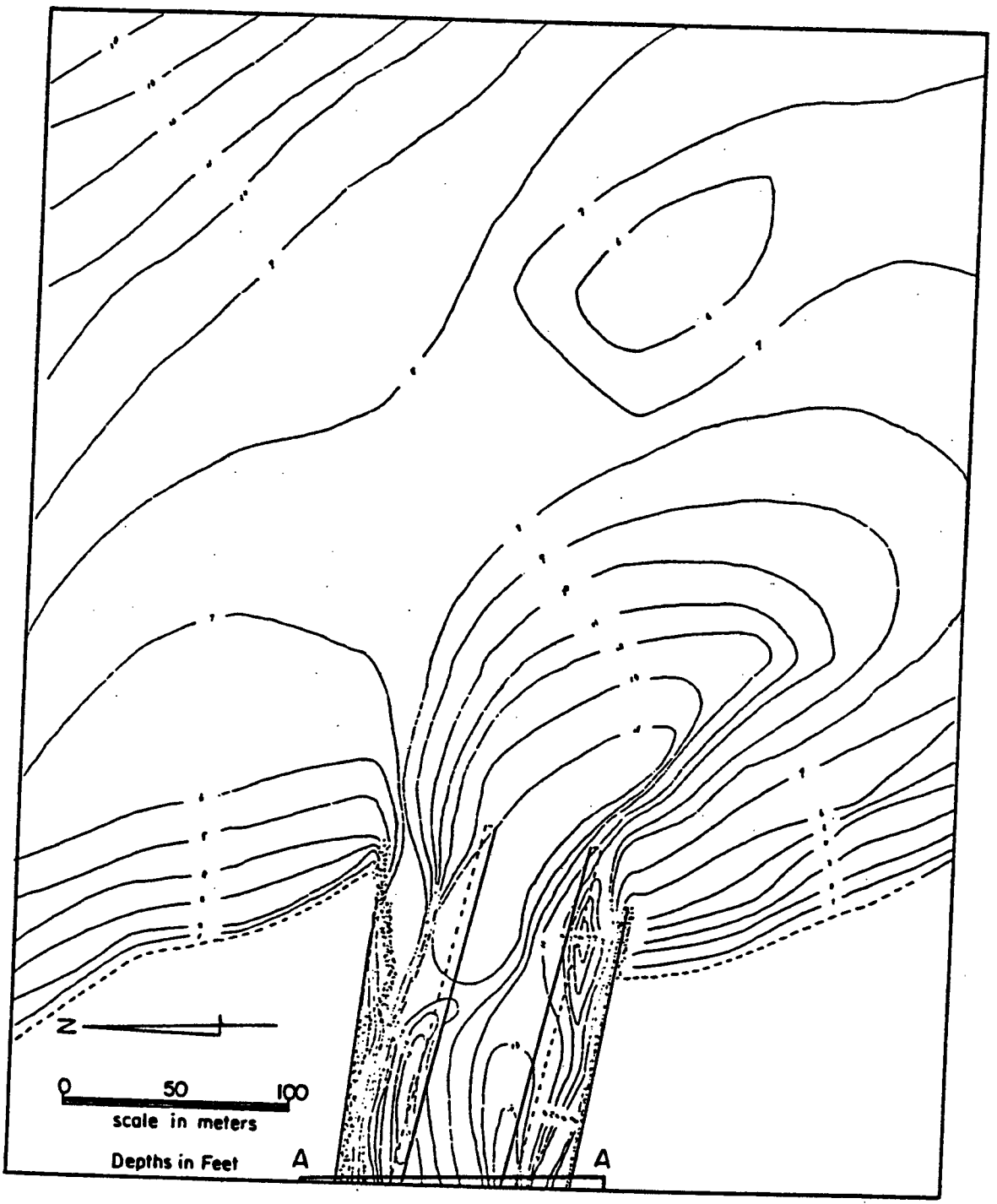

Fig. F-1. Inlet Mouth and Offshore Bathymetry. Horizontal Scale is in Meters. Depths are in Feet Below MSL.

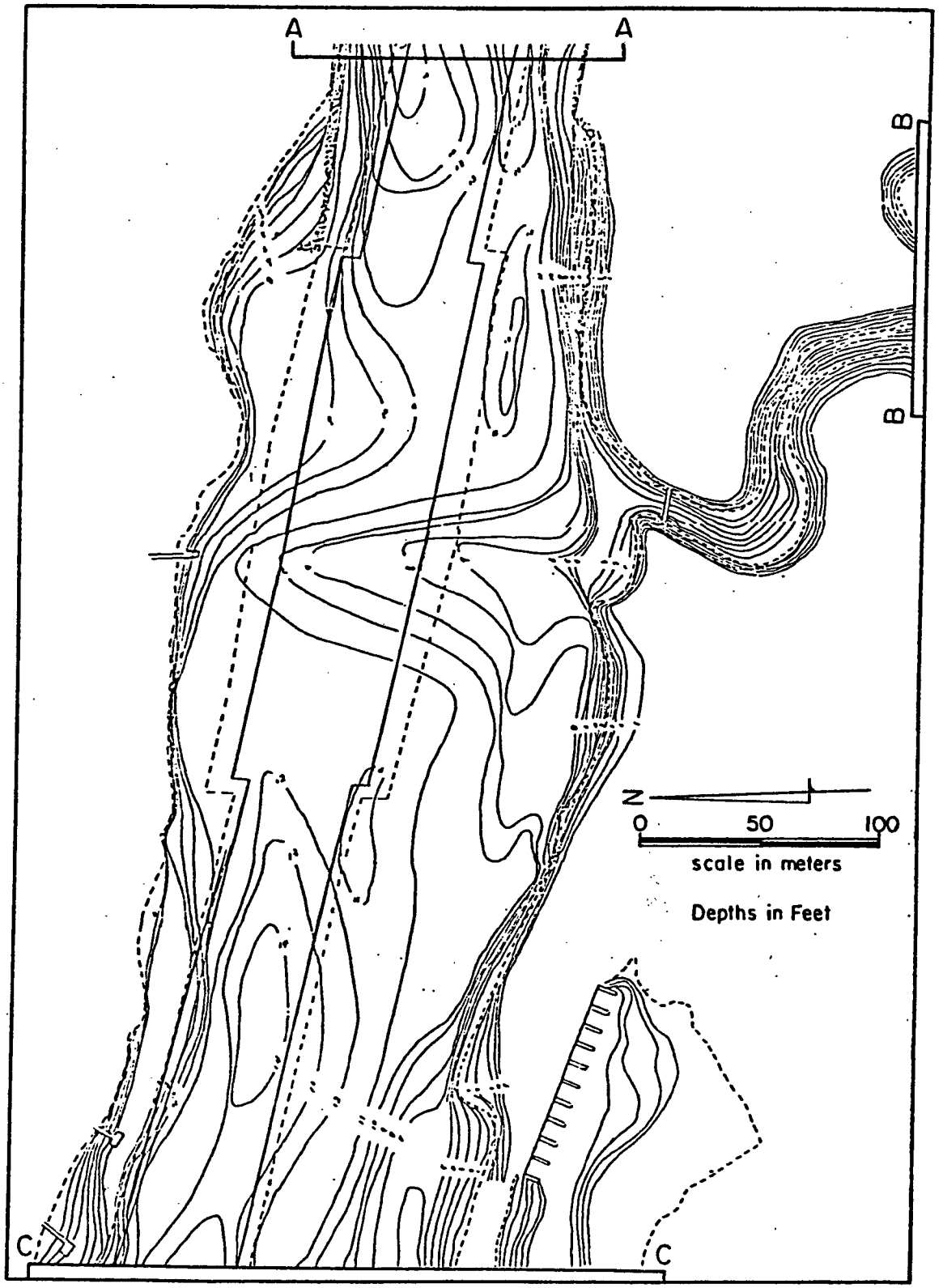

Fig. F-2. Bathymetry of Main Channel Region (Note: Sand Trap is Full).

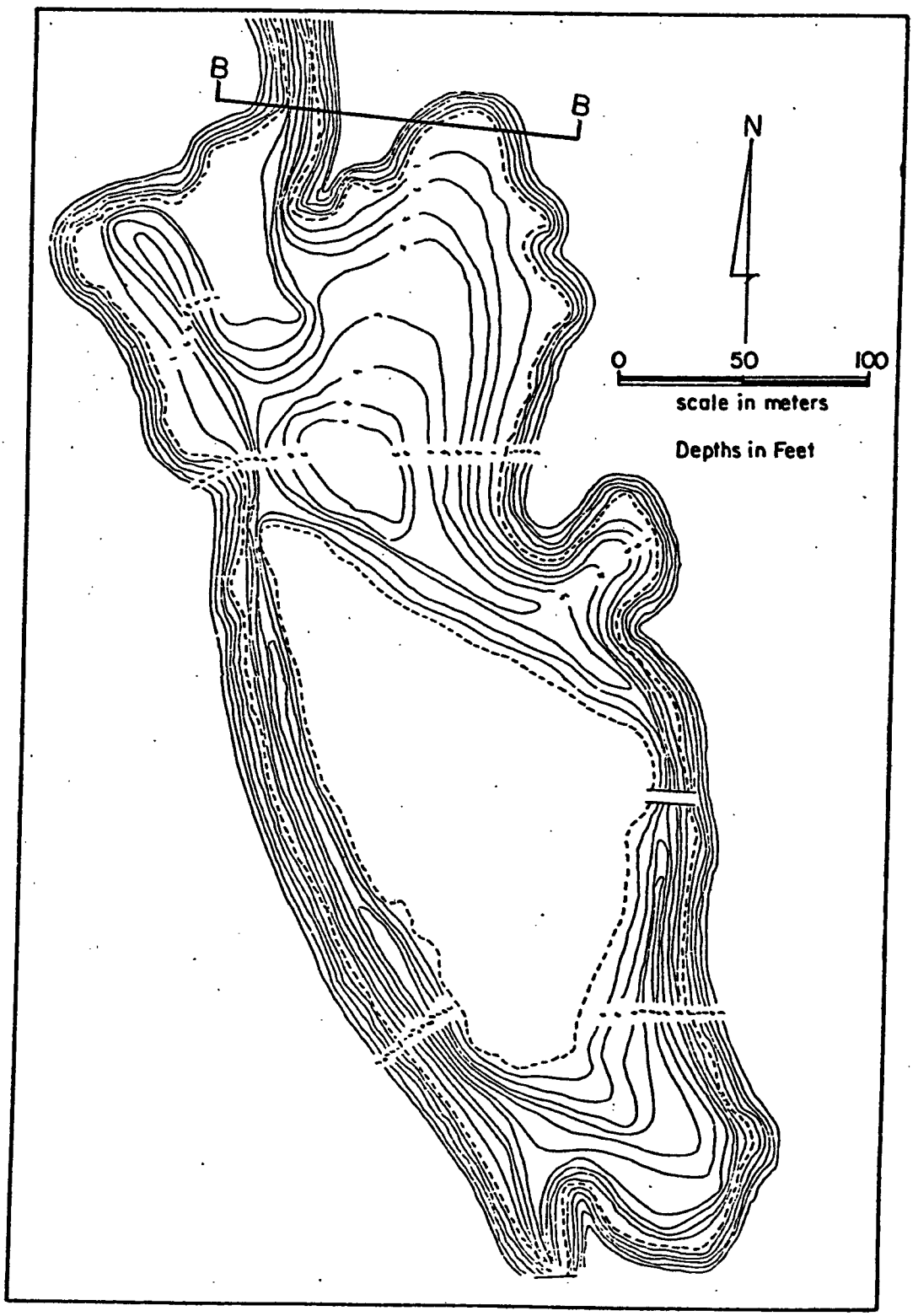

Fig. F-3. Bathymetry of Dubois Park Lagoon.

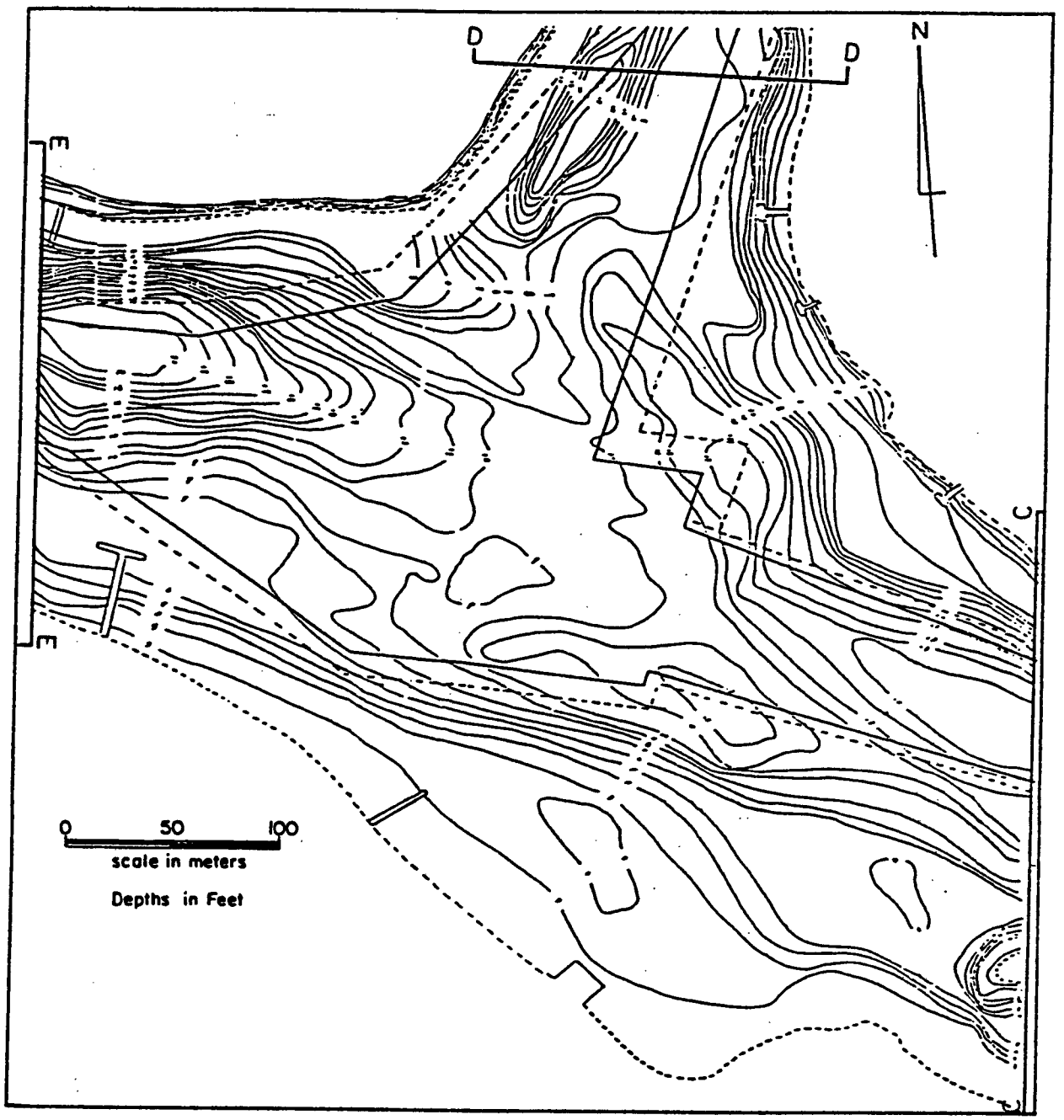

Fig. F-4. Bathymetry of Area West of Main Channel where the Inlet/Channel Splits into two Reaches of the Intracoastal Waterway.

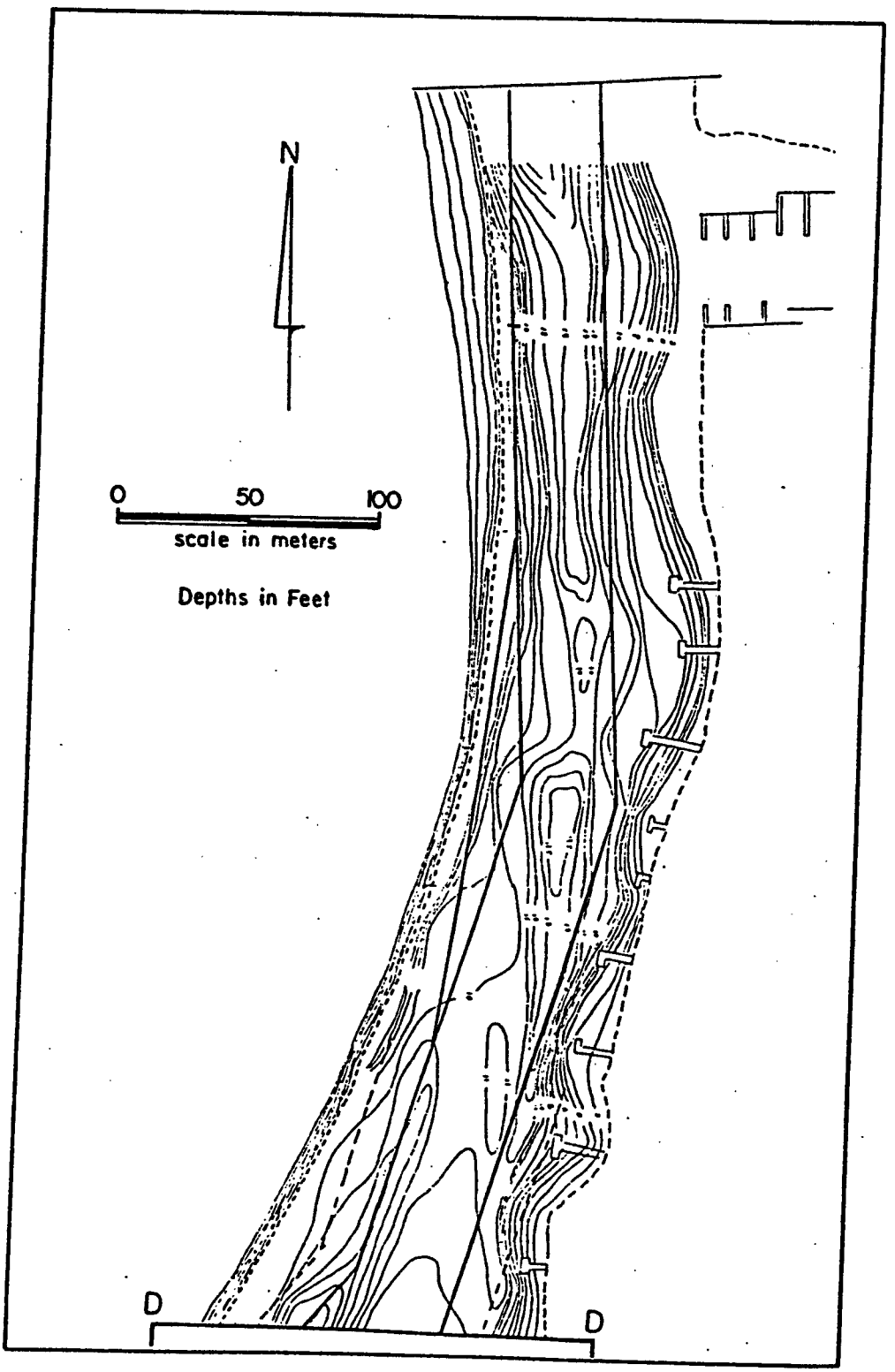

Fig. F-5. Bathymetry of North Reach of the Intracoastal Waterway.

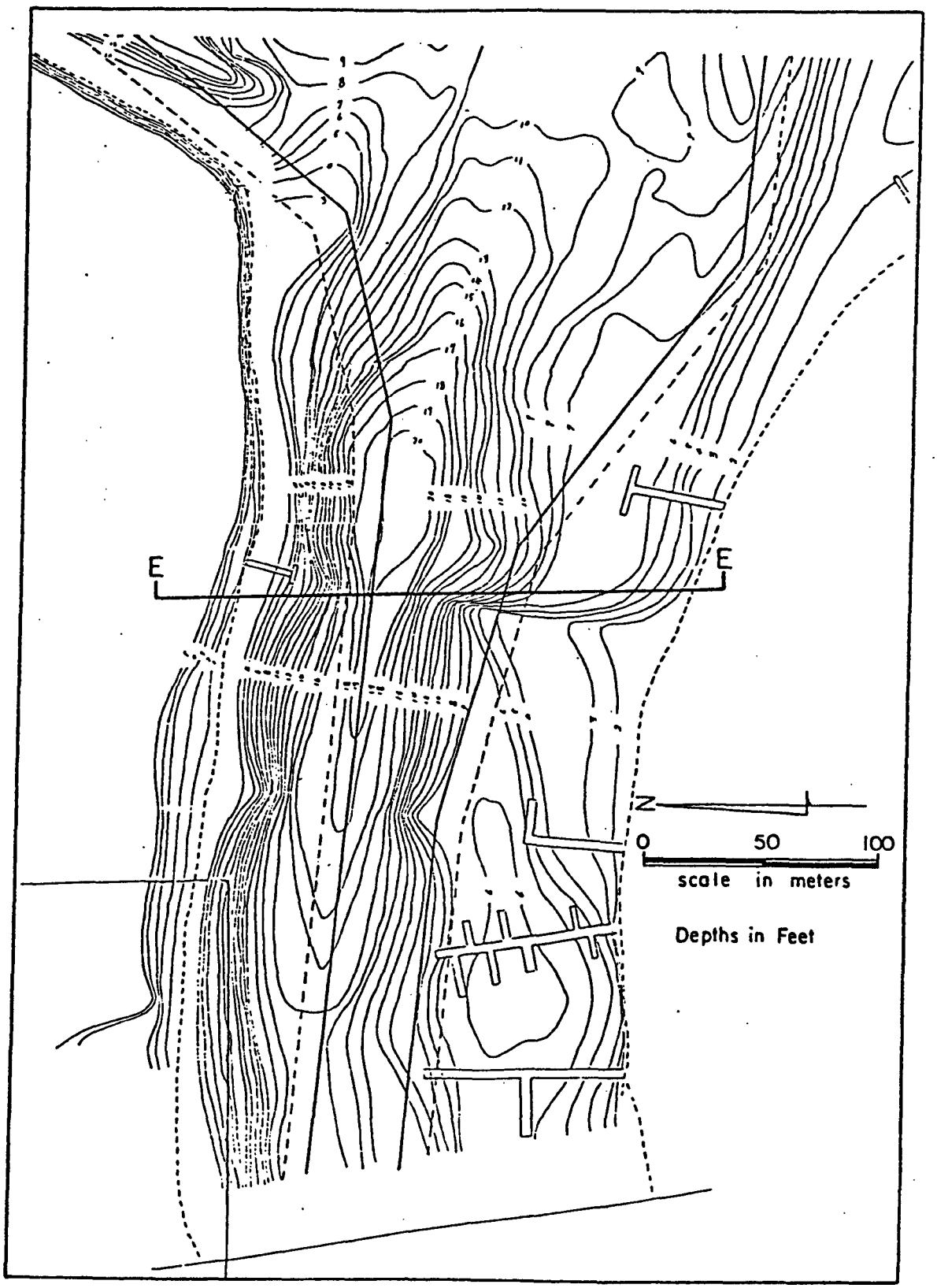

Fig. F-6. Bathymetry of the West Reach of the Intracoastal Waterway.

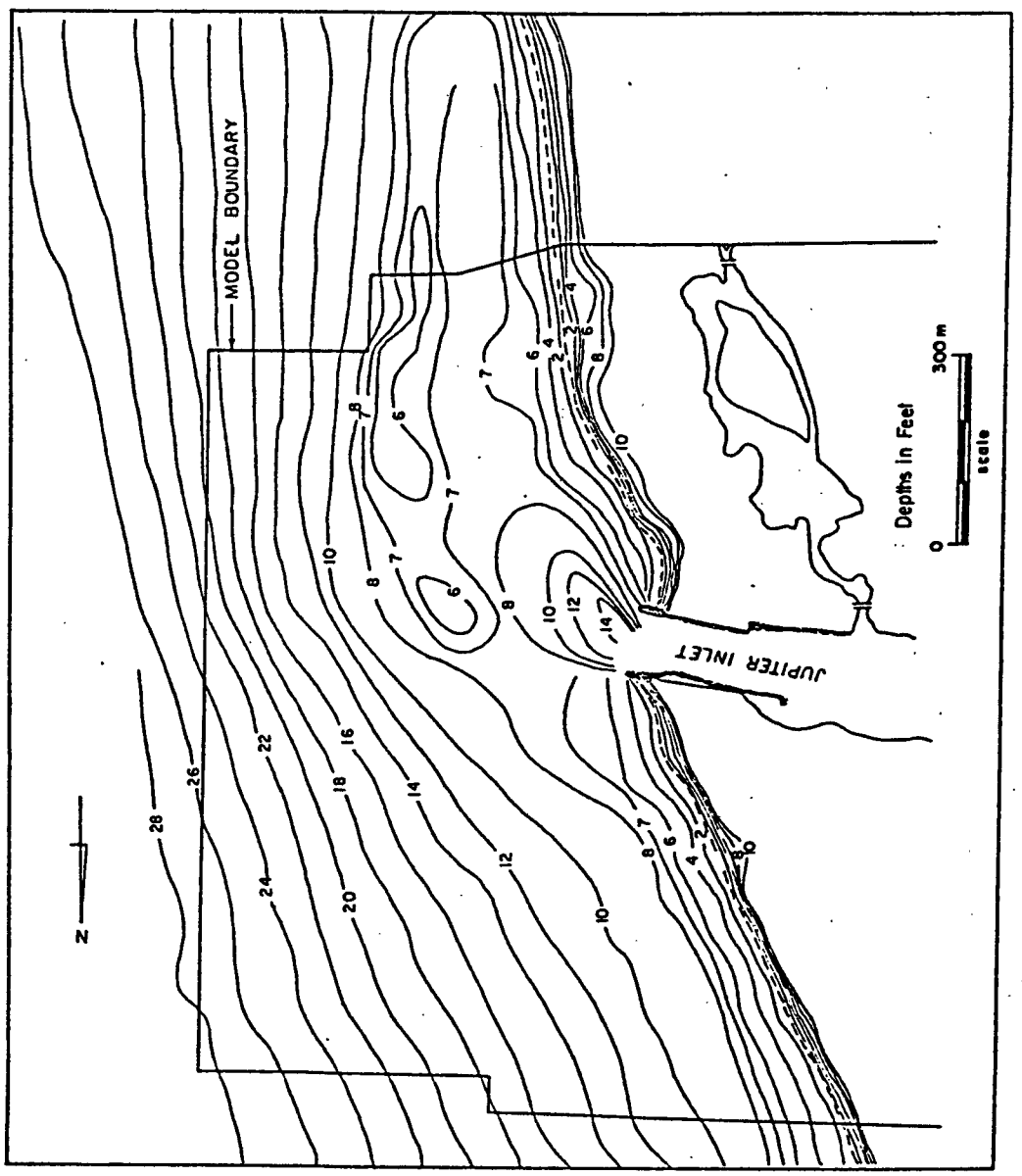

Fig. F-7. Offshore Bathymetry.

APPENDIX G

WAVEMAKER SETTING

The following is a simplified discussion of the theory behind generating desired wave height, period, length, and direction of approach via a "snake-type" wavemaker with specific references to the model.

The theory (Dean, 1984) is based on the premise that the volume of water displaced by the wavemaker should be equal to the crest volume of the resulting wave form (Galvin, 1964). For example, consider a flap-type wavemaker with a maximum stroke S in water of depth h as shown in Fig. G-1:

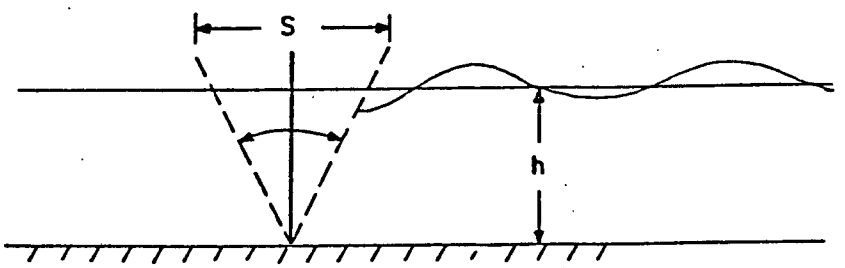

Fig. G-1. Flap-type Wavemaker

The volume of water displaced over the stroke is Sh/2; the volume of water in a wave crest is:

$$\int_0^{L/2} \frac{H}{2} \sin kx \, dx = \frac{H}{k} \qquad \text{(G-1)}$$

where L is the wave length, H is the wave height, k is the wave number ($2\pi/L$) and x is the direction of wave propagation. Equating these two volumes:

$$\frac{Sh}{2} = \frac{H}{k} \tag{G-2}$$

or

$$\frac{H}{S} = \frac{kh}{2} \tag{G-3}$$

Where H/S is the height to stroke ratio. This relationship, shown in Fig. G-2, is valid in the shallow water region where $kh < \pi/10$, i.e. $h/L < 0.05$, which is the case at all points in the ocean portion of the model.

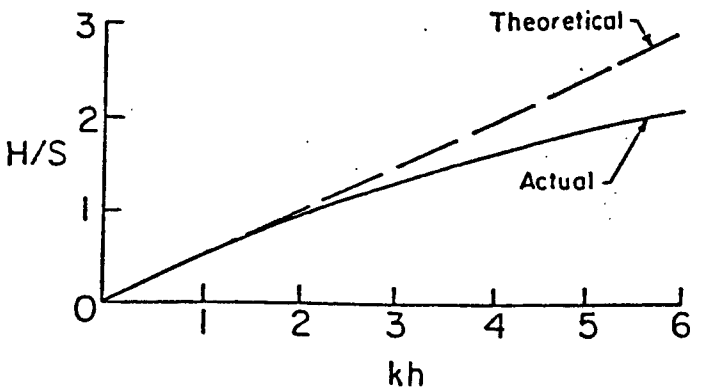

Fig. G-2. Flap-Type Wavemaker Theory. Wave Height to Stroke Versus Relative Depths (Dean, 1984).

Since S is the stroke, its horizontal displacement x is

$$x = \frac{S}{2} \sin\sigma t \tag{G-4}$$

where σ is the wavemaker frequency and t is time. The speed of the wavemaker and hence the initial wave speed is U where:

$$U = \frac{dx}{dt} = \frac{S}{2}\,\sigma\cos\sigma t \qquad \text{(G-5)}$$

From Equation (G-2) the wave height, H, can be determined as:

$$H = \frac{Shk}{2} \qquad \text{(G-6)}$$

The "snake-type" wavemaker consists of a series of flaps that may be set at different phase angles so as to generate waves from different directions. To examine the generation of specific wave directions by a "snake-type" generator, consider the following. A wavemaker is located along the y-axis, propagating waves in the x direction in the x-y plane (Fig. G-3). For simplicity assume the wavemaker to be infinitely long.

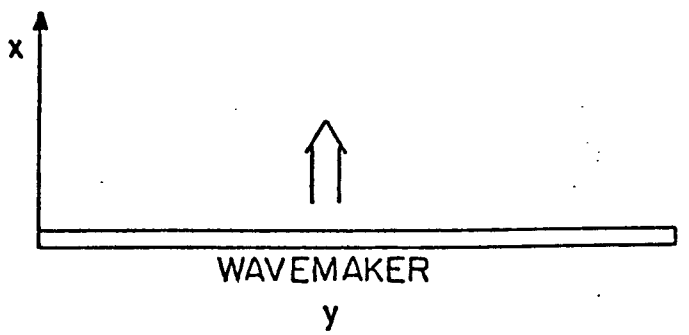

Fig. G-3. Schematic of Wavemaker Generating Waves in the x-y Plane

The motion of the wavemaker at x=0 generates velocities in the x-direction, u(y,z;t) which may be simply expressed as

$$u(y,z;t) = U(z)\cos(\lambda y - \sigma t) \quad \text{on} \quad x = 0 \qquad \text{(G-7)}$$

where λ is the y-component of the wave number k_p of the generated wave. This represents a horizontal velocity at the wavemaker which consists of a periodic motion propagating in the +y direction. The

propagation of such waves must satisfy the boundary value problem expressed as

$$\frac{\partial^2\phi}{\partial x^2} + \frac{\partial^2\phi}{\partial y^2} + \frac{\partial^2\phi}{\partial z^2} = 0 \quad \text{in} \quad \begin{array}{l} 0 \leq x \leq \infty \\ -\infty \leq y \leq \infty \\ -h \leq z \leq 0 \end{array} \tag{G-8}$$

where ϕ represents the velocity potential function of the propagating wave.

Generation of a directional wave at an angle θ from the perpendicular to the wavemaker as defined in Fig. G-4

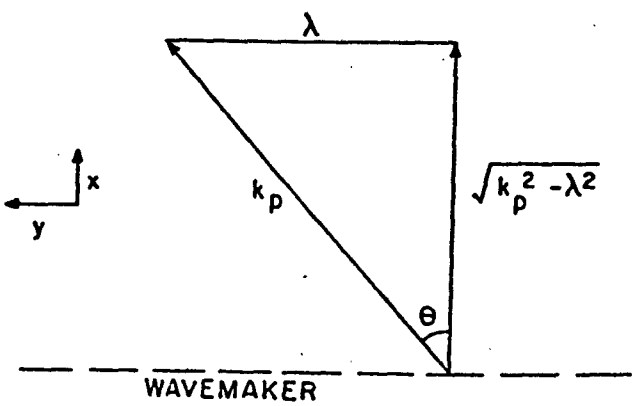

Fig. G-4. Definition for Wave Direction θ

where λ is the wave number in the y-direction and $\sqrt{k_p^2 - \lambda^2}$ is the wave number in the x-direction, results in a wave number k_p in the propagation direction. Furthermore,

$$\lambda = k_p \sin\theta \tag{G-9}$$

and

$$\sqrt{k_p^2 - \lambda^2} = k_p \cos\theta \qquad \text{(G-10)}$$

These expressions relate the wave length of the wavemaker displacement to the desired wave angle. Once λ is calculated, the phase angle of each of the wave generator paddles, ω, may be determined so as to generate the desired wave direction, θ, from the following relationship:

$$\omega = \frac{W}{\lambda} \times 360^0 \qquad \text{(G-11)}$$

where W is the width of one paddle and $\lambda = k_p \sin\theta$.

Three wave directions were generated in the wave basin; directions corresponding to northeasterly, easterly and southeasterly waves at the inlet. These directions would correspond to deepwater θ values of -25°, 20°, and 65° relative to the inlet shoreline where 0° represents the direction normal to the shoreline and directional angles are positive clockwise. These deep water waves were then refracted (see Appendix E) into the prototype depth corresponding to the depth of the wavemaker in the model (h_m = 0.56 m; h_p = 27 m) and angles θ for this depth were calculated. The wavemaker is oriented at a 96° azimuth relative to the orientation of the model shoreline so 6° were subtracted from θ calculated for the wavemaker depth thereby resulting in the required wave directions. From these θ values, the phase lag of the generator paddles to produce the required wave directions was determined from the procedure previously outlined. Table G-1 presents the results of these calculations, an example of which is presented below:

Given: Deep water direction (Northeast) = 25°, wave period T = 10.7 sec, water depth h = 27 m, wave direction corresponding to depth at wavemaker = -26°, and paddle width W = 0.23 m.

Calculation: Deep water wave length

$$L_o = gT^2/2\pi = 179 \text{ m.}$$

From Shore Protection Manual:

$$h/L_o = 0.1508$$

$$\therefore L/L_o = 0.8197$$

$$\therefore L = 160 \text{ m}$$

$$\therefore K_p = 2\pi/L = 0.03936 \text{ m}^{-1}$$

$$\therefore \lambda = K_p \sin\theta = (0.03936)(\sin 26^0)$$

$$\lambda = (0.0172) = 2\pi/L_y \text{ m}^{-1}$$

$$\therefore L_y = \text{wave length in the y-direction}$$

$$= 2\pi/(0.0172)$$

$$= 364.1 \text{ m}$$

$$L_{y_{model}} = 364.1 \text{ m}/49 = 9.09 \text{ m}$$

$$\therefore \omega = \frac{0.23}{7.43} \times 360 = 11^0$$

Generation of these wave directions at the wavemaker should, through refraction (assuming the ocean bathymetry is correctly modeled), result in the required nearshore wave direction at the wave gage. This was found to be the case as these nearshore wave directions were obtained to within $\pm$ 5° using the prescribed wave generator wave angles and phase angles.

Table G-1. Paddle Phase Angles for Various Wave Approach Angles

Deepwater Wave Direction	Wave Period (sec)	Wave Direction at Generator (Deg)	Phase Angle (Deg)
-25°(NE)	5.9	-31	-38.5
-25°(NE)	10.7	-26	-11
20°(E)	5.9	15	19.5
20°(E)	10.7	11	2
65°(SE)	5.9	60	65
65°(SE)	10.7	40	16

APPENDIX H

WEIR CALIBRATION

Figure 4.1 in the text shows the location of each weir box while Fig. 4.7 gives the dimensional parameters of the two types of boxes. The weirs were calibrated by determining the coefficients C_V and C_R in the following two equations (4-1 and 4-2 in the text) based on a known discharge Q for known values of H, L, and θ (King, 1976).

V-Notched Weir: $$Q = \frac{8}{15} C_V \tan(\theta/2)\sqrt{2g}\, H^{5/2} \qquad (4\text{-}1)$$

Rectangular-Notched Weir: $$Q = C_R L\, H^{3/2} \qquad (4\text{-}2)$$

The following calculations illustrate the procedure by which C_V for box 1 (a V-notched weir) and, subsequently, the discharge through the weir (as a function of H) were determined. Table H-1 provides pertinent information for all five weirs.

Weir Box 1: V-notched, $\theta = 60°$. For $H = 0.1335$ m, $Q = 0.00626$ m^3/sec was measured.

From equation D-1:

$$0.00626 = \frac{(8)}{(15)} C_V(\tan 30^0)\left(\sqrt{2*9.806}\right)(0.1335)^{5/2}$$

$$\therefore\ C_V = 0.705$$

and

$$Q = 3.12\ H^{5/2}$$

where H is in meters and Q is in cubic meters per second.

Table H-1. Weir Calibration

Weir Number	Type	θ (deg)	L (m)	C_V or C_R	Q (m^3/sec)
1	V-Notched	60	-	0.705	$3.12\ H^{5/2}$
2	V-Notched	60	-	1.105	$4.89\ H^{5/2}$
3	Rectangular	-	0.46	0.515	$0.24\ H^{3/2}$
4	Rectangular	-	0.46	1.510	$0.69\ H^{3/2}$
5	Rectangular	-	0.61	2.871	$1.75\ H^{3/2}$

APPENDIX I

ROUGHNESS ELEMENT THEORY

The following theory and equations apply to Fig. I-1 representing a turbulent flow velocity profile over a roughness element, where $\bar{u}$ is the depth-mean velocity and $\alpha\bar{u}$ is the corresponding velocity at an elevation λ equal to the roughness element height.

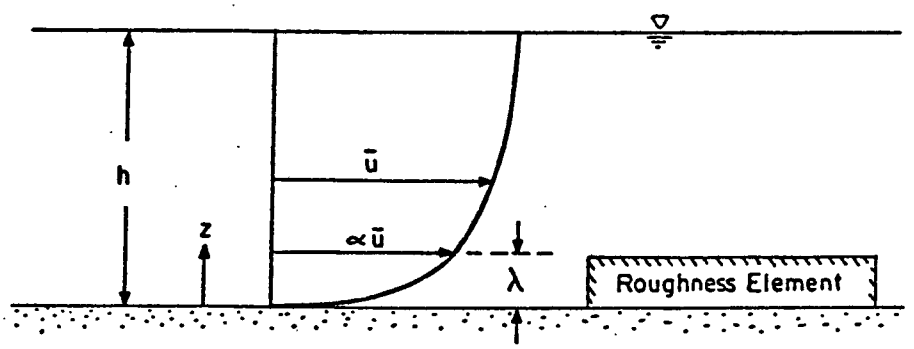

Fig. I-1. Schematic of a Roughness Element in a Velocity Field

For the situation represented in Fig. I-1 the total bed shear stress, τ on the fluid is equal to the sum of the bed friction stress and the drag force due to the roughness element. This relationship may be expressed as:

$$\tau = \frac{\rho f \bar{u}^2}{8} + \frac{\rho C_D (\alpha\bar{u})^2 A_p N}{2} \qquad \text{(I-1)}$$

where ρ is the fluid density, f is the friction factor of the model bed, C_D is the roughness element drag coefficient (which is selected to be

1.0), A_p is the projected area of roughness element, and N is the number of roughness elements per unit bed area.

The bed shear stress τ may also be expressed in relation to the energy grade line slope S as follows:

$$\tau = \gamma RS \tag{I-2}$$

$$= \rho g R \frac{\Delta h}{\ell} \tag{I-3}$$

where γ is the unit weight of the fluid, g is the acceleration due to gravity and R is the hydraulic radius. The slope S may also be expressed as head loss Δh over a distance ℓ.

Equating Equations (I-1) and (I-3) results in

$$\frac{\Delta h}{\ell} = \frac{\tau}{\rho g R} = \frac{\rho \bar{u}^2}{\rho g R} \left(\frac{f}{8} + \frac{C_D \alpha^2 A_p N}{2}\right) \tag{I-4}$$

The one-seventh approximation relating surface velocity u_{max} to velocity u at an elevation z (Schlichting, 1951) may be expressed as:

$$\frac{u_z}{u_{max}} = \left(\frac{z}{h}\right)^{1/7} \tag{I-5}$$

where h is the total depth. Applying equation (I-5) to the depth averaged velocity $\bar{u}$ results in:

$$\frac{\bar{u}}{u_{max}} = \frac{1}{h} \int_0^h \frac{z^{1/7}}{h^{1/7}} dz = \frac{7}{8} \tag{I-6}$$

Applying this same approximation to the average velocity over the depth of the roughness element, and defining $u_{EFF}^2 = (\alpha \bar{u})^2$ yields:

$$\frac{u_{EFF}^2}{u_{max}^2} = \frac{1}{\lambda} \int_0^{\lambda} \frac{z^{2/7}}{h^{2/7}} dz = \frac{7}{9} \left(\frac{\lambda}{h}\right)^{2/7} \qquad \text{(I-7)}$$

Consequently:

$$\alpha^2 = \frac{u_{EFF}^2}{\bar{u}^2} = \frac{\frac{7}{9} \left(\frac{\lambda}{h}\right)^{2/7} u_{max}^2}{\left(\frac{7}{8} u_{max}\right)^2} = 1.016 \left(\frac{\Delta}{h}\right)^{2/7}$$

$$\therefore \alpha^2 \approx \left(\frac{\lambda}{h}\right)^{2/7} \qquad \text{(I-8)}$$

Therefore as an example, for $\lambda/h = 0.1$, $\alpha^2 = (0.1)^{2/7} = 0.52$; hence $\alpha = 0.72$. The value of α may be substituted into equation (I-4) to determine N, the number of roughness elements per area necessary to achieve a head loss of Δh over a length ℓ, and hence the desired energy grade line slope S. Ultimately, this procedure was not used in the model study, since the desired energy grade line slopes, as determined by differences in water surface elevations, were obtained within acceptable margins of error (Section 4.5). As a result, the required flow conditions were satisfactorily reproduced in the model without using roughness elements.

APPENDIX J

TEST RESULTS

This appendix contains pertinent data resulting from the tests described in Chapter VI. Bottom velocities, wave heights and P values are presented in tabular form for each solution scheme. Figures are included to indicate the specific locations where these measurements were made.

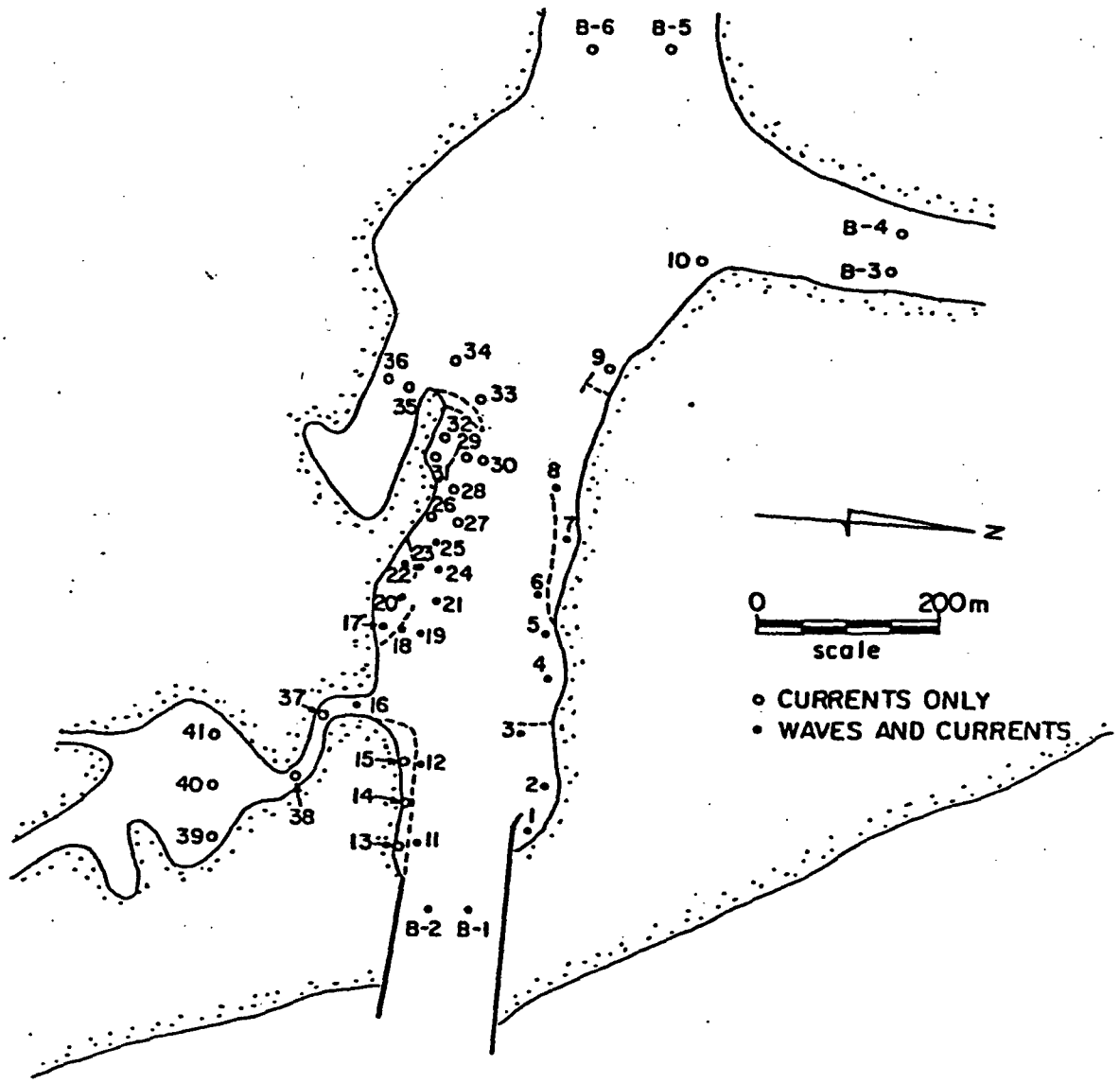

Fig. J-1. Locations of Measurements Made in the Model for the Existing Conditions and those under Phase One.

Table J-1a. Bottom Velocities, Wave Heights and P Values during Flood Tide for the Existing Condition and the Condition under Phase One

	EXISTING CONDITION			CONDITION AFTER PHASE ONE				EXISTING CONDITION			CONDITION AFTER PHASE ONE		
Location**	u_B* (m/s)	H (m)	P	u_B* (m/s)	H (m)	P	Location**	u_B* (m/s)	H (m)	P	u_B* (m/s)	H (m)	P
B-1	1.30	1.00	77.34	1.30	1.00	77.34	19	0.61	0.25	1.43	0.90	0.25	5.78
B-2	1.10	0.75	27.07	1.10	0.76	27.10	20	0.59	0.25	7.49	0.25	0.12	-0.14
B-3	0.50	0.0	1.24	0.54	0.0	1.38	21	0.61	0.25	1.96	0.90	0.12	4.84
B-4	0.98	0.0	7.66	0.96	0.0	7.12	22	0.20	0.25	1.09	0.09	0.25	-0.69
B-5	0.66	0.0	2.94	0.66	0.0	2.94	23	0.67	0.25	2.52	0.40	0.12	0.22
B-6	0.47	0.0	1.00	0.46	0.0	0.99	24	0.61	0.25	1.43	0.45	0.12	0.46
1	0.18	0.31	0.89	0.20	0.25	2.37	25	0.81	0.25	5.64	0.62	0.12	-3.97
2	0.35	0.31	2.79	0.36	0.31	2.83	26	0.62	0.0	4.64	0.54	0.0	1.07
3	0.75	0.19	5.04	0.65	0.25	8.76	27	0.63	0.0	1.85	0.37	0.0	0.01
4	0.31	0.19	0.42	0.32	0.12	0.47	28	0.69	0.0	3.34	0.66	0.0	3.28
5	0.47	0.19	2.19	0.37	0.25	0.46	29	0.81	0.0	4.94	0.83	0.0	5.26
6	1.20	0.19	14.46	0.93	0.37	9.74	30	0.63	0.0	1.85	0.77	0.0	4.41
7	0.48	0.19	2.55	0.16	0.25	-0.67	31	0.10	0.0	-0.88	0.10	0.0	-0.90
8	0.74	0.0	2.96	0.15	0.12	-0.81	32	0.17	0.0	-0.64	0.09	0.0	-0.92
9	0.81	0.0	4.86	0.22	0.0	-0.65	33	0.42	0.0	0.34	0.09	0.12	-0.89
10	0.33	0.0	0.0	0.22	0.0	-0.63	34	0.34	0.0	0.04	0.18	0.12	-0.47
11	0.61	0.62	23.04	0.78	0.75	143.27	35	0.17	0.0	-0.64	0.08	0.0	-0.92
12	0.17	0.62	0.65	0.39	0.62	27.44	36	0.17	0.0	-0.64	0.09	0.0	-0.91
13	0.08	0.0	-0.96	0.05	0.0	-0.98	37	0.45	0.0	0.48	0.40	0.0	0.16
14	0.08	0.0	-0.96	0.05	0.0	-0.98	38	0.45	0.0	0.48	0.40	0.0	0.16
15	0.08	0.0	-0.96	0.05	0.0	-0.98	39	0.09	0.0	-0.70	0.07	0.0	-0.73
16	0.25	0.25	0.04	0.30	0.37	0.72	40	0.17	0.0	0.08	0.15	0.0	-0.16
17	0.20	0.37	2.71	0.19	0.12	-0.40	41	0.09	0.0	-0.70	0.07	0.0	-0.73
18	0.67	0.25	2.52	0.93	0.25	6.25							

*u_B refers to "Bottom Velocity" measured 0.15 m above bottom.

**Locations are shown in Fig. J-1.

Table J-1b. Bottom Velocities, Wave Heights and P Values during Ebb Tide for the Existing Condition and the Condition under Phase One

EXISTING CONDITION				CONDITION AFTER PHASE ONE			EXISTING CONDITION				CONDITION AFTER PHASE ONE		
Location**	u_B* (m/s)	H (m)	P	u_B* (m/s)	H (m)	P	Location**	u_B* (m/s)	H (m)	P	u_B* (m/s)	H (m)	P
B-1	1.73	0.0	16.96	1.70	0.0	15.66	19	1.23	0.0	8.08	1.35	0.0	12.15
B-2	1.93	0.0	21.37	1.90	0.0	20.62	20	0.35	0.0	0.08	0.17	0.0	-0.74
B-3	0.43	0.0	0.64	0.46	0.0	0.76	21	1.23	0.0	9.90	1.23	0.0	9.90
B-4	0.60	0.0	2.28	0.56	0.0	1.84	22	0.20	0.0	-0.63	0.09	0.0	-0.92
B-5	0.92	0.0	6.73	0.88	0.0	6.26	23	1.00	0.0	6.19	1.08	0.0	7.48
B-6	0.94	0.0	7.01	0.90	0.0	6.46	24	0.92	0.0	4.11	1.05	0.0	6.95
1	0.64	0.0	3.97	0.40	0.0	0.45	25	1.04	0.0	8.76	1.08	0.0	9.52
2	0.40	0.0	1.05	0.32	0.0	0.30	26	1.01	0.0	11.37	0.77	0.0	3.32
3	1.20	0.0	9.49	1.05	0.0	8.94	27	0.78	0.0	3.45	0.75	0.0	3.06
4	0.63	0.0	2.56	0.16	0.0	-0.77	28	0.87	0.0	5.78	0.82	0.0	5.16
5	1.10	0.0	9.90	0.75	0.0	2.38	29	1.52	0.0	19.88	1.17	0.0	11.26
6	1.36	0.0	12.28	1.14	0.0	6.86	30	1.18	0.0	9.01	1.08	0.0	7.38
7	1.13	0.0	10.48	0.16	0.0	-0.84	31	0.10	0.0	-0.88	0.10	0.0	-0.88
8	0.74	0.0	2.96	0.85	0.0	3.36	32	0.09	0.0	-0.91	0.09	0.0	-0.91
9	1.05	0.0	8.90	0.32	0.0	-0.26	33	0.61	0.0	1.66	0.44	0.0	0.38
10	0.58	0.0	2.06	0.45	0.0	0.46	34	0.52	0.0	1.44	0.36	0.0	-0.07
11	1.56	0.0	13.64	1.60	0.0	14.01	35	0.17	0.0	-0.64	0.17	0.0	-0.67
12	1.16	0.0	8.79	1.17	0.0	8.86	36	0.17	0.0	-0.64	0.17	0.0	-0.65
13	0.08	0.0	-0.96	0.05	0.0	-0.98	37	0.53	0.0	1.01	0.53	0.0	1.01
14	0.08	0.0	-0.96	0.05	0.0	-0.98	38	0.53	0.0	1.01	0.53	0.0	1.01
15	0.08	0.0	-0.96	0.05	0.0	-0.98	39	0.18	0.0	0.22	0.18	0.0	0.22
16	0.50	0.0	0.80	0.83	0.0	2.57	40	0.17	0.0	0.08	0.17	0.0	0.08
17	0.10	0.0	-0.91	0.09	0.0	-0.92	41	0.18	0.0	0.22	0.18	0.0	0.22
18	1.33	0.0	11.79	1.39	0.0	13.01							

*u_B refers to "Bottom Velocity" measured 0.15 m above bottom.

**Locations are shown in Fig. J-1.

Table J-1c. Bottom Velocities, Wave Heights and P Values during a 1.5 m Storm Surge for the Existing Condition and the Condition under Phase One

	EXISTING CONDITION			CONDITION AFTER PHASE ONE				EXISTING CONDITION			CONDITION AFTER PHASE ONE		
Location**	u_B* (m/s)	H (m)	P	u_B* (m/s)	H (m)	P	Location**	u_B* (m/s)	H (m)	P	u_B* (m/s)	H (m)	P
B-1	2.46	1.62	498.50	2.42	1.62	496.72	19	1.28	0.50	26.83	1.88	0.25	24.64
B-2	2.11	0.93	114.65	2.02	0.88	109.55	20	0.60	0.50	10.16	0.40	0.12	0.82
B-3	0.54	0.0	1.64	0.56	0.0	1.76	21	1.28	0.50	32.75	1.88	0.25	24.64
B-4	1.26	0.0	13.45	1.32	0.0	13.95	22	0.31	0.37	1.54	0.21	0.25	-0.27
B-5	1.28	0.0	13.80	1.28	0.0	13.80	23	1.33	0.0	11.84	1.37	0.0	12.56
B-6	0.72	0.0	3.68	0.72	0.0	3.68	24	1.28	0.12	10.11	1.88	0.12	25.10
1	0.52	0.37	7.49	0.46	0.37	6.29	25	1.36	0.0	15.60	1.04	0.0	7.80
2	0.30	0.50	1.79	0.21	0.50	0.64	26	0.94	0.0	9.68	1.16	0.0	15.26
3	1.26	0.50	28.65	1.88	0.50	80.19	27	0.86	0.0	4.39	0.88	0.0	4.64
4	0.43	0.50	3.73	0.39	0.37	2.06	28	0.90	0.0	6.38	0.90	0.0	6.38
5	0.72	0.25	6.38	1.13	0.25	10.48	29	0.78	0.0	4.56	0.80	0.0	4.84
6	1.97	0.37	53.99	2.00	0.37	42.34	30	0.72	0.0	2.74	0.76	0.0	3.16
7	0.73	0.25	6.80	0.59	0.25	2.38	31	0.08	0.0	-0.93	0.21	0.0	-0.55
8	0.90	0.0	4.90	0.29	0.12	-0.41	32	0.15	0.0	-0.73	0.20	0.0	-0.57
9	1.24	0.0	12.89	0.42	0.0	0.26	33	0.52	0.0	1.48	0.20	0.0	-0.64
10	0.52	0.0	1.43	0.38	0.0	0.02	34	0.42	0.12	0.69	0.10	0.0	-0.91
11	0.45	0.62	4.71	0.42	0.75	7.08	35	0.15	0.0	-0.73	0.20	0.0	-0.53
12	0.44	0.87	9.43	0.42	0.62	6.11	36	0.15	0.0	-0.73	0.20	0.0	-0.51
13	1.58	0.12	20.80	0.98	0.12	7.09	37	0.70	0.0	2.57	0.62	0.0	2.40
14	1.12	0.12	9.95	0.70	0.12	3.25	38	0.84	0.0	4.14	0.76	0.0	3.96
15	0.72	0.12	3.50	0.46	0.12	1.36	39	0.23	0.0	0.92	0.21	0.0	0.84
16	0.89	0.75	31.13	0.79	0.37	6.58	40	0.30	0.0	2.28	0.28	0.0	2.16
17	0.44	0.25	2.12	0.21	0.12	-0.50	41	0.23	0.0	0.92	0.21	0.0	0.84
18	1.33	0.50	34.67	1.85	0.50	72.94							

*u_B refers to "Bottom Velocity" measured 0.15 m above bottom.

**Locations are shown in Fig. J-1.

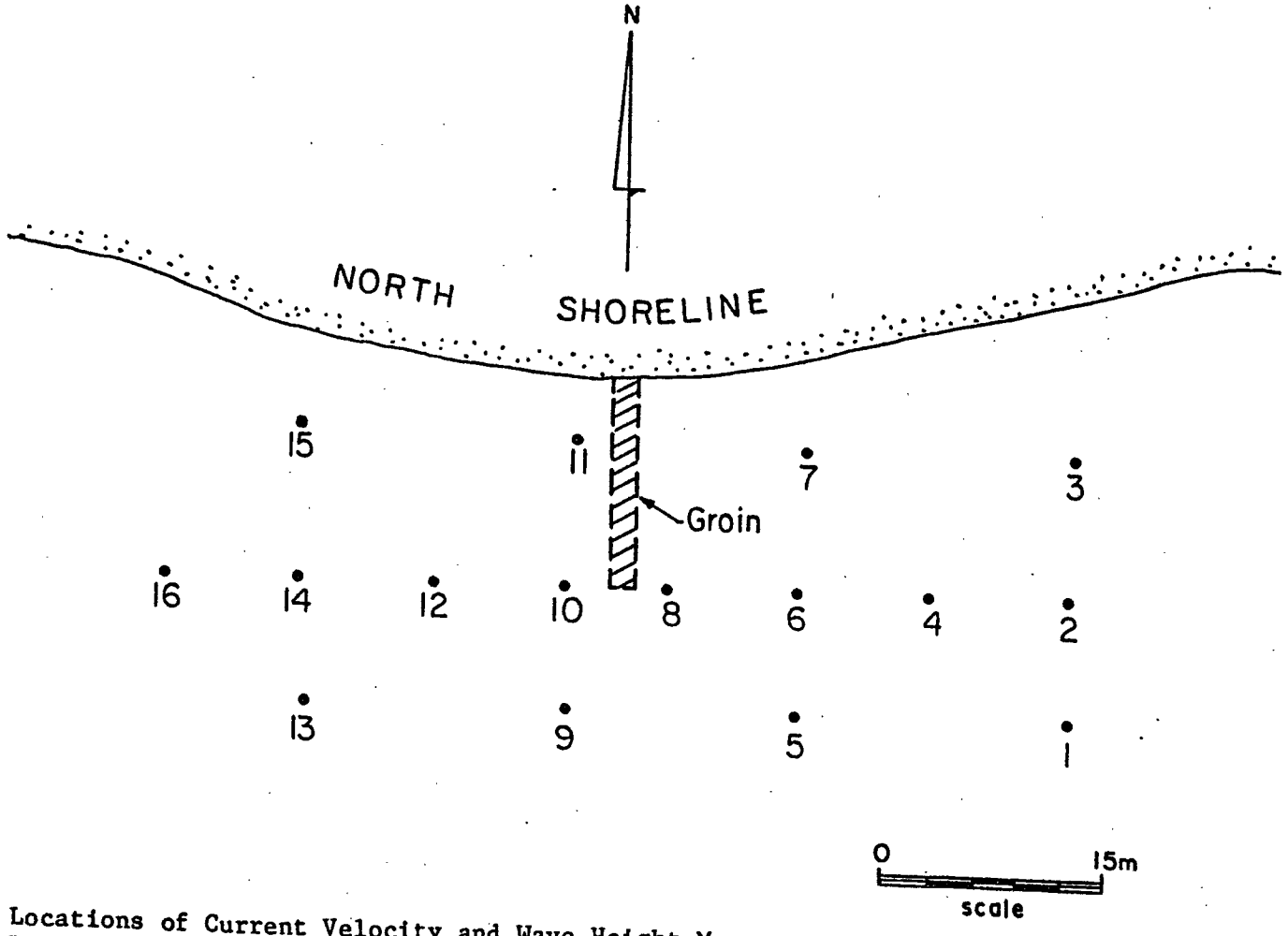

Fig. J-2. Locations of Current Velocity and Wave Height Measurements Made in the Model with and without the Remnants of the Existing Northshore Groin.

Table J-2a. Bottom Velocities, Wave Heights and P Values at Locations Shown in Fig. J-2 with the Groin Remnants in Place

	FLOOD			STORM			EBB		
Location**	u_B* (m/s)	H (m)	P	u_B* (m/s)	H (m)	P	u_B* (m/s)	H (m)	P
1	1.02	0.62	23.82	1.90	0.87	143.45	1.17	0.0	7.20
2	0.32	0.50	2.55	0.81	0.62	30.81	0.97	0.0	5.75
3	0.17	0.37	0.22	0.35	0.37	3.89	0.17	0.0	-0.73
4	0.32	0.50	2.55	0.64	0.50	13.18	0.81	0.0	3.69
5	0.58	0.62	7.10	1.17	0.75	41.46	1.31	0.0	9.38
6	0.32	0.50	2.55	0.64	0.50	13.18	0.97	0.0	5.75
7	0.35	0.37	3.89	0.69	0.50	30.15	0.17	0.0	-0.73
8	0.48	0.37	4.38	0.64	0.62	19.36	0.97	0.0	5.75
9	0.73	0.50	8.51	1.46	0.62	49.65	1.17	0.0	7.20
10	0.32	0.37	1.39	0.48	0.37	4.38	0.81	0.0	3.69
11	0.35	0.12	0.67	0.35	0.25	1.90	0.17	0.0	-0.73
12	0.32	0.25	0.57	0.64	0.37	8.56	1.13	0.0	8.19
13	0.58	0.25	2.33	1.31	0.37	21.84	1.17	0.0	7.20
14	0.32	0.25	0.57	0.64	0.25	5.26	0.97	0.0	5.75
15	0.35	0.12	0.67	0.52	0.12	2.76	0.17	0.0	-0.73
16	0.48	0.12	1.30	0.97	0.12	8.22	1.29	0.0	11.00

*u_B refers to "Bottom Velocity" actually measured 0.15 m above the bottom.
**Locations are shown in Fig. J-2.

Table J-2b. Bottom Velocities, Wave Heights and P Values at Locations Shown in Fig. J-2 with no Groin

	FLOOD			STORM			EBB		
Location**	u_B* (m/s)	H (m)	P	u_B* (m/s)	H (m)	P	u_B* (m/s)	H (m)	P
1	1.02	0.62	23.82	2.04	0.87	166.53	1.17	0.0	7.20
2	0.32	0.62	4.09	0.81	0.75	43.23	0.97	0.0	5.75
3	0.17	0.37	0.22	0.35	0.37	3.89	0.17	0.0	-0.73
4	0.32	0.37	1.39	0.76	0.50	18.50	1.13	0.0	8.19
5	0.58	0.50	5.09	1.21	0.75	45.00	1.31	0.0	9.38
6	0.32	0.50	2.55	0.76	0.62	26.12	1.29	0.0	11.00
7	0.17	0.37	0.22	0.52	0.50	10.68	0.28	0.0	-0.27
8	0.32	0.37	1.39	0.81	0.62	30.81	1.13	0.0	8.19
9	0.80	0.50	10.32	1.46	0.62	49.65	1.31	0.0	9.38
10	0.32	0.37	1.39	0.81	0.62	30.81	1.13	0.0	8.19
11	0.17	0.37	0.22	0.35	0.50	6.79	0.35	0.0	0.10
12	0.36	0.37	2.04	0.64	0.62	19.36	1.13	0.0	8.19
13	0.73	0.37	6.05	1.31	0.37	21.84	1.17	0.0	7.20
14	0.48	0.25	2.52	0.64	0.37	8.56	1.29	0.0	11.00
15	0.35	0.25	1.90	0.52	0.37	10.00	0.35	0.0	0.08
16	0.56	0.25	3.79	0.97	0.25	13.09	1.29	0.0	11.00

*u_B refers to "Bottom Velocity actually measured 0.15 m above the bottom.
**Locations are shown in Fig. J-2.

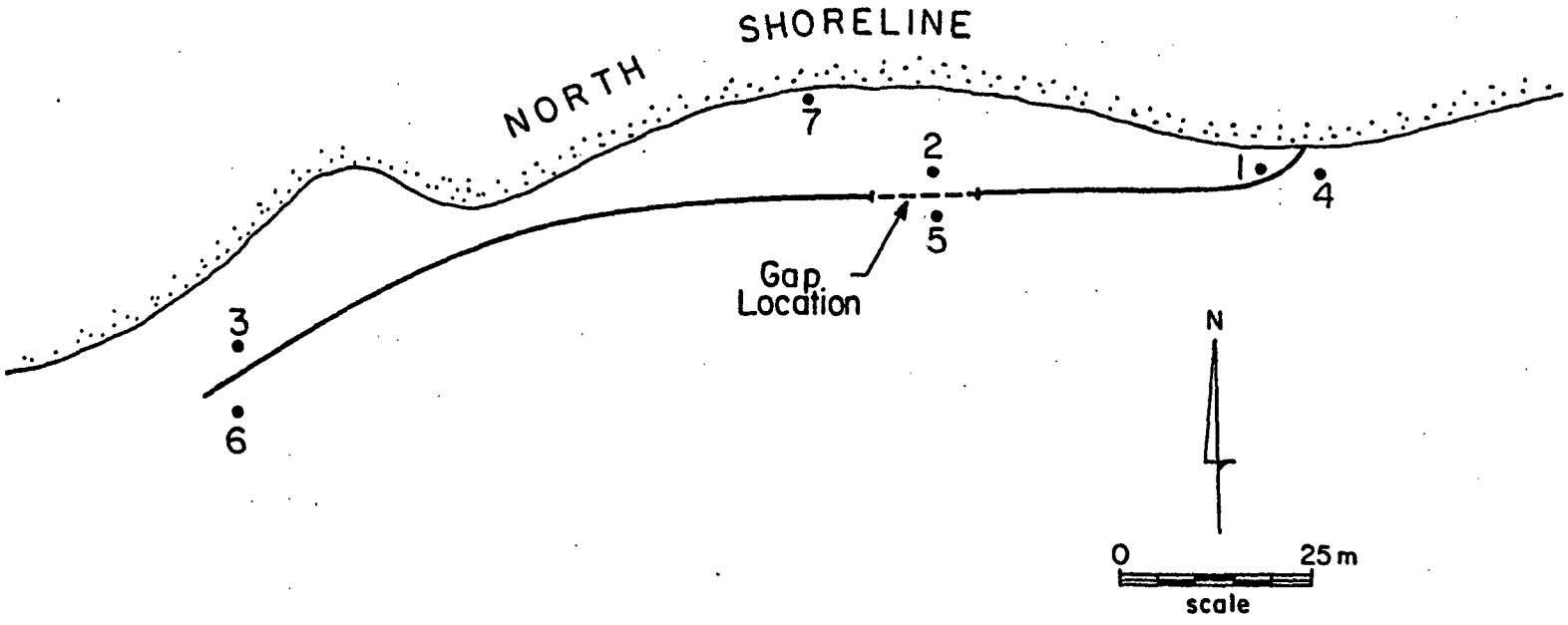

Fig. J-3. Locations of Current Velocity Measurements Made in the Model near the Proposed Flow Deflector with and without a 6 m Gap as Shown.

Table J-3. Bottom Velocities, Wave Heights and P Values near the Flow Deflector with and without a 6 m Gap as Shown in Fig. J-3

	NO GAP						GAP					
	EBB		EBB w/T**		FLOOD		EBB		EBB w/T**		FLOOD	
Location***	u_B* (m/s)	P	u_B* (m/s)	P	u_B* (m/s)	P	u_B* (m/s)	P	u_B* (m/s)	P	u_B* (m/s)	P
1	0.08	-0.95	0.08	-0.95	0.15	-0.83	0.16	-0.81	0.16	-0.81	0.23	-0.61
2	0.15	-0.83	0.15	-0.83	0.15	-0.83	0.46	1.03	0.62	2.60	0.53	1.50
3	0.23	-0.61	0.20	-0.70	0.23	-0.61	0.31	-0.31	0.39	0.08	0.38	0.04
4	0.24	-0.65	0.14	-0.96	0.46	1.43	0.24	-0.65	0.16	-0.84	0.70	4.5
5	0.38	-0.15	0.30	-0.26	0.29	1.14	0.60	1.17	0.60	1.17	0.58	1.06
6	0.60	1.17	0.40	-0.04	0.66	1.62	0.75	2.39	0.45	0.22	0.52	0.63
7	0.08	-0.95	0.08	-0.95	0.23	-0.61	0.16	-0.81	0.16	-0.81	0.31	-0.30

*u_B refers to "Bottom Velocity" measured 0.15 above the bottom.

**T-Groin in place ~ 100 m west of west end of deflector.

***Locations are shown in Fig. J-3.

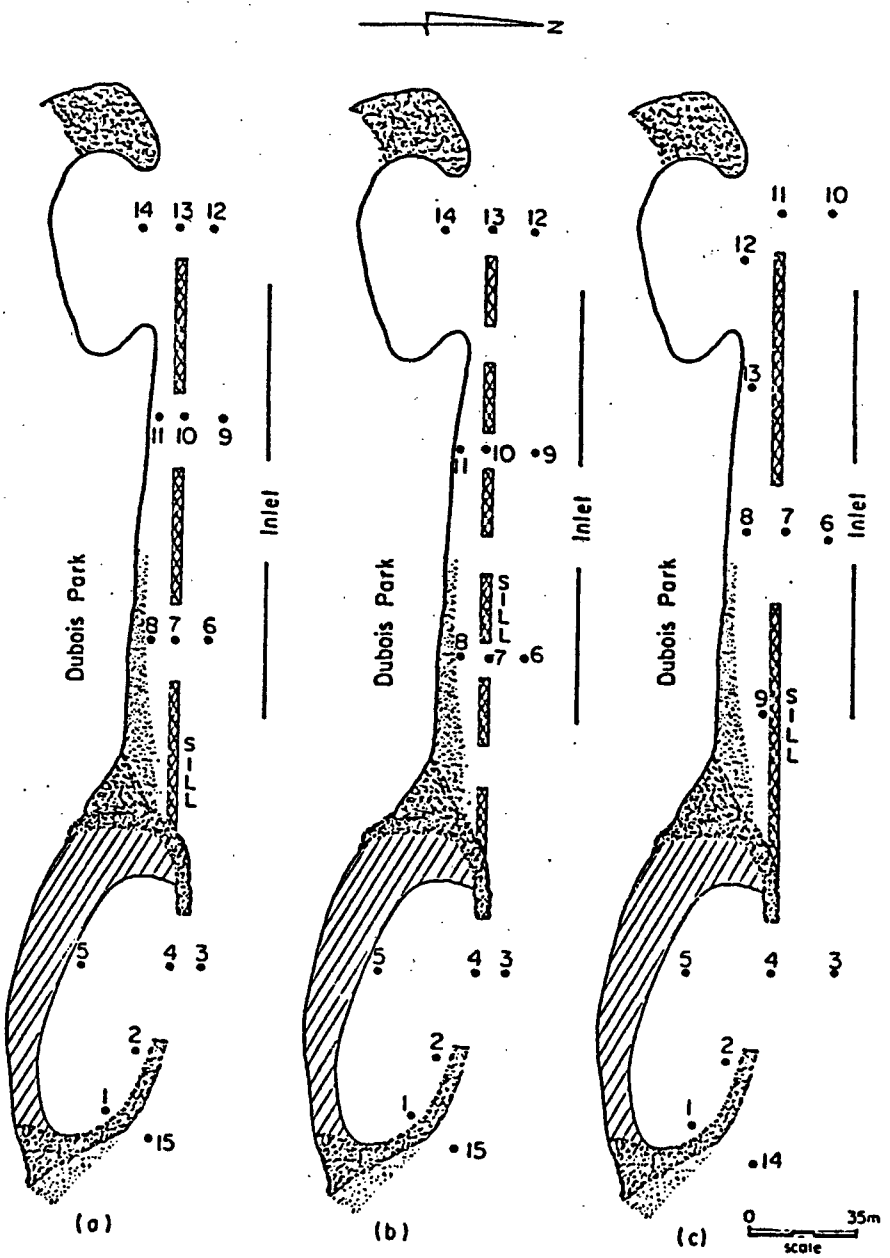

Fig. J-4. Locations of Current Velocity and Wave Height Measurements Made in the Model for the Three Proposed Sill Schemes.

Table J-4. Bottom Velocities, Wave Heights and P Values Resulting from the Placement of a Sill between the Groins at the Dubois Park Beach

	FLOOD			STORM			EBB		
Location**	u_B* (m/s)	H (m)	P	u_B* (m/s)	H (m)	P	u_B* (m/s)	H (m)	P
21	0.60	0.25	3.53	1.13	0.40	23.18	0.70	0.0	2.59
17	0.14	0.0	-0.81	0.28	0.20	1.95	0.20	0.0	-0.64
20	0.23	0.15	0.25	0.23	0.25	1.14	0.16	0.0	-0.76
22	0.14	0.15	-0.48	0.19	0.15	-0.77	0.06	0.0	-0.97

*u_B refers to "Bottom Velocity" measured 0.15 m above the bottom.

**Locations refer to Fig. J-1.

Table J-5a. Bottom Velocities, Wave Heights and P Values for the Three Sill Schemes Shown in Fig. J-4 during a Flood Tide

	Sill Scheme a			Sill Scheme b			Sill Scheme c		
Location**	u_B* (m/s)	H (m)	P	u_B* (m/s)	H (m)	P	u_B* (m/s)	H (m)	P
1	0.18	0.12	-0.47	0.18	0.06	-0.60	0.18	0.06	-0.61
2	0.17	0.06	-0.67	0.17	0.0	-0.72	0.17	0.0	-0.72
3	0.93	0.19	8.67	0.93	0.06	5.91	0.93	0.06	5.91
4	0.65	0.19	5.36	0.65	0.12	4.15	0.65	0.12	4.15
5	0.12	0.19	-0.71	0.12	0.12	-0.74	0.12	0.12	-0.74
6	0.77	0.06	3.80	0.62	0.06	2.07	0.70	0.06	2.88
7	0.48	0.06	1.40	0.40	0.12	1.01	0.40	0.12	1.01
8	0.26	0.12	0.02	0.17	0.12	-0.55	0.17	0.12	-0.55
9	0.77	0.0	3.33	0.62	0.0	1.77	0.70	0.0	2.50
10	0.48	0.0	1.11	0.40	0.0	0.47	0.39	0.0	0.08
11	0.17	0.0	-0.71	0.17	0.0	-0.70	0.32	0.0	-0.06
12	0.62	0.0	1.77	0.46	0.0	0.95	0.17	0.0	-0.70
13	0.32	0.0	-0.06	0.32	0.0	-0.06	0.17	0.0	-0.70
14	0.17	0.0	-0.70	0.17	0.0	-0.70	1.13	0.25	18.36
15	1.13	0.25	18.36	1.13	0.25	18.36	-	-	-

*u_B refers to "Bottom Velocity" measured 0.15 m above the bottom.

**Locations are shown in Fig. J-4.

Table J-5b. Bottom Velocities, Wave Heights and P Values for the Three Sill Plans Shown in Fig. J-4 during an Ebb Tide

	Sill Scheme a			Sill Scheme b			Sill Scheme c		
Location**	u_B* (m/s)	H (m)	P	u_B* (m/s)	H (m)	P	u_B* (m/s)	H (m)	P
1	0.18	0.0	-0.67	0.18	0.0	-0.67	0.18	0.0	-0.67
2	0.17	0.0	-0.72	0.17	0.0	-0.72	0.17	0.0	-0.72
3	0.77	0.0	3.33	0.77	0.0	3.33	0.77	0.0	3.33
4	0.81	0.0	4.87	0.81	0.0	4.87	0.81	0.0	4.87
5	0.09	0.0	-0.91	0.09	0.0	-0.91	0.09	0.0	-0.91
6	0.93	0.0	5.23	0.77	0.0	3.33	0.93	0.0	5.23
7	0.81	0.0	4.87	0.65	0.0	2.76	0.81	0.0	4.87
8	0.68	0.0	3.82	0.68	0.0	3.82	0.68	0.0	3.82
9	0.93	0.0	5.23	0.77	0.0	3.33	0.93	0.0	5.23
10	0.81	0.0	4.87	0.81	0.0	4.87	0.94	0.0	5.42
11	0.68	0.0	3.82	0.68	0.0	3.82	0.64	0.0	2.68
12	0.88	0.0	4.58	0.88	0.0	4.58	0.41	0.0	0.72
13	0.56	0.0	1.82	0.56	0.0	1.82	0.68	0.0	3.82
14	0.38	0.0	0.48	0.38	0.0	0.48	0.81	0.0	3.70
15	0.81	0.0	3.70	0.81	0.0	3.70	-	-	-

*u_B refers to "Bottom Velocity" measured 0.15 m above the bottom.

**Locations are shown in Fig. J-4.

Table J-5c. Bottom Velocities, Wave Heights and P Values for the Three Sill Plans Shown in Fig. J-4 during a 1.5 m Storm Surge (Flood Tide)

	Sill Scheme a			Sill Scheme b			Sill Scheme c		
Location**	u_B* (m/s)	H (m)	P	u_B* (m/s)	H (m)	P	u_B* (m/s)	H (m)	P
1	0.23	0.19	-0.19	0.23	0.19	-0.19	0.23	0.19	-0.19
2	0.22	0.19	-0.27	0.22	0.19	-0.27	0.22	0.19	-0.27
3	1.29	0.31	20.45	1.29	0.31	20.45	1.29	0.31	20.45
4	0.88	0.31	12.18	0.88	0.31	12.18	0.88	0.25	10.31
5	0.21	0.25	-0.27	0.21	0.25	-0.27	0.21	0.25	-0.27
6	1.14	0.12	10.30	1.00	0.12	7.65	0.86	0.25	9.35
7	0.73	0.12	4.88	0.58	0.12	2.76	0.58	0.12	2.01
8	0.30	0.12	0.16	0.30	0.12	0.16	0.30	0.12	0.16
9	1.14	0.06	9.13	1.00	0.12	7.65	0.86	0.19	6.22
10	0.73	0.06	-0.48	0.58	0.06	2.33	0.86	0.0	4.31
11	0.30	0.0	-0.07	0.30	0.0	-0.07	0.44	0.0	0.73
12	0.86	0.0	4.31	0.93	0.0	5.23	0.22	0.0	-0.48
13	0.44	0.0	0.73	0.44	0.0	0.73	0.30	0.06	0.01
14	0.30	0.0	-0.07	0.30	0.0	-0.07	1.90	0.37	56.73
15	1.90	0.37	56.73	1.90	0.37	56.73	-	-	-

*u_B refers to "Bottom Velocity" measured 0.15 m above the bottom.

**Locations are shown in Fig. J-4.

REFERENCES

Bruun, P. M., Stability of Tidal Inlets, Elsevier Publishing Co., Amsterdam, 1978.

Bruun, P., and Gerritsen, F., "By-Passing of Sand by Natural Action at Coastal Inlets and Passes," Coastal Engineering Laboratory, Report No. 15, University of Florida, Gainesville, Florida, 1958.

Bruun, P. M., Chiu, T. Y., Gerritsen, F., and Morgan, W. H., "Storm Tides in Florida as Related to Coastal Topography," Engineering Progress at the University of Florida, Vol. 16, No. 1, Florida Engineering and Industrial Experiment Station, University of Florida, Gainesville, Florida, 1962.

Bruun, P. M., Battjes, S. A., Chiu, T. Y., and Purpura, J. A., "Coastal Engineering Model Studies of Three Florida Coastal Inlets," Florida Engineering and Industrial Experiment Station, Report No. 6, Vol. 20, University of Florida, Gainesville, Florida, 1966.

Bodge, K. R., and Dean, R. G., "Longshore Sediment Transp#rt in the Swash Zone," University of Florida Department of Coastal and Oceanographic Engineering, Gainesville, Florida, In Preparation.

Coastal and Oceanographic Engineering Laboratory, "Coastal Engineering Investigation of St. George Island Channel," Florida Engineering and Industrial Experiment Station, Report No. 7, University of Florida, Gainesville, Florida, 1970.

Dean, R. G., and Walton, T. L., "Sediment Transport Processes in the Vicinity of Inlets with Special Reference to Sand Trapping," Estuarine Research, Vol. 2, Academic Press, New York, 1975, pp. 129-149.

Dean, R. G., and Dalrymple, R. A., Water Wave Mechanics for Engineers and Scientists, Prentice-Hall, Inc., Englewood Cliffs, New Jersey, 1984.

Escoffier, F. F., and Walton, T. L., "Inlet Stability Solutions for Tributary Inflow," Journal of the Waterways, Port, Coastal and Ocean Division, ASCE, Vol. 105, No. WW4, November 1979, pp. 341-355.

Flick, R. E., and Guza, R. T., "Paddle Generated Waves in Laboratory Channels," Journal of the Waterways, Port, Coastal and Ocean Division, ASCE, Vol. 106, No. WW1, February 1980, pp. 79-96.

Florida Coastal Data Network, "Wave Data Report No. 2 - January 1983," Department of Coastal and Oceanographic Engineering, University of Florida, Gainesville, Florida, 1983.

Galvin, C. J., "Wave-Height Prediction for Wave Generation in Shallow Water," Technical Memorandum No. 4, U.S. Army Corps of Engineers, Coastal Engineering Research Center, Washington, D.C., 1964.

Hayter, E. J., "Verification of the Hydrodynamic Regime of a Tidal Waterway Network," M.S. Thesis, University of Florida, Gainesville, Florida, March, 1979.

Hicks, S. D., Debaugh, H. A. Jr., and Hickman, L. E. Jr., Sea Level Variations for the United States, 1855-1980, National Ocean Service Tides and Water Level Branch, Rockville, Maryland, 1983.

Jarrett, S. T., "Tidal Prism - Inlet Area Relationships," GITI Report No. 3, U.S. Army Corps of Engineers, Fort Belvoir, Virginia, 1976.

Jones, C. P., "An Evaluation of Sand Bypassing Systems at Tidal Inlets in Florida," M.S. Thesis, University of Florida, Gainesville, Florida, 1977.

Keulegan, G. H., "Tidal Flow in Estuaries: Water Level Fluctuations of Basins in Communications with Seas," Committee on Tidal Hydraulics Technical Bulletin No. 14, U.S. Army Corps of Engineers, Waterways Experiment Station, Vicksburg, Mississippi, 1967.

King, H. W., and Brater, E. F., Handbook of Hydraulics, 6th Edition, McGraw-Hill, New York, 1976.

LeMehauté, B., "Similitude in Coastal Engineering," Journal of the Waterways, Harbors, and Coastal Engineering Division, ASCE, Vol. 102, No. WW4, November 1976, pp. 317-335.

Lin, P. M., "Modeling Sedimentaton at Inlet and Coastal Regions," Proceedings of the 13th Conference on Coastal Engineering, ASCE, Vol. 2, Vancouver, B.C., Canada, 1972, pp. 883-911.

Macrae, S. W., "Facilities at the Coastal and Oceanographic Engineering Laboratory of Florida," University of Florida, Gainesville, Florida, Unpublished, 1977.

McPherson, B. F., Sabankas, M., and Long, W. A., "Physical, Hydrological, and Biological Characteristics of the Loxahatchee River Estuary, Florida," U.S. Geological Survey, Water-Resources Investigations, Report 82-350, Tallahassee, Florida, 1982.

Mehta, A. J., "Hydraulics of Tidal Inlets, Simple Analytic Models for the Engineer," Coastal and Oceanographic Engineering Laboratory, Report No. 19, University of Florida, Gainesville, Florida, 1975.

Mehta, A. J., "Bed Friction Characteristics of Three Tidal Entrances," Coastal Engineering II, Elsevier Scientific Publishing Co., Amsterdam, 1978, pp. 69-83.

Mehta, A. J., and Christensen, B. A., "Incipient Sediment Motion in Entrances with Shell Beds," Proceedings of the Symposium on Inland Waters for Navigation, Flood Control and Water Diversions, ASCE, 1976, pp. 960-977.

Mehta, A. J., and Sheppard, D. M., "Monitoring (Performance) Study at Matanzas Closure," First Annual Report, Coastal and Oceanographic Engineering Laboratory, Report No. 24, University of Florida, Gainesville, Florida, 1977.

Mehta, A. J., and Sheppard, D. M., "Performance Study at Matanzas Closure," Final Report, Coastal and Oceanographic Engineering Laboratory, Report No. 7, University of Florida, Gainesville, Florida, 1979.

Myers, J. J., Holm, C. H., and McAllister, R. F., Handbook of Ocean and Underwater Engineering, McGraw-Hill, New York, 1969.

National Oceanographic and Atmospheric Association, "Flood Insurance Study, Palm Beach County, Florida," Project No. 4, Washington, D.C., 1971.

National Oceanographic and Atmospheric Association, "Climatological Data," National Climatic Center, Vol. 84, No. 1-12, Ashville, N.C., 1980.

O'Brien, M. P., "Equilibrium Flow Areas of Inlets on Sandy Coasts," Journal of the Waterway and Harbors Division, ASCE, Vol. 95, No. WW1, February 1969, pp. 43-52.

O'Brien, M. P., and Clark, R. R., "Hydraulic Constants of Tidal Entrances 1: Data from NOS Tide Tables, Current Tables, and Navigation Charts," Coastal and Oceanographic Engineering Laboratory Technical Report, No. 21, University of Florida, Gainesville, Florida, 1973.

Richardson, T. W., and McNair, E. C., Jr., "A Guide to the Planning and Hydraulic Design of Jet Pump Remedial Sand Bypassing Sands," Technical Report, HL-81-1, U.S. Army Corps of Engineers, Waterways Experiment Station, Vicksburg, Mississippi, 1981.

Sager, R. A., and Hales, L. Z., "Inlets," Coastal Hydraulic Models, Special Report No. 5, U.S. Army Corps of Engineers Coastal Research Center, Fort Belvoir, Virginia, 1979, pp. 453-517.

Sainflou, M., "Treatise on Vertical Breakwaters," Annals des Ponts et Chausses, Paris, 1928.

Schlichting, H., Boundary Layer Theory, McGraw-Hill, New York, 1979.

Shields, I. A., "Applications of Similarity Principles and Turbulence Research to Bed-Load Movement," Berlin, 1936.

Sorensen, R. M., "An Investigation of Ship-Generated Waves," Journal of Waterways and Harbors Division, ASCE, Vol. 93, No. WW1, 1967, pp. 85-99.

Sorensen, R. M., Basic Coastal Engineering, John Wiley & Sons, New York, 1978.

U.S. Army Corps of Engineers, Jacksonville District, "Survey on Jupiter Inlet, Florida," 1966.

U.S. Army Corps of Engineers, Coastal Engineering Research Center, Shore Protection Manual, U.S. Government Printing Office, Washington, D.C., 1977.

U.S. Army Corps of Engineers, Waterways Experiment Station, "Dredging-Survey of Portable Hydraulic Dredges," Technical Report, HL-83-4, Vicksburg, Mississippi, 1984.

U.S. Geological Survey, "Water Resources Data, Florida Water Year 1981," Water Data Report FL-81-2B, Vol. 2B, Tallahassee, Florida, 1981.

U.S. Naval Weather Service Command, Summary of Synoptic Meteorological Observations, Vol. 4, Asheville, North Carolina, 1970.

van de Kreeke, J., and Wang, J. D., "Tidal Hydraulics and Salt Balance of Lake Worth," Rosensteil School of Marine and Atmospheric Science, University of Miami, 1976.

Walton, T. L., "Littoral Drift Estimates Along the Coastline of Florida," Sea Grant Report #13, Coastal and Oceanographic Engineering Laboratory, University of Florida, Gainesville, Florida, 1976.

Walton, T. L., and Adams, W. D., "Capacity of Inlet Outer Bars to Store Sand," Proceedings of the 15th Conference on Coastal Engineering, ASCE, Vol. 2, Honolulu, Hawaii, 1976, pp. 1919-1937.

Wiegel, R. L., Oceanographical Engineering, Prentice-Hall, Englewood Cliffs, New Jersey, 1964, pp. 359.